Evaluation of Green's functions in complex media by decomposition of the Time Reversal Operator: Application to Medical Imaging and aberration correction

Jean-Luc Robert

Universite Paris 7 – Denis Diderot
Ecole Doctorale de Physique Macroscopique

DOCTORAT DE PHYSIQUE

Specialite: **Acoustique Physique**

JEAN-LUC ROBERT

ESTIMATION DE FONCTIONS DE GREEN DANS LES MILIEU COMPLEXE PAR DECOMPOSITION DE L'OPERATEUR RETOURNEMENT TEMPOREL: APPLICATION A L'IMAGERIE MEDICALE ET A LA CORRECTION D'ABERRATION

Directeur de these: Mathias FINK

Chapter 1. Introduction

L’imagerie medicale par echographie a subi un important developement au cours des vingt dernieres annees. Les principales raisons de ce developement sont dues au faible cout de la modalite par rapport aux autres methodes disponibles (CT-scan, IRM), a la mobilite des appareils (des appareils portables commencent meme a etre disponibles), au caractere non-invasif et non-radioactif de la methode, ou encore a la possibilite de visualiser des images en temps reels, contrairement aux autres modalites. Recemment, les echographes ont acquis la possibilite d’imager des volumes en 3 dimensions, comme par exemple un cœur qui bat ou le visage d’un bebe.

Les applications sont nombreuses : detection de cancers, diagnostic prénatal ou encore visualisation d’ecoulements sanguins grace au mode Doppler.

Cependant, la qualite des images est severemment degreades chez un certains nombre d’individus, a cause de l’inhomogeneite des tissus traverses. On parle d’aberration. Cette degradation limite la capacite diagnostique des ultrasons. Des exemples sont presentes de la Figure 1 a la Figure 3. La detection des cancers du sein, entre autre, est particulierement affecte. En effet le sein est un milieu particulierement heterogene, et les frequences utilisees pour cette application sont elevees, ce qui augmente la sensibilite au probleme.

La correction des aberrations est donc un sujet important. Cette these s’interesse au developement d’une methode basee sur le retournement temporel pour corriger les aberrations. Les resultats developes dans ce manuscript sont toutefois plus general et s’appliquent aussi a d’autre domaines.

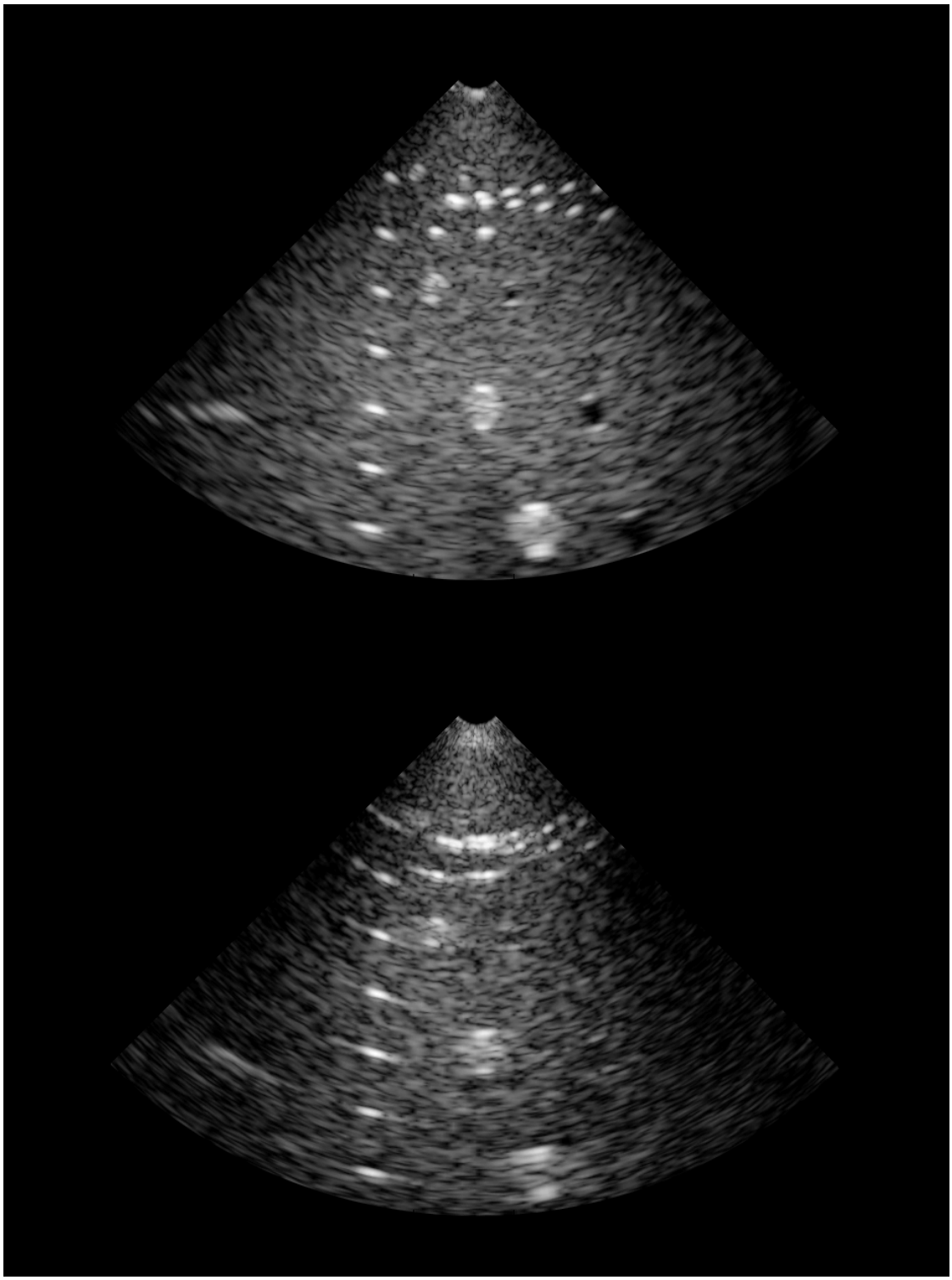

Figure 1 Image d'un phantom medical, imitant les tissus biologiques, sans aberration (haut), et en presence d'un aberrateur (bas). Les points sont moins bien resolus, et les cysts deviennent invisibles.

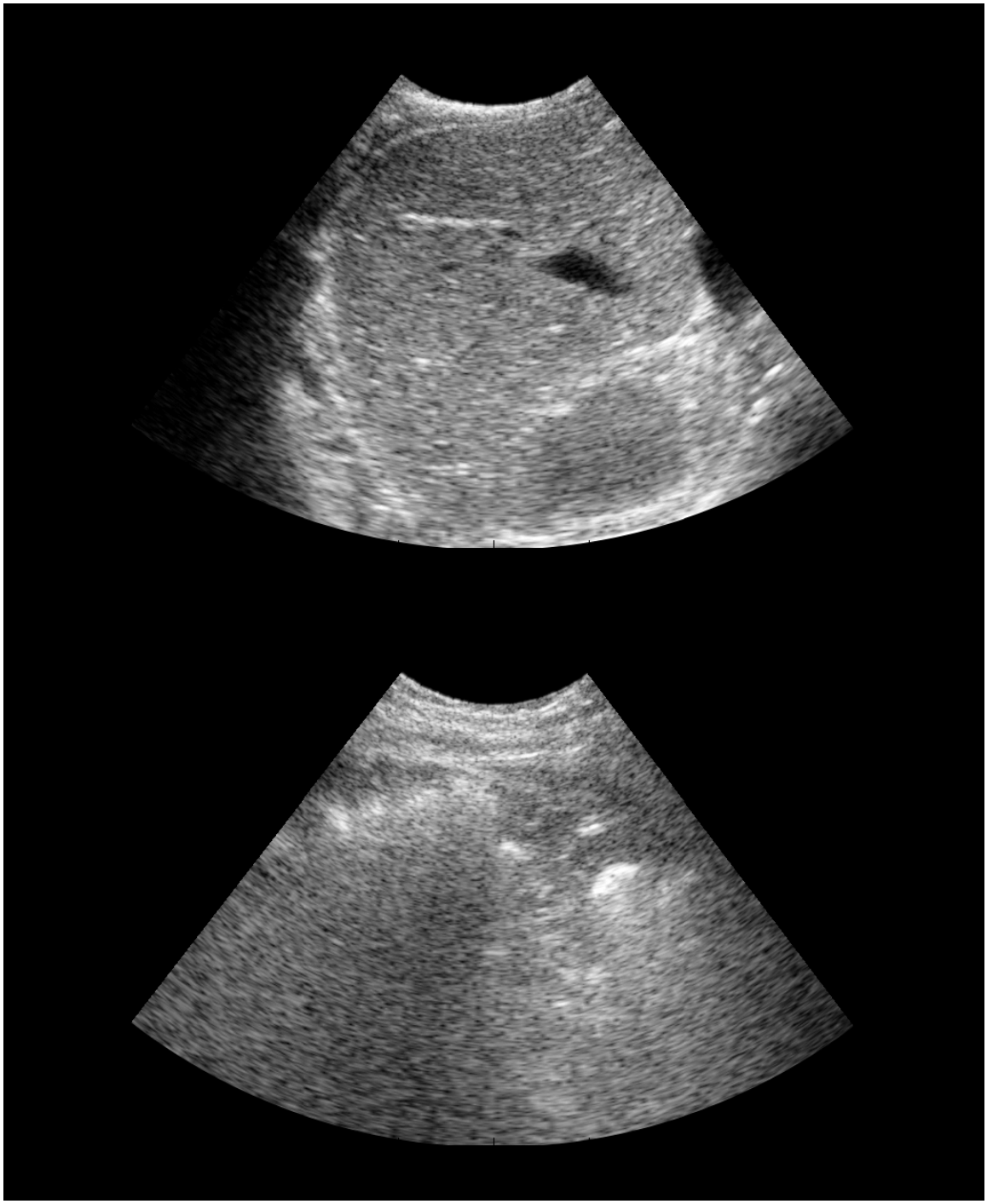

Figure 2 Image du foie chez un patient facile (haut) et difficile, c'est a dire dont l'image est degreadee par le phenomene d'aberration (bas). Il est aise de reconnaître des structures comme les vaisseaux sanguins dans le premier cas, mais quasiment impossible dans le second cas.

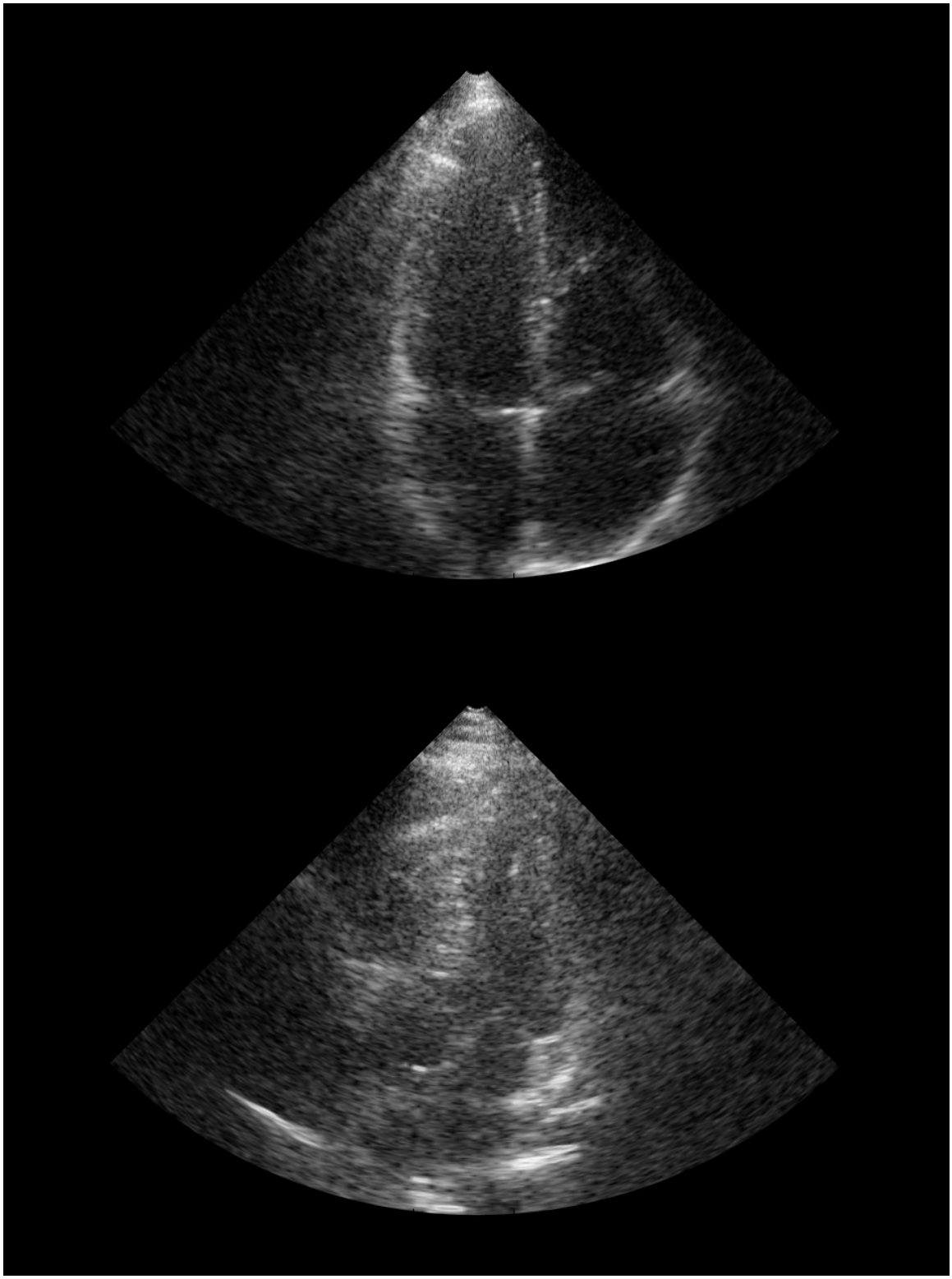

Figure 3 Images cardiaques chez un patient facile (haut) et difficile (bas). On distingue aisement les quatre compartiments du cœur dans l'image superieur, mais cela est plus difficile pour l'image du bas.

I. FOCALISATION DANS DES MILIEUS HOMOGENES ET HETEROGENES

La plupart des applications en acoustique repose sur la possibilité de focaliser les signaux. Par exemple, pour former une image d un milieu diffusant, on insonifie le milieu par un faisceau ultrasonore, et on reçoit les échos des diffuseurs au moyen d'une barrette échographique. La résolution de l'image, et donc sa qualité, dépend de la focalisation du faisceau. En effet, si le faisceau insonifie plusieurs diffuseurs a la fois, les échos de ces diffuseurs sont reçus simultanément, et il n'est pas possible de séparer les diffuseurs lors de la formation de l'image. Apres la réception, une nouvelle focalisation est applique, appelle focalisation en réception. Cette focalisation s'effectue habituellement en appliquant des délais a chaque voie, et en les sommant. Cette opération est appelée *Beamforming* ou formation de voie.

I.A. Focalisation en milieu homogène

I.A.1. Le concept de « delay and sum »

Il y a quelques années, la focalisation nécessitait l'emploie de lentilles. Aujourd'hui, elle s'effectue électroniquement. Une barrette est en effet constituée d'un certain nombre de transducteurs, indépendants les uns des autres. Chaque transducteur peut transmettre une impulsion ultrasonore a un temps donne.

Pour focaliser en un point P de l'espace, il faut que le transducteur i transmette une impulsion avec un délai t_i correspondant au temps de propagation du transducteur au point P, $t_i(P)=r_i(P)/c$ ou $r_i(P)$ est la distance entre P et le transducteur, et c est la vitesse du son. Ainsi, les fronts d'onde de tous les transducteurs arrivent en même temps au point

P et interfère constructivement. Ailleurs, les fronts d'onde interfèrent destructivement, car ils arrivent decales. Ainsi, l'énergie est concentre dans le voisinage de *P*. *P* est appele point focal. Les delais t_i correspondant a la propagation dans un milieu homogene sont souvent appeles *delais geometriques*.

En reception, l'echo du diffuseurs situe au point *P* arrive a la barette et est converti en signal electrique. Les signaux recus par chaque transducteur arrivent decalles. Le delai correspond au temps de propagation depuis *P* et est donc l'oppose des t_i. La focalisation en reception s effectue en retardant les signaux de chaque voies par t_i, et en les sommant. Ainsi, les signaux correspondant au point *P* s'ajoutent constructivement, tandis que les signaux provenant d'autres points interferent destructivement.

Il est souvent pratique de considerer une approche monochromatique (a une frequence, aussi appelee bande etroite par reference a la largeur de la bande passante) car les calculs y sont simplifies. L'approche precedente est connue sous le nom d'approche impulsionelle, ou bande large.

Dans l'approche monochromatique, le decallage des signaux devient un dephasage. Le signal applique sur le transducteur *i* devient

$$H_i = e^{jkr_i(P)} \Big/ r_i(P) = e^{j\omega t_i(P)} \Big/ r_i(P)$$

Eq.1. 1

I.A.2 Fonction de Green

La fonction e^{jkr}/r est connue sous le nom de *fonction de Green monochromatique* pour un espace libre a trois dimensions. Elle represente le champ emit par une source ponctuelle (voir par exemple (Goodman) chapitre 3).

Par abus de langage, le vecteur H dont les coordonnées sont les H_i est appele fonction de Green du point P dans ce document. H represente en quelques sortes les coordonnees du point P dans la base de la barette, appelée *base canonique*. Dans le domaine temporel, on appelera le front d'onde provenant de P et recu par la barette, la fonction de Green temporelle de P. Rigoureusement, une fonction de Green temporelle est le signal recu quand la source emet un dirac, mais dans ce document on etend le terme aux signaux a bande passant limite (par la fonction de transfert des transducteurs).

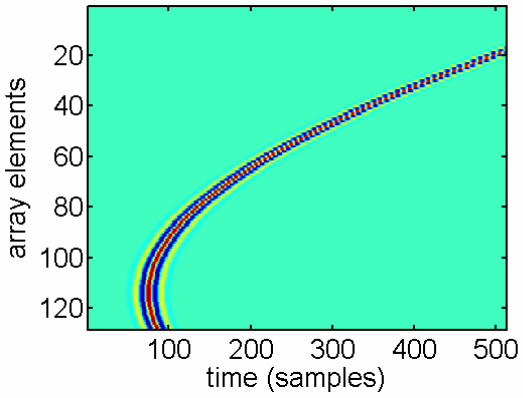

Figure 4 Une fonction de Green temporelle

I.A.3 Retournement temporel des fonctions de Green et focalisation

La fonction de Green H est le signal recu par la barette lorsqu'un pulse est emis au point P. En vertu de l'invariance par retournement temporel, si l'on transmet le retourne temporel (conjugue en monochromatique) de la fonction de Green, on genere

une onde qui focalise au point *P*. Ce resultat est valide non seulement en milieu homogene, mais aussi dans n'importe quel milieu pouvu que l attenuation soit negligeable (Fink). C'est pour cela qu'il est interessant de savoir estimer les fonctions de Green, tout specialement dans les milieux homogenes ou l'on ne la connaît pas theoriquement, comme nous allons le voir dans la partie suivante.

I.B Focalisation en milieu heterogene

I.B.1.Origine du probleme en imagerie medicale

Lorsque le milieu est homogène et que la vitesse du son y est connu, il est simple de focaliser, comme nous l'avons vu dans le paragraphe précèdent. Un exemple simple est le cas de l'eau, par exemple lors d'expérience realise dans un laboratoire.

En premiere approximation, le corps humain peut aussi etre considere comme milieu homogene car les tissus sont constitues en majorite d'eau. C'est l'approximation faites par les appareils d'echographie. Cela donne de bons résultats dans la plupart des cas.

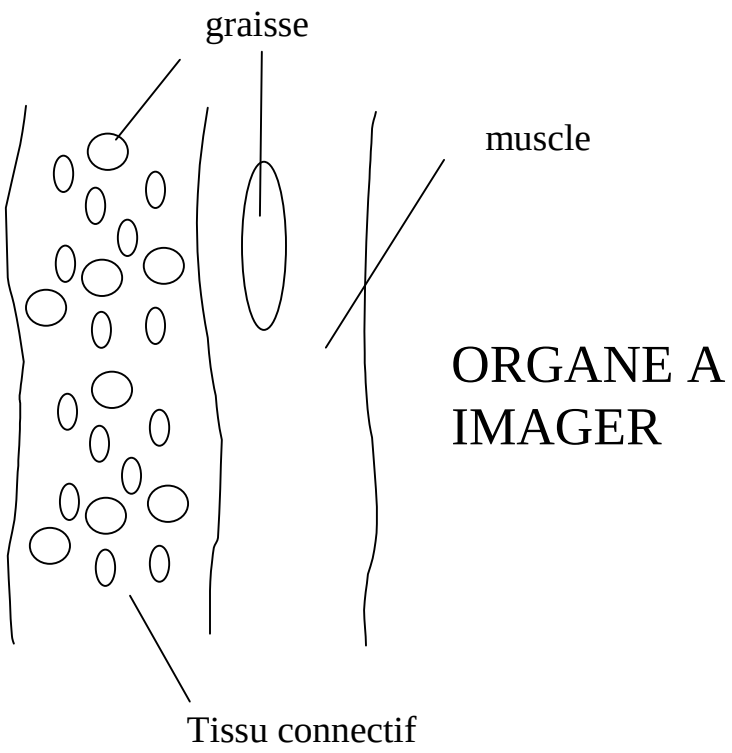

Figure 5 Schema des couches de tissus gras et musculaires en surface de l'organe a imager

Cependant, en realite, la vitesse du son diffère d'un tissu a un autre, car la compressibilite et l'elasticite des tissus (dont dépend la vitesse du son) varie. Les differences sont particulierement importante dans la couche grasse, constitue de lobule de graisse (1450 m/s) entoure par du tissu connectif (1615 cm/s) comme on le voit sur la Figure 5(Hinkelman, Mast et al.; Mast, Hinkelman et al.). La traversee de cette couche (importante chez les patients obeses) entraine un decallage des fronts d'onde emis par chaque transducteurs, qui n'arrivent plus en phase au point focal. L'image est alors de pauvre qualite, et il est difficile de faire un diagnostic. On parle *d'aberrations*.

I.B.2. Solution generale : retournement temporel de la fonction de Green

Pour focaliser dans le milieu heterogene, et obtenir une image de bonne qualite, il faut connaître la fonction de Green de chaque point dans le milieu. En effet, comme on l'a vu dans le paragraphe precedent, en transmettant le retourne temporel de la fonction de Green, on genere une onde qui focalise en *P*. Cela est vrai tant que l'invariance par retournement temporel est valide, c'est-à-dire tant que l'attenuation est negligeable. C'est en general le cas dans le corps humain, et c'est l'hypothese qui est faite dans ce document. Une exception est le crane.

Contrairement au cas homogene, on ne peut pas calculer a l'avance les fonctions de Green de chaque point du milieu. En effet, elles sont differentes pour chaque patient. Il est donc necessaire de savoir estimer les fonctions de Green du milieu heterogene a partir du signal echographique. Idealement, un algorithme de correction d'aberration se fait en 3 etapes :

- Acquisition du signal echographique en utilisant les fonctions de Green homogenes
- Estimation des fonctions de Green heterogenes a partir du signal echographique
- Nouvelle acquisition utilisant les fonctions de Green estimées

On parle dans ce cas d'imagerie adaptative, car la focalisation s'adapte au milieu.

En general, la fonction de Green dans un milieu heterogene ne peut pas etre considere comme une simple loi de retard (les signaux sur chaque voies sont identiques mais retarde les uns par rapport aux autres) Il se produit des phenomenes d'interferences, diffraction et quelque fois aussi de réflexion multiple. Les signaux sont donc en général

deforme temporellement (la déformation étant différente pour chaque voies) et l'amplitude varie selon les voies. Un exemple est montre Figure 6.

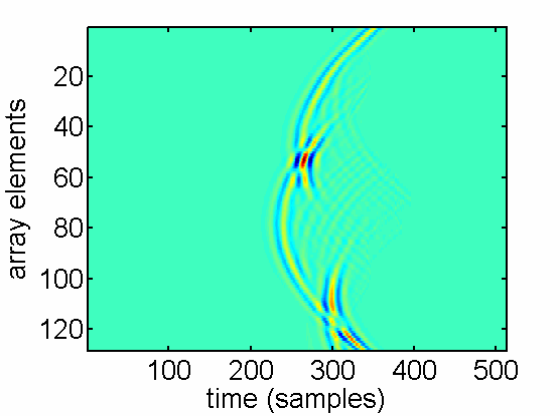

Figure 6Exemple de fonction de Green dans un milieu heterogene (la simulation utilise le modele de l'ecran en champ lointain developpe dans la section I.B.4)

Pour focaliser en transmission, il faut etre capable de transmettre le retourne temporel du front d'onde représente Figure 6. Cela nécessite des voie equipees de filtres programmable individuellement (du type mirroir a retournement temporel), ce dont ne sont pas equipes les appareils d'echographie actuels. En reception, l'equivalent du retournement temporel est la convolution par un match-filter (Dorme and Fink 1995) illustre par la Figure 7. Cela aussi necessite une architecture couteuse pour les appareils d'echographie.

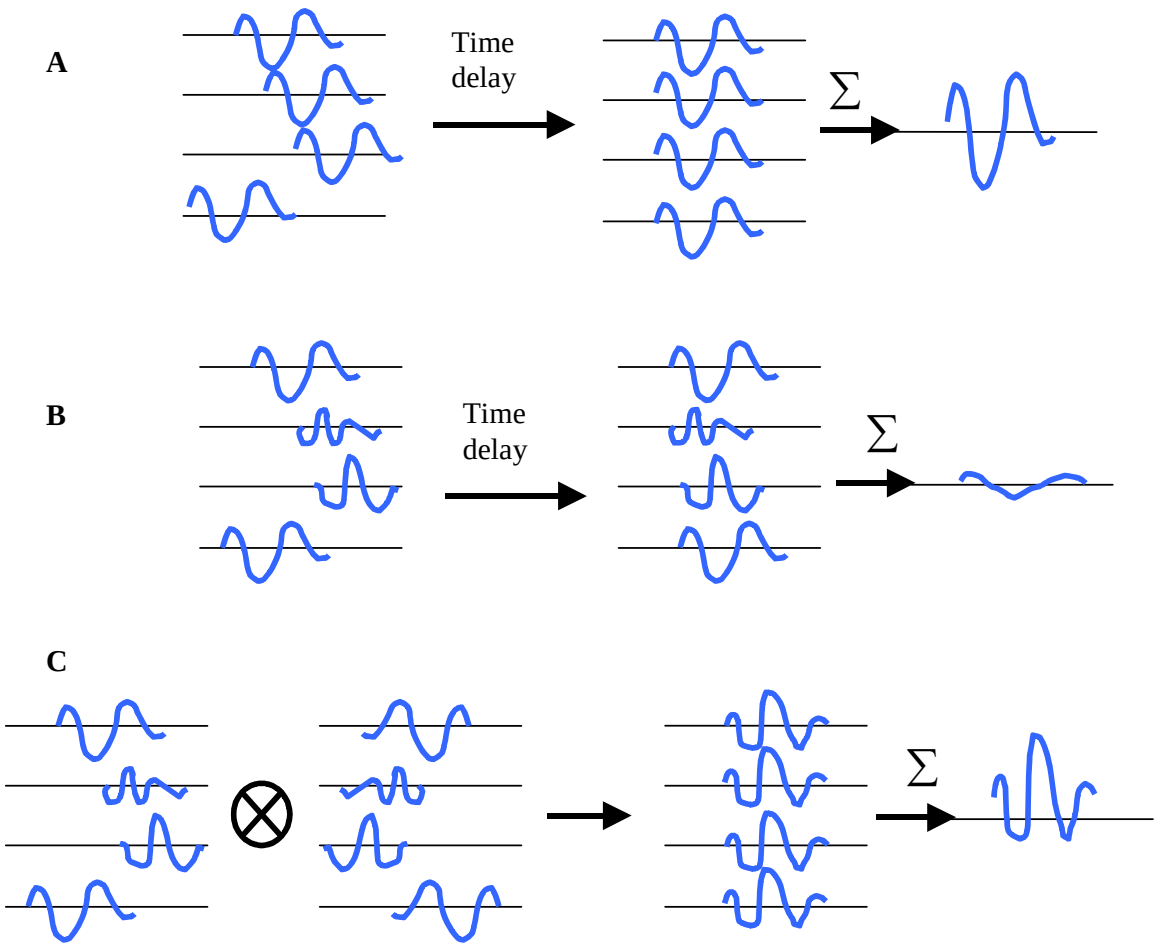

Figure 7 Comparaison entre le beamforming classique (retard et somme) et l'approche match-filter. A) En general, la focalization est effectue par alignement des signaux sur chaque voie. Lorsque les signaux sont ajoutes les uns aux autres, les signaux provenant du point d'interet (point focal) s'ajoutent constructivement. B) Si les signaux sur chaque voie ont des formes differentes, les alignes n'est plus suffisant C) Dans l'approche match-filter, on convolue les signaux sur chaque voix par le retourne temporal de la function de Green du point focal. Si les signaux recus provienent effectivement du point focal, on obtient un pic des fonctions sur chaque voie (la convolution d'un signal par son retourne temporel, qui est equivalent a l'auto-correlation du signal, a un fort maximum correspondant a la superposition exacte des signaux) On peut alors ajouter constructivement les signaux entre eux, tous les pics ayant lieux au meme moment.

Dans le formalisme monochromatique, une fonction de Green heterogene dans le cas general s'ecrit sous la forme

$$H_i(\omega, P) = a_i(\omega, P) e^{j\left(\omega t_i(P) + \phi_i(\omega, P)\right)}$$

Eq.1. 2.

Ou en general, $\phi_i(\omega, P)$ n'est pas lineaire en ω. La fonction de Green heterogene est donc la fonction de Green homogene de l'Eq.1. 1, multipliee par le filtre

$a_i(\omega, P) e^{j\left(\phi_i(\omega, P)\right)}$.

Un autre obstacle pour l'implementation est le besoin d'estimer la fonction de Green pour chaque point ou l'on veut focaliser. Lorsque l'on veut faire une image d'un milieu, on focalise typiquement sur plusieurs centaines de points. En general, on peut cependant considerer que la fonction de Green d'un point *P* est valable pour les points de son proche voisinage, a condition de rajouter un retard correspondant a la propagation homogene. La region dans laquelle cette aproximation est valide est appelle isoplanatic patch

Afin d'implementer des algorithmes de correction d'aberration en temps reel dans un echographes, des modeles simplifies ont ete introduits. Ces modeles sont aussi utiles pour simuler simplement une aberration. Ils seront utilises au long de cette these.

I.B.3. Ecran de phase en champ-proche (near-field phase screen)

C'est le modele le plus simple, et utilise par la quasi-totalite des méthodes de correction d'aberration. Dans ce modele, toute l'heterogeneite est suppose etre concentre dans une couche mince immediatement apres la barette. Le reste du milieu est homogene.

Dans ce cas, un front d'onde emis par un point du milieu arrive intact jusqu'à l'heterogeneite (aberrateur). Chaque point du front d'onde subi un delai different lors de la traversee de l'heterogeneite (car ils traversent des tissus different). L'effet de l'aberrateur est donc d'introduire un delai τ_i sur chaque element, en plus du delai geometrique $t_i(P)$ correspondant a la propagation dans le milieu homogene. On modelise alors l'heterogeneite par un ecran d'epaisseur nulle, situe devant la barette, qui introduit un simple delai lors du passage de l'onde. Une fonction de Green typique dans ce modele est represente Figure 8. On observe bien le delai introduit par l'aberrateur.

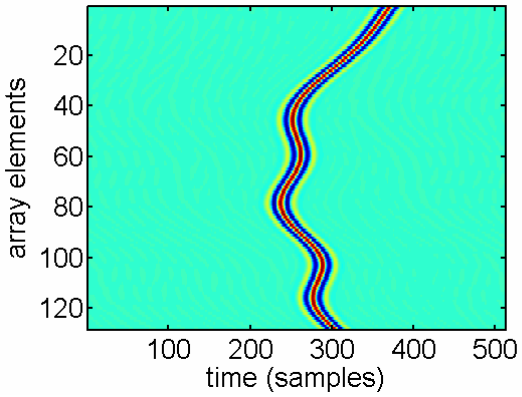

Figure 8 Fonction de Green dans le modele de l'ecran en champ proche

Dans le formalisme monochromatique (Eq.1. 2), le delai se traduit par un dephasage $\phi_i(\omega, P)$, lineaire en fonction de la frequence, et independant de *P :*

$$\phi_i(\omega) = \omega\tau_i$$

Eq.1. 3

.

Il y a de nombreux avantages a travailler avec un ecran champ-proche :

- La focalisation peut etre rectifie simplement en compensant les retards τ_i, ce qui est tres simple a implementer dans un scanner.

- La correction ne depend pas du point *P* auquel on veut focaliser. En effet, pour chaque point, l'ecran introduit les meme retard τ_i. La loi de retard totale pour focaliser en *P* est $t_i(P)+\tau_i$. Une fois que les τ_i ont ete estime, il est possible de focaliser n'importe ou dans le milieu, en ajustant les delais geometriques. On a donc besoin d'estimer une seule fonction de Green, en utilisant une des methodes presentes plus tard. On peut ensuite en deduire les fonctions de Green de tous les autres points.

Ce modele est tres simple a utiliser, mais n'est pas tres realiste. En effet, l'heterogeneite est rarement concentre sur une faible epaisseur a la surface du transducteur, mais est en general distribuee sur plusieurs centimetres. L'ecran champ proche peut etre vu comme une approximation a l'ordre 0 d'un aberrateur reel.

Les corrections d'aberration basees sur ce modele permettent en general une legere amelioration de la qualite de l'image, mais a notre connaissance, la plupart des implementations cliniques ont ete decevantes.

I.B.4. Ecran de phase en champ-lointain (far-field phase screen)

Un modele plus complet est obtenu si l'on place l'ecran de phase non plus a la surface de la barette, mais en profondeur dans le milieu. Ce modele est appele *ecran de phase en champ lointain.* Il offre une meilleur approximation de l'effet des heterogeneites.

Dans ce modele, certaines composantes du front d'onde sont retardes lors de la traversee de l'ecran, comme dans le modele champ-proche. Cependant, lorsque le front d'onde continue de se propager vers la barette, les diverse composantes qui sont maintenant dephasees, interferent. Il en resulte une deformation temporelle du front

d'onde, et une variation de son amplitude en fonction de l'azimuth. Une facon de regarder le probleme est de considerer chaque point de l'ecran de phase comme une source secondaire. Le phenomene d'interference (diffraction) apparaît car les sources secondaire sont hors-phase. Ces phenomenes de distortion et d'interferences sont observes dans le cas d'heterogeneites distribues. Le modele en champ lointain est donc plus complet que l'ecran en champ proche, car il prend en compte, au 1er ordre, ces effets. Une fonction de Green typique obtenue dans le modele de l'ecran de phase en champ lointain est represente Figure 9.

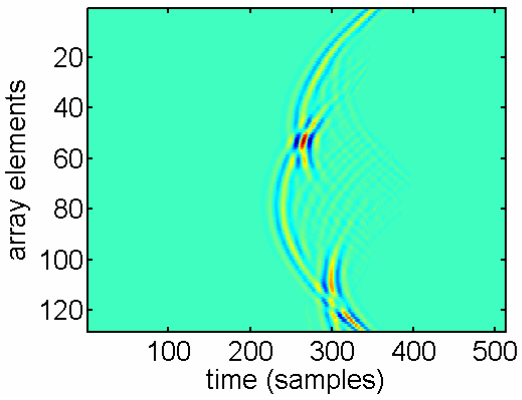

Figure 9 Fonction de Green dans le cas d'un ecran de phase en champs lointain

Ce modele a ete propose initialement par (Liu and Waag) puis (Dorme and Fink). Il est repris est developpe dans le chapitre 2 de cette these.

II. METHODES D'ESTIMATION DE FONCTIONS DE GREEN

On peut classifier les méthodes en différentes catégories. Le premier critère est l'approximation considérée. On différenciera les méthodes reposant sur l'approximation de l'écran champ proche (dans ce cas, on n'estime pas vraiment la fonction de green, mais

la meilleure loi de retard qui approche la fonction) et les méthodes qui estiment complètement la fonction de Green.

Certaines méthodes ne s'appliquent qu'au speckle, d'autres seulement aux diffuseurs ponctuels. En imagerie médicale, la majorité du milieu est constitue de speckle, et donc il est impératif que la méthode soit capable d'estimer les fonctions de Green a partir du speckle.

Le speckle est le signal qui a un aspect granuleux ou neigeux, observable dans la quasi-totalité des images médicales. Il est aussi observe dans d'autres domaines comme le contrôle non-destructif. Le speckle apparaît lorsque le milieu contient une grande densité de diffuseurs microscopiques, comme c'est le cas dans les tissus biologiques ou les diffuseurs sont les structures cellulaires. Dans ce cas, un grand nombre de diffuseurs sont présents dans une cellule de résolution (le volume insonifie a un instant donne par le système ultrasonore) et l'écho obtenu est la somme de la contribution de chacun des diffuseurs, qui sont légèrement dephases les uns par rapport aux autres. Le problème est similaire au problème de marche aléatoire. La somme des signaux est aléatoire et obéit aux lois statistiques, présentées dans le chapitre 4.

Figure 10 Image d'un foie. La plupart du signal, qui a un aspect « neigeux » est du speckle. Il y a aussi quelques diffuseurs étendus (vaisseaux sanguins), mais pas de diffuseurs ponctuels.

II.A Methode reposant sur le modèle écran en champ-proche (estimation de loi de retards seulement)

Ces méthodes sont particulièrement intéressantes pour l'implémentation en temps réel et a faible coût d'une correction d'aberration. Toutefois les qualités d'images obtenues sont moyennes.

II.A.1. Methodes de cross-correlation de signaux (O'Donnell)

Cette méthode a été proposée par (Flax and O'Donnell 1988; O'Donnell and Flax 1988). Elle consiste à calculer la fonction de corrélation de signaux reçus par des éléments voisins de la barrette, i and $i+1$. Le pic de la fonction de corrélation indique la

différence de temps d'arrivée entre les signaux. Les fronts d'ondes sont alignes auparavant de façon a enlever les délais géométriques $t_i(P)$, correspondant a la partie homogène de la propagation. Les différences de temps d'arrivée correspondent donc aux différences de retard introduits par l'aberrateur, τ_{i+1}-τ_i. La connaissance des différences de retard pour chaque couple de voisins permet de remonter à la loi $\tau_{i.}$

La méthode permet d'estimer les délais a partir écho de diffuseurs ponctuels, ou bien du speckle. De nombreuses variantes ont été developpees. Dans certaines, la fonction de corrélation est normalisée, dans d'autres la covariance remplace la corrélation (Silverstein and Ceperley 2003). Enfin, dans d'autres approches, le calcul des fonctions de corrélation est remplace par la somme de la différence entre les signaux au carre, ou par la somme de la valeur absolue de la différence (Friemel, Bohs et al. 1995; Viola and Walker 2003). Enfin, dans une dernière approche, le retard est estime a partir de la corrélation entre le signal reçu par un element et un signal de référence(Rigby, Chalek et al. 2000).

Une variante a été propose par (Gauss, Trahey et al. 2001; Fernandez, Gammelmark et al. 2003). Cet algorithme est connu sous le nom de LMS (Least Mean Square) Dans ce cas, les fonctions de corrélation ne sont calcules non plus uniquement entre pairs éléments voisins, mais aussi entre proche voisins. Le profil de retard optimal est ensuite obtenu en minimisant la distance entre le profil et les délais estimes, grâce a la méthode des moindres carre (LMS). Le fait d'utiliser les corrélations entre proche voisin, et non pas seulement voisins immédiats, augmente la robustesse dans le speckle. Nous reviendrons sur cela dans le chapitre 4.

II.A.2 Maximisation de l'intensité du speckle

Cette méthode a été propose par (Levin, Gregg et al. 1989) Elle est base sur le fait que intensité du speckle augmente avec la qualité de la focalisation. L'algorithme ajuste les retards sur les voies de façon a maximiser intensité du speckle dans une région d'intérêt.

Cette méthode est spécifique au speckle.

II.B. Methodes estimant la fonction de Green complète

Ces méthodes sont plus efficaces que les précédentes, et font l'objet de la plupart des travaux récents. Cependant, leur implémentation sur des échographes commerciaux est encore loin d'être à l'ordre du jour. Une comparaison des performances de ces méthodes et faites dans le chapitre 4.

II.B.1 Itération du retournement temporel et méthode DORT

L'itération du retournement temporel (Prada, Wu et al.) permet d'estimer la fonction de Green du diffuseur le plus brillant du milieu. On insonifie d'abord le milieu et on enregistre les échos. Ensuite, on reemet les signaux retournes temporellement. Ceux-ci focalisent sur les diffuseurs, et un nouvel écho est genere. A chaque itération, écho des diffuseurs les plus faible sont atténues par rapport au diffuseur le plus brillant. Au bout d'un grand nombre itération, seul écho du diffuseur le plus brillant est reçu.

Les fonctions de Green des autres diffuseurs peuvent être obtenues en utilisant la méthode DORT (Décomposition de l'Opérateur Retournement Temporel) (Prada and Fink; Prada, Manneville et al.). La méthode est base sur l'acquisition de Opérateur Retournement Temporel qui décrit le processus de retournement temporel entre la

barrette et les diffuseurs. Opérateur Retournement temporel est habituellement défini par le produit KK^H ou $K_{i,j}$ est le signal reçu par éléments *j* lorsque une impulsion est transmise par éléments *i*.

Les vecteurs propres de l'opérateur retournement temporel correspondent aux invariants du retournement temporel. Dans le cas ou les diffuseurs sont bien résolus, chaque invariant correspond à la fonction de Green d'un diffuseur. La méthode est décrite plus précisément dans le chapitre 2.

Les méthodes basées sur le retournement temporel sont les plus puissantes (au moins tant que l'atténuation est négligeable. Cependant la méthode DORT, dans sa version originale, est loin d'être utilisable dans le domaine médicale Cela est lie entre autre a la nature des diffuseurs et aux modes d'acquisition des échographes Le sujet de cette thèse est précisément d'adapter la méthode a un tel environnement.

Opérateur Retournement Temporel peut aussi être interprète comme une matrice de covariance (Prada and Thomas; Gruber, Marengo et al.). Cela est particulièrement intéressant pour faire le lien avec les autres méthodes d'estimation, qui sont pour la plupart basées sur le calcul de fonctions de corrélation Ainsi, le coefficient (i,j) de Opérateur Retournement Temporel est le coefficient de corrélation (a une fréquence donnée) entre les signaux reçus par les éléments i et j de la barrette La corrélation est à entendre au sens deterministique (car les signaux sont des échos de diffuseurs ponctuels. La corrélation est moyenne sur l'ensemble des transmissions (chaque transmission pouvant être vue comme une nouvelle *réalisation* du milieu.

II.B.2 Décomposition de la matrice de corrélation spatiale

Cette méthode a été proposée par (Varslot, Krogstadt et al.), pour le speckle. Elle consiste à construire dans un premier temps une matrice de corrélation spatiale des signaux diffuses par une région de speckle, a un certain nombre de fréquences. Par exemple, le coefficient (i,j) de cette matrice, est le coefficient de corrélation (a une fréquence donnée) des signaux reçus par les éléments i et j de la barrette La corrélation est à entendre au sens statistique (le signal est ici un signal aléatoire, le speckle) : Le moyennage s'effectue sur diverses réalisations de la distribution de speckle. L'aspect statistique du speckle et de la corrélation spatiale est développe en détail dans le chapitre 4.

Ensuite, une décomposition de la matrice est effectuée. Le 1^{er} vecteur propre est la fonction qui maximise intensité du speckle. D'après ce que l'on a vu en II.A.2, cette fonction peut être interprète comme une fonction de Green d'un point dans la région d'intérêt.

Cette méthode semble très similaire a la méthode DORT : toutes deux impliquent la décomposition d'une matrice de corrélation Toutefois, l'une s'applique à des diffuseurs deterministiques tandis que l'autre s'applique à des signaux aléatoires. Nous reviendrons sur la similarité entre les deux méthodes dans le chapitre 4, lorsque nous généralisons la méthode DORT au speckle.

II.B.3.Methodes de corrélation dans le domaine fréquentiel

Cette méthode est utilisée par (Waag and Astheimer; Waag and Astheimer). Elle est l'équivalent fréquentiel de la méthode II.A.1. Les signaux reçus sont alignes de façon à supprimer le retard correspondant à la propagation homogène, $t_i(P)$. La transformée de

Fourier est ensuite effectuée, et le coefficient de corrélation entre voisins est calcule à un certain nombre de fréquences. La phase du coefficient de corrélation donne $\phi_{i+1}(\omega,P)- \phi_i(\omega,P)$, d'après Eq.1. 2.. Le déphasage introduit par l'aberration peut donc en être déduit et corrige. L'avantage par rapport aux méthodes temporelles est la possibilité de prendre en compte des termes de phases non-lineaires en fonction de la fréquence, et qui ne se traduisent donc pas par un simple retard.

III. MODELES POUR LES SIGNAUX

Nous présentons brièvement les modèles et approximations pour les signaux acoustiques qui seront utilises dans ce manuscrit.

III.A Formule de Rayleigh-Sommerfeld

Le champ acoustique genere par une barrette peut être décrit par la formule de Rayleigh-Sommerfeld. Nous supposons que la pression applique dans le plan de la barrette est continue. Soit *E(X)* ce signal. Le champ de pression dans le milieu, a un point *M* de coordonnées (x,z) est donne par

$$P(x) = \frac{1}{j\lambda}\int_{barrette} E(X)\, e^{jk\sqrt{z^2+(x-X)^2}} \Big/ \sqrt{z^2+(x-X)^2}\cos\theta \cdot dX$$

Eq.1. 4

ou $e^{jk\sqrt{z^2+(x-X)^2}} \Big/ \sqrt{z^2+(x-X)^2}$ est la fonction de Green du point *M*, et θ est l'angle sous lequel est observe le point. Le terme en *cos* est en général néglige. Mathématiquement, la

formule Eq.1. 4 peut alors être interprétée comme la projection du signal *E(X)* sur la fonction de Green du point considère.

III.A.2 Approximation de Fresnel en coordonnes cartésiennes

Pour des point tels que z>>(x-X), on fait en général l'approximation de Fresnel

$$\sqrt{z^2+(x-X)^2} \approx z+\frac{1}{2}\frac{(x-X)^2}{z}$$

Eq.1. 5

L'Eq.1. 4 devient alors

$$P(x,z)=\frac{e^{j2\pi\frac{z^2+x^2}{\lambda z}}}{Z}\int_{barrette}E(X)e^{j\frac{X^2}{\lambda z}}e^{j2\pi\frac{xX}{\lambda z}}dX$$
$$=Ke^{j\frac{x^2}{\lambda z}}TF\left\{E(X)e^{j\frac{X^2}{\lambda z}}\right\}\left[\frac{x}{\lambda z}\right]$$

Eq.1. 6

ou *K* est une constante indépendante de *x*, et TF désigne la transformée de Fourier. Le champ est donc donne par la transformée de Fourier du signal applique dans le plan de la barrette multiplie par un terme de phase. Lorsque l'on focalise en un point, ce terme de phase est annule, et le signal peut être considère comme la transformée de Fourier de l'ouverture. En général, pour une ouverture de taille *D*, et sans apodization, le signal observe dans le plan focal est donne par $\mathrm{sinc}\left(\frac{\pi x}{\lambda z/D}\right)$, et la résolution est $\lambda z/D$.

III.A.3 Approximation de Fresnel en coordonnées polaires

Lorsque l'on utilise une mode d'acquisition sectoriel (phase array, les points focaux sont situes sur un arc de cercle), les coordonnes polaires sont utilisées.

L'approximation de Fresnel s'écrit alors

$$\sqrt{r^2 + X^2 - 2rX\sin\theta} \approx r + \frac{1}{2}\frac{X^2}{r} - X\sin\theta$$

Eq.1. 7

Le terme de gauche, exprimant la distance entre un point de la barrette et le point *M*, est obtenu par le théorème d'Al Kashi. On obtient alors

$$P(x,z) = K \cdot TF\left\{ E(X) e^{j\frac{X^2}{\lambda r}} \right\}\left[\frac{\sin\theta}{\lambda}\right]$$

Eq.1. 8

Le champ sur l'arc de cercle focal est alors $\mathrm{sinc}\left(\frac{\pi D\sin\theta}{\lambda}\right)$, et la résolution est donnée par $\Delta\sin\theta = \lambda/D$.

Souvent, l'approximation supplémentaire $\sin\theta \approx \theta$ est effectuée

III.D La propagation comme un filtre passe-bas

Comme l'indique la formule Eq.1. 8, seule les détails dont la fréquence spatiale (dans la coordonnée sinθ) est inférieure a $D/2\lambda$ sont transmis, et reçus (car la même formule est valable en réception) L'image observe a donc un contenu fréquentiel limite. La propagation agit comme un filtre passe-bas. Cela n'est pas valable seulement dans le plan focal, mais a toutes distances.

Une formule similaire être donnée en coordonnées cartésiennes La fréquence maximale est $D/2z\lambda$. Une démonstration rigoureuse fait intervenir la technique du spectre angulaire (voir (Goodman) pp.55-61). En effet Eq.1. 6 ne convient pas à cause du terme de phase dépendant de x a l'extérieur de l'intégral.

IV. PLAN DE LA THESE

Le principal but de cette thèse est d'adapter une méthode basée sur le retournement temporel, la méthode DORT, a l'imagerie médicale La plupart des résultats concernent aussi d'autres domaines de l'imagerie acoustique, et le manuscrit est écrit de façon assez générale

Un premier obstacle a l'utilisation de la méthode DORT conventionnelle en échographie médicale est le mode d'acquisition utilise. La méthode DORT est basée sur le *full data set*, c'est à dire que les transmissions sont effectuées avec chaque éléments individuellement et a tour de rôle. Ceci n'est pas praticable dans le domaine médical, pour diverse raison évoquée dans le chapitre 2. Une adaptation de la méthode au mode d'acquisition focalise utilise par les échographes est l'objet du chapitre 2. Dans ce même chapitre, le modèle des transducteurs virtuels qui permet de traiter de façon simple et élégante la méthode DORT à partir de transmissions focalisées est présente. La nouvelle méthode est baptisee FDORT (F pour focalise) Nous verrons aussi que cette méthode permet de résoudre le problème de l'écran en champ lointain comme s'il s'agissait d'un écran en champ proche.

La méthode DORT fonctionne bien sur des diffuseurs ponctuels lorsqu'ils sont dans l'eau, mais moins bien lorsqu'ils sont entoures de speckle. Nous proposons une solution également dans le chapitre 2. Enfin, ce chapitre traite aussi du problème du déplacement des cibles. En effet, dans le corps humain, les diffuseurs sont en perpétuel mouvement, et propose une implémentation rapide de la méthode

Le plus gros inconvenient de DORT, est que la méthode a été developee pour des diffuseurs ponctuels. Ce type de diffuseurs est virtuellement inexistant dans un milieu complexe comme le corps humains. La grande majorité des diffuseurs présents dans les tissus biologique est le speckle, et il est donc fondamental de trouver une méthode fonctionnant avec ce type de signal. Ceci est l'objet du chapitre 4. Ce chapitre présente une théorie statistique de la méthode pour les signaux aléatoires, et fait le lien avec un théorème important, le théorème de Van Cittert Zernike. Des exemples de correction d'aberration seront presentes.

Un autre type de diffuseurs trouves dans les tissus sont les diffuseurs *étendus*, c'est à dire dont la taille dépasse la cellule de résolution du système Il s'agit par exemple des parois de vaisseaux. Ce type de diffuseurs est l'objet du chapitre 3. Ce chapitre est place avant celui sur le speckle, car certains résultats de ce chapitre seront utiles pour l'analyse dans le speckle.

Finalement, échographie médicale utilise des signaux larges bandes, alors que la méthode DORT est principalement une méthode monochromatique. Des méthodes permettant d'obtenir les fonctions de Green temporelles sont développes dans le chapitre

5. En particulier, nous présentons la décomposition de Opérateur Retournement Temporel dans le domaine temporel, ce qui fait intervenir un tenseur d’ordre 4.

Dorme, C. and M. Fink (1995). "Focusing in transmit--receive mode through inhomogeneous media: The time reversal matched filter approach." The Journal of the Acoustical Society of America **98**(2): 1155-1162.

Dorme, C. and M. A. Fink (1996). "Ultrasonic beam steering through inhomogeneous layers with a time reversal mirror." Ultrasonics, Ferroelectrics and Frequency Control, IEEE Transactions on **43**(1): 167-175.

Fernandez, A. T., K. L. Gammelmark, et al. (2003). "Synthetic elevation beamforming and image acquisition capabilities using an 8 /spl times/ 128 1.75D array." Ultrasonics, Ferroelectrics and Frequency Control, IEEE Transactions on **50**(1): 40-57.

Fink, M. (1992). "Time reversal of ultrasonic fields. I. Basic principles." Ultrasonics, Ferroelectrics and Frequency Control, IEEE Transactions on **39**(5): 555-566.

Flax, S. W. and M. O'Donnell (1988). "Phase-aberration correction using signals from point reflectors and diffuse scatterers: basic principles." Ultrasonics, Ferroelectrics and Frequency Control, IEEE Transactions on **35**(6): 758-767.

Friemel, B. H., L. N. Bohs, et al. (1995). "Relative performance of two-dimensional speckle-tracking techniques: normalized correlation, non-normalized correlation and sum-absolute-difference." **2**: 1481-1484 vol.2.

Gauss, R. C., G. Trahey, et al. (2001). "Wavefront estimation in the human breast." Proc. SPIE **4325**: 172-181.

Goodman, J. W. Introduction to Fourier Optics, Mc Graw-Hill.

Gruber, F. K., E. A. Marengo, et al. (2004). "Time-reversal imaging with multiple signal classification considering multiple scattering between the targets." The Journal of the Acoustical Society of America **115**(6): 3042-3047.

Hinkelman, L. M., T. D. Mast, et al. (1998). "The effect of abdominal wall morphology on ultrasonic pulse distortion. Part I. Measurements." The Journal of the Acoustical Society of America **104**(6): 3635-3649.

Levin, N., E. T. Gregg, et al. (1989). "Phase aberration correction in medical ultrasound using speckle brightness as a quality factor." The Journal of the Acoustical Society of America **85**(5): 1819-1833.

Liu, D.-L. and R. C. Waag (1994). "Correction of ultrasonic wavefront distortion using backpropagation and a reference waveform method for time-shift compensation." The Journal of the Acoustical Society of America **96**(2): 649-660.

Mast, T. D., L. M. Hinkelman, et al. (1998). "The effect of abdominal wall morphology on ultrasonic pulse distortion. Part II. Simulations." The Journal of the Acoustical Society of America **104**(6): 3651-3664.

O'Donnell, M. and S. W. Flax (1988). "Phase-aberration correction using signals from point reflectors and diffuse scatterers: measurements." Ultrasonics, Ferroelectrics and Frequency Control, IEEE Transactions on **35**(6): 768-774.

Prada, C. and M. Fink (1994). "Eigenmodes of the time reversal operator: a solution to selective focusing in multiple-target media." Wave motion **20**: 151-163.

Prada, C., S. Manneville, et al. (1996). "Decomposition of the time reversal operator: Detection and selective focusing on two scatterers." The Journal of the Acoustical Society of America **99**(4): 2067-2076.

Prada, C. and J. L. Thomas (2003). "Experimental subwavelength localization of scatterers by decomposition of the time reversal operator interpreted as a covariance matrix." The Journal of the Acoustical Society of America **114**(1): 235-243.

Prada, C., F. Wu, et al. (1991). "The iterative time reversal mirror: A solution to self-focusing in the pulse echo mode." The Journal of the Acoustical Society of America **90**(2): 1119-1129.

Rigby, K. W., C. L. Chalek, et al. (2000). "Improved in vivo abdominal image quality using real-time estimation and correction of wavefront arrival time errors." **2**: 1645-1653 vol.2.

Silverstein, S. D. and D. P. Ceperley (2003). "Autofocusing in medical ultrasound: the scaled covariance matrix algorithm." Ultrasonics, Ferroelectrics and Frequency Control, IEEE Transactions on **50**(7): 795-804.

Varslot, T., H. Krogstadt, et al. (2004). "Eigenfunction analysis of stochastic backscatter for characterization of acoustic aberration in medical ultrasound imaging." The Journal of the Acoustical Society of America **115**(6): 3068-3076.

Viola, F. and W. F. Walker (2003). "A comparison of the performance of time-delay estimators in medical ultrasound." Ultrasonics, Ferroelectrics and Frequency Control, IEEE Transactions on **50**(4): 392-401.

Waag, R. C. and J. P. Astheimer (2005). "Statistical estimation of ultrasonic propagation path parameters for aberration correction." Ultrasonics, Ferroelectrics and Frequency Control, IEEE Transactions on **52**(5): 851-869.

Waag, R. C. and J. P. Astheimer (2006). "Statistical estimation of ultrasonic propagation path parameters for aberration correction." The Journal of the Acoustical Society of America **119**(5): 3376.

Chapter 2. The Time Reversal Operator with Virtual Transducers: FDORT

II. INTRODUCTION AND PRESENTATION OF THE METHOD

The DORT method is very efficient to extract the Green's function of points scatterers in simple cases, like wires in water for example. A weakness of the original method is that it is based on *full data sets.* This means that the signals are transmitted with one element at the time.

In more complex situation, like medical ultrasound, full data sets are rarely used. Rather, sets of focused transmits are used. A focused transmits is generated by firing a group of elements, with delays $r_i(P)/c$, where $r_i(P)$ is the distance between the element i and the focal point P. There are two main advantages to using the focused transmits over the full data sets in imaging. (Gammelmark and Jensen; Lokke Gammelmark and Arendt Jensen; Jensen, Holm et al.)

- The signal-to-noise ratio (SNR) is improved because more energy is transmitted for each transmits. Usually, it is improved by a factor $\sqrt{N}$ for random noise (for example electronic noise due to the transducers) or a factor N for deterministic noise (for example an active scatterer, like a distant ship in underwater acoustics, or waves generated by the body), where N is the number of elements fired for each focused transmits.

- It is more robust to motion. Indeed, to make the image of a point P, only the transmit focusing at, or near P is needed with a focused sets. With a full data sets, the focusing in transmission as to be reconstructed from the different transmits. As there is a lap of time between the first and last transmits used, the scatterers may have moved.

We presents here a generalization of the DORT method using a focused transmit scheme, this method is termed FDORT.

The FDORT method is illustrated in Figure 11. A beam is transmitted, and the received signals are recorded for each element. The Fourier transform of the signals is then taken. The Fourier coefficient at frequency ω for the signal received by element *j* when the beam *i* is transmitted gives the element $K_{ij}(\omega)$ of the transfer matrix $K(\omega)$.

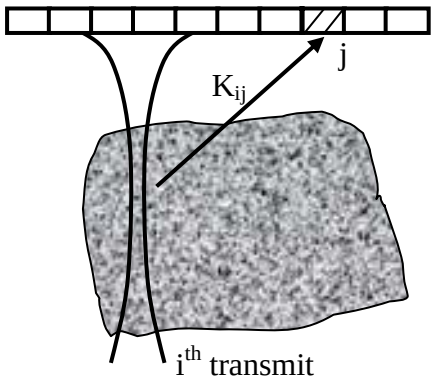

Figure 11 Acquisition of the transfer matrix with the FDORT method. It differs from the conventional DORT method by the use of focused transmit. The element K_{ij} of the matrix is the signal received by element *j* after the i^{th} focused beam has been transmitted.

Different transmit sequences using groups of elements (like Hadamard codes) have previously been proposed with the DORT method to improve the SNR. More recently, acquisitions using orthogonal codes have been proposed to improve the SNR and the motion robustness in a wave-guide (Folegot, de Rosny et al.). These schemes were interpreted as alternative bases where the Time Reversal Operator could be expressed.

Although the focused beams can also be interpreted, under certain conditions, as a new orthogonal basis, as it will be shown in III.C, we also propose a more intuitive and more general approach based on the concept of virtual transducers, and show that the

FDORT method can be seen as a simple DORT method between a virtual array, whose elements are the transmits foci, and the physical array. This is a new interpretation compared to a previous paper about the method (Robert, Burcher et al.).

First (Section II), we develop the formalism of the DORT method, in the case of 2 distinct arrays. The main results are summarized.

Then, we develop the concept of virtual transducers and virtual arrays. The main beam sequences are reviewed.

In the three last sections are presented applications of the FDORT method that take advantage of the focused beams benefits. This includes focusing through a far-field phase screen, extracting the Green's function of scatterers embedded in speckle and a fast implementation of DORT in the case where the region of interest is limited.

III. THE DORT METHOD BETWEEN TWO DIFFERENT ARRAYS

II.A. The transfer matrix and the time reversal operator

The theory of the D.O.R.T. method has been thoroughly covered in the literature (Prada and Fink 1994; Prada, Manneville et al. 1996). It is introduced here to set the formalism. The method is based on a matrix description that describes a transmit-receive process performed by an array of transducers(Prada and Fink 1994; Prada, Manneville et al. 1996), or between 2 different arrays (an array of M transmitters and an array of L receivers)(Prada, Tanter et al. 1997). Most of D.O.R.T. experiments are conducted using the same array in transmission and reception, but in order to introduce the modified method in Section III, between the array of virtual transducers and the array of real transducers, we will consider in the following the general case of 2 different arrays, shown in Figure 12.

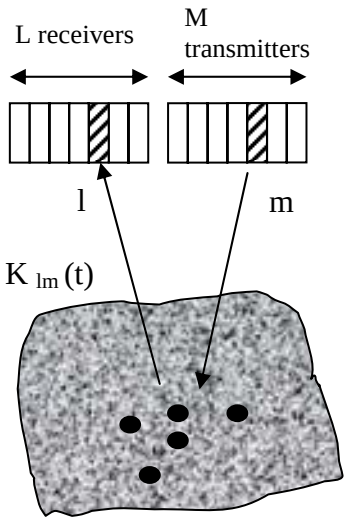

Figure 12 The DORT method between two arrays

If the system (propagating medium and electro acoustic response) is linear and time-invariant, the process of transmitting and receiving can be described by a collection of filters: each transmitting element m and each receiving element l are linked by an interelement impulse response $k_{lm}(t)$, so that:

$$r_l(t) = e_m(t) \otimes k_{lm}(t)$$

where $r_l(t)$ is the signal received on the l^{th} transducer when $e_m(t)$ is transmitted on the m^{th} transducer, as seen in Figure 12. Thus when the input of the element number m is a delta impulse, the output of the element number l is $r_l(t) = k_{lm}(t)$. The Fourier transform yields: $R_l(\omega) = K_{lm}(\omega)$. The repetition of the process for each pair (l,m) of transmitting and receiving element leads, at a given frequency, to the transfer matrix $\mathbf{K}(\omega)$:

$$\mathbf{K}(\omega) = \begin{bmatrix} K_{11} & K_{12} & \cdots & K_{1M} \\ K_{21} & K_{22} & & \\ \vdots & & \ddots & \\ K_{L1} & & & K_{LM} \end{bmatrix}$$

The matrix K describes the transmit-receive process between the arrays and is therefore depending on the scattering medium. If a signal $\mathbf{E(\omega)} = [E_1(\omega), E_1(\omega), \ldots, E_M(\omega)]^T$, where $E_m(\omega)$ is the input of the element m, at the frequency ω, and ^{T} is the transpose (that transform a 1*M line vectors into a M*1 column vector) is transmitted into the medium, the received echo is given by the following matrix formulation:

$$\mathbf{R(\omega)=K(\omega)E(\omega)}$$

where $\mathbf{R(\omega)}=[R_1(\omega), R_2(\omega), \ldots, R_L(\omega)]^T$, $R_l(\omega)$ being the signal received by the l^{th} element of the receive array. $\mathbf{E(\omega)}$ and $\mathbf{R(\omega)}$ are vectors expressed respectively in the transmit and receive basis, formed by the elements of the arrays.

The time reversal operator is then defined(Prada, Tanter et al. 1997) as $\mathbf{T_{Tx}} = \mathbf{K^H K}$ in the transmit (Tx) basis or by $\mathbf{T_{Rx}} = \mathbf{K K^H}$ in the receive (Rx) basis, where ^{H} stand for the hermitian, or conjugate, transpose (transpose followed by complex conjugation). For all the results recalled here, there is no need for **K** to be either symmetric or square (which is obviously not the case if L is not equal to M) as it was in the earliest papers(Prada and Fink 1994; Prada, Manneville et al. 1996). Then in general $\mathbf{K^H K}$ and $\mathbf{K K^H}$ are different, but both have the same rank, equal to the rank of **K**.

As $(\mathbf{K^H K})^\mathbf{H} = \mathbf{K^H K}$ (the same hold in the receive basis) the time reversal operator is hermitian positive in an orthogonal basis and thus can be diagonalized. Moreover, the eigenvalues are real and positive, and the eigenvectors are orthogonal.

Practically, the diagonalisation of the time reversal operator is not used. Indeed, the diagonalization is mathematically equivalent to the singular value decomposition (svd) of **K:**

$$\mathbf{K=USV^H}$$

where **S** is a L×M diagonal matrix completed by lines of zeros, containing the singular values of **K**; **U** is a L×L unitary matrix whose columns are the eigenvectors of $\mathbf{K K^H}$ (here the time reversal operator expressed in the receive basis); **V** is the M×M matrix whose columns are the eigenvectors of $\mathbf{K^H K}$.

II.B. Case of isotropic, pointlike scatterers and single scattering

II.B.1. Expression of the transfer matrix

In the case of isotropic point scatterers and under the Born approximation, the eigenvectors and eigenvalues of the time reversal operator can be theoretically calculated. For clarity, the number of point scatterers is assumed to be two. Let **P** and **Q** be the scatterers' positions. We denote by $\mathbf{H_{Rx}}(P)$ and $\mathbf{H_{Tx}}(P)$ the monochromatic Green's functions of **P** expressed in the Rx and Tx bases respectively. For example, $\mathbf{H_{Tx}}(\mathbf{P})$ is a 1*M vector and $\mathbf{H_{Tx}}(\mathbf{P})_i$ describes the propagation between the i^{th} element and **P**. Let $D(\mathbf{P})$ and $D(\mathbf{Q})$ be the reflectivity of each scatterer. We also assume the absence of noise and we omit the acousto-electrical responses of the transducers, as they have no influence on the results.

A transmit-receive process can be divided into 3 stages, as seen in FIGURE CYCLE: propagation from the Tx array to the scatterers, reflection on the scatterers, and finally propagation to the Rx array. The transmit-receive process between Tx element m and Rx element n is then:

$\mathbf{K}_{nm} = \mathbf{H_{Tx}}(\mathbf{P})_m * D(\mathbf{P}) * \overline{\mathbf{H}}_{\mathbf{Rx}}(\mathbf{P})_n + \mathbf{H_{Tx}}(\mathbf{Q})_m * D(\mathbf{Q}) * \overline{\mathbf{H}}_{\mathbf{Rx}}(\mathbf{Q})_n$ and finally, one can write the transfer matrix as the product of 3 terms(Prada and Fink 1994):

$$\mathbf{K}=(\mathbf{H_{Rx}})^H \mathbf{D}\, \mathbf{H_{Tx}}$$

where $\mathbf{H_{Rx}} = \begin{pmatrix} H_{Rx}(\mathbf{P})_1 & H_{Rx}(\mathbf{P})_2 & \cdots & H_{Rx}(\mathbf{P})_N \\ H_{Rx}(\mathbf{Q})_1 & H_{Rx}(\mathbf{Q})_2 & \cdots & H_{Rx}(\mathbf{Q})_N \end{pmatrix}$

and $\mathbf{D} = \begin{pmatrix} D(\mathbf{P}) & 0 \\ 0 & D(\mathbf{Q}) \end{pmatrix}$

$\mathbf{H_{Tx}}$ has the same structure as $\mathbf{H_{Rx}}$; its rows are the Green functions expressed in the Tx array. It follows that the rank of **K** is equal to the number of scatterers.

II.B.2. Time reversal operator from the scatterers' point of view

In the receive basis, the time reversal operator becomes:

$$\mathbf{K K^H = (H_{Rx})^H D H_{Tx}\ H_{Tx}^H D H_{Rx}}$$

Although experimentally we only have access to the time reversal operator expressed from the point of view of one of the arrays, in order to understand the properties of its eigenvectors, it is more convenient to express it from the point of view of the scatterers, in other words in the scatterers' basis. As depicted in FIGURE, the time reversal process can be seen as a cycle. From the scatterers' point of view, the cycle begins at the scatterers location and is seen as follows: The scatterers emit an echo toward the Tx array, which backpropagates the echo toward the scatterers. The signal is reflected by the scatterers, received by the Rx array and backpropagated one more time toward the scatterers.

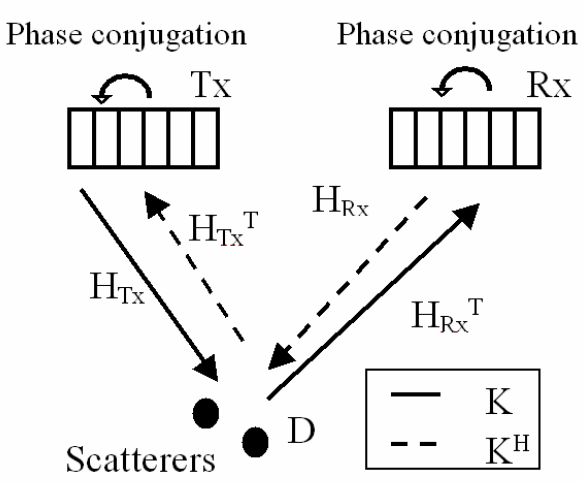

Figure 13 The time reversal process can be seen as a full cycle between 3 *actors:* the Tx array, the Rx array and the scatterers. Propagation between the *actors* is described by H_{Tx} and H_{Rx}. Reflection from the scatterers is equivalent to a multiplication by D, and the backpropagation by the arrays is equivalent to a phase conjugation, included in the hermitian transpose ^{H}. K describes the one-way propagation between Tx and Rx, represented by the solid line. The time reversal operator can be expressed mathematically from the point of view of any of these 3 *actors*. Then one has to start from the desired *actor* and make a full cycle.

Let $\mathbf{T_{scat}}$ be the time reversal operator in the scatterer basis; as there are two scatterers, $\mathbf{T_{scat}}$ is a 2*2 matrix and $\mathbf{T_{scat,ij}}$ is the signal received by scatterer i after a full time reversal process when the initial echo was sent by scatterer j. $\mathbf{T_{scat}}$ is expressed as

$$\mathbf{T_{scat} = D\, H_{Tx}\, H_{Tx}^H\, D\, H_{Rx}\, H_{Rx}^H}$$

Eq.2. 1

Furthermore,

$$\mathbf{H_{Rx}}\,\mathbf{H_{Rx}}^{\mathbf{H}} = \begin{pmatrix} \| \mathbf{H_{Rx}}(\mathbf{P}) \|^2 & < \mathbf{H_{Rx}}(\mathbf{Q}) \mid \mathbf{H_{Rx}}(\mathbf{P}) > \\ < \mathbf{H_{Rx}}(\mathbf{P}) \mid \mathbf{H_{Rx}}(\mathbf{Q}) > & \| \mathbf{H_{Rx}}(\mathbf{Q}) \|^2 \end{pmatrix}$$

Eq.2. 2

And a similar expression holds for $\mathbf{H_{Tx}}\,\mathbf{H_{Tx}}^{H}$. Because **D** is already diagonal, a condition for the expression of $\mathbf{T_{scat}}$ to be diagonal is:

$$<\mathbf{H_{Rx}}(\mathbf{P})|\mathbf{H_{Rx}}(\mathbf{Q})> = 0$$

Eq.2. 3

which means that $\mathbf{H_{Rx}}\,\mathbf{H_{Rx}}^{\mathbf{H}}$ is diagonal, and

$$<\mathbf{H_{Tx}}(\mathbf{P})|\mathbf{H_{Tx}}(\mathbf{Q})> = 0$$

Eq.2. 4

which means that $\mathbf{H_{Tx}}\,\mathbf{H_{Tx}}^{H}$ is diagonal. In other words, the Green functions of the scatterers are orthogonal in both the transmit (Eq.2. 4) and the receive (Eq.2. 3) bases.

II.B.3. Physical interpretation

There is a physical interpretation of the scalar products from Eq.2. 3 and Eq.2. 4. Using time-reversal arguments, transmitting $\overline{\mathbf{H}}_{\mathbf{Rx}}(\mathbf{Q})$ with the receive array results in focusing on the point **Q**. The field received at the point **P** when transmitting such a signal is expressed as

$$\sum_{i=1}^{L} \overline{\mathbf{H}}_{\mathbf{Rx}}(\mathbf{Q})_i * \mathbf{H_{Rx}}(\mathbf{P})_i = <\mathbf{H_{Rx}}(\mathbf{P})|\mathbf{H_{Rx}}(\mathbf{Q})>$$

Eq.2. 5

This is deduced from the interpretation of the rayleigh-sommerfeld formula as a projection on a Green function (Chapter 1.III.A). Thus the scalar product is equal to zero if it is possible to focus on one scatterer without sending energy to the other one. The scatterers are then said to be well resolved or well separated.

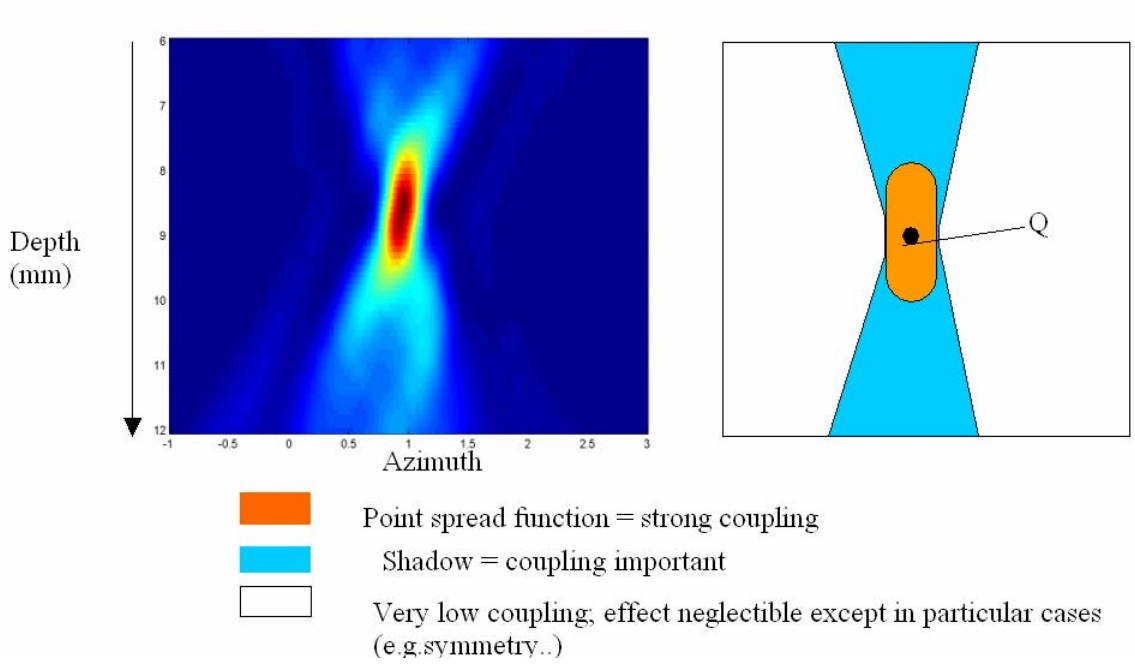

Figure 14 The scalar product between the Green's functions of two points *P* and *Q* is proportional to the field at *P* when one focus on *Q*. The scalar product, and therefore the coupling between the scatterers, is high if the points are not resolved (orange zone). Points in the light blue zone may also be coupled with the scatterer Q.

II.B.4. Eigenvectors

The conditions of Eq.2. 3 and Eq.2. 4 are satisfied if the scatterers are well resolved from the point of view of both arrays. In this case, Eq.2. 1 shows that the time reversal operator is diagonal in the scatterers' basis. The two eigenvectors of the time reversal operator expressed in the Rx basis associated with non-zero eigenvalues are then the scatterers' Green's functions, $\mathbf{H_{Rx}(P)}$ and $\mathbf{H_{Rx}(Q)}$ expressed in the Rx array. Identically,

eigenvectors of the time reversal operator expressed in the Tx basis are the Green function in the Tx array. The svd of K gives the eigenvectors in both the Rx and Tx array. Moreover, the eigenvalue corresponding to the scatterer **P** is

$$\lambda = ||\mathbf{H_{Tx}(P)}||^2 \, ||\mathbf{H_{Rx}(P)}||^2 \, D(\mathbf{P})^2$$

If the targets are not well resolved, there is a coupling between them through the non-zero diagonal terms of Eq.2. 3 and the eigenvectors are expressed as a linear combination of the Green functions(Prada, Manneville et al. 1996). The transmission of such an eigenvector does not lead to point focusing but DORT still provides useful information in this case.

IV. FOCUSED BEAMS AND VIRTUAL TRANSDUCERS

III.A. Virtual transducer model

The decomposition of the Time Reversal Operator between two physical arrays has been presented in the previous Section. Now, it is shown that the focused transmits used in the FDORT method can be considered as virtual transducers.

When a transmit is focused on a point *P*, at depth *Z*, the evolution of the wave-front can be separated in two different steps, as seen in Figure 15. First, one observes a wave that converges to the focal point *P*. As the wave gets closer from *P*, the lateral size of the wave-front reduces. When the wave-front is at *P*, most of the energy is concentrated in an area of lateral width $\lambda Z / D$ where *D* is the aperture size, and λ is the wave-length. The wave-front is at *P* at time $t_0 = Z/c$, where *c* is the speed of sound.

The wave-front does not stop at *P*, and one observes then a wave that diverges from the point *P*, propagating outward.

III.A.1.Virtual transducer for $t>t_0$

For an observer located at a depth greater than *Z*, it looks like the wave is originating from a *virtual transducer* located at *P*. The equivalent virtual transducer is not isotropic, but has a directivity pattern with an angle θ, as shown in Figure 16, so that it generates the same cone of sound as the focused transmit.

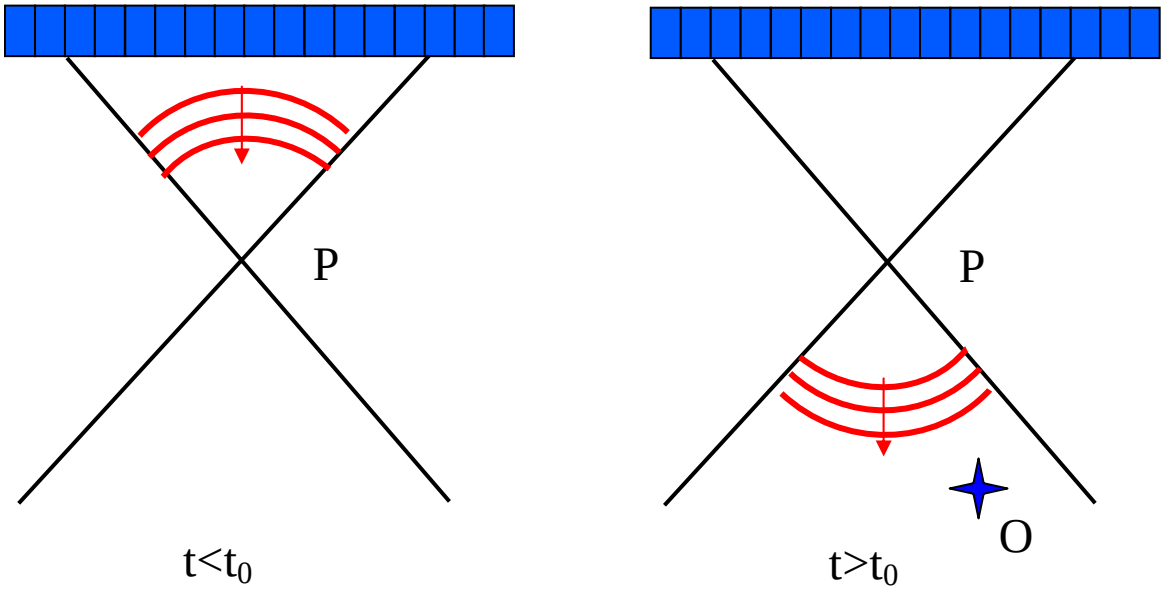

Figure 15 Wave-front resulting from a focused transmit, before (left) and after (right) it reaches the focal point *P*. For $t<t_0$, the wave is propagating inward, converging toward *P*. For $t>t_0$, the wave is propagating outward, diverging from *P*. An observer *O* located in the sound cone, hear the wave-front as if it were coming from a virtual transducer located at *P*.

The angle θ of the cone is defined by the geometrical relationship

$$\tan\left(\theta/2\right)=\frac{D/2}{Z}$$

Eq.2. 6

as seen in Figure 16. Most of the time, the angles are small, and

$$\theta = D/Z$$

Eq.2. 7

is a good approximation. The directivity of a transducer is defined as the width of the main lobe. The Fresnel relationship in polar coordinates teaches that the field is given by the Fourier transform of the transducer, scaled by a factor λ. Therefore, a virtual element of width $\lambda Z/D$ would be a good approximation. In fact, a more accurate equivalent virtual transducer would be a sinc function whose main lobe width is $\lambda Z/D$

$$\sin c\left(\frac{\pi X}{\lambda Z/D}\right)$$

Eq.2. 8

so that, at the limit, in the focal plane (plane of the virtual transducer) the field of the virtual transducer and the field of the focused transmit are equal (in the focal plane, the field of a focused beam can be well approximated by a sinc).

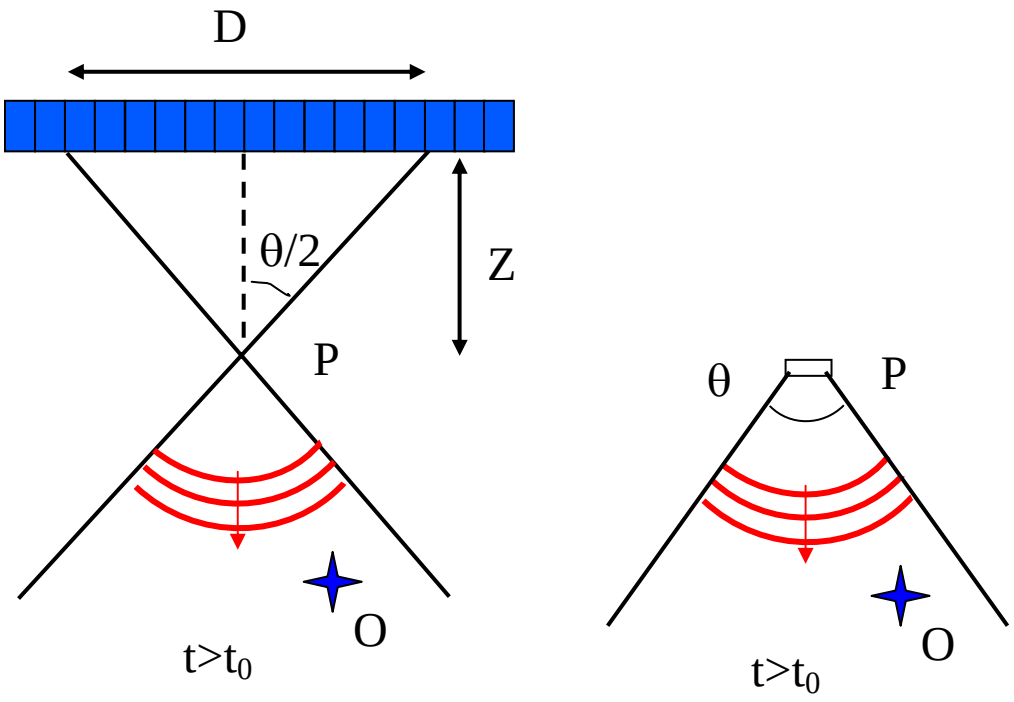

Figure 16 Wave-front for the focused transmit (left) and for an equivalent virtual transducer (right) located at *P*, with a directivity angle θ, transmitting a pulse at t_0. For the observer *O*, both fields are very similar.

The shape of the virtual transducer does not really matter. What is important for the following is that for an observer *O*, deeper than Z, the wave-front of a focused transmit generated at *t=0* is (almost) the same as the wave-front from a virtual transducer located at *P*, with a directivity angle $\theta = D/Z$, and generated at $t=t_0$.

By spatial reciprocity, the same concept applies in reception, if a static focused receive on *P* is used. Let us imagine that the observer generates a pulse at *t=0*, then the signal recorded by the array focused in reception on *P*, would be the same as the signal recorded by the virtual transducer t_o seconds earlier.

In this work, the focused beams will be used mainly in transmission. But all the results could be generalized to the reception as well.

III.A.2 Virtual transducer for $t<t_0$

For $t<t_0$, the wave-front is converging toward the focal point. It is like observing the wave-front emitted by a transducer at the focal spot, but in a movie played backward. For an observer located shallower than *Z*, the wave-front appears as the time-reversed of a wave-front emitted at $t=-t_0$ by a virtual transducer facing the array, as shown in Figure 17. The virtual transducer has the same directivity $\theta = D/Z$ as the one discussed in the previous part.

In reception, the analogy is the same: by spatial reciprocity, the signal recorded by the array focused on *P* would be the time-reversed of the signal recorded by a virtual transducer located at *P*.

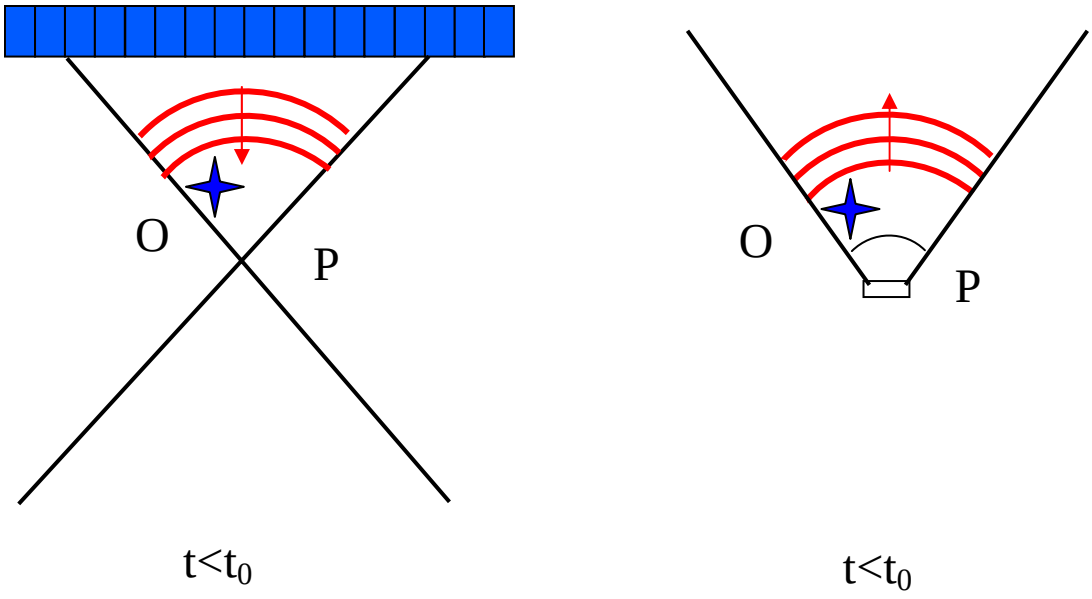

Figure 17 Wave-front for the focused transmit (left) and for an equivalent virtual transducer (right) located at *P*, with a directivity angle θ, transmitting a pulse at $-t_0$. For the observer *O*, the wave-front of the focused beam is the time-reversed of the wave-front for the virtual transducer.

The strong analogy between a focused beam and a transducer can actually be understood by the fact that they can both be seen as a Green's function. When a real element is fired, the signal propagating in the medium is the Green's function of the element. On the other hand, when one focus on a point *P*, one actually transmit the Green's function of the point *P*. The real transducer has only a forward (propagating outward) component because there is effectively a source. The virtual transducer has both backward and forward component because there are no sources or sinks.

A similar concept of virtual sources can be found in the literature, for example (Gammelmark and Jensen 2003).

III.B. The DORT method between a real array and a virtual array

It has been shown that the focused transmits were equivalent to virtual transducers. The FDORT method uses focused transmits and per-element receives, therefore it is equivalent to a DORT method between a *virtual array* whose elements are the foci for each transmits, and the real physical array. It is then possible to use the results of Section.2.I, for DORT between two different arrays.

III.B.1. The focused transfer matrix and its singular vectors

The notation K now refers to the transfer-matrix for the FDORT method. In this case, K_{ij} is the signal received by element j when the i^{th} focused beam is transmitted. Using the virtual transducer model, it can be seen as the inter-element response between the virtual transducer i and the real transducer j. Therefore, the matrix K describes a time-reversal operator between the virtual array and the real array. The results of the Section III.A can then be used.

The singular value decomposition (SVD) of the K matrix gives $\boldsymbol{K=USV^H}$, where U would contain the invariants of the Time Reversal Operator in the physical array (also termed *canonical array)* and V would contain the invariants expressed in the virtual array. In the case of resolved, point scatterers, U contains the Green's function of each scatterers in the physical array, while V contains the Green's function of the same scatterers in the virtual array. For scatterers located shallower than the focal depth ($t<t_0$), V contains actually the conjugate of the Green's function, because the wave-fronts for the focused transmits are the time-reversed of the virtual transducers wave-fronts.

The conditions for the scatterers Green's function to be separated is that they are resolved from both the real and virtual arrays point of view. The resolution of the virtual array actually depends on the focused beams sequence. This is discussed in Section.III.B.2.

III.B.2. Example of virtual arrays and properties

There are several possibilities of choosing a scheme of focused beams. Here are the most popular ones. The consequences of each scheme on the FDORT properties are discussed.

III.B.2.a Linear scan

In a linear scan, only a sub-aperture of the total array is usually used for a transmit. The consecutive transmits are obtained by translation of the sub-aperture. As a result the virtual array is linear, as shown in Figure 18. This scan sequences is typically used when the region to image is a rectangle whose lateral extent is equal or less than the

array width. The directivity of the elements depends on the size of the sub-aperture and on the focal depth as stated in Eq.2. 6 and Eq.2. 7.

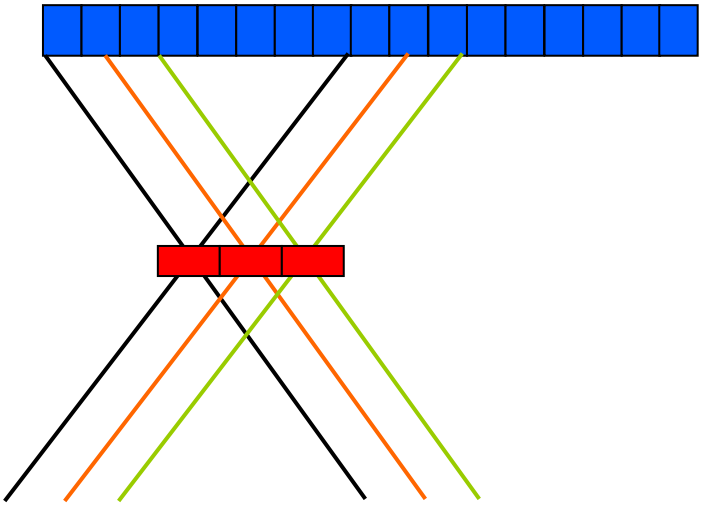

Figure 18 Example of a linear scan sequence (only the first few beams are shown), with corresponding virtual array in red.

Resolution: An important parameter is the resolution of the virtual array, as it is a condition to separate the Green's function of scatterers. The resolution is proportional to the ratio z/d, where z is the distance to the virtual array, and d is the width of the virtual array. As can be seen from Figure 19, the resolution is in this case the same for every depth, and is limited by the directivity of the virtual transducers. Indeed, if z increases, the number of virtual transducers that the point can hear increases also, because of the directivity. In a good approximation, the resolution for any point is given by the formula $\lambda Z / D$, where Z is the focal depth (and not the depth of the scatterers) and D is the size of the transmit aperture. The resolution at any depth is then given by the resolution chosen for the focal depth. In general, the resolution is less good than the resolution obtained with the conventional DORT method where the full aperture is used at every depth.

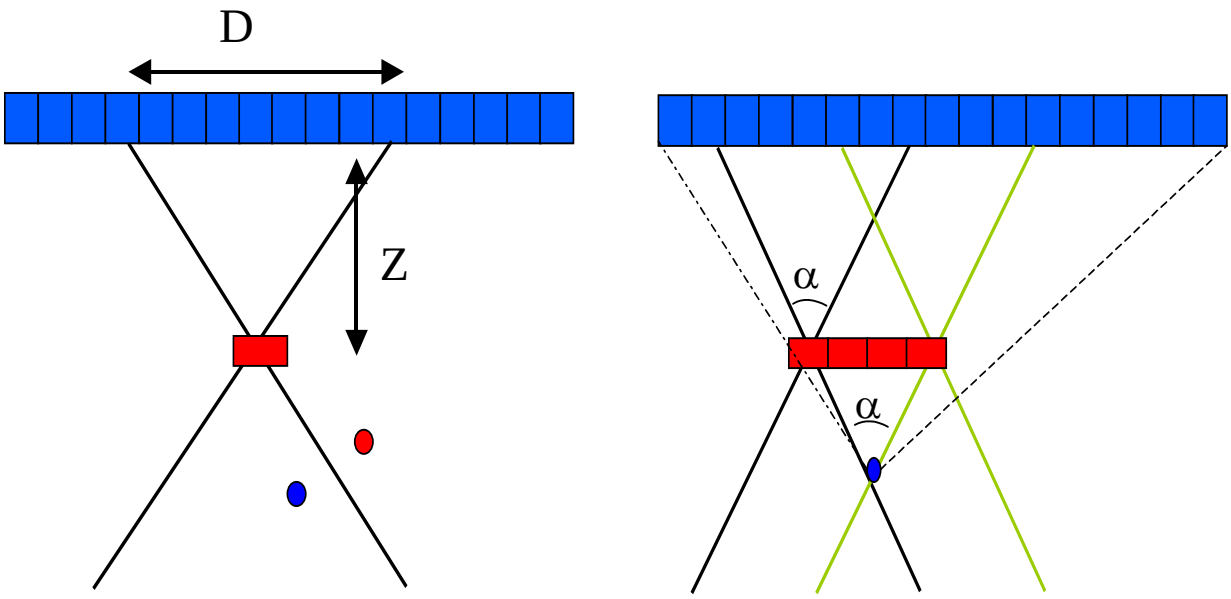

Figure 19 Left: each transducer has a directivity function corresponding to the sound cone of the beam. Therefore, only the scatterer inside the cone, like the blue scatterer, will hear and be heard by the virtual transducer. The red scatterer does not hear the virtual transducer. Right: because of this directivity effect, a scatterer (in blue) hears only a limited number of virtual transducer. The virtual array that insonifies a given point has then a limited size, which limits the resolution of the FDORT method with linear scan. It can be seen geometrically, that the angle α between the scatterer and the virtual array is the same as the angle of the beams. Therefore, the resolution for any point in the medium, independently of its depth is the same and is equal to the resolution of the focus, $a = \lambda Z / D$. **The angle that would be obtained with the full aperture is shown in dash line.**

Transducers spacing: A key parameter is the separation between two consecutives virtual transducers. A way of determining this is to use similar design rules as for an array of real transducers (Angelsen 2000) (6.21). Another approach, involving the orthogonality between the Green's functions, is discussed in the next Section.

When the element spacing in an array is too large, grating lobes appear. Indeed, the Fresnel approximation in polar coordinates states that the field at the focal radius is

given by the Fourier transform of the aperture, with scaling by λ. For a continuous aperture, this gives the well-known sinc shape of the beam pattern. However, an array is not continuous but made of a few discrete elements. In a 1st approximation, each element can be considered as a point. In this case, it is like the continuous array has been sampled, or multiplied by a dirac comb. Let *a* be the distance between two elements. In the Fourier domain, this results in a periodic repetition of the sinc at a period $\Delta \sin\theta = \lambda / a$. The repetitions of the sinc form so-called grating lobes. The first grating lobes are then at an angle $\Delta \sin\theta = \lambda / a$ from the main lobe. The further apart are the transducer in an array, the closer from the main lobe are the grating lobes. In fact, each element is not a point, but has a finite extent, which give him a directivity. For example, an element equivalent to a virtual transducer has a shape in $\sin c\left(\frac{\pi X}{\lambda Z / D}\right)$ (Eq.2. 8). Therefore, the array is better modelized by the Dirac comb convolved by the sinc. In the Fourier domain, the field of the point-like array is multiplied by the directivity function (here the Fourier transform of the sinc) The directivity should be narrow enough so that the grating lobes are suppressed. In our case, the directivity is approximately given by $\Delta \sin\theta = D / Z$ (Eq.2. 7). The worst case happens when the main lobe is steered on the edge of the directivity function, and therefore the appropriate spacing between transducers is $a \le \lambda Z / D$. If the spacing between elements is larger than this, the method may not be able to separate two scatterers when a scatterer is in the main lobe while the other one is in a grating lobe.

In ultrasound, the signals are often broad-band, and in this case, the spacing at the center frequency can be chosen. The beam spacing required for FDORT is significantly less than the beam spacing used in imaging modes.

To summarize, with a linear scan, both the resolution and the maximum spacing is equal to $\lambda Z / D$, which is the inverse of the spatial bandwidth.

III.B.2.b Sector scan (or phase scan)

In a sector scan, the full aperture is usually used for a transmit. The consecutive transmits are then obtained by steering (rotating) the beam. Thus, the foci are located on a circle at a constant radius from the array center. This is shown in Figure 20. Therefore, the virtual array is a curved array. The sector scan is especially interesting when the zone to image is a sector.

Resolution: A geometrical derivation similar to the one in Figure 19 shows that with this scheme the resolution of the virtual array is the same as the real array. Indeed, as shown in Figure 20, the angle between the blue scatterer and the virtual array is the same as the angle between the scatterer and the real array. Thus with such a transmit sequences, the performance of FDORT in terms of scatterers separation is identical to DORT, and is equal to $\Delta \sin\theta = \frac{\lambda}{D}$.

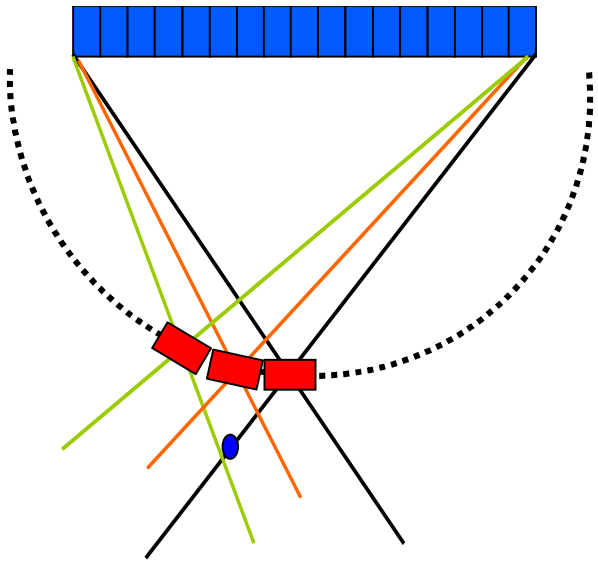

Figure 20 Example of sector scan. The foci are located on a circle, and the beams are steered.

Transducers spacing: The maximum transducers spacing is derived in III.C, using orthogonality condition between the transmits. It is found that the distance between two consecutive virtual transducers is $\Delta \sin\theta = \frac{\lambda}{D}$.

III.B.2.c Hybrid scan

The hybrid scan is shown in Figure 21. It combines the advantages of linear and sector scan. The whole aperture is used for each transmit, which results in a resolution identical to the DORT method, as shown for the blue scatterer in Figure 21. However, the foci are located on a line at constant depth, and thus the virtual array is linear, which makes the method more intuitive.

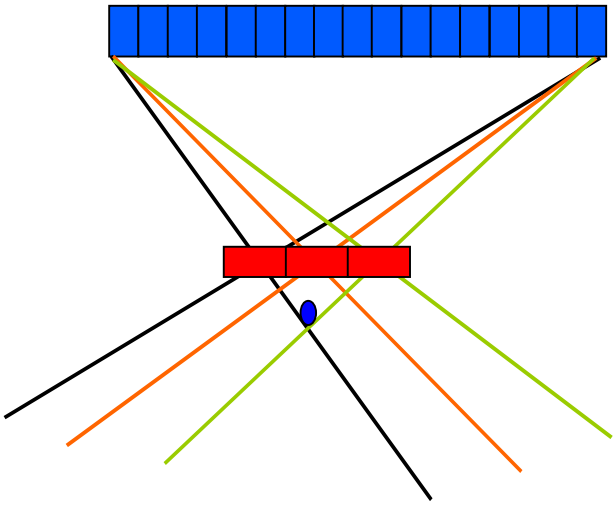

Figure 21 Hybrid scheme. The foci are on a line, but the full aperture is used for each beam. Thus the resolution is the same as DORT. The angle between a scatterer (blue point) and the virtual array is the same as the angle between the scatterer and the real array.

III.B.3. Simulations

Two point scatterers located at depth 30mm have been simulated using Field II (J.A.Jensen). One of the point was twice brighter than the other. An array with 128 elements and 7.3 MHz center frequency was used. Three sets of acquisition were performed, using the hybrid scheme of Section III.B.2.c., with a beam spacing equal to 0.2 mm. The focal depths were respectively 10mm, 30mm (scatterers depth) and 60mm (deeper than scatterers). For each case, the transfer matrix K was built for several frequencies ranging from 0 to 12 Mhz, using a Fast Fourier Transform of the received signal. The SVD of each matrix was performed. According to III.B.1, the singular vector U gives the Green's function in the physical array, whereas the singular vector V gives the Green's functions in the virtual array.

The temporal eigenvectors for each scatterer were then reconstructed by taking the Fourier transform of the monochromatic eigenvectors.

In Figure 22 are shown the eigenvalues in function of the frequency. There are two non-zero eigenvalues, indicating the presence of 2 scatterers in the medium. The two first temporal eigenvectors in the real array are shown in Figure 23. Each eigenvector is the temporal Green's function, or wave-front of one of the scatterer. In Figure 24 shows the amplitude and phase of the 1st eigenvector *U* at the center frequency. These results are very similar to what one would obtain with the classical DORT method.

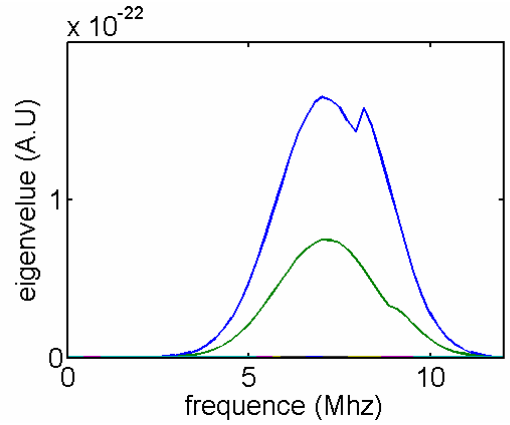

Figure 22 Evolution of the eigenvalues in function of the frequency. There is one non-zero eigenvalue for each point scatterer.

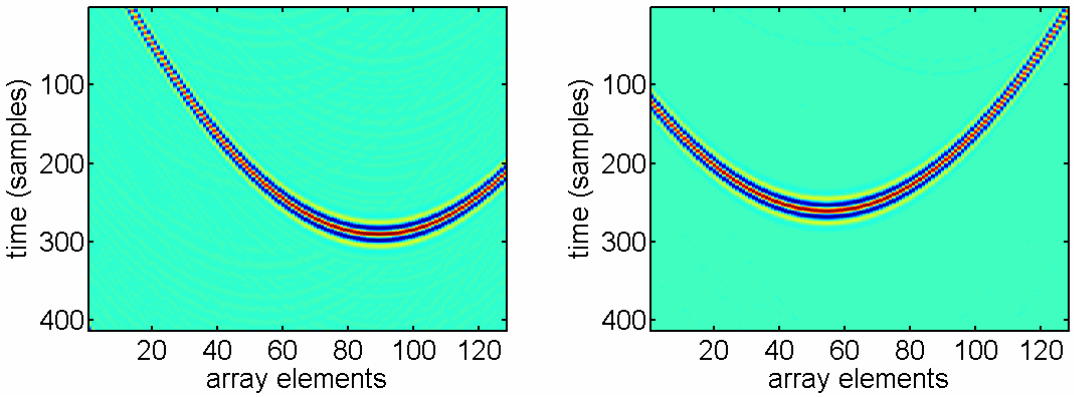

Figure 23 Temporal eigenvectors expressed in the real array. They correspond to each scatterer's wave-front.

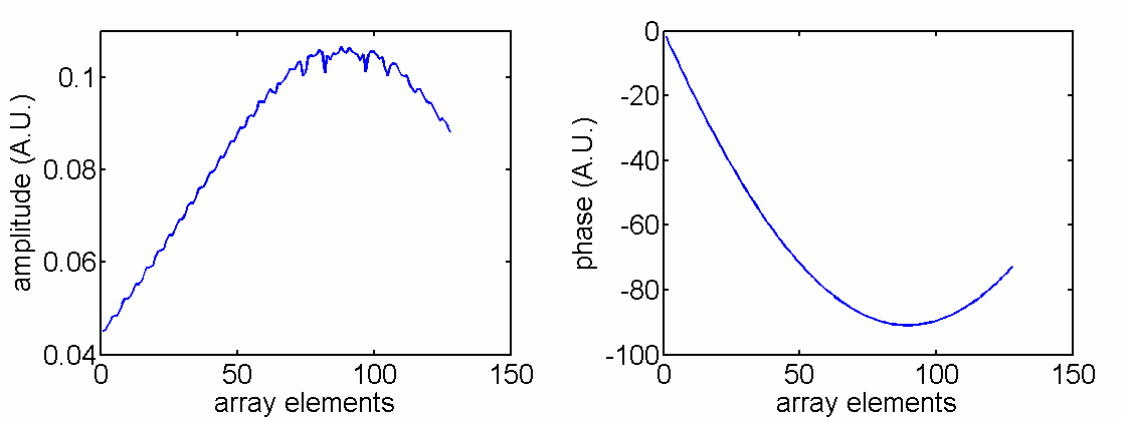

Figure 24 Amplitude and phase of the 1st singular vector *U* at the center frequency. It represents the monochromatic Green's function of the first scatterer.

However, with FDORT, additional information can be obtained from the other singular vector *V*. It gives the Green's function in the virtual array. The position of the virtual array can be adjusted by changing the focal depth. Three cases can be distinguished: the scatterers can be retrospectively deeper than, as the same depth as, or shallower than the virtual array. It is important to understand that in all cases the ability to separate the scatterers is the same, and that the singular vector *U* are similar. Changing the focal depth is simply a way of changing the point of view. Examples of applications will be developed in Sections IV. And V.

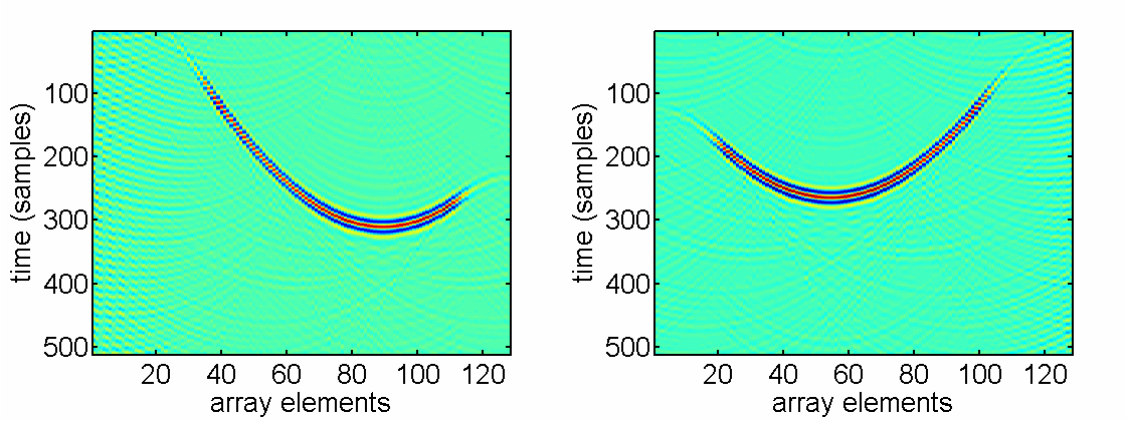

Figure 25 Temporal singular vectors expressed in the virtual array at depth 10mm. It is obtained by the Fourier transform of the frequency domain vector *V*. The wave-fronts are truncated on the edges because of the directivity of the virtual transducers. The scatterers do not hear the virtual transducers on the edges.

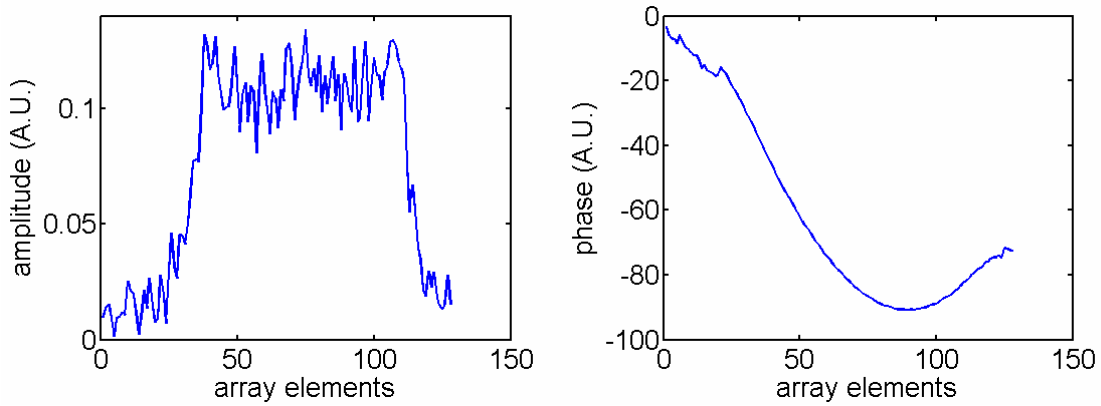

Figure 26 Phase and amplitude of the 1st singular vectors *V* . It represents the monochromatic Green's function of the brightest scatterer expressed in the virtual array. The directivity pattern of the transducers is clearly visible in the amplitude term.

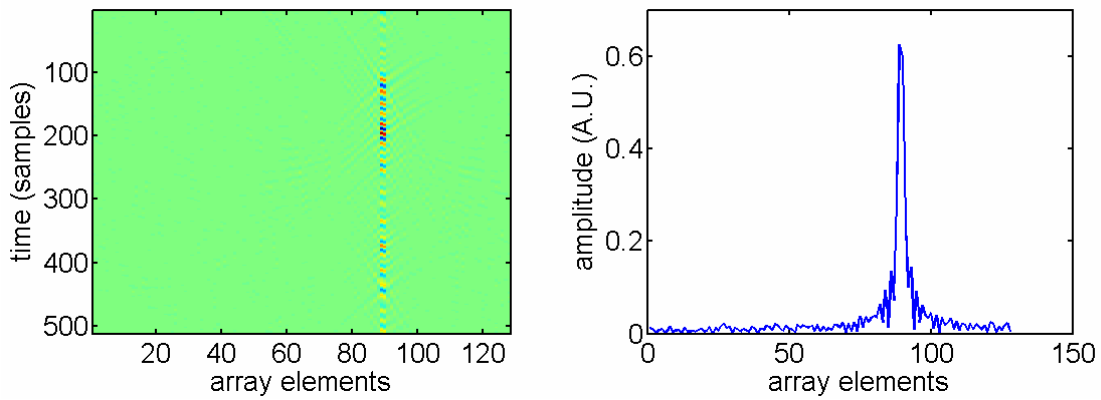

Figure 27 First temporal singular vector, and amplitude of the first monochromatic singular vector at the center frequency, for the virtual array located at 30 mm, in the scatterers plane. In this plane the virtual transducers, or transmit beams, are sinc functions, with a narrow main lobe, and only a few insonify significantly the scatterer. The sinc function variation can be noticed in the amplitude.

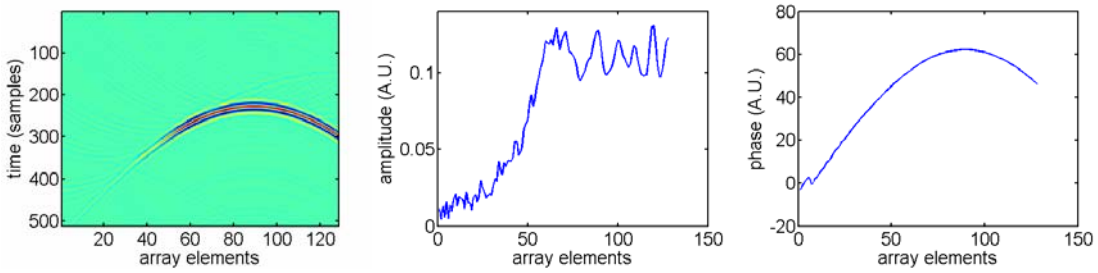

Figure 28 First Temporal singular vector, amplitude, and phase of the 1st singular vector *V* at the center frequency for the virtual array located at 60mm. The curvature of the wave-front and of the phase are inversed compared to Figure 23 to Figure 26, because the scatterer is now shallower than the focal depth, and as explained in Section III.A.2., the signals are time-reversed in this case.

III.C. The focused transmits as an orthogonal basis

The DORT method has been implemented in the past with transmits sequences other than single elements transmits. In these cases, orthogonal combinations of array elements were used. The interest of using this kind of transmits is increasing the SNR.

The focused beams can themselves be considered as an orthogonal basis. Each focused beam is the Green's function of the corresponding focal point. For one frequency, it is given by $H_i = e^{jkr_i(P)} \big/ r_i(P)$. The condition of orthogonality of Green's functions is given by Eq.2. 5 : the Green's functions of two points *P* and *Q* are orthogonal if it is possible to focus with the array on *P* without sending energy on *Q*.

For the linear scan, in the focal plane, the field is given by $\sin c\left(\frac{\pi X}{\lambda Z / D}\right)$, according to Chapter 1.III.B.1. The main lobe of the sinc is centered on the focus, here the point *P*. The points that are not insonified, and therefore whose Green's function are orthogonal to *P*'s Green's function, are the points located at the *zeros* of the sinc. The distance between these points is $a = \lambda Z / D$. Therefore, by choosing foci that are separated by

$$a = \lambda Z / D$$

Eq.2. 9

in the focal plane, each beam will be orthogonal to every other, and one is able to build an orthogonal family of beams.

For the phase scan, one needs to reason on a line at constant radius from the center of the array, in polar coordinates. The Fresnel approximation of Chapter 1.III.B.2 states that, in the focal radius, the field is the Fourier transform of the aperture, for the spatial frequency $\sin\theta / \lambda$. The field for a beam focusing on θ = 0, is then given by

$\sin c\left(\frac{\pi D \sin\theta}{\lambda}\right)$. The other beams will then be orthogonal if their foci are located at angles such that

$$\sin\theta / \lambda = n / D$$

Eq.2. 10

where n is an integer. In other words, $\Delta \sin\theta = \frac{\lambda}{D}$.

In the case where the array elements have a width equal to $\lambda/2$, which is the condition to have a directivity angle equal to π (half-plane), the array image the half-plane. To span the whole field of view, one needs foci ranging from $\sin\theta$=-1 to $\sin\theta$=+1. Combined with Eq.2. 10, this yields $\frac{D}{\lambda/2}$ beams, which is also equal to the number of element in the array. In this case, the canonical basis and the beam basis are two equivalent orthogonal basis of the same space.

It is easy to see the beams as an orthogonal basis in the case where the foci are in the very far-field. In this case, the Fraunhoffer approximation is valid, and the signal applied in the array to generate a beam is $e^{j2\pi\frac{\sin\theta}{\lambda}x}$. Together with Eq.2. 10, this yields $e^{j2\pi\frac{n}{D}x}$. This forms a family of Fourier coefficients, which is a well-known orthogonal basis. They are the basis of Fourier series (UNSER). A similar result could also be derived in the Fresnel aproximation, using properties of the Fourier transform.

Note: only the sector scan can form an orthogonal basis of the same space as the canonical basis. With the linear scan, it has been seen in III.B.2.a that some resolution

was lost compared to the canonical basis. The space span by a linear scan is then a sub-space of the canonical space.

The interpretation of the beams as an orthogonal basis is a nice result, although it is not essential for the present application. The FDORT method works well in general with families of beams that are not an orthogonal basis (for example if the spacing between beams is smaller than the orthogonality condition). The virtual transducer model is a more general and more intuitive approach.

The condition of orthogonality for the beams, stated in Eq.2. 9 and Eq.2. 10, is equivalent to the grating lobe condition given in III.B.2. This gives an upper-bound on the distance between beams that yield optimal results. If the spacing is greater than the upper-bound, the performance of the method is reduced. However, it is possible to use a spacing smaller than the bound although the beams are no longer orthogonal. This will just requires using more beams to span the whole space. There will be some redundancy, but is not a problem for FDORT, as the SVD will makes sense of the information.

The orthogonal basis provides all the information on the space, and thus a full-performance FDORT, with the smallest number of beams possible (minimum entropy). It leads to information optimization. It is then helpful when the number of beams is an issue. As acquiring a new beam takes time, it yields a faster implementation.

An orthogonal basis can be required for some signal processing algorithm. A good reference is (Trees).

III.D Link to back-propagation

Let Q be the position of a scatterer. Its Green's function is $H(Q)$. Let P_m be the foci of a focused beam. Focusing on P_m is equivalent to delay the signals of the physical

array by $r_i(P_m)/c$ and summing. In a monochromatic formalism, it is equivalent to project the signals on P_m Green's function. Therefore, the echo from Q heard by P_m is expressed as $S_m = \langle H(Q) \mid H(P_m) \rangle$. According to Eq.2. 5, S_m is also the field at position P_m when the echo from the scatterer Q is back-propagated from the array. Again, this shows that the focused beams act like virtual transducers that *probe* the value of the field at distance. The difference with the previous virtual transducer interpretation is that here the virtual transducers do not have a directivity, they are isotropic. However, the field is now the back-propagated field, which means that the signal is non-zero only in a cone.

To summarize, there are 2 ways to interpret the virtual transducers:

- either as transducers with a directivity probing the free space field from the scatterer
- or as isotropic transducer probing the back-propagated field of the transducer

The interest of this interpretation is to give a physical interpretation of the change of basis between the canonical basis (physical array) and the focused basis (virtual array). The change of basis is obtained by a back-propagation of the signals from the array plan to the focal plan.

V. APPLICATION TO FOCUSING THROUGH A FAR-FIELD PHASE SCREEN

IV.A Changing a far-field phase screen problem into a near-field phase screen problem using a virtual array

IV.A.1 Heuristics

It has been seen in Chapter 1 that the far-field phase screen was a better model for the heterogeneities than a near-field model (where the phase screen is supposed to be immediately in front of the array). However, the far-field model is much more complicated to deal with than the near-field phase screen model. First, time delays are no longer enough to correct the aberration, and a match-filter/ time reversal is necessary. Second, with a near-field phase screen, if one knows the Green's function of a single point in the medium, one is able to focus anywhere in the medium as the aberration does not depend on the position. With the far-field phase screen, the aberration depends on the position. Thus the knowledge of a point Green's function enables to focus only in the neighborhood of the point.

This is where the virtual transducers are helpful. Indeed, in the case where the aberrator is in the far-field, it is possible to use an array of virtual transducers close to the phase screen. This is feasible by choosing a focal depth for the focused transmit that is slightly shallower than the phase screen. In this case, the aberrator is still in the far-field for the physical array, but it is in the near-field for the array of virtual transducers (the

virtual elements are immediately in front of the aberrator)! This means that we can benefit from the advantage of a near-field phase screen when we are working with the virtual transducers.

IV.A.2 Example

We illustrate this with a simulated example. The simulation setup is illustrated in Figure 29

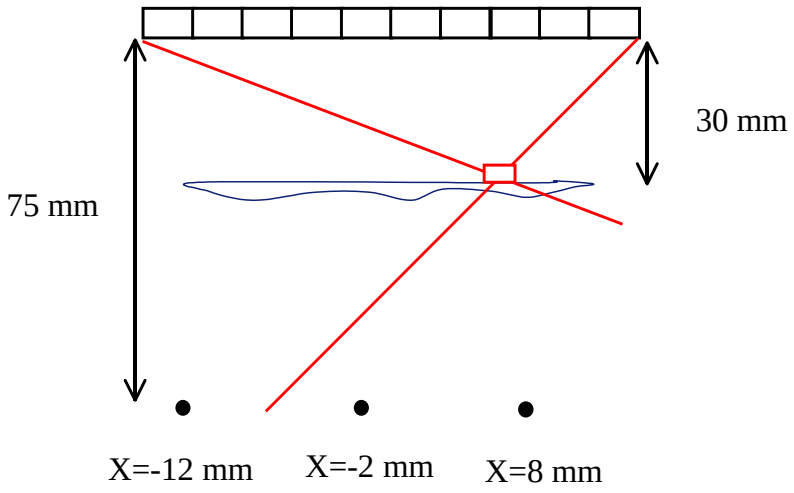

Figure 29 Simulation setup. A virtual transducer with its directivity pattern is shown in red.

A phase-screen, that applies a differential delay of 100 ns in average, with a spatial correlation of 4.5mm, was located at 30 mm from an array (128 elements of 0.2mm). Three point scatterers were located at a depth of 75 mm, and at an azimuth of respectively -12, -2, and +8 mm. FDORT was performed using the hybrid scheme, with foci at z=30 mm, in the phase screen plan. The spacing between the virtual transducers (foci) was 0.2 mm, which is slightly below the orthogonal condition (0.23 mm). The monochromatic singular vectors were computed both in the physical array, and the virtual

array. The temporal invariants of the time reversal were computed by Fourier transform, in the temporal frequency dimension, of the singular vectors. The temporal Green's function for the physical array are shown in Figure 30 while the temporal Green's function in the virtual array are shown in Figure 31.

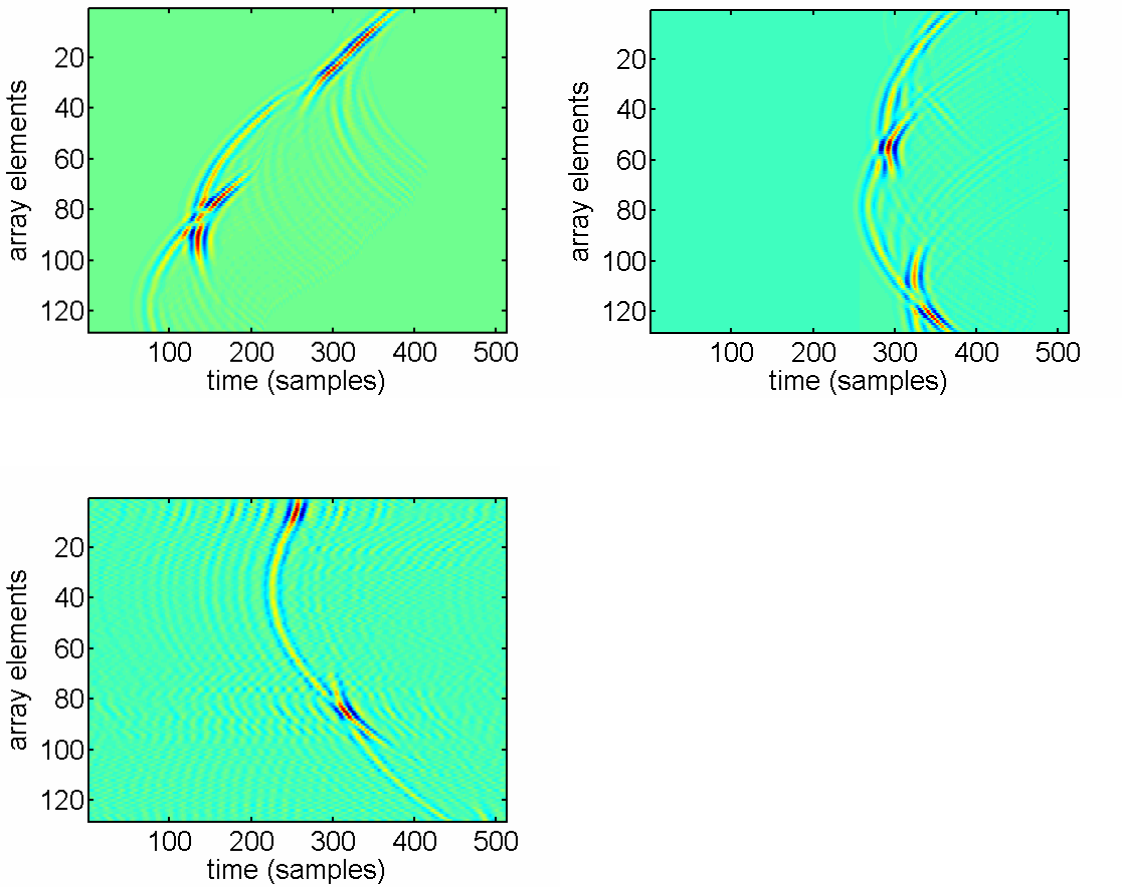

Figure 30 Temporal Green's function of the 3 scatterers (resp. -12,-2 and 8 mm) in the physical array. Because of the far-field phase screen, the signals are distorted in time, and there are important variations of amplitude across the array. Moreover, the effect of the aberration depends on the position of the scatterer. For example, the amplitude peaks are at different position for each scatterer.

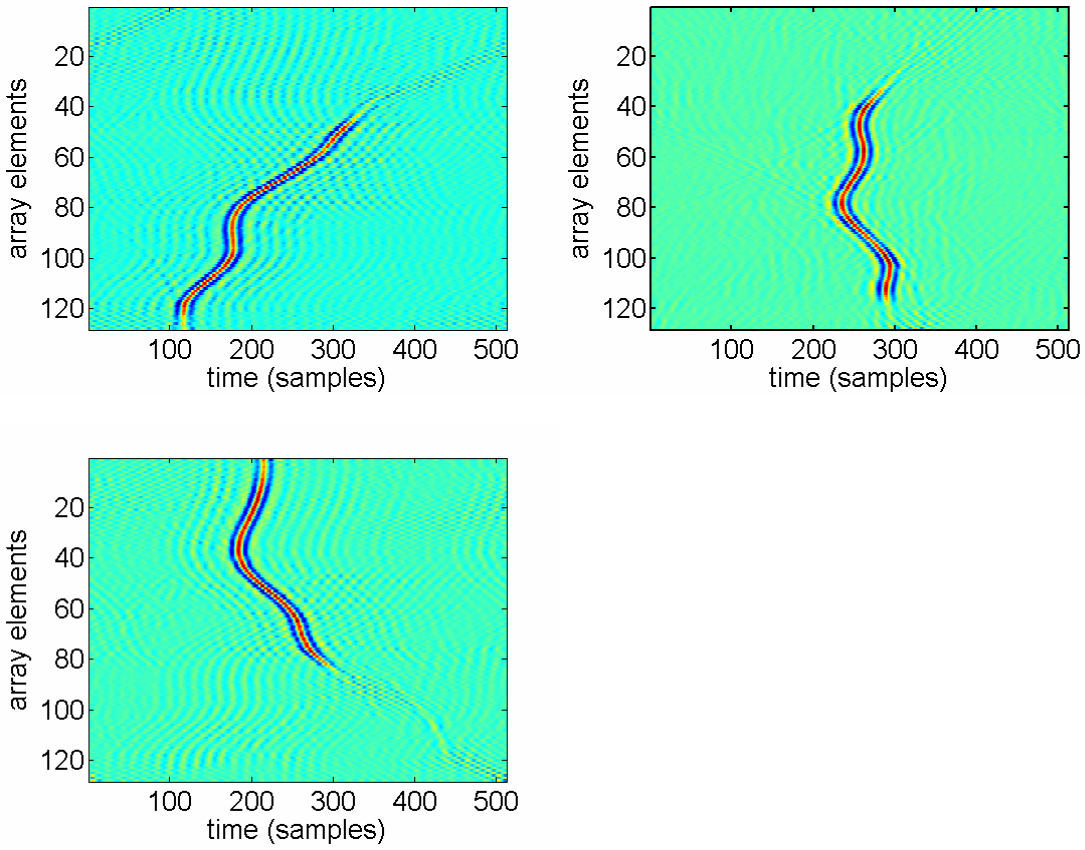

Figure 31 Temporal Green's functions (resp. -12,-2 and 8 mm) in the virtual array, located just behind the phase screen. The wave-fronts are merely delayed by the aberration. There is no distortion of the pulse or variation of amplitude. For each scatterer, the signal is received only by about 80 virtual elements, because of the directivity of the virtual transducers.

It is obvious in this example that from the virtual array point of view, the aberration acts as a near-field phase screen. The wave-fronts are merely delayed, and the aberration delays are the same for all scatterers. The only difference with a true phase screen as shown in FIGURE CHAPTER I is due to the directivity of the virtual transducers. This phenomenon is fully predicted by our model though, as described in section III. For example, one can see that the virtual transducer depicted in Figure 29 cannot *hear* the leftmost (x= -12 mm) scatterer.

IV.B Steering from the virtual array

With the far-field phase screen, the knowledge of the Green's function of the 3 scatterers enables to focus only in the immediate neighborhood (isoplanatic patch) of the point. The size of the isoplanatic patch, which is the area where the aberration effect is constant, depends on the strength of the phase screen and the distance to the array. With the phase screen chosen in the simulations, the isoplanatic patch is very narrow, as seen in Figure 32. The Green's function of a scatterer located at -12 mm was used to focus at this point and at neighbor points. To focus at neighbor points, a steering term was added to the phase of the Green's function, which corresponds to the difference in geometrical delays between the reference point and the new point. This is equivalent to consider that the term due to the aberration is the same for all points. Both amplitude and phase of the Green's function are used.

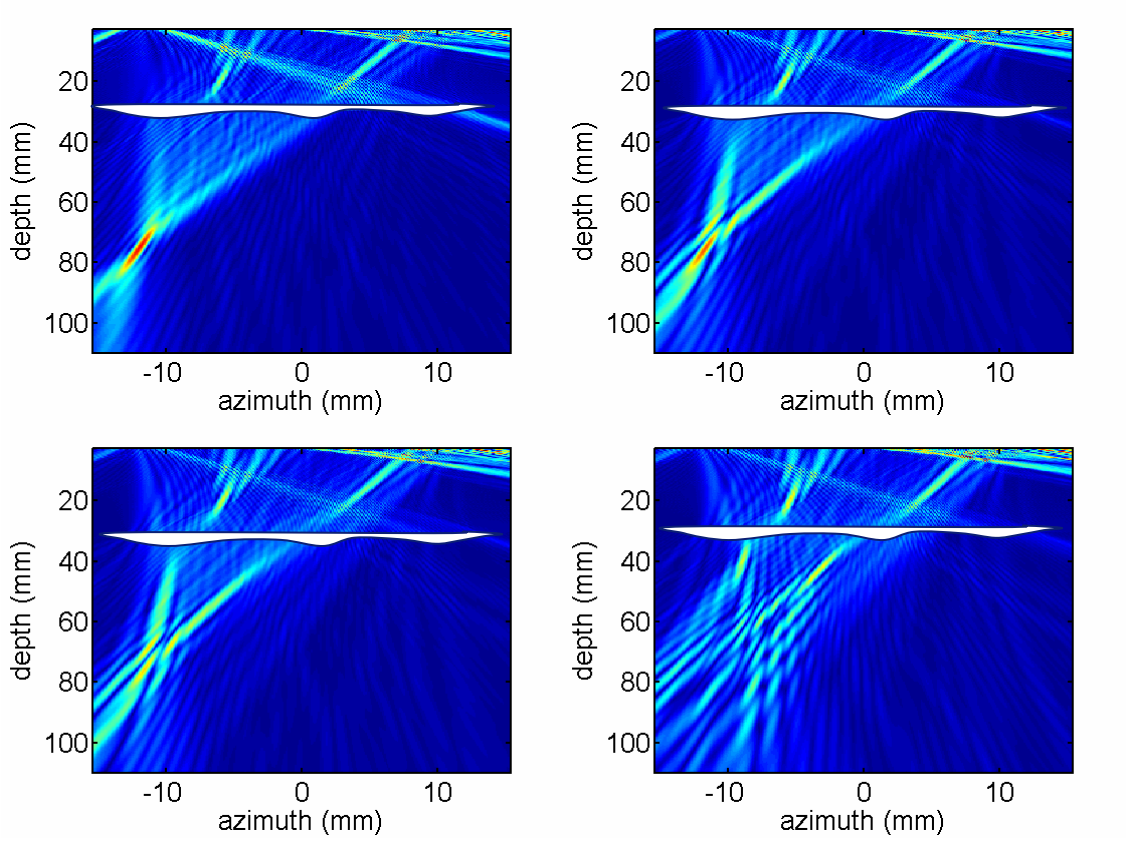

Figure 32 Focusing from the physical array at, respectively from top left to bottom right: -12 mm, -11.7 mm, -11.5 mm, -10 mm. The Green's function for the scatterer at -12 mm was used to correct the aberration. Therefore the focusing is perfect at – 12 mm. However it degrades very rapidly, as the aberration varies with the position.

The focusing degrades very rapidly. At only 0.5 mm from the reference point, the focusing can be considered as relatively poor.

The same steering process was then performed from the virtual array, to focus at the same neighbor point. In this case, the focusing on neighbor point was very good, even if the point was far away from the reference. The focusing on a point at x=-10mm is shown in Figure 33, and is much better than the focusing on the same point from the physical array shown in Figure 32.

From the virtual array, we can in theory focus anywhere in the medium using the knowledge of a single Green's function, because the phase screen is near-field. However, as seen in Figure 31, because of the directivity of the virtual transducers, one Green's function gives only information about a part of the phase-screen. For example, the Green's function of the scatterers at x= -12 mm, gives a non-zero signal only on the 80 left-most virtual transducers. Therefore, only the delay experienced by these 80 transducers can be deduced. To characterize completely the phase screen delay, it is necessary to use another scatterer that is *heard* by the remaining virtual transducers. The scatterer at x=8mm is suitable. From the knowledge of these two Green's functions, one can characterize completely the phase screen, and then focus on any point in the medium using the proper geometrical delay.

Using the unwrapped phase of the Green's functions for the two scatterers at –12 mm and 8 mm, we were able to deduce the delay profile shown in Figure 34. The estimated profile was very close from the true profile. Then, using this profile we were able to focus anywhere in the medium by adding the proper geometrical delay, $r_i(P)/c$, where $r_i(P)$ is the distance between a point and the virtual tranducer i. The focusing on a point at x= -2 mm is shown in Figure 33. The focusing was not obtained from the measured Green's function of the scatterer located at this point, but by steering using the knowledge of only the 2 other Green's function (x = -12 and x= 8 mm). Using the virtual transducers, we were then able to achieve a very good focusing on a point that was 1 cm away from the closest estimated Green's function, through a far-field phase screen.

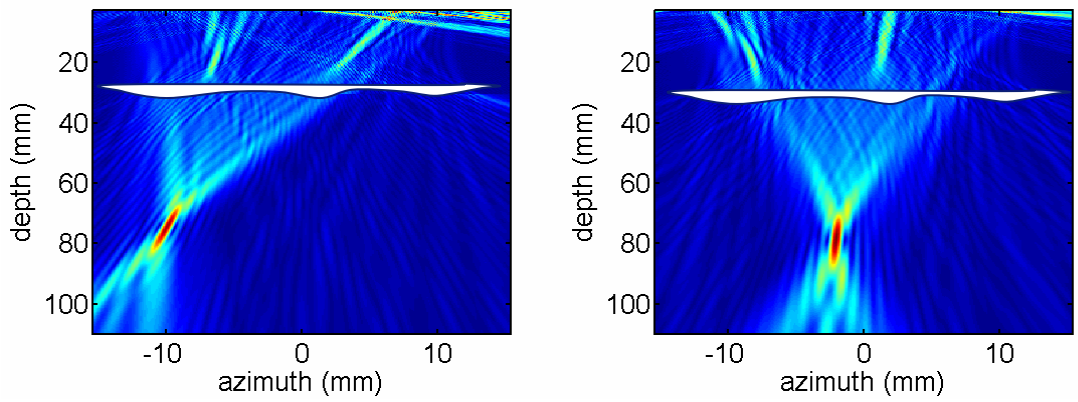

Figure 33 Focusing from the virtual array at respectively, from left to right, -10 mm and – 2 mm. The reference Green's function was at –12mm in the 1st case, and –12 mm and + 8 mm in the second case.

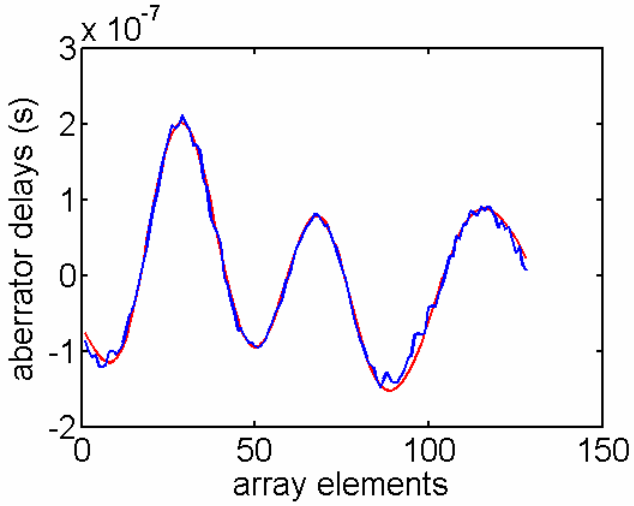

Figure 34 Estimated delay profile of the phase screen (blue) compared to the true delay profile (red).

In conclusion, with appropriate virtual transducers, one is able to focus on any point through a far-field phase screen, using the knowledge of only two Green's functions. This is remarkable, as the size of the isoplanatic patch (seen from the physical array) was hardly 0.5mm. In addition, the focusing from the virtual array requires only time-delaying the signal, and not a complete match-filter.

IV.C Practical implementation

IV.C.1 Determination of the phase screen position

In a practical setting, the depth of the phase screen is not necessarily known. We investigate here a few criterion to determine this depth.

IV.C.1.a Criterion based on the amplitude

If the phase screen only delays the wave-front, and does not introduce any attenuation, the amplitude of the wave-front immediately after going through the phase screen is approximately constant. During the propagation after the phase screen, interferences lead to amplitude variation. The 1st criterion is then based on the field amplitude. The monochromatic Green's function of the scatterer at x=-2mm of the previous example is numerically back-propagated in an homogeneous medium, as shown in Figure 35. As the wave-front gets closer from the phase-screen plane (z=30mm), the amplitude variation becomes smoother. After the phase-screen plane, amplitude variation reappears, because the phase screen was not modeled in the back-propagation.

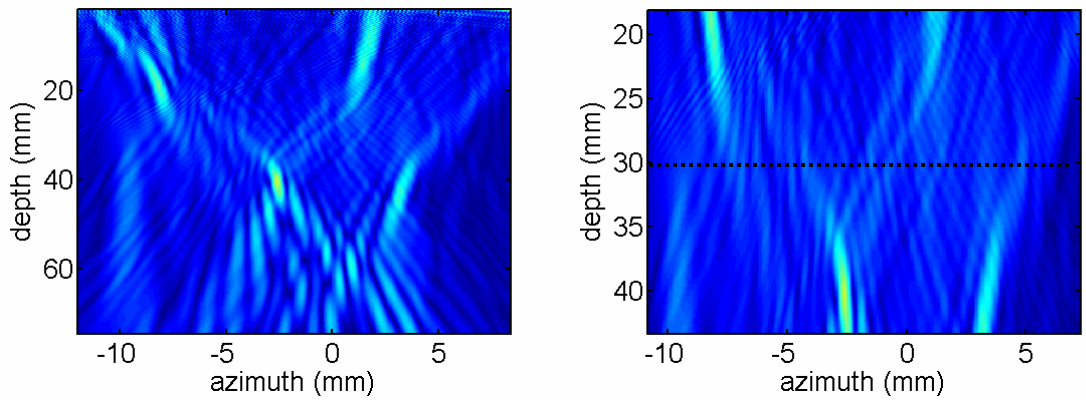

Figure 35 Field due to the back-propagation of a Green's function. Right: zoom around the phase screen depth. The plane where the amplitude is approximately constant indicates the phase-screen position.

IV.C.1.b Criterion based on the distortion

The drawback of the previous approach is that, in a real setting, an aberration often introduces amplitude variation through attenuation, and not merely time-delays. An approach proposed by (Liu and Waag) and (Dorme and Fink) is to use a wave-front similarity factor. Indeed, the propagation after the phase screen does not lead only to amplitude variation, but also to pulse distortion. The criterion is based on the correlation between pulses at two distant location of the wave-front. By numerical back-propagation in a homogeneous medium, the wave-front is computed at any depth. For each depth, a similarity factor is computed by correlation of the pulses. The phase-screen depth is given by the maximum of the similarity factor.

IV.C.1.c Criterion based on spatial invariance of the aberration effect

A third property of the near-field phase screen can be used. In the near-field phase screen model, the aberration effect is independent on the position. One can focus

anywhere in the medium by adjusting the geometrical delays. For a far-field phase screen, the aberration term depends on the position. It can vary significantly from one position to the other. It is approximately constant only in the isoplanatic patch.

The criterion compares then the back-propagated field for 2 different scatterers. Immediately after the phase screen, the field differs only by the steering term. In the Fresnel approximation, it is a linear phase shift. Far from the phase-screen, the fields are more different, as the aberration effect is no longer the same. Both the amplitude and phase variation is different for the 2 scatterers.

Therefore, we numerically back-propagate two Green's function, at the central frequency. Ideally, the 2 scatterers should be far enough so that the aberration effect is significantly different. However, if they are too far apart, their wave-front will cross two different part of the phase-screen, and the signals can no longer be compared.

Let $P_A(x,z_0)$ and $P_B(x, z_0)$ be the field for the two Green's functions at depth z_0. In the phase-screen plane, these two functions should differ only by a phase shift. Therefore the Fourier transform of the product $P_A(x,z_0)\, P_B(x, z_0)^*$ should exhibit a strong peak whose position depends on the phase shift. The value of the peak maximum corresponds to the correlation between the aberration term for the 2 scatterers. In order to normalize the criterion, we define the criterion as $C = \frac{\max\left[FT\left\{P_A(x,z_0)P_B(x,z_0)^*\right\}\right]}{\sqrt{\int |P_A(x,z_0)|^2 dx \int |P_B(x,z_0)|^2 dx}}$. This criterion is equal to 1 if $P_A(x,z_0)$ and $P_B(x, z_0)$ are identical except for a linear phase term. If $P_A(x, z_0)$ and $P_B(x, z_0)$ differs by their amplitude or phase (other than linear shift), the criterion decreases. To highlight the position of the phase screen, $1/(1-C)$ is plot.

The curve in Figure 36 has been obtained by comparison of the Green's function of 2 scatterers separated by 2 mm, with the phase-screen of Figure 29.

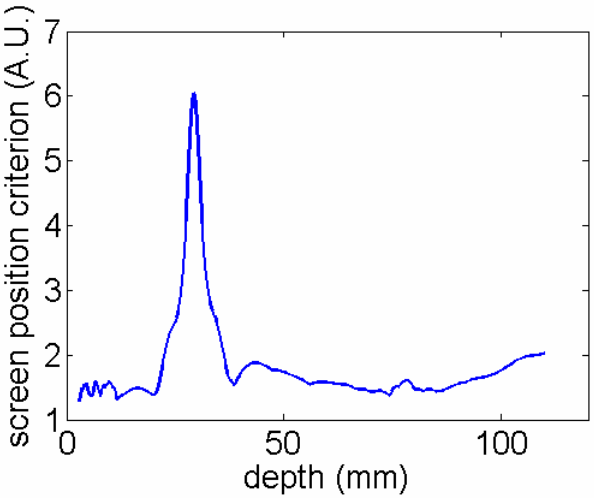

Figure 36 Criterion based on spatial invariance of the aberration effect. The peak indicates the position of the phase-screen.

This criterion yields an accurate position of the phase-screen, and requires the back-propagation for only one frequency. However, 2 scatterers have to be available.

IV.C.2 Application to Real Experiments

In Section IV.B, it was shown how it was possible to focus from the virtual array of transducer in a numerical experiment. We now describe how this can be done in a real experiment, where we want to be able to focus on any point through a far field phase screen. In a real experiment, we don't have access directly to the virtual transducers, but to the physical transducers. In order to focus on a point, we need to know the signal to apply to each physical transducer. Therefore, we need to express the Green's function in the real array.

We already know how to generate each focused beam (virtual transducer) from the physical array. The signal applied in the real array to form a few focused beams are shown in Figure 37. We also know how to focus from the array of virtual transducer on any point in the medium. We just have to apply the appropriate delay to each virtual transducer. This means that some focused beams are transmitted later than others. Therefore, if we delay the wave-fronts corresponding to each focused beam by the appropriate amount, and add the signals together, we obtain the signal to transmit in order to focus on any point in the medium. This is illustrated in Figure 37.

Note: This operation is equivalent to backpropagating the signal from the virtual array to the canonical array, as proposed in (Dorme and Fink). In the case where the virtual transducers forms an orthogonal basis, it is also equivalent to change bases (from the basis of focused beams to the canonical basis; the Green's function of each focal point is then the coordinate of each focused beam in the canonical basis)

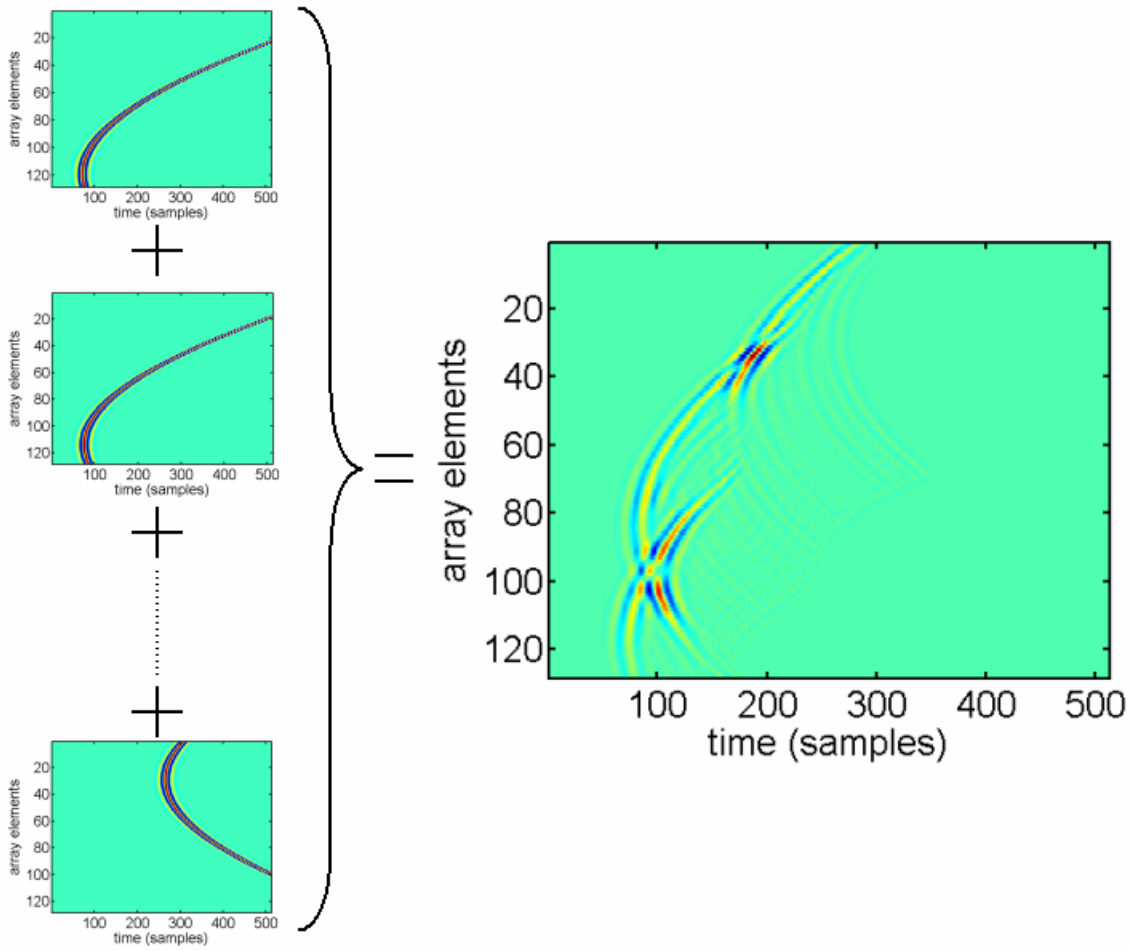

Figure 37 To compute the Green's function of any point in the medium in the physical array, one merely has to add the wave-front corresponding to each virtual transducer that insonify the point with the proper time delays. The virtual transducers that do not insonify the point (because of the directivity) are not summed.

The method was used to synthesized the Green's function of the point at x=-2mm (Figure 29). The Green's function obtained is very close to the Green's function measured when a scatterer is present at this point (Figure 38).

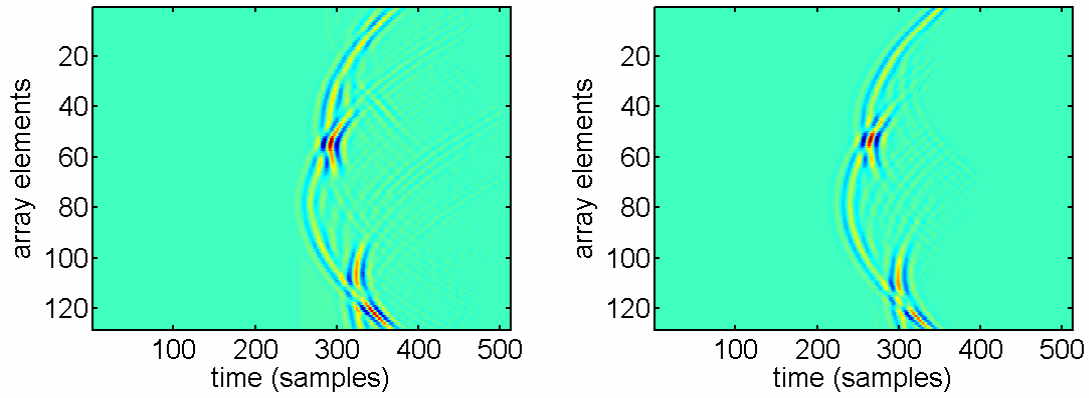

Figure 38 Temporal Green's function of the point at x=-2mm, measured (left) and synthesized using the method described in this section (right)

This method is particularly interesting has it shows how a complicated wave-front, where the pulse is distorted and the amplitude varies, can be synthesized by a mere sum of simpler wave-fronts. Match filter processing is very costly to implement in practice, as it requires filters on each channel. This shows that it can be reduced to a series of delay-and-sum.

IV.C.3 Application to imaging

To image a medium, one has to focus in transmission and reception on every point of the medium. One way to use the method in imaging is to compute the match-filters for every point in the medium, and do match-filter processing. However, the advantage of imaging compared to a focusing experiment, is that the focusing can be done numerically. For example, a full data set can be acquired, and the focusing on each point is achieved *a posteriori* by processing the full data set.

The full data set does not have to be acquired in the physical array though. It can also be acquired in the virtual array. A full data set in the virtual array is obtained when a signal is transmitted successively by each virtual transducer (focused beams), and for

each transmit, the signal is received by all virtual transducers. Receiving with a virtual transducer is equivalent to focusing in receive on the location of the desired virtual transducer. Focusing in receive on a point *P* is achieved by delaying the signals received by the physical transducers by $r_i(P)/c$ and summing them. Before, we were using the virtual transducers (focusing) only in transmit. Now we are using them both in transmit and in receive.

In practice, the full data set in the virtual array would be acquired the following way:

- a focused beam is transmitted
- the received signals are recorded by every physical transducers
- the signals are delayed and summed to reconstruct the signals received by each virtual transducer
- the process is repeated for every focused transmit

Once the full data set in the virtual array is obtained, it is very easy to image the medium. Two parts of the medium can be distinguished: deeper and shallower than the virtual array.

We consider first the deeper part. Focusing in this part is equivalent to focusing through the near-field phase screen (from the point of view of the virtual array). This is done by adding the phase screen delays to the geometric delays.

Let us consider now the shallower part. There is no phase screen between the virtual array and this part, and simple geometric delays can be used. However, we have seen in section.III.A.2 that an observer located shallower than the virtual array was

observing a time-reversed version of the signal emitted by the array (because the wave-fronts are converging to the virtual transducers). For this observer, the signal from the furthest virtual transducer is the first signal observed. Therefore, the delays have to be inversed when focusing in this part of the medium from the virtual array.

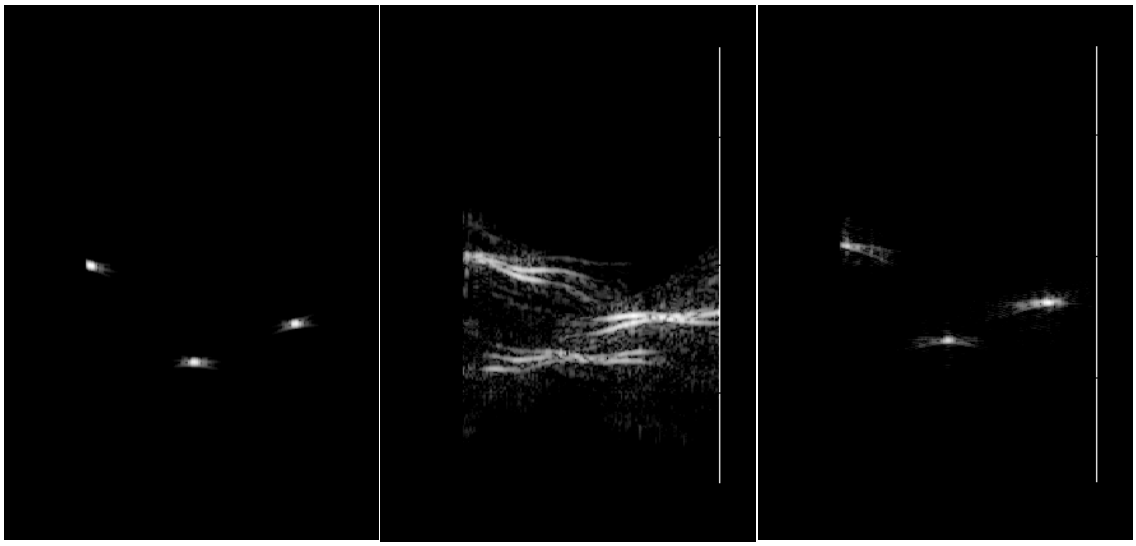

Figure 39 From left to right: image of an unaberrated point-scatterer phantom, image of the same phantom with a 100ns rms phase-screen located at 30mm; and image of the aberrated phantom corrected using the FDORT method. The corrected image is not perfect, but much better than the aberrated image.

VI. FDORT WITH TIME GATING

The DORT method is able to detect and focus on well separated point scatterers, like wires (which can be considered point-like in the 2-D geometry of the experiments), in water, even in the presence of a strong aberrator(Prada, Manneville et al. 1996). In medical applications, however, the scatterers are embedded in tissue that generates a

speckle signal. The DORT process was performed on a tissue-mimicking phantom with wire-targets, represented in Figure 40.

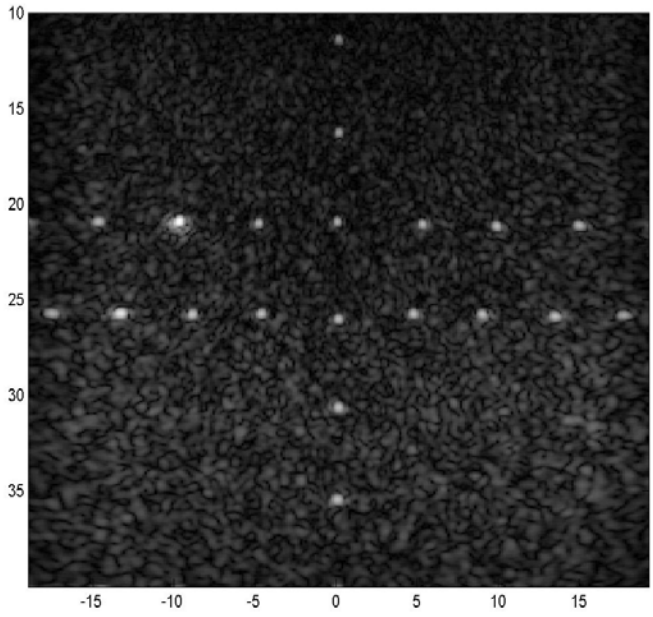

Figure 40 Phantom used for the experiments

Eigenvalues and numerical backpropagation of the second eigenvector are shown in Figure 41. Due to speckle, the eigenvectors become too noisy and DORT fails: Focusing on the wires' locations is very poor.

It is desirable to have a method that can offer the same kind of performance as DORT in such an environment, where the targets are embedded in speckle. A mere implementation of the FDORT method as described earlier is not a solution for this problem, and leads the same results as DORT. However, we are now presenting a method, based on FDORT with time gating, on a linear scan, that provides an excellent solution of this problem. This solution takes advantage of a property of focused beams

and cannot be implemented as efficiently with a full data sets. This section is taken from (Robert, Burcher et al.).

We start by an analysis of the noise and then present the solution.

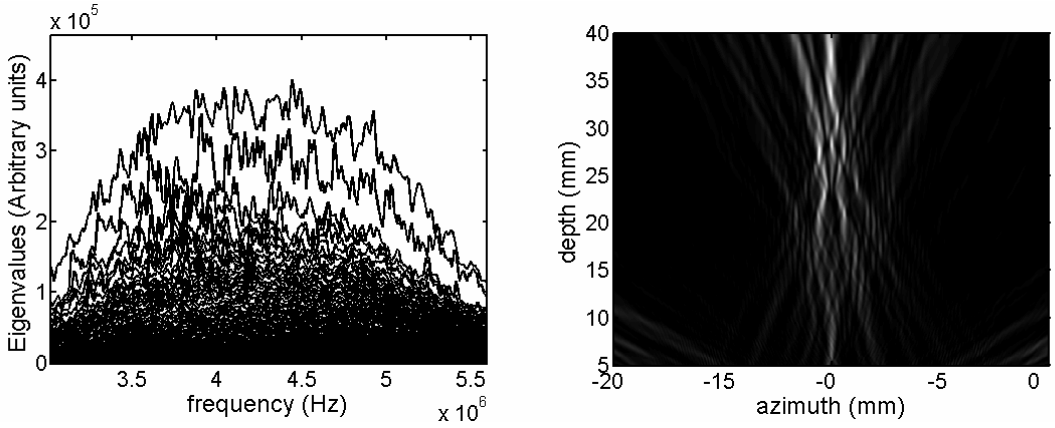

Figure 41 FDORT on a tissue mimicking phantom, performed with the whole received signal. Left: singular values in function of the frequency. It shows that lots of eigenvalues have an important magnitude and it is hard to make a clear distinction between significant targets eigenvalues and noise eigenvalues; Right: Field resulting from the numerical backpropagation at 4.3 MHz (close to the central frequency) of the 2nd eigenvector.

V.A. Influence of noise on eigenvectors and eigenvalues

Signals from scatterers other than the ones we want to detect (here the wires in the phantom) are considered as a noise. In this case these are sub-resolution scatterers generating speckle signal. Two cases can be distinguished:

a. Ideally separated scatterers These are not coupled with the targets; they are located outside the coupling area for each target, as depicted in Figure 14. They give rise to new non-zero eigenvalues, but do not affect the eigenvectors corresponding to the targets that still enable perfect focusing. The focusing properties are preserved, but as there are more

non-zero eigenvalues, it is more difficult to determine which eigenvectors correspond to the targets.

b. Non ideally separated scatterers They are located in the shadow (light blue area in Figure 14) of the target and therefore are coupled with the target. There are more non-zero eigenvalues, as in the previous case, but here the eigenvectors are affected: They are no longer equal to the Green functions of individual targets, but are linear combinations of the targets' Green functions and Green functions from noise scatterers coupled with the targets. The resulting eigenvectors can be very complex in the presence of speckle signals, as hundreds of sub-resolution scatterers are coupled with the target. FIGURErepresents, in a clinical image, all the scatterers coupled with the target, located at a depth of 25 mm. The focusing properties are in this case dramatically degraded, as seen in Figure 41.

V.B. A solution: FDORT with time gating

V.B.1. Principle

We are here interested to reduce the effect of the last kind of noise, which has the worst influence. The noise comes from the set of scatterers coupled with the target, contained in a conical shape centered on the target. Laterally, in the target plane, the zone of coupling is narrow. It is the resolution cell of the array. This limitation is due to the finite size of the array and affect usual beamforming imaging. Axially the coupled zone is much more extended. This limit is not present in classical beamforming. It is due to the fact that the temporal resolution is not exploited by DORT or FDORT because of

their only monochromatic nature. An important amount of information is then lost. In conventional imaging, the axial resolution comes from the broadband nature of the signal.

To solve this difficulty, impulsive and monochromatic approaches have to be mixed. At any given time τ, an incident ultrasound beam illuminates only a volumetric distribution of scatterers, called the isochronous volume(Fink and Cardoso 1984; Jean-Francois and Mathias 1991; Mallart and Fink 1994) . Now, selecting within the received signal an analysis time window $[\tau,\tau+\Delta\tau]$ (Figure 43) is equivalent to selecting only echoes from scatterers located in a well-defined volume whose lateral extension is equal to the lateral extension of the beam, and whose axial extension Δz is related to $\Delta\tau$. If we repeat this process for every beam, the union of all the volumes gives a slice of the medium of width Δz, represented in Figure 42.

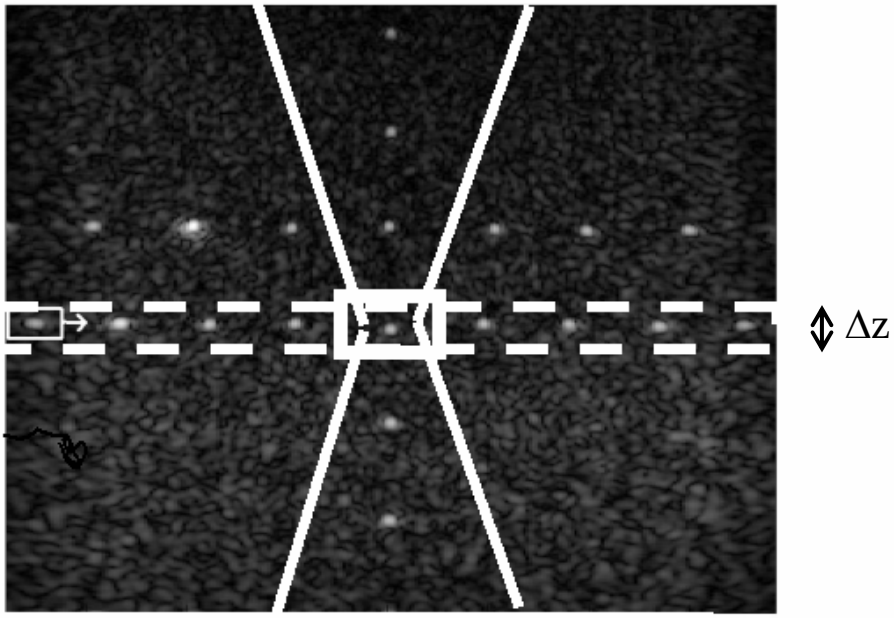

Figure 42 Tissue-mimicking phantom used for the experiments. The zone of coupling for one scatterer is indicated by the white conical shape. Scatterers inside this area are coupled with the

scatterer. The box drawn with dashed lines indicates the slice obtained by time gating the signals. This reduces the influence of the coupled scatterers.

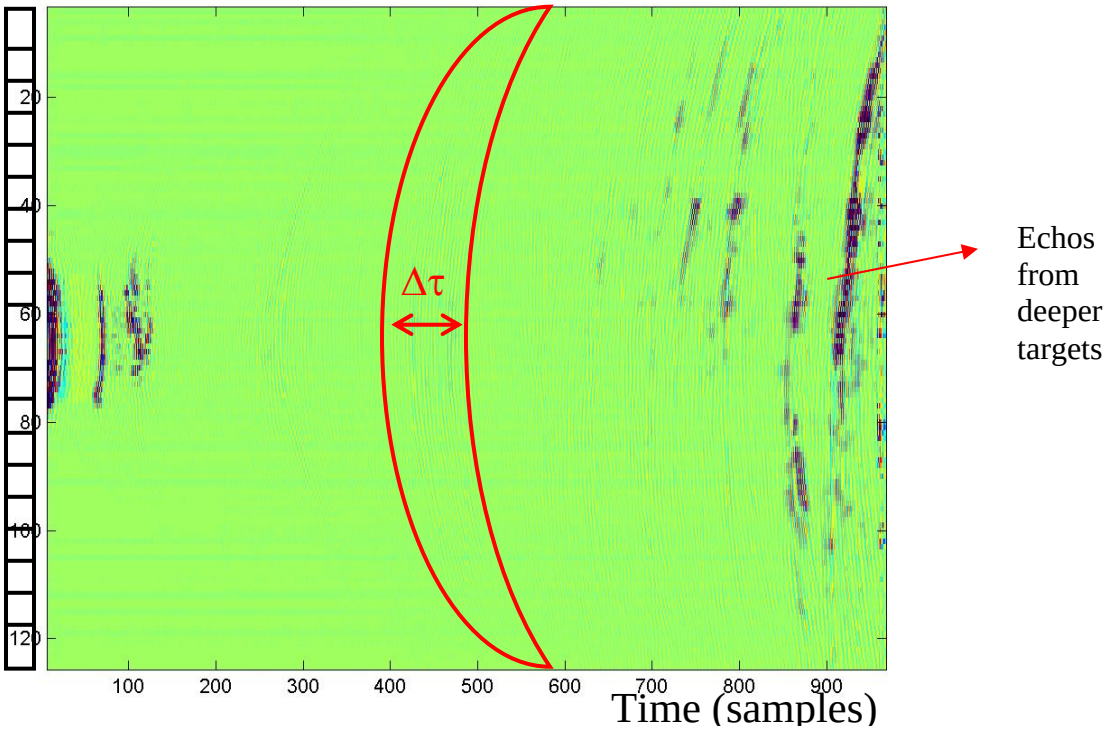

Figure 43 Per channel received signal for a given transmission. A time window suitable for the algorithm is shown in red. It enables to select signal from the slice in Figure 42.

From the point of view of FDORT, using time windows is similar to having an empty medium outside this slice. Therefore, there is no coupling with scatterers outside of the slice. Thanks to time gating, the zone of coupling narrows axially and tends to the limit set by the temporal resolution; targets from different depths can then be fully decoupled if advantage is taken from the impulsive approach.

Such a process is possible only with focused pulse transmission. Indeed, the narrow directivity pattern leads to a direct relationship between propagation time and depth. If a single element transmission is used, as in the classical DORT method, the

whole medium is insonified and it is no longer feasible to select signals from a given depth.

The method has been presented here with a linear scan. It can also be done with a phased scan, but in this case, slices of radius are taken, rather than slices of depth.

V.B.2. Experiments

Experiments are carried out on the medical phantom represented in Figure 40, using a Philips HDI-5000 and a 1-D linear array at 4.3 MHz center frequency.

For each transmission the signals on all N received elements are recorded. The signals are gated in time, keeping only the signal from $z-0.5\Delta z$ to $z+0.5\Delta z$. The window width is chosen to be slightly longer than the pulse width. For the m^{th} transmission pulse, gating in depth is achieved using the geometrical focal law focusing along the beam m at depth z.

Figure 44 shows the eigenvalue spectrum and the numerical backpropagation of the second eigenvector obtained using the FDORT method in the medical phantom at the depth of 9 wires. It demonstrates a great improvement in the focusing ability of the first eigenvectors, compared to the results in Figure 41. To obtain the focal law of each wire, one needs to repeat the process for several depth ranges.

In conclusion, the FDORT method can still be performed to detect point targets in the presence of speckle noise, but the medium needs to be sampled in thin slices to decouple the targets from the speckle noise. The number of significant eigenvalues is the number of targets in the slice, and the eigenvectors are the corresponding Green functions. Targets localization is now feasible, as shown in Figure 45.

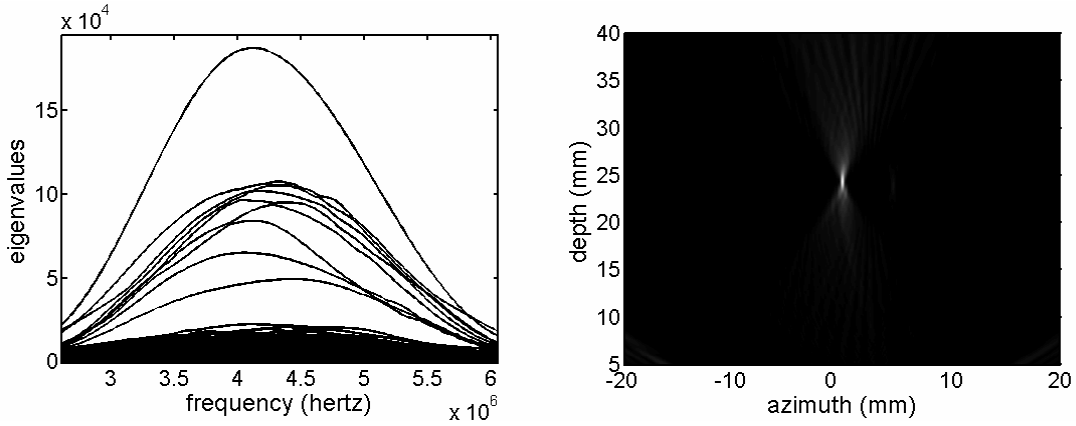

Figure 44 FDORT on a tissue mimicking phantom, performed in the slice shown in Figure 42. Left: singular values in function of frequency (MHz).: 9 eigenvalues have now significant magnitudes compared to the others; Right: Field resulting from the numerical backpropagation at 4.3 MHz (close to the central frequency) of the 2nd eigenvector. A good focusing is now obtained.

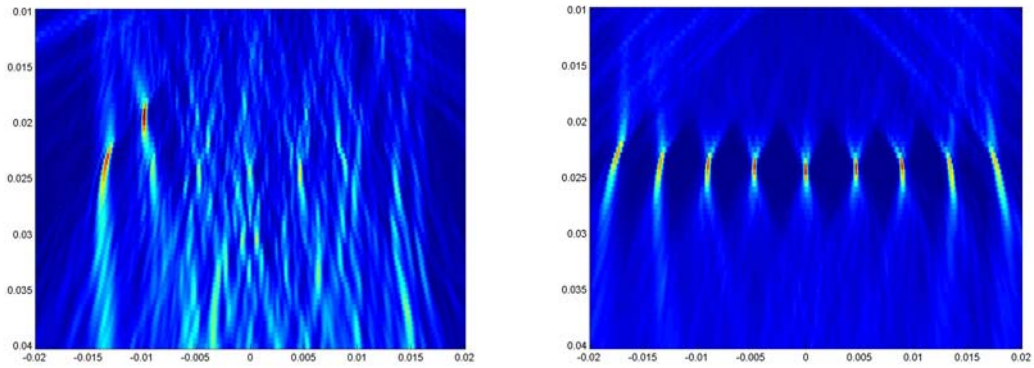

Figure 45 Targets localization in speckle. Left: field resulting from the numerical backpropagation of the 9 first eigenvectors without the time gating. Right: same with the time gating: the focusing and wires localization is very clean.

VII. LOCAL FDORT

VI.A. FDORT in a limited region of space

VI.A.1. Principles

The DORT method using the elements basis is well adapted when the zone of interest (the zone when one wants to detect and extract the Green's function of scatterers) is the whole half plane. In most cases, though, the zone of interest is narrower, and can be limited to a small region of space. Intuitively, there is less information to extract from a small region of space than from the whole half space, and we should not need as many transducers in this case. It also seems that the most efficient use of the transducers would be to place them in the middle of the region of interest, which is possible with virtual transducers; in this case we would need only a few transducers to listen to all the signals from the region.

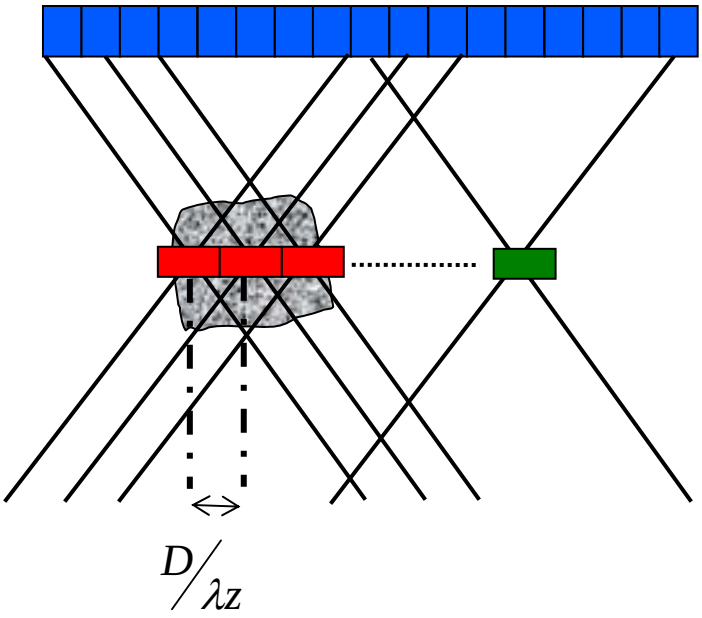

Figure 46 When the region of interest (gray) is limited, it is most efficient to have the transducers at a depth corresponding to the middle of the region. This is possible with virtual transducers. The number of transducers needed is reduced. Indeed, most of the virtual transducers, like the green one, are not providing any information and do not need to be transmitted. In this example, only the 3 red virtual transducers are necessary. This allows a much faster implementation of the method as only a few transmits are necessary.

It is possible to develop this point more rigorously by considering the beams as a basis for the Green's function. The focused beams are particularly interesting because they are *spatially localized*, especially near the focal depth. Indeed, each beam insonifies a narrow region of space. Retrospectively, each point is insonified by a limiting number of beams, or virtual transducers. This is very obvious in Figure 27, when the scatterer is at the focal depth. The amplitude of the Green's function is non-zero only on very few virtual transducers. Therefore, all the information on the point is concentrated in few vectors. It is then possible to perform FDORT on a small region of space with only a few

beams. No performance is lost because the beams that are not used did not carry any information on the region of interest.

This is illustrated in Figure 47 and Figure 48. First, we have projected the normalized Green's function of the points on a sub-space of only 5 consecutive orthogonal beams of the phase scan. Figure 47 (left) shows that almost all points in a triangular slice are completely described by this 5 beams. Indeed, the projection in the sub-space is close to 1. On the opposite, the 5 beams carry no information on points outside the slice; their projection in the sub-space is equal to zero. By adding more beams in the sub-space, one can increase the size of the slice (Figure 47 - right). This basis is particularly efficient, as the number of transmits needed depends on the size of the region of interest.

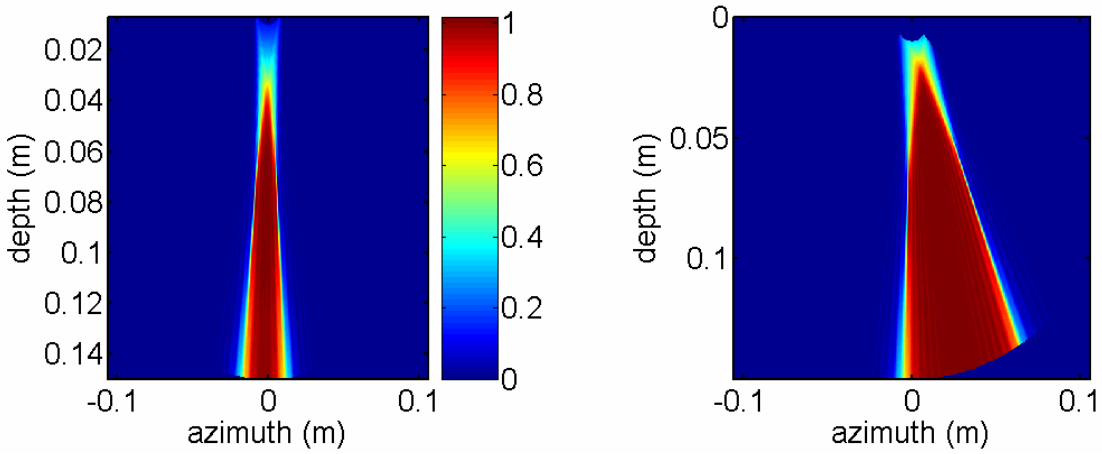

Figure 47 In dark red is shown the sub-space spanned by 5 (left) and 16 (right) consecutive orthogonal beams in a phase scan. The map represents the projection of the normalized Green's function of each point of the space in the sub-space. When the projection is 1 (or close to 1) the Green's function can be described entirely by the family of beams. . The dark red area is basically the area where FDORT can be performed at full performance.

The same as been done for the hybrid scan, in Figure 48. In this case, the beams are well localized around the focal depth (50 mm). The zone that is completely represented is diamond shaped and center around the focal depth.

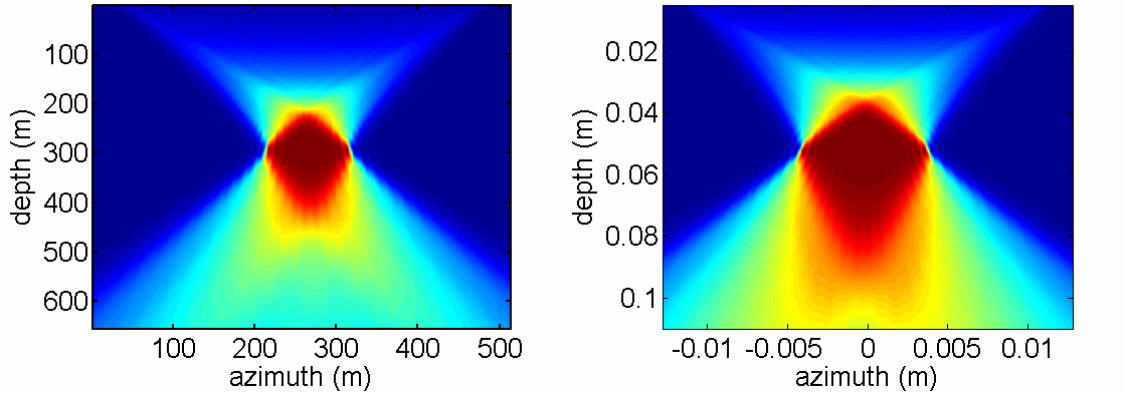

Figure 48 In dark red is shown the sub-space spanned by 10 (left) and 20 (right) consecutive orthogonal beams with the hybrid scan, The results with a linear scan are similar.

The problem with the canonical basis traditionally used with DORT is that if we want to decompose a Green function in this basis, we will have a significant component on most of the vectors. This is because each real element insonifies most of the space (Figure 49). Then, if we want to perform a synthetic aperture acquisition with only a few elements in transmission, we lose part of the information and obtain different results than if we were using all the elements. (Reducing the number of element in transmission is equivalent to using a smaller array, which will yield a lower resolution).

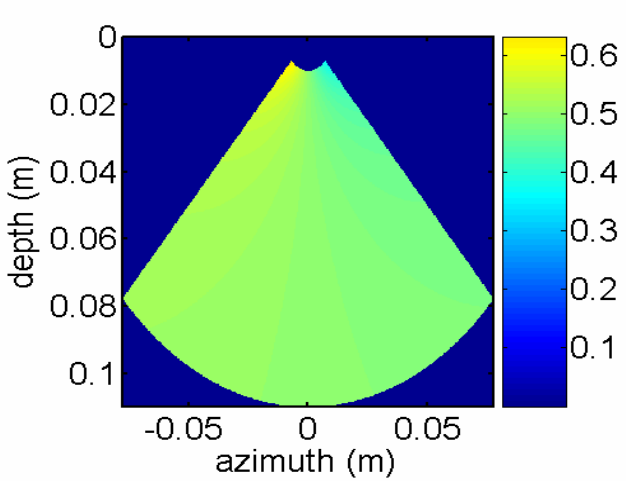

Figure 49 Same for the canonical basis (conventional DORT method) The points Green's function have been projected on the 32 first elements of the canonical basis (out of 64 elements) No point is completely described. The projection is about 0.5, which means half the information is missing. This missing information translates in decreased performance (decreased resolution)

VI.A.2 Fast FDORT method and target detection in 3D

The reduction in number of transmits can be significant. For example, it the targets are known to be within an angle of 30 degrees, the number of transmits can be reduced by about 6 compared to the whole 180 degrees half plane, by using a phased scan. The process is speed up considerably.

This is especially important if we want to detect target in a 3D volume, with a 2D array. Indeed, 2D arrays can have 1000 to 10000 elements, and it is completely unrealistic to acquire a full data set with such an array. If we have an idea of the region where the targets are, the FDORT method can still be performed with a relatively low number of focused transmits.

VI.A.3 Quantity of information in a region of space

We can go further and show that the focused beams are very close to the optimal family of vectors one can use to extract information from a limited region of space. Indeed let us imagine that we want to extract the information from a region of space of width *L*, and relatively narrow in depth. To simplify, let us reason in a monochromatic formalism, and for a linear scan. As the beam evolves relatively slowly in the depth dimension, it is possible to do the derivation at only one depth. We would like to find the most optimal basis, that is to say the smallest family of vector where one can express all the Green's functions of the region.

As the medium is seen by an array of limited size, the highest spatial frequencies are lost during the propagation from the medium to the array (Chapter 1.III.B.3). The image of the medium can then be represented by a function whose spatial frequencies spectrum has a width equal to $D/\lambda z$ where d is the depth of the medium slice we are considering. The image of the medium is then a band-limited function. It is also limited in space, in an interval of length *L*, which is the size of the region of interest. The sub-space of band-limited and space limited functions has been extensively studied, notably by Slepian *et al. (Goodman; Slepian and Pollack 1961; Frieden 1971)*, as it is a frequent problem in engineering. It is treated in more detail in Chapter 3. The dimension of such a sub-space is equal to the space-bandwidth product, in this case $N = LD/\lambda z$. As λ/Dz is also the size of the resolution cell of the array, *N* is the equal to the number of resolution cells in the interval *L*. This means that one needs at least *N* vector, when using the most optimal basis, to extract all the information. This is also approximately what we obtain

with the focus beams, when they are separated by $D/\lambda z$ (orthogonal condition, Eq.2. 9) A similar result can be obtained in polar coordinate for the phase scan.

VI.B Application to moving scatterers

VI.B.1 Problem

It is in general difficult to use the DORT method (with the canonical basis) when the scatterers are moving. Indeed, between the first and the last transmits needed to build the Time Reversal Operator, a given target moves. Therefore everything happens as if there were several targets: the first one corresponding to the initial position of the target, and the last one corresponding to the final position. As a consequence, even if only one scatterer is present in the medium, several non-zero eigenvalues are observed, as shown in Figure 50. This happens especially when the motion of the scatterer is lateral. In this case, the number of non-zero eigenvalues is equal to the lateral displacement of the scatterer, expressed in number of resolution lengths, between the first and last transmits. Indeed, if the target has moved the equivalent of 3 resolution lengths, the DORT method will *see* 3 different resolved scatterers (this problem is similar to the extended object problem developed in Chapter 3). Moreover, the ability of the method to separate different scatterers decreases (Figure 51). Finally, if the motion is important, the first eigenvector no longer looks like a point Green's function (Figure 52). This is because it corresponds to a combination of the Green functions corresponding to all the positions, which leads to interferences (again, this is similar to the extended object problem and is described in Chapter 3)

VI.B.2 Motivations

This problem is important, because in practice few targets stay still. In medical imaging, the body of a patient is constantly moving. The abdomen moves due to the breathing. Cardiac imaging is particularly affected by motion. A typical motion for the abdomen is 4 cm/s. In the heart, certain parts (like the valves) reaches speed over 20 cm/s (Lokke Gammelmark and Arendt Jensen 2003). This means that during one acquisition of the canonical Time Reversal Operator (about 1/30 s) the displacement of a scatterer can reach 5 mm!

In underwater acoustics, most of the targets are also moving. In addition, the medium itself is moving and therefore the Green's functions are changing over time. The case of an underwater wave-guide is found in (Folegot, Rosny et al. 2005).

A typical application of Time Reversal with moving scatterers is lithotripsy(Thomas and Fink 1998). A kidney stone is tracked in real time by iterative Time Reversal. After a few iterations of the iterative Time Reversal, one obtains the Green's function from the brightest scatterer (supposed to be the stone) The Green's function is then used to focus on the stone with an intense wave, and destroy it. If several bright scatterers other than the stone are present, it might be helpful to use the DORT method instead of an iterative Time Reversal.

VI.B.3 Solution

As we have seen in VI.A, the advantage of the focused beams is that only a limited number of beams are insonifying a given scatterer. For a scatterer at the focal depth, this is only 2 or 3 beams. For most other scatterers not too far from the focal depth, it is less than 10. This means that the time between the 1st and last transmits that insonify

a target is considerably reduced compared to the canonical method. Therefore the displacement of the scatterer is also reduced. In general, it can be reduced 10 times or more compared to the canonical method. If only a subset of transmits are used as explained in VI.A, it is possible to update the Green's function at a higher rate. However, the computing time necessary for the Fourier Transform and SVD is limiting the speed.

Simulation setup: An array with 7.3 Mhz center frequency has been simulated. In the 1st case, a single scatterer at depth 70 mm was simulated. It was moving with a lateral speed equal to 4 cm/s in a 1st case, and 20 cm/s in a 2nd case. These are observed speeds for motion in the human body. In a 3rd case, 2 scatterers located 3 mm apart were simulated. Both were moving with the same lateral speed of 4 cm/s. For each case, DORT (canonical basis) and FDORT (beam focused at 65mm, hybrid scheme) were performed. The results are displayed in the following figures.

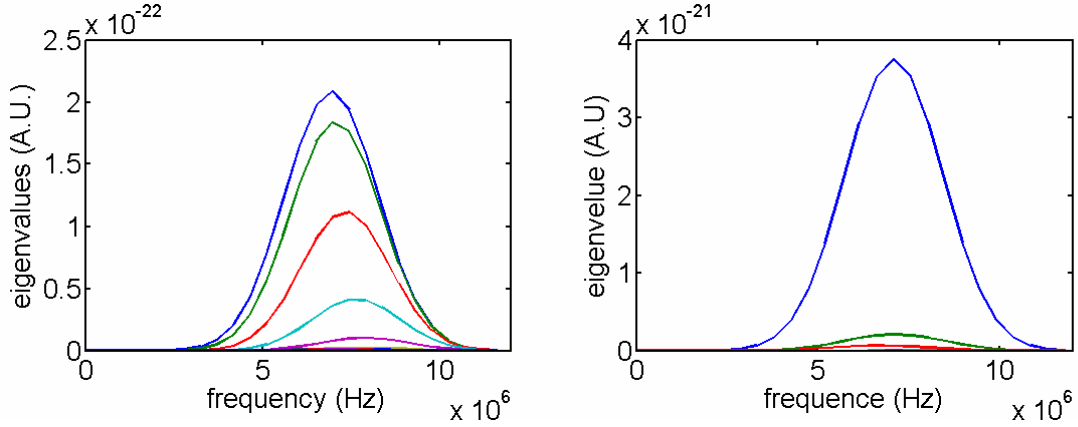

Figure 50 Single point-scatterer moving at 4 mm/s. With DORT (left) several non-zero eigenvalues are observed. With FDORT (right), only one significant eigenvalue is observed.

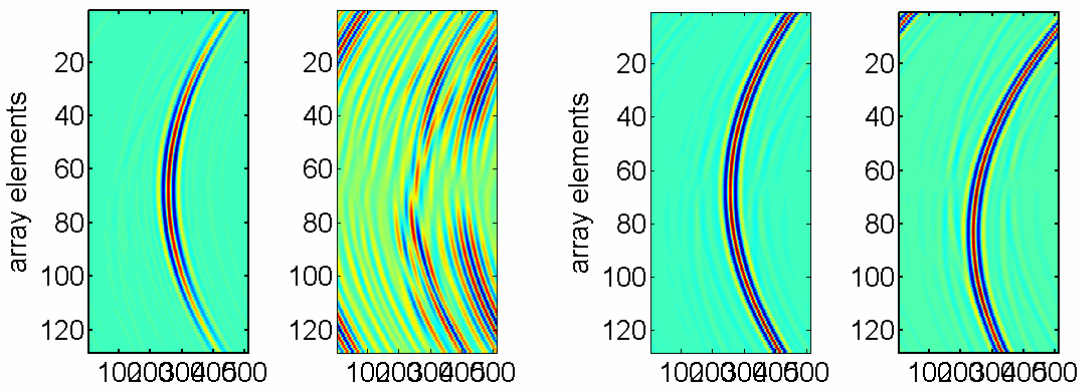

Figure 51 Two point-scatterers distant from 3 mm. With DORT (left), the 1st eigenvector correspond to the Green's function from one scatterer, but the 2nd eigenvector is a mixture of several signals corresponding to the 2 scatterers. With FDORT, the scatterers are well resolved, and the 2 first eigenvectors correspond to their respective Green's functions. This is what we would observe without motion.

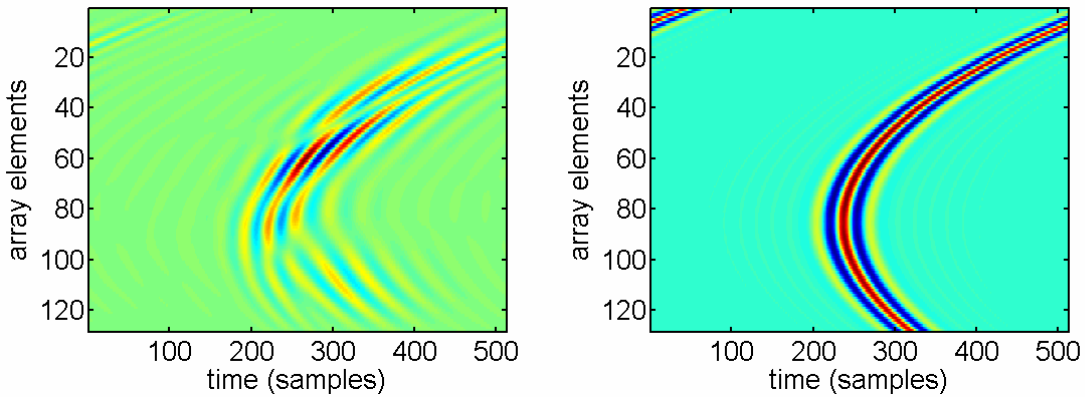

Figure 52 Single scatterer moving at 20 cm/s (typical speed in the heart). With DORT (left), the observed first eigenvector is due to interferences between Green's function for successive position of the scatterer. The FDORT method (right) is robust at such speed.

VI.C. Application to small objects detection

In Section V. we proposed gating the signal in depth to reduce coupling. In Section VI.A, it was shown how the method could be applied to a volume of limited

lateral dimension. Thus, using FDORT, we can specify the size of the volume where the method is performed: in azimuth by setting which transmits are processed, and in depth by setting the width of the time window. This can be used to perform a local FDORT method(Robert, Burcher et al.). An application of this algorithm is the detection of small objects.

One of the challenges of breast ultrasonic imaging is improved detection of small microcalcifications, which can be associated with cancer. Small microcalcifications are often hard to distinguish because of their small size and because they are embedded in speckle.

VI.C.1. Influence of the scatterer nature in the DORT method

When the scatterer size is less than a wavelength, the scatterer is associated with only one non-zero eigenvalue. However, for deterministic scatterers whose size is greater than a wavelength, two or more eigenvalues are observed[10]. The extended objects problem will be developed further in Chapter III.

A way of detecting small deterministic scatterers like the microcalcifications is to use the Local FDORT method and to consider the ratio of the first two eigenvalues. If a point scatterer is present at the location, the first eigenvalue is higher than the second one, and the ratio is dramatic. If there is only speckle or an extended reflector, like a cyst edge, the eigenvalues are of similar magnitude and the ratio is close to 1. Considering only the first eigenvalue is not enough, as it is proportional to the echogenicity (reflectivity) which is often greater for extended objects or even speckle; the ratio takes into account the size difference.

VI.C.2. The moving window FDORT

Local FDORT gives access to the local properties of the medium. Thus it gives the eigenvalues and the ratio of the eigenvalues at a specific location, the location of the window. To scan the medium, one needs to move the window at a series of locations. This can be done in depth by translating the time gate or in azimuth by changing the transmits processed. For example, the first window may use transmits 1 to 10, the second window transmits 2 to 11, and so on. For each location, the sizes of the windows are the same. Eigenvalues are computed for each position. This is the moving window FDORT.

VI.C.3. In vivo experiments and results

Experiments are carried out on clinical data. Acquisitions are performed on a healthy female volunteer, using a Philips HDI-5000 scanner with a 1-D linear array probe, at 7.3 MHz center frequency. Local FDORT is performed in a window whose dimension is $\Delta z = 0.7$ mm and $\Delta x = 1$ mm (5 transmits). The window is moved along the white line depicted on Figure 53.b at a constant depth, where a microcalcification has been identified, using a moving window FDORT. Figure 53.c shows the variation of the first eigenvalues versus azimuth, at the center frequency. Looking only at the first eigenvalue, which is proportional to the reflectivity, we cannot distinguish the microcalcification from the other scatterers. However, when considering the ratio λ_1/λ_2, in Figure 53.d, the microcalcification appears clearly. Averaging over several frequencies within the bandwidth improves the results. The process can be repeated for several depths, and a 2D color map can be plotted, but at significant computational cost.

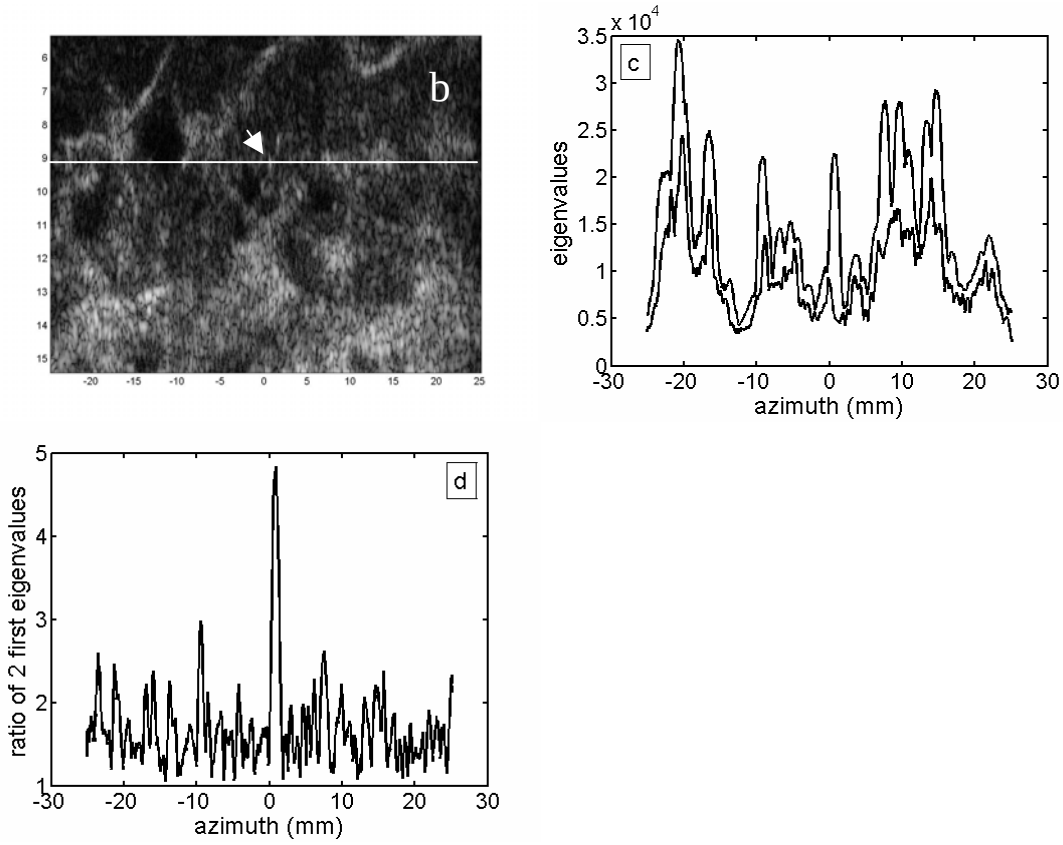

Figure 53 b) A scatterer identified as a microcalcification is shown by the white arrow. c) The first two eigenvalues are plotted versus the azimuth. The first eigenvalue is proportional to the echogenicity, but considering the second eigenvalue adds additional information. d) Ratio of the first two eigenvalues versus the azimuth: the position of the microcalcification is indicated by a high ratio.

Finally, the eigenvector corresponding to the identified microcalcification has been used in focusing. The resulting field in the medium has been computed and the results are displayed in Figure 54. This demonstrates the good focusing property of FDORT's eigenvectors in a clinical application.

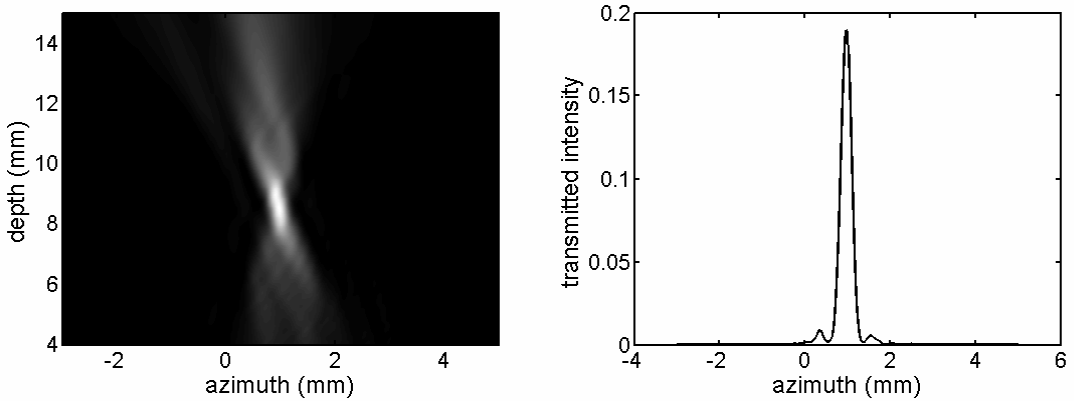

Figure 54 Focusing achieved in breast clinical data using a microcalcification as a point scatterer. The 1st eigenvector has been numerically backpropagated. Left: intensity of the resulting field. Right: intensity versus azimuth at the depth of the microcalcification.

VIII. CONCLUSION

We have seen how the FDORT method can be intuitively described by a Time Reversal process between the physical array and an array of virtual transducers located at the beams foci. With appropriate beams (phased or hybrid scan), the performance, in terms of scatterers resolution, is the same as the conventional DORT method. We give a condition in term of beam spacing for the beams to form an orthogonal basis.

The focused beams offer a few advantages compared to the original method. The SNR is better, and the problems due to targets motion are reduced, as only a reduced number of focused beams typically insonified a given scatterer.

An important application of the virtual transducers is the problem of the far-field phase screen. By choosing appropriately the location of the virtual transducers, one is able to transform the problem in a near-field phase screen problem. Focusing through the far-field phase screen on any point of the medium is now possible by steering from the

virtual array. It requires the knowledge of only one or two Green's function. Moreover, the virtual array model offers a solution to focus through the far-field phase screen using only two successive delay-and-sum operations instead of a full match-filter usually costly to implement.

A drawback of the DORT method is that it is a monochromatic approach, and therefore the resolution in depth is poor. A solution mixing monochromatic and broadband formalism is proposed. It is based on the relationship between time of arrival and depth, valid in the case of the focused beams. Spectacular results are obtained for the detection of targets embedded in speckle.

Finally, the focused beams are an efficient basis to use when the region of interest is small, because their energy is concentrated in space. In this case, only a few beams are necessary, and the method is faster. A local method taking advantage of theses properties has been designed for small objects detection.

REFERENCES

Angelsen, B. A. (2000). Ultrasound Imaging, Vol. I www.ultrasoundbook.com.

Dorme, C. and M. A. Fink (1996). "Ultrasonic beam steering through inhomogeneous layers with a time reversal mirror." Ultrasonics, Ferroelectrics and Frequency Control, IEEE Transactions on **43**(1): 167-175.

Fink, M. A. and J. F. Cardoso (1984). "Diffraction Effects in Pulse-Echo Measurement." Sonics and Ultrasonics, IEEE Transactions on **31**(4): 313-329.

Folegot, T., J. de Rosny, et al. (2005). "Adaptive instant record signals applied to detection with time reversal operator decomposition." Journal of the Acoustical Society of America **117**(6): 3757-3765.

Folegot, T., J. d. Rosny, et al. (2005). "Adaptive instant record signals applied to detection with time reversal operator decomposition." The Journal of the Acoustical Society of America **117**(6): 3757-3765.

Frieden, B. R. (1971). Evaluation, design, and Extrapolation methods for optical signals based on use of the prolate functions, North Holland publishing company.

Gammelmark, K. L. and J. A. Jensen (2003). "Multielement synthetic transmit aperture imaging using temporal encoding." Medical Imaging, IEEE Transactions on **22**(4): 552-563.

Goodman, J. W. Statistical Optics, Wiley Classics Library.

J.A.Jensen (1996). "Field: A program for simulating ultrasound systems." Med. Biol. Eng. Comp., col. 10th Nordic-Baltic Conference on Biomedical Imaging **4**(1): 351-353.

Jean-Francois, C. and F. Mathias (1991). "Echographic diffraction filters and the diffraction function for random media through an instantaneous time-frequency approach." The Journal of the Acoustical Society of America **90**(2): 1074-1084.

Jensen, J. A., O. Holm, et al. (2005). "Ultrasound research scanner for real-time synthetic aperture data acquisition." Ultrasonics, Ferroelectrics and Frequency Control, IEEE Transactions on **52**(5): 881-891.

Liu, D.-L. and R. C. Waag (1994). "Correction of ultrasonic wavefront distortion using backpropagation and a reference waveform method for time-shift compensation." The Journal of the Acoustical Society of America **96**(2): 649-660.

Lokke Gammelmark, K. and J. Arendt Jensen (2003). Duplex synthetic aperture imaging with tissue motion compensation.

Mallart, R. and M. Fink (1994). "Adaptive focusing in scattering media through sound-speed inhomogeneities: The van Cittert Zernike approach and focusing criterion." The Journal of the Acoustical Society of America **96**(6): 3721-3732.

Prada, C. and M. Fink (1994). "Eigenmodes of the time reversal operator: a solution to selective focusing in multiple-target media." Wave motion **20**: 151-163.

Prada, C., S. Manneville, et al. (1996). "Decomposition of the time reversal operator: Detection and selective focusing on two scatterers." The Journal of the Acoustical Society of America **99**(4): 2067-2076.

Prada, C., M. Tanter, et al. (1997). Flaw detection in solid with the D.O.R.T. method.

Robert, J.-L., M. Burcher, et al. (2006). "Time reversal operator decomposition with focused transmission and robustness to speckle noise: Application to microcalcification detection." The Journal of the Acoustical Society of America **119**(6): 3848-3859.

Slepian, D. and H. O. Pollack (1961). "Prolate spheroidal wave functions,Fourier analysis and uncertainty, I." Bell Syst. Tech. J. **40**: 43-64.

Thomas, J. L. and M. Fink (1998). "Stone tracking with time-reversal techniques." The Journal of the Acoustical Society of America **103**(5): 3071-3071.

Trees, H. V. (2002). Optimum Array Processing - Detection, Estimation, and Modulation Theory, Wiley-Interscience.

UNSER, M. (2000). "Sampling- 50 years after shannon." Proceedings of the IEEE **88**(4): 569-587.

Chapter 3. Extended Objects

I. INTRODUCTION

In the case of rigid point-scatterers, the DORT theory is well understood: the number of non-zero singular values is equal to the number of scatterers, and the singular vectors correspond to the scatterers Green functions. A scatterer is considered poine-like if its size is much smaller than the resolution cell, $\lambda Z / L$, where L is the size of the imaging aperture, and Z the depth of the scatterer. In media like biological tissue, there are virtually no point-scatterer. Example of scatterers (except speckle, which will be reviewed in Chapter 4) includes vessels, microcalcifications, or kidney stones. These scatterers are typically the size of one or a few resolution cells.

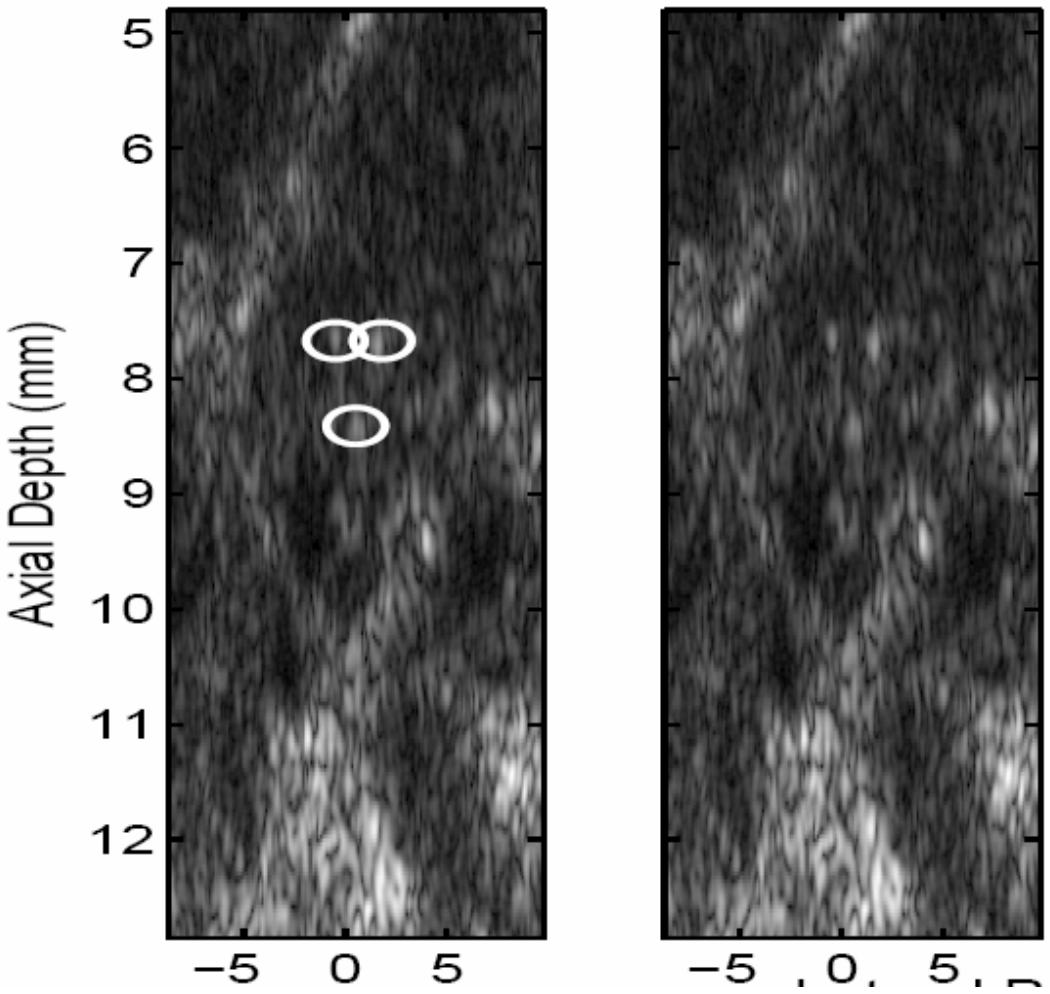

Figure 55 Microcalcifications in the breast (shown by circle in the left panel)

Microcalcifications in the breast are particularly important because they can be associated with cancerous cellular activity. Usually, the presence of a single microcalcification is not alarming, but the presence of a cluster of microcalcifications can be a serious symptom. It is usually hard to differenciate a clutter from a single microcalcification with ultrasound, because microcalcifications have typically the size of the resolution cell.

The amplitude of the DORT matrix eigenvectors obtained in-vivo for a microcalcification are shown in Figure 56,and the amplitude of the numerically backpropagated fields are shown in Figure 57.

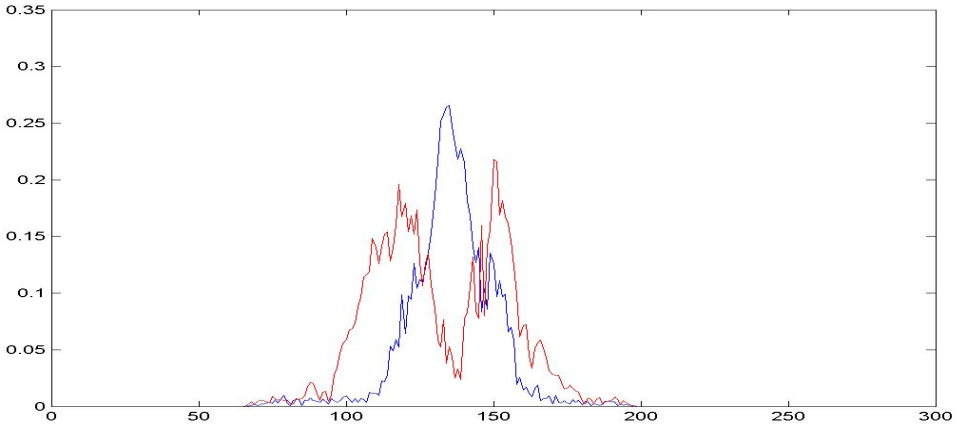

Figure 56 Amplitude (in arbitrary units) of the two first singular vectors for an in-vivo microcalcification.

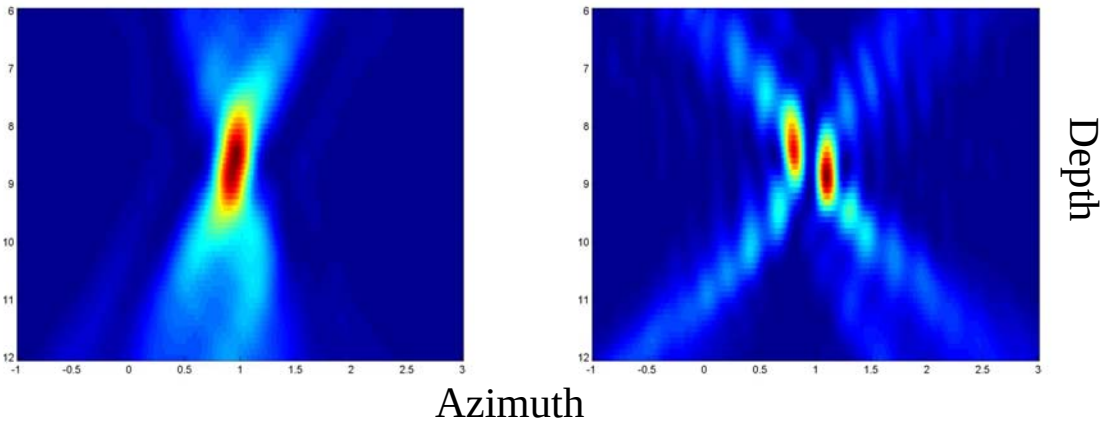

Figure 57 Amplitude of the fields obtained by numerical backpropagation of the two singular vectors.

This chapter does not focus only on Green's function estimate, but rather on different applications of the DORT (or FDORT that gives similar results) with regard to

extended objects in medical imaging. After presenting a theory for small rigid objects, we will review the applications to tomography and microcalcification diagnosis.

A theory of DORT with cylindrical objects has been proposed by inver. He proposes a solution based on Hermite-Gaussian modes for scatterers much larger than the resolution cell, and a solution based on Legendre polynomials for scatterers whose size is about the resolution cell. Our analyze is based on slightly different approximations and on a flat objects, and yield the Prolate Spheroidal Functions as solutions in both cases. We will show that asymptotically, our solutions tend to *Aubry et al.* solutions.

II. THEORY

II.A Expression of the time reversal operator for an extended object

II.A.1 Continuous formalism

For any given frequency, the signal R received by the array is linked to the transmit signal E by the transfer matrix K

$$R = KE$$

Eq.3. 1

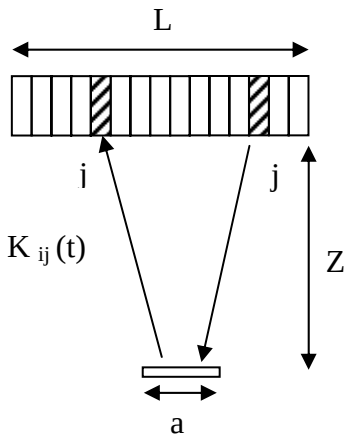

Figure 58 Set-up

The time reversal operator is defined by KK^H. The invariants of the time reversal operator are practically the singular vectors of *K*. Eq.3. 1 can be rewritten with explicit summation.

$$R_i = \sum_{j=1}^{N} K_{ij} E_j$$

Eq.3. 2

where *N* is the number of elements. Using a continuous formalism is easier in our case. We introduces X_T and X_R, the coordinates of a point of the array, resp. in transmission and in reception. The equation becomes

$$R(X_R) = \int_{-L/2}^{L/2} K(X_R, X_T) E(X_T) dX_T$$

Eq.3. 3

where $K(X_R, X_T)$ is called the *Kernel* of the integral equation, and is the equivalent of the matrix *K* in discrete formalism. The matrix coefficients are then given by $K_{ij}=K(X_i,X_j)$ where i and j are 2 array elements. The discrete and continuous problem are equivalent if the sampling requirements are met, which is the case in most arrays.

II.A.2 Kernel in the Fresnel approximation

The Kernel can be derived easily in the case of the Fresnel approximation (see Chapter 3.III.A.2). The derivations are done in Appendix. For an object whose scattering distribution is *d(x)*, we find that the kernel is given by

$$K(X_R, X_T) = e^{j\frac{2\pi X_R^2}{\lambda Z}} e^{j\frac{2\pi X_T^2}{\lambda Z}} FT^{-1}\left\{ d(x) e^{j\frac{4\pi x^2}{\lambda Z}} \right\}\left[\frac{X_R + X_T}{\lambda Z} \right]$$

Eq.3. 4

where FT^{-1} stands for the inverse Fourier Transform. The term $FT^{-1}\left\{ d(x) e^{j\frac{4\pi x^2}{\lambda Z}} \right\}\left[\frac{X_R + X_T}{\lambda Z} \right]$ is the Fresnel transform of the object scattering distribution (The Fresnel transform of a function *f(x)* being defined as $\int E(X) e^{j\frac{2\pi X^2}{\lambda z}} e^{j2\pi\frac{xX}{\lambda z}} dX$) Basically, the amplitude of the kernel is given by the Fresnel transform of the object. The amplitude depends only on $X_R + X_T$ (anti-Toeplitz), which gives the particular symmetry of the matrix (see Figure 59).

II.A.3 Kernel for objects of size a< $\sqrt{\lambda Z}$

For an object small enough, $FT\left\{ d(x) e^{j\frac{2x^2}{\lambda Z}} \right\}\left[\frac{X_R + X_T}{\lambda Z} \right]$ may be approximated by $FT\{d(x)\}\left[\frac{X_R + X_T}{\lambda Z} \right]$. Indeed the variation of the parabolic phase term is negligible over a short distance. This approximation is known as the Fraunhoffer approximation, and will be considered true for the remaining of the derivations. We are assuming the Fraunhoffer approximation in the object plane only, and not for the array plane. The

condition for the object size is $a^2 < \lambda Z$. A typical depth in medical ultrasound is *Z=50mm*, and a typical wave-length ranges from λ*=0.2mm* (linear arrays) to λ*=0.5mm* (phased arrays). In practice, we had a good fitting between theory and simulation results for objects was *a<4mm* (linear arrays) or *a<10mm* (phased). The approximation is validated for most scatterers present in medical ultrasound. Therefore, Eq.3. 4 becomes

$$K(X_R, X_T) = e^{j\frac{2\pi X_R^2}{\lambda Z}} e^{j\frac{2\pi X_T^2}{\lambda Z}} FT^{-1}\{d(x)\}\left[\frac{X_R + X_T}{\lambda Z}\right]$$

Eq.3. 5

The amplitude of the kernel is given by the Fourier Tranform of the object.

We also assume that the object has a rectangular scattering distribution (1 inside the object, 0 outside). Its Fourier transform is then a *sinc* function. Under the Fraunhoffer approximation, and for a rectangular object, the expression of the kernel simplifies to

$$K(X_R, X_T) = e^{j\frac{2\pi X_R^2}{\lambda Z}} e^{j\frac{2\pi X_T^2}{\lambda Z}} \operatorname{sinc}\left[\frac{\pi a(X_R + X_T)}{\lambda Z}\right]$$

Eq.3. 6

The amplitude of the kernel for an object that met the Fraunhofer condition and for a larger object are shown in Figure 59 and Figure 60.

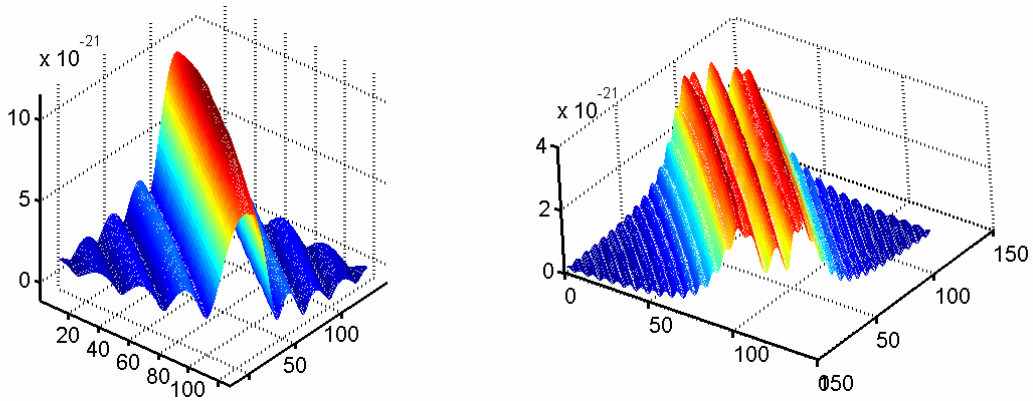

Figure 59 Left: Amplitude of the *K* matrix for an object of size a, such as $a^2 < \lambda Z$ (Fraunhofer approximation). In this case, the Fresnel transform simplifies to a simple Fourier transform. For a rectangular object, this yields a sinc. Right: Same for a larger object (a^2=64mm, while λZ=10mm) The phase term in the Fresnel transform can no longer be neglected.

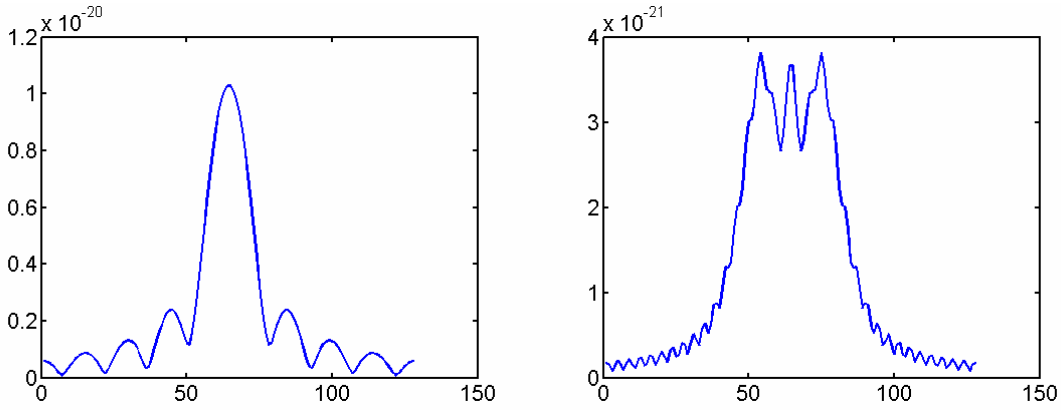

Figure 60 **Amplitude along the diagonal in the 2 cases of** Figure 59**, the sinc pattern (left) and Fresnel transform of a square aperture pattern (right) are obvious.**

II.B Invariants of the Time Reversal Operator: The Prolate Spheroidal functions

Finding the invariants of the time reversal operator is equivalent to computing the singular functions of the kernel K. In continuous formalism, the singular functions of the

Kernel are a set of functions *E(X)* and *R(X)* constituting an orthonormal basis of the transmit, resp. receive, arrays, and such that

$$\mu R(X_R) = \int_{-L/2}^{L/2} K(X_R, X_T) E(X_T) dX_T$$

Eq.3. 7

where μ is the associated singular value. Using Eq.3. 6, we obtain

$$\mu R(X_R) e^{j\frac{-X_R^2}{\lambda Z}} = \int_{-L/2}^{L/2} \mathrm{sinc}\left[\frac{\pi a(X_R + X_T)}{\lambda Z}\right] E(X_T) e^{j\frac{X_T^2}{\lambda Z}} dX_T \qquad -L/2 < X_R < L/2$$

Eq.3. 8

The equation can be solved by choosing a function *W(X)* such as *W(X)=* $R(X)e^{j\frac{-X^2}{\lambda Z}} = E(-X)e^{j\frac{X^2}{\lambda Z}}$; Eq.3. 8 becomes

$$\begin{aligned}\mu W(X_R) &= \int_{-L/2}^{L/2} \mathrm{sinc}\left[\frac{\pi a(X_R + X_T)}{\lambda Z}\right] W(-X_T) dX_T \\ &= \int_{-L/2}^{L/2} \mathrm{sinc}\left[\frac{\pi a(X_R - X_T)}{\lambda Z}\right] W(X_T) dX_T\end{aligned} \qquad -L/2 < X_R < L/2$$

Eq.3. 9

Eq.3. 9 is a well-studied Fredholm equation of 2nd order, with hermitian kernel, and the solutions have been found by Slepian {slepian} They are called the Prolate Spheroidal Wave-functions. These functions have also been studied in optics (Goodman 1975; Goodman 1985) (Frieden 1971) in problems closest from the present one. They depend on only one parameter, $N = \frac{La}{\lambda Z}$, which can be interpreted as the number of resolution cell in the objects. (Boyd 2004) provides a good mathematical overview.

The main result is that the number of non-zeros singular values is proportional to the parameter N , in our case, the number of resolution cells that fit in the object. This is an intuitive result. More precisely, the *N* first singular values are equal, and the following singular values drop rapidly to zero.

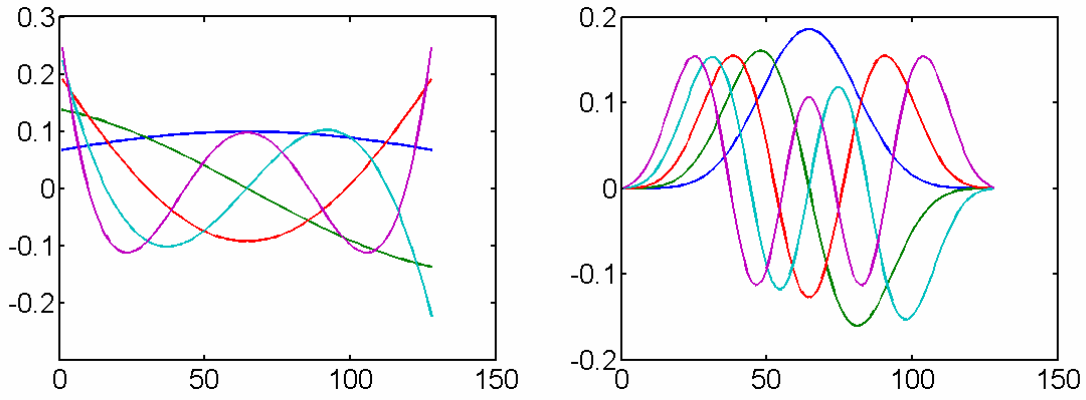

Figure 61 Five first Spheroidal Prolate function for *N=1 (left)* and *N=10.*

The singular vectors (the Prolate Spheroidal functions) have the interesting properties to be the invariants of the Finite Fourier Transform, in other words, eigenvectors in the array space or in the object space have the same shape.

They are the natural basis of the space of simultaneously band-limited and time-limited functions. No functions can be completely band-limited and time-limited at the same time, but the Prolates are the closest functions to be. They are the most concentrated simultaneously in time and frequency. This is why there are of such interest in information theory, signal processing or optics. The consequence of this property in our application is that they maximize the concentration of energy simultaneously in the array plane and the object plane.

The invariants of the Time Reversal Operator are derived from the Prolate functions using:

$$R_i(X) = W_i(X)e^{j\frac{X^2}{\lambda Z}} \qquad E_i(X) = W_i(-X)e^{j\frac{-X^2}{\lambda Z}} = W_i(X)e^{j\frac{-X^2}{\lambda Z}}$$

Eq.3. 10

where $W_i(X)$ is the i^{th} Prolate function, and the last equality is due to the symmetry of the functions.

The phase of the singular vectors corresponds then to a focusing on the object.

These results are valid for small objects, such as $a^2 < \lambda Z$. This is the case for most objects encountered in medical imaging. Solution for larger objects are discussed in Appendix B.

III. RESULTS

III.A. Results with a one-dimensional array

III.A.1 Object with N=10

An extended object has been simulated with field II. The parameters were the following: λ=0.2*mm* (center frequency), *a=4mm, Z=50mm and L=25mm.* Therefore *N=10.*

The theoretical singular values are compared with the simulation results in Figure 62. There is a good agreement between theory and simulation. In simulation, the singular values start decreasing earlier, which is likely due to the directivity. The directivity could be taken into account using perturbation theory (Aubry, Rosny et al. 2006). It confirms that the number of non-zero singular values is about *N.*

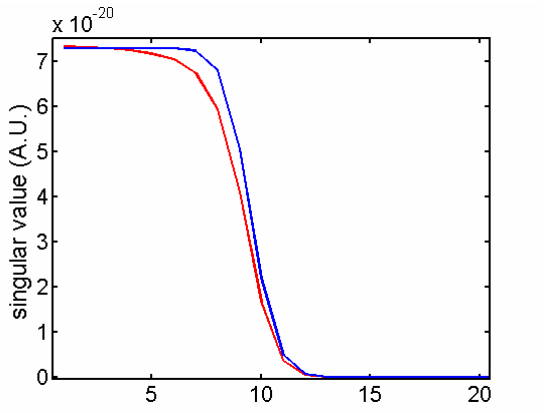

Figure 62 Analytical (blue) and simulated singular values for an object with *N=10*.

It is also interesting to look at the evolution of the singular values with the frequency in Figure 63. The number of non-zero singular values increases versus the wavelength. This is obvious in Figure 63 (right) where the singular values have been normalized by the 1st one to get rid of the effect of the bandwidth. This is a typical property of Prolate functions (Goodman 1985). This is in agreement with the fact that the resolution increases with the frequency. Thus more resolution cell fits in the objects.

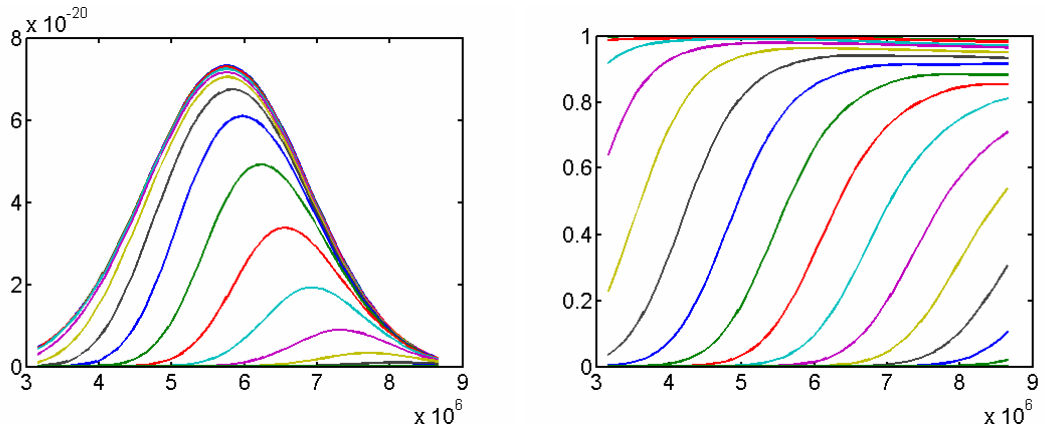

Figure 63 Singular values in function of the frequency. On the right panel, the singular values have been normalized to get rid of the bandwidth effect. As the frequency increases, more points are resolved in the object.

A few singular functions obtained in simulation are compared to the Prolate functions (analytical solutions) in Figure 64.

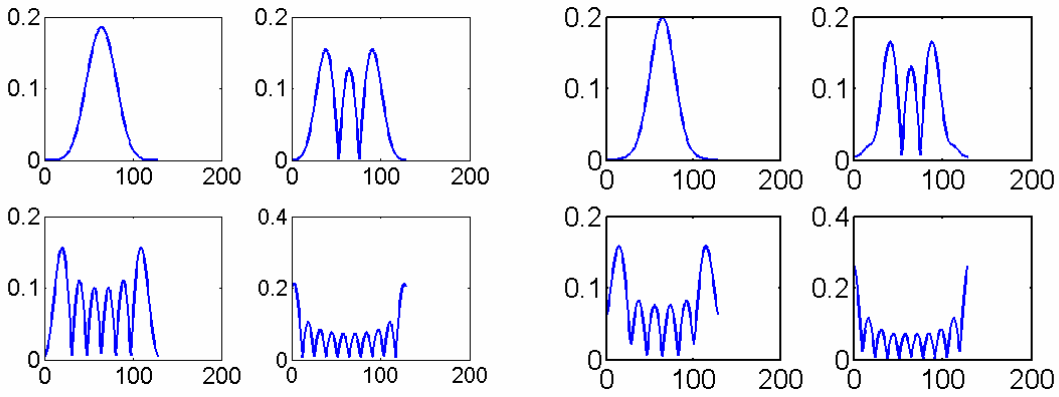

Figure 64 Left: Analytical results, the Prolate functions for *N=10* (*1st, 3rd, 6th and 10th are shown)* Right: simulation results.

Note: It is not always easy to observe the prolate with a rectangular objects, as all the singular vectors have identical singular values. We often observe a mixture.

III.A.2 Scatterer whose size is about the resolution cell (N=1) "resonance region"

Another important case are the scatterers whose size is just about the wave-lengths. They are particularly hard to characterize on an image. This is the case for the micro-calcifications. An example with *N=1.2* is shown in Figure 65 and Figure 66.

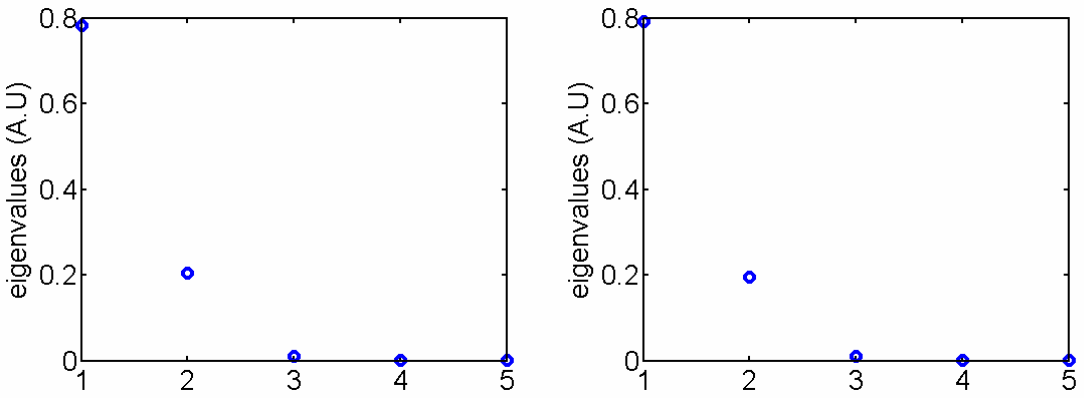

Figure 65 Analytical (left) and simulated (right) singular values for an object in the so-called resonance region (about the size of the resolution cell) *N=1.2* in this case. One singular value is dominant but a second singular value has also a relatively large value. This 2nd singular value is important to characterize the shape of the object.

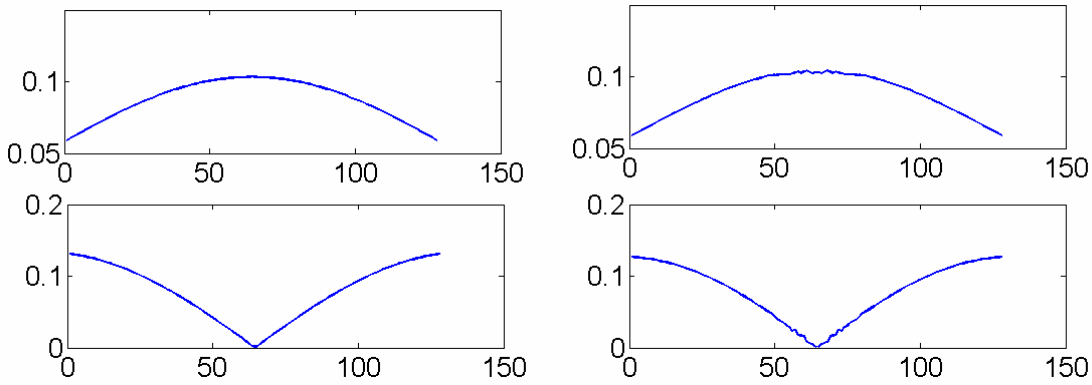

Figure 66 Amplitude of the first two invariants for *N=1.2*. Analytical solutions (left) and simulated (right). The agreement is almost perfect.

III.B Application to Green's function estimation and focusing

As seen Eq.3. 10, the solution in homogeneous medium, is the homogeneous Green's function modulated by the Prolate functions. The amplitude modulation originates from the interferences between several points of the object. The same results can be generalize to a heterogeneous medium, if the isoplanatic patch is about the size of the object. In this case, the invariants become

$$R_i(X) = W_i(X)e^{j\left(\frac{X^2}{\lambda Z}+\phi\right)} \qquad E_i(X) = W_i(X)e^{j\left(\frac{-X^2}{\lambda Z}-\phi\right)}$$

Eq.3. 11

Where ϕ is the phase term due to the heterogeneity.

As a result of the amplitude modulation, the Green's function cannot be estimated as precisely from extended object as from point scatterers. For example, if one considers the 1st invariant, one will have a good estimate of the Green's function in the central elements where the amplitude is important, but no estimate for the outer elements where the amplitude is zero.

If the object is relatively small, say one or two resolution cells, the width of the amplitude function is still close to the array width, as seen in Figure 66 and the effect is negligible. The 1st invariant can be considered almost as a point Green's function. The focusing is illustrated in Figure 67, where the field resulting from the backpropagation of the 4 first invariants for the small objects are shown. The 1st invariant leads to a sharp focus. The same result is obtained in presence of an aberration.

For larger object, a loss of resolution is occurred, because of the narrow amplitude factor seen in Figure 64. As a results, the focal spot obtained by time reversal

of the 1st invariant is broad (Figure 68). The large is the object, the broader is the focal spot.

Moreover, if the object is not flat but has a complex shape, the kernel of Eq.3. 9 is no longer a sinc, and the solution *W* will likely be complex, and not real like the prolate. In this case, the phase of the invariants will be equal to the phase of the Green's function plus the phase of *W*, according to Eq.3. 10. The phase estimate is then biased.

To conclude, an extended object can still be used to estimate Green's function if its size is relatively small, but larger objects, especially if they have a complex shape, may introduce an error in the estimate.

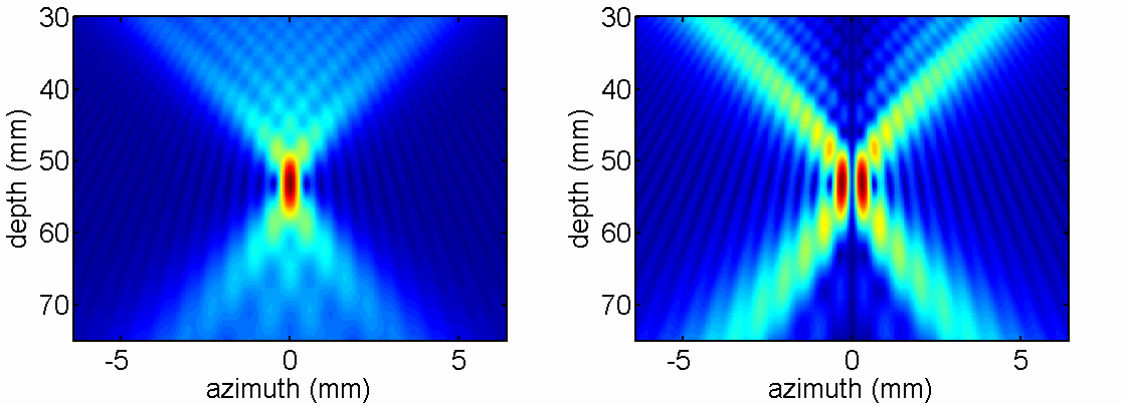

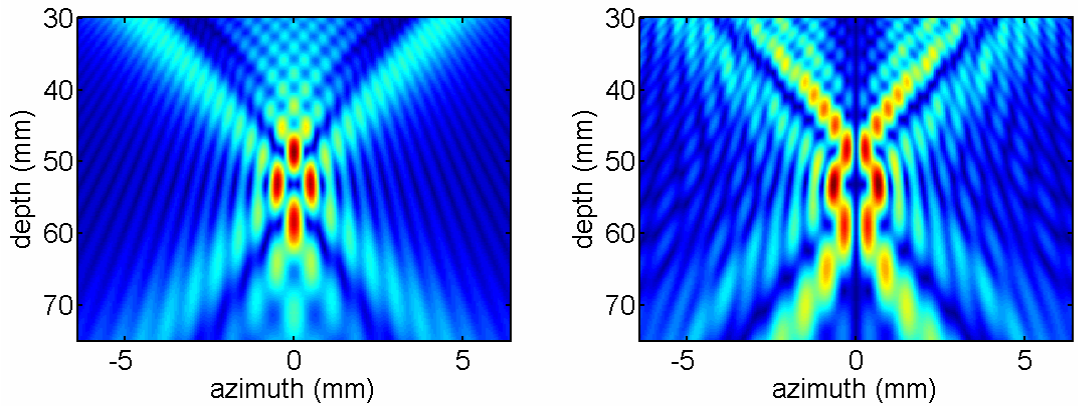

Figure 67 Field resulting from the backpropagation of the first four invariants for the small object (resonance region) The 1st invariant (top left) yield a focusing comparable to the Green's function of a point. The other invariants cannot be used for focusing because of the lobes.

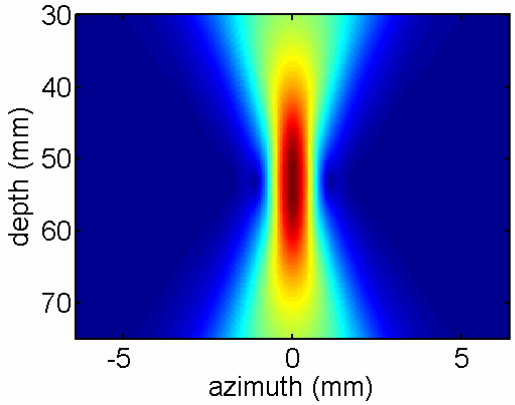

Figure 68 Backpropagation of the 1st invariants for the object with *N=10*. The resolution is not suitable.

III.B Results with a 2D array

Most of the new medical probes are 2D-array that image a 3D volume. It is interesting to look at the analytical solutions for some 3D objects.

The solutions have a simple form if the object scattering distribution is separable in Cartesian coordinates $d(x,y) = d(x)d(y)$. This is the case, for example, for a wire aligned with one of the array directions (we have then $d(x,y) = \delta(x)1(y)$) or for a

rectangular plate ($d(x, y) = box(x)box(y)$, where box is the box function) Indeed, in that case, the kernel is also separable (property of the Fourier Transform) For symmetry reason, the solutions are separable too, and we have $R(X,Y) = R_X(X)R_Y(Y)$, where R_X and R_Y are solutions to the respective 1D equations, and $E(X,Y) = E_X(X)E_Y(Y)$. This is derived in Appendix B.

The number of singular values is Nx*Ny ie the number of 2D resolution cells in the object.

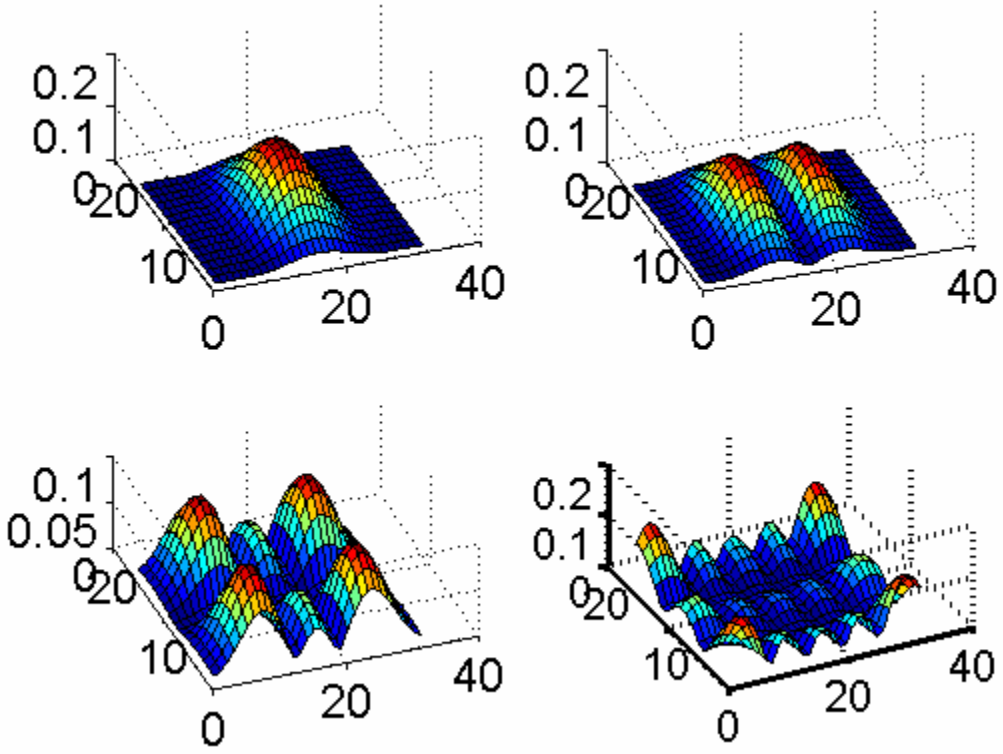

Figure 69 Selected invariants for a simulated rectangular plate imaged with a 2D array. The object size was roughly 5 resolution cells in azimuth * 3 resolution cells in elevation. The invariants can be described by a cartesian product of Prolate functions. Here are shown the modes (1,1), (1,2), (2,3), and (3,5).

.

IV. COMPARISON WITH PREVIOUS WORK

(Aubry, Rosny et al. 2006) have proposed a solution based on Hermite-Gaussian modes for scatterers much larger than the resolution cell (when the edge effect of the array are negligible), and a solution based on Legendre polynomials for scatterers whose size is about the resolution cell (in this case the edge effect is dominant).

We can find these functions as asymptotic limit of our solutions. Indeed, for a small parameter N (the number of resolution cell in the object), or near the edges, the Prolate functions can be approximated by Legendre Polynomials(Boyd 2004).

Similarly, for large N, the Prolate functions can be well approximated by Hermite-Gaussian modes, with a width equal to $1/\sqrt{N}$.

$$W_i(X) \approx e^{-N\frac{X^2}{2}} H_i(\sqrt{N}X)$$

However, the solutions based on Hermite Gaussians seem to be valid also for larger scatterers that do not met the Fraunhofer approximation. They cover the solutions derived in Appendix B. Also the Hermite-Gaussian modes in (Aubry, Rosny et al. 2006) are derived for a cylindrical object, which influences the width of the modes.

The prolate are better solutions for the scatterers in the Fraunhoffer regimen, in particular in the transition region between Legendre and Hermite-gaussian solutions. Moreover, the results about the number of non-zero eigenvalues could not be derived in (Aubry, Rosny et al. 2006) because the finite size of the array is not taken into account.

V. APPLICATIONS: SUPER-RESOLUTION, TOMOGRAPHY AND MICROCALCIFICATION DIAGNOSIS

The problem with image in the resonance region (about the resolution cell) is that they are difficult to differentiate from pure point-scatterers on a conventional image. This is backed up by the fact that they have one dominant singular values. However, the other singular-values, even tough they are small, are not completely equal to zero and carry information on the object size and shape (the 2^{nd} singular value is obviously non-zero, but even the following singular values are non-zero when plotted on a logarithmic scale). The aim of inverse methods is to use and amplify the information in the others singular vectors. The more singular vectors can be used and the better the resolution is. However, the singular values become so small at some point, that the noise limits the possible resolution. Also, the accuracy of the model of the medium used in the reconstruction seriously limits the resolution. The inverse methods do not allow to reconstruct the missing information lost during the propagation (high spatial frequencies), and do not violate the law of physics. Rather, they work by assuming additional information on the object, in general that the edges are sharp.

Most inverse methods are based on the decomposition of the Covariance matrix, and a link between Covariance matrices and Time Reversal Operator has been done in (Gruber, Marengo et al. 2004) Therefore, the methods can be used directly with the time Reversal Invariants. A general reference for array processing algorithm is (Trees 2002) One of the algorithm is the minimum variance, also known as Capon, algorithm. An expression of the Minimum Variance algorithm using DORT's eigenvector is given in (Prada and Thomas 2003) As an illustration, the minimum Variance method has been

used with the small scatterer in the resonance region. The profile at the focal depth has been reconstructed using the usual backpropagation method , and with the Minimum Variance method (Figure 70)

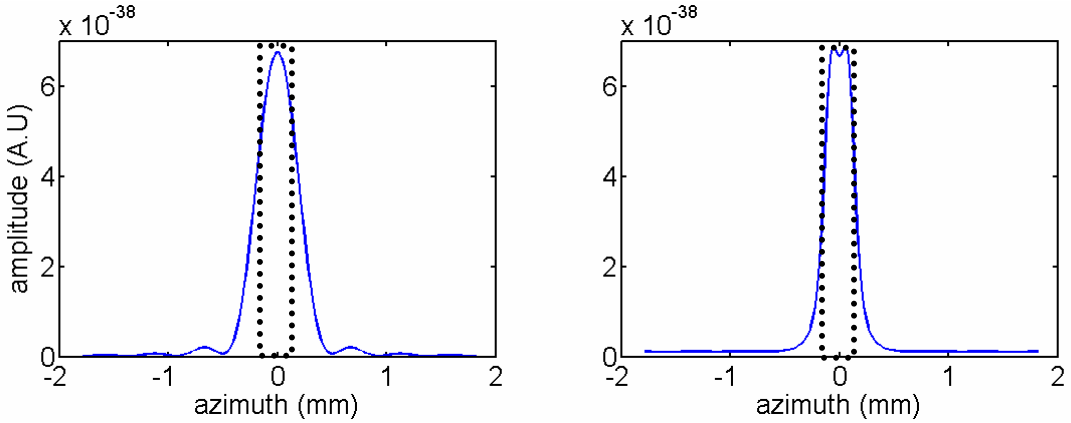

Figure 70 Profile of the object at center frequency. It is the object convolved by the beam pattern (sinc). It is then a low-pass filtered version of the object (the propagation act as a lo-pass filter) Right: profile obtained with the minimum variance algorithm. The real object is in dash line.

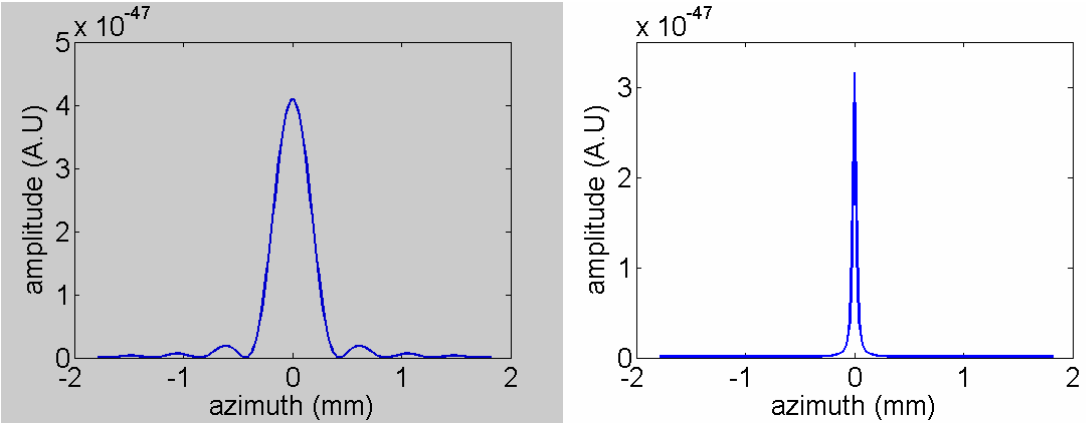

Figure 71 Same as Figure 70, but for a point scatterer. With the conventional profile, it is very difficult to make the difference between the point and the extended object. With the Minimum variance method, the difference is obvious, and it is easy to asset the size of the scatterer.

These methods are good to increase the resolution in the azimuth dimension, but not in the depth dimension (they are monochromatic methods). This is why some researchers use them with an enclosing array, or cavity, in a setup similar to tomography.

(Mast, Nachman et al. 1997; Waag, Liu et al. 1997) use a formalism similar to our (but in spherical coordinate and plane wave approximation) Their inverse method is also based on variance minimization, and account for multiple scattering. More recent work account for heterogeneities (Waag 2006). High resolution images of phantom are shown. (Lewis, Liu et al. 2006) used an advanced inverse scattering method from the electromagnetic inverse community to determine the shape of microcalcifications and differenciate between clutter and single microcalcification. Simulation in homogeneous medium are impressive, but in-vivo applications are much more challenging.

VI. CONCLUSION

The invariants of the Time Reversal Operator for a small flat object whose size *a* is such as $a^2 < \lambda Z$, are the Prolate Spheroidal functions. The number of non-zero singular values is roughly equal to the number of resolution cells in the object.

If the object is small enough (a few resolution cells), the 1st invariant is a good estimate of the Green's function. For larger objects, the estimate is only good for central elements and a loss of resolution occurs.

The main application of Time Reversal Invariants in medical imaging is the characterization of small scatterers. Indeed, the invariants can be used in inverse filtering methods that allows a reconstruction of the objects with higher resolution. This is especially promising for microcalcifications characterization, which remains a challenge of ultrasound imaging.

APPENDIX A: DERIVATION OF THE KERNEL

Let X_T , resp. X_R be the coordinate in the array plane for the transmit, resp. the receive, process, and x the coordinate in the object plane. Let d(x) be the scattering distribution of that object. The derivation is done under the Fresnel approximation (see Chapter 3.III.A.2) First, a signal E(X) is transmitted by the array. Using the Fresnel approximation, (valid for x<<Z and X<<Z) the pressure field $P_i(x)$ received by the object is

$$\begin{aligned} P_i(x) &= \frac{e^{j2\pi\frac{Z^2+x^2}{\lambda Z}}}{Z}\int_{aperture} E(X_T)e^{j\frac{X^2}{\lambda Z}}e^{j2\pi\frac{xX}{\lambda Z}}dX \\ &= Ke^{j\frac{x^2}{\lambda Z}}FT\left\{E(X_T)e^{j\frac{X_T^2}{\lambda Z}}\right\}\left[\frac{x}{\lambda Z}\right] \end{aligned} \qquad (1)$$

where $K = \frac{e^{j2\pi\frac{Z^2}{\lambda Z}}}{Z}$ depends only on Z, and $FT[\ ]_{fx=\frac{x}{\lambda Z}}$ stands for the Fourier transform at frequency $x/\lambda Z$. The pressure backscattered by the object, expressed in the object plane at depth Z, is given by

$$P_b(x) = d(x)P_i(x) \qquad (2)$$

and finally the signal received by the array is given by the Fresnel transform of $P_b(x)$

$$\begin{aligned} R(X_R) &= Ke^{j\frac{X_R^2}{\lambda Z}}FT\left\{P_b(x)e^{j\frac{x^2}{\lambda Z}}\right\}\left[\frac{X_R}{\lambda Z}\right] \\ &= K^2e^{j\frac{X_R^2}{\lambda Z}}FT\left\{d(x)e^{j\frac{2x^2}{\lambda Z}}FT\left\{E(X_T)e^{j\frac{X_T^2}{\lambda Z}}\right\}\left[\frac{x}{\lambda Z}\right]\right\}\left[\frac{X_R}{\lambda Z}\right] \end{aligned} \qquad (3)$$

Using the relationship relating the Fourier Transform of a product of functions to the convolution product of the Fourier transform of the functions, noting that

$$FT\left\{FT\left\{E(X_T)e^{j\frac{X_T^2}{\lambda Z}}\right\}\left[\frac{x}{\lambda Z}\right]\right\}\left[\frac{X_R}{\lambda Z}\right] = E(-X_R)$$ and not $E(X_R)$ as the second transform is

not an inverse Fourier Transform, and omitting the factor K yields

$$R(X_R) = e^{j\frac{X_R^2}{\lambda Z}}\int_{-L/2}^{L/2} FT\left\{d(x)e^{j\frac{2x^2}{\lambda Z}}\right\}\left[\frac{X_R + X_T}{\lambda Z}\right]E(X_T)e^{j\frac{X_T^2}{\lambda Z}}dX_T \qquad -L/2 < X_R < L/2 \quad (4)$$

Finally

$$K(X_R, X_T) = e^{j\frac{X_R^2}{\lambda Z}}e^{j\frac{X_T^2}{\lambda Z}}FT^{-1}\left\{d(x)e^{j\frac{2x^2}{\lambda Z}}\right\}\left[\frac{X_R + X_T}{\lambda Z}\right]$$

APPENDIX B: LARGER OBJECTS

If the objects become to large (or its curvature does not cancel it), it is no longer possible to ignore the phase term in $FT\left\{d(x)e^{j\frac{2x^2}{\lambda Z}}\right\}$. In this case, the kernel of Eq.3. 7 is no longer the Fourier Transform of the object, but its Fresnel Transform. It is not easy to derive the new analytical solutions, but, intuitively, they are very close to be the Fresnel transform of the Prolate functions, at least for the first functions, that are not localized on the edge. In the following we are then neglecting the array edge effect, which is an approximation done in {Aubry} to derive the Hermite-gaussian solutions.

Indeed, let's take $W_1(x)$, the 1st Prolate function. Its Fresnel transform can be chosen to be $\tilde{W}_1(X) = FT^{-1}\left\{W_1(x)e^{j\frac{-x^2}{\lambda Z}}\right\}[\frac{X}{\lambda Z}]$ (9)

The amplitude of the Fresnel transform is still the 1st Prolate function, but dilated REFERENCE. Thus, if the phase term is not varying very fast, we can consider that $\tilde{W}_1(X)$, the Fresnel transform of $W_1(X)$ (the prolate in the object plane) will still be a function concentrated in the array plane. Let assume that $E(X) = \tilde{W}_1(X) e^{j\frac{-X^2}{\lambda Z}}$ is transmitted with the array. Then, in the object plane, the field is proportional to

$$P_i(x) = e^{j\frac{x^2}{\lambda Z}} FT\left\{\tilde{W}_1(X)\right\} \tag{10}$$

using eq(1). We have neglected the effect of the finite-size of the aperture, using the assumption that the function was concentrated in the aperture. Using (9) the field becomes

$$P_i(x) = W_1(x) \tag{11}$$

and using eq(3), the signal received by the array would be:

$$\begin{aligned} R(X) &= e^{j\frac{X^2}{\lambda Z}} FT\left\{W_1(x) e^{j\frac{x^2}{\lambda Z}}\right\}\left[\frac{X}{\lambda Z}\right] \\ &= e^{j\frac{X^2}{\lambda Z}}\left[FT\left\{W_1(x) e^{j\frac{-x^2}{\lambda Z}}\right\}\left[\frac{-X}{\lambda Z}\right]\right]^* \\ &= e^{j\frac{X^2}{\lambda Z}}\left[FT^{-1}\left\{W_1(x) e^{j\frac{-x^2}{\lambda Z}}\right\}\left[\frac{X}{\lambda Z}\right]\right]^* \\ &= E(X)^* \end{aligned} \tag{12}$$

We have used the fact that $W_1(x)$ was real and concentrated in the object. For the 1st inequality we use the formula $FT\{f(x)^*\}[X] = FT\{f(x)\}[-X]^*$, and for the 2nd equality we replace the Fourier Transform evaluated for -X by the inverse Fourier transform evaluated for –X. If we time reverse the received signal, we see that the proposed solution is an invariant of the time reversal process. For the functions on the edge, the derivation is no longer exactly valid; indeed because of the dilatation property of the Fresnel transform, the Fresnel transform of the functions may no longer be concentrated in the aperture.

In fig.we compare the eigenvalues for the case where the phase term may no longer be neglected to the eigenvalues of eq(7). The number of non-zero eigenvalues is still the same, proportional to the number of resolution cells, but the last non-zero eigenvalues are lower when the phase term is not neglected (this may be physically related to the dilatation introduced by the Fresnel transform that spead a part of the energy out of the array)

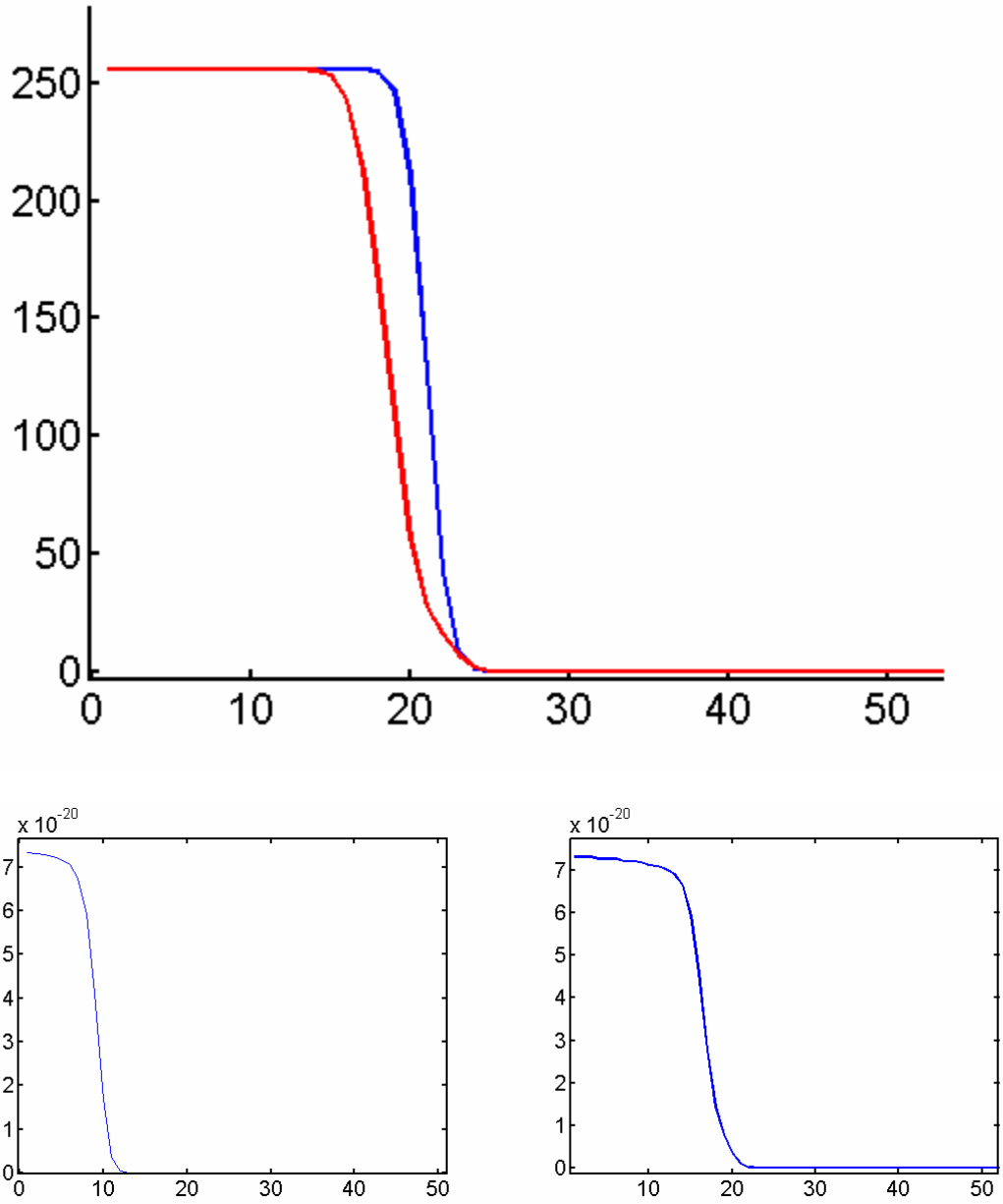

Figure 72 **Blue: theoretical eigenvalues distribution at center frequency when the Fresnal phase term is neglectible; red: same with the phase term; ((a^2=64mm, while λZ=10mm)) this does not change the number of eigenvalues, still proportional to the number or resolution cell. Bottom: Eigenvalues distribution from simulation, for 2 objects of different size (corresponding to the 2 cases of** Figure 59**)**

APPENDIX C: INVARIANTS FOR 3D OBJECTS WITH 2D ARRAYS

The singular value equation becomes

$$\mu R(X_R, Y_R) = e^{j\frac{X_R{}^2+Y_R{}^2}{\lambda Z}} \iint_{array} \text{kernel2D}\left[\frac{X_R + X_T}{\lambda Z}, \frac{Y_R + Y_T}{\lambda Z}\right] E(X_T, Y_T) e^{j\frac{X_T{}^2+Y_T{}^2}{\lambda Z}} dX_T dY_T \quad -$$

$L/2 < X_R, Y_R < L/2$ (13)

where kernel2D is the 2-D Fresnel transform of the object

$$\text{kernel2D} = FT\left\{ d(x,y) e^{j\frac{2(x^2+y^2)}{\lambda Z}} \right\}\left[\frac{X}{\lambda Z}, \frac{Y}{\lambda Z}\right] \quad (14)$$

DORT with a 2D array

The discrete equivalent of the 1D equation was the singular-problem of a matrix given by

$$K_{i,j} = \text{ker}\, nel(X_i, X_j)$$

Similarly, the discrete equivalent of eq.(13) is the singular problem for a tensor given by

$$K^{2D}{}_{i,j,k,l} = \text{ker}\, nel2D(X_i, Y_j, X_k, Y_l)$$

and the problem reads $\mu R_{i,j} = K^{2D}{}_{i,j,k,l} E_{k,l}$ (15)

using Einstein's notation, and with the conditions that the singular matrices R, respectively E, constitute an orthonogonal basis of the receive, respectively transmit space. K^{2D} is the generalization of the transfer matrix to 2D arrays. $K^{2D}{}_{i,j,k,l}$ is then the signal received by element (i,j) when a pulse is fired by element (k,l). Practically, the singular problem (15) can be rewritten in term of a matrix singular problem. Each pair (i,j) may be indexed by a number α, $1 \le \alpha \le N^2$, and each pair (k,l) may be indexed by β $1 \le \beta \le N^2$. Eq(15) becomes then

$$\mu \tilde{\tilde{R}}_\alpha = \tilde{\tilde{K}}^{2D}{}_{\alpha,\beta} \tilde{\tilde{E}}_\beta \qquad (16)$$

where $\tilde{\tilde{R}}$ and $\tilde{\tilde{E}}$ are $N^2 \times 1$ vectors and $\tilde{\tilde{K}}^{2D}$ is a $N^2 \times N^2$ matrix. The singular decomposition of $\tilde{\tilde{K}}^{2D}$ can easily be performed numerically.

Analytical solutions for separable kernels

Solutions of eq(13) have a simple form if the object reflectivity function is separable in Cartesian coordinates $d(x,y) = d(x)d(y)$. This is the case, for example, for a wire aligned with one of the array directions (we have then $d(x,y) = \delta(x)1(y)$) or for a rectangular plate ($d(x,y) = box(x)box(y)$, where box is the box function) Indeed, in that case, the kernel is alos separable (property of the Fourier Transform) For symmetry reason, the solutions are separable too. $R(X,Y) = R_X(X)R_Y(Y)$ and $E(X,Y) = E_X(X)E_Y(Y)$. Eq(13) finally becomes

$$\mu R_X(X_R)e^{j\frac{X_R^2}{\lambda Z}} R_Y(Y_R)e^{j\frac{Y_R^2}{\lambda Z}}$$
$$= \int \text{kernel}_X\left[\frac{X_R + X_T}{\lambda Z}\right] E_X(X_T)e^{j\frac{X_T^2}{\lambda Z}} dX_T \int \text{kernel}_Y\left[\frac{Y_R + Y_T}{\lambda Z}\right] E_Y(Y_T)e^{j\frac{Y_T^2}{\lambda Z}} dY_T \quad (17)$$

and the equations for the X and Y quantities can be solved independently

$$\mu R_X(X_R)e^{j\frac{X_R^2}{\lambda Z}} = \int \text{kernel}_X\left[\frac{X_R + X_T}{\lambda Z}\right] E_X(X_T)e^{j\frac{X_T^2}{\lambda Z}} dX_T$$

with $\text{kernel}_X = FT\left\{d(x)e^{j\frac{2x^2}{\lambda Z}}\right\}\left[\frac{X}{\lambda Z}\right]$, this is exactly the equation we have for a 1D object with reflectivity d(x) ; we have a similar equation for Y.

The solutions of eq(17) are then the products of the solutions of the 1D equations. The singular value is the product of the singular values of the two 1D problems.

The number of non-zero singular values is equal to the number of pairs of X non-zero singular values and Y non-zero singular values. Let N_X be the number of X non-zero singular value and N_Y the same for the Y axis, then the number of non-zero values for the 2D problem is $N_X N_Y$, which is again proportional to the number of resolution cells in the object (2D resolution cell in that case)

Aubry, A., J. d. Rosny, et al. (2006). "Gaussian beams and Legendre polynomials as invariants of the time reversal operator for a large rigid cylinder." The Journal of the Acoustical Society of America **120**(5): 2746-2754.

Boyd, J. P. (2004). "Prolate Spheroidal Wavefunctions as an alternative to Chebyshev and Legendre polynomials for spectral element and pseudospectral algorithms." journal of computational physics **199**: 688-716.

Frieden, B. R. (1971). Evaluation, design, and Extrapolation methods for optical signals based on use of the prolate functions, North Holland publishing company.

Goodman, J. W. (1975). Statistical Properties of Speckle Pattern. Laser Speckle and Related Phenomena. J. C. Dainty. Berlin, Springer-verlag**:** 9-75.

Goodman, J. W. (1985). Statistical Optics, Wiley Classics Library.

Gruber, F. K., E. A. Marengo, et al. (2004). "Time-reversal imaging with multiple signal classification considering multiple scattering between the targets." The Journal of the Acoustical Society of America **115**(6): 3042-3047.

Lewis, M. A., P. Liu, et al. (2006). "Linear sampling method for acoustic inverse scattering in breast microcalcification detection." The Journal of the Acoustical Society of America **120**(5): 3025-3025.

Mast, T. D., A. I. Nachman, et al. (1997). "Focusing and imaging using eigenfunctions of the scattering operator." The Journal of the Acoustical Society of America **102**(2): 715-725.

Prada, C. and J. L. Thomas (2003). "Experimental subwavelength localization of scatterers by decomposition of the time reversal operator interpreted as a covariance matrix." The Journal of the Acoustical Society of America **114**(1): 235-243.

Trees, H. V. (2002). Optimum Array Processing - Detection, Estimation, and Modulation Theory, Wiley-Interscience.

Waag, R. (2006). "Image reconstruction using eigenfunctions of a scattering operator." The Journal of the Acoustical Society of America **120**(5): 3023-3023.

Waag, R. C., D. L. Liu, et al. (1997). "Imaging with eigenfunctions of the scattering operator." The Journal of the Acoustical Society of America **101**(5): 3091-3091.

Chapter 4. FDORT In Speckle

I. INTRODUCTION

In a biological medium, like the human body, there are actually very few *well resolved* point scatterers. Most of the signal is speckle. Speckle is due to the presence of a large number of sub-resolution scatterers. The observed signal results from the interferences between the wave-fronts from all the insonified scatterers and has a random aspect. Therefore the speckle has to be dealt with in terms of statistics. As speckle is more abundant than nicely resolved point scatterers, it is a requirement for aberration correction in medical ultrasound to be able to extract Green functions of the medium from speckle signal.

Unfortunately, Time Reversal methods are originally designed for deterministic scatterers only. In this chapter, we show that FDORT can also be used to extract Green's functions from pure speckle signal. In this case, we select signal coming from around the focal depth, by gating the signal in time. Although the original FDORT algorithm gave decent results in speckle, a slight modification of the algorithm is better suited for estimation in speckle. This will be described and justified in Sec.III.A.

We start by giving a review of the main properties of and tools used for speckle.

In Sec.III, we show that for random speckle signal, KK^H can be interpreted as a spatial correlation matrix described by the Van Cittert- Zernike theorem(Mallart and Fink 1994). This links this method to the work of others (Msoy, Angelsen et al. 2004; Msoy, Varslot et al. 2005) and yield an interesting interpretation of the 1st eigenvalue. With speckle, a 3rd interpretation is possible as a time reversal operator for an equivalent virtual object, which leads to physical meaning for the eigenvectors. The variance of the estimate of the Green's function is also discussed.

In Sec. IV we will see that in presence of an aberration, the FDORT method in speckle need to be iterated. It usually converges to the Green's function after a few iterations. Experimental results in phantom are presented.

Our method is then compared to other's in Sec.V. Finally a unique feature of the FDORT method is developed: the ability to separate the signal of interests from strong interferences, in Sec.VI.

The main contributions of this work are the Sections III and IV. The Section VI is also interesting and can be read easily. The Section V is more technical and but given for completeness.

As this paper makes a link between DORT and random signal processing (like the VanCittert Zernike theorem), notations of both fields are used, so that the reader can refer easily to the original papers. Thus, the signal received by array element j for the i^{th} transmit is K_{ij} in DORT notations which highlights the fact that it is a coefficient of the transfer matrix K, and S_j^i in statistical notation, which highlight the fact that it is the i^{th} realization of the signal received by element j.

II. BASIC STATISTICAL PROPERTIES OF SPECKLE SIGNALS

This Section summarizes speckle concept that are helpful to understand the work exposed in this thesis. A reader familiar with random signal processing and speckle phenomena can start directly the section III.

A. Randomness of the speckle

Tissues viewed by an ultrasound medical scanner acquire a granular appearance. The details structure of this granularity bears no obvious relationship to the macroscopic properties of the imaged tissue, but rather it appears random. This is due to the fact that an ultrasound pulse insonifies many sub-resolution scatterers at the same time.

1. The scattering or isochronous volume

Indeed, let $S_m(x,t)$ be the signal received by array element *m,* at time *t,* when the transmits is focused at the lateral position (azimuth) *x*. This is illustrated in Figure 73. Because the wave-front has a certain extent laterally (the beam width) and axially (the pulse-length), the echos of many scatterers are received simultaneously by the array. The volume of scatterers that contribute to a sample, $S_m(x,t)$, of the signal, is called, in this document, the *scattering volume.* It is also known as the isochronous volume(Fink, Cardoso et al. 1984). The scattering volume is delimited laterally by the width of the beam, and axially by the length of the pulse. In other word, the volume is delimited by the wave-front at frozen time *t* for a transmit at *x*. To be accurate, one has to consider round-trip wave-front. In our case, we are interested by focused transmits, and single element receive. Therefore, the lateral extension is given by the transmit only. The axial extension is given, around the focal depth, by the convolution of the transmit pulse by the receive pulse. The scattering volume is shown in Figure 73

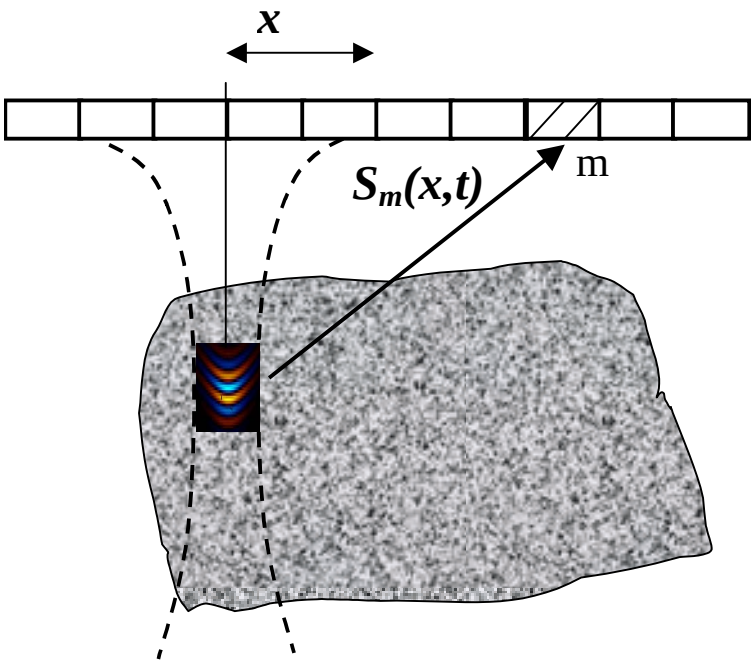

Figure 73 The signal $S(x_b,t_b)$ is due to the sum of the scatterers located in the scattering volume or isochronous volume at time t_b. The scattering volume is delimited by the wave-front.

2. The model of fully developed speckle

Thus $S_m(x,t)$ is the sum of the contribution of all scatterers located in the scattering volume at time *t*. The resulting backscattered signal is then the sum of many coherent components, but that have different phases, resulting in an interference pattern.

Usually, the model of *fully developed speckle* is used. In this model, the signals from different scatterers are supposed to be independent. In a monochromatic formalism, this means that the phase and amplitude of a given scatterer are independent of the other scatterers.

Therefore, the sum $S_m(x,t)$ can be seen as a random walk, that is to say the sum of many independent complex signals as seen in Figure 74. The statistics of a random walk is given by the central limit theorem.

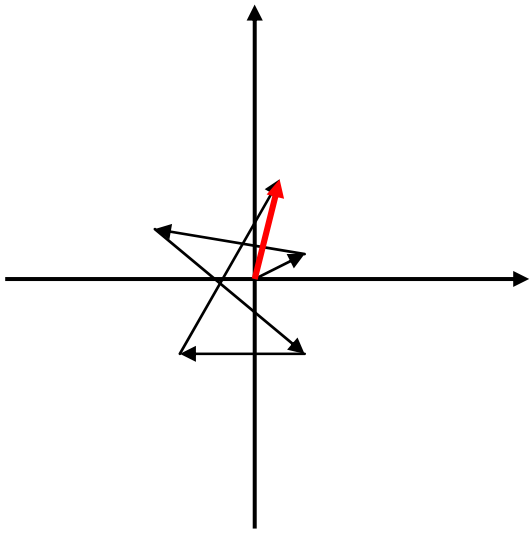

Figure 74 Model of the random walk for speckle signal. The resulting signal (red) is the sum of many coherent components that have random phases. The amplitude of the resulting signal has then a Gaussian distribution.

The speckle can then only be rigorously described using statistics. The intensity of one realization of the speckle (one point in the image), or a sample of received signal $S_m(x,t)$ do not carry useful information as they are random. However expected, or average, values are meaningful. To compute an average value, one needs several realizations of the random signal. Ideally, a different realization would be obtain using the same scattering volume, but with a different random scattering distribution. To have N realizations, one would then need to repeat N times the experiment, but changing the random medium each time. This is not feasible in practice, and a better solution will be developed in Section III.A.

Speckle statistics has been developed in optics, and very good references are (Goodman 1975; Goodman 1985)

The fully developed speckle approximation assumes there is no correlation between neighbor scatterers. This is obviously not exactly the case in practice, as the scattering distribution follows the material structure. However, the approximation is good as long as the correlation length of the distribution is significantly smaller than the size of the scattering volume.

B. First order statistics

First order statistic gives the statistics for a single sample of signal, whereas second order statistics is the statistic for product of samples (correlation). The statistics of the speckle are fully described by the random walk in the complex plane, and by the central limit theorem, which states that the sum of a large number of independent random variables has a Gaussian (or normal) statistics. First order statistics are not important for this work, and they are summarized here quickly, following (Goodman 1975).

- The complex signal (monochromatic formalism) has a Gaussian circular statistics (Gaussian in the complex plane). The real and imaginary parts have Gaussian statistics with zero mean.
- The phase has a uniform statistics, any value of the phase as the same statistics $1/2\pi$.
- The intensity has a Rayleigh probability distribution. Its variance is equal to its mean value.
- A sum of samples (beamformed signal) enjoy the same statistics, aside of a scaling constant.

C. Second order statistics

Second order statistic is the statistic of square of, or product of random variables. In particular, it gives the cross-correlation of signals. It is important for speckle processing.

1. Van Cittert Zernike theorem

The Van Cittert-Zernike theorem has been introduced by (Mallart and Fink 1994) to derive the spatial correlation function of the signal backscattered by speckle, that is to say the correlation $< S_m S_n^{*} >$ between signals received by a pair of array elements m and n.

The theorem states that the correlation function is given by the Fourier transform of the transmit beam intensity profile in the random mirror plane

$$\left\langle S_m S_n^{*} \right\rangle = \exp j\left(\frac{2\pi}{\lambda Z}\left(X_m^{2} - X_n^{2} \right) \right) \cdot \beta \cdot P\left(\frac{X_m - X_n}{\lambda Z} \right)$$

where $P(X)$ is the Fourier transform of the transmit beam intensity, β is a real constant, and $\frac{2\pi}{\lambda Z}\left(X_m^2 - X_n^2\right)$ is the difference of geometric curvature between the 2 elements. In an homogeneous medium, the transmit field at the focal depth is a sinc function, the intensity is a sinc^2 and then the spatial correlation function is a triangle function. This is illustrated in Figure 75.

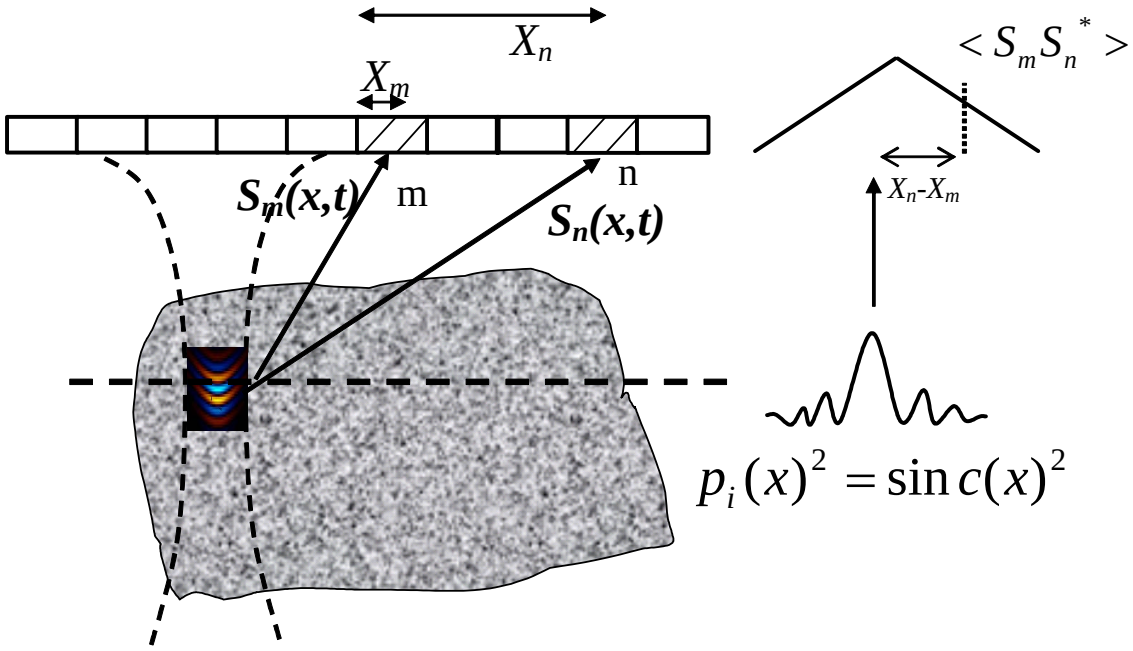

Figure 75 The Van Cittert Zernike theorem expresses the cross-correlation $< S_m S_n^* >$ between two samples received by different receive elements *m* and *n* from the same scattering volume. The theorem states that the spatial correlation function is given by the Fourier transform of the intensity distribution $p_i(x)^2$, here a triangle. The correlation decrease then linearly in function of the distance between elements X_m-X_n.

A derivation based on (Mallart and Fink 1994) is provided in the following. The spatial correlation matrix is then introduced. Finally, the Van Cittert Zernike theorem is derived

for an inhomogeneous medium. Usually, in presence of aberration, the intensity distribution is broader as the focus is not as good, and then the spatial correlation function is narrower. The derivations are included because they are a good way to be familiar with the speckle formalism, but they are not required to understand the work of the thesis. A reader can therefore jump to II.C.2.

Theorem for a homogeneous medium

The analysis is done in a monochromatic approach, but the signals are supposed to be originating from a volume located at a certain depth only. This means that the signals are gated in time to select echoes from a given depth prior to take the Fourier transform. This is like taking a slice of the medium. We suppose also that the signals are gated at the focal depth.

Following (Mallart and Fink 1994), the scattering volume can be modeled as a random mirror (Figure 76). All the quantities introduced here are in the frequency domain, but the index ω will only be specified the first time the quantity is used for clarity. Let $r(x,\omega)$ be the scattering coefficient of the random mirror. Let $p_i(x,\omega)$ be the incident field, and $p_b(x,\omega)$ the backscattered field at the surface of the plane, such as

$$p_b(x) = p_i(x) r(x)$$

Eq.4. 1

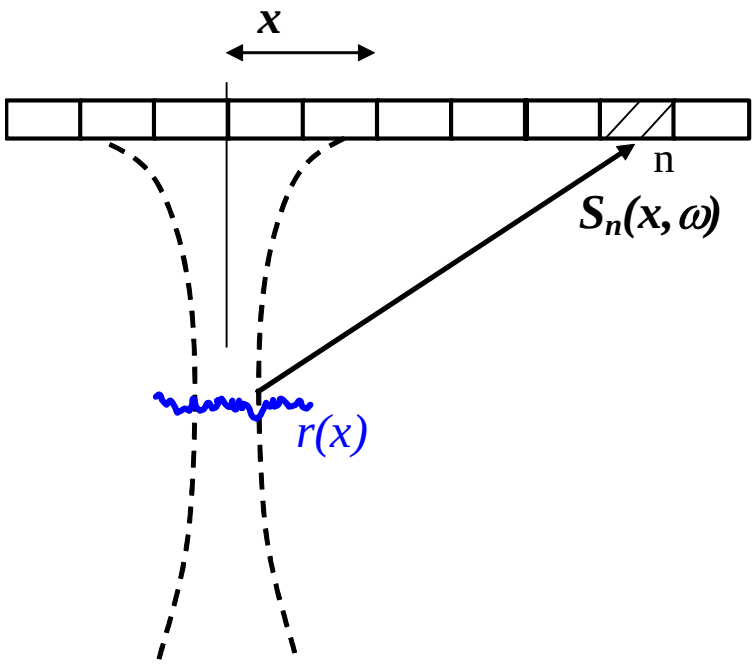

Figure 76 The scattering distribution is replaced by a random mirror whose reflectivity is a random function *r(x)*

If the lateral distribution of the incident field is not too broad so that we can use the Fraunhoffer approximation, the received field P(X) on the array can be expressed as the Fourier transform of $p_b(x)$. X is the coordinate on the array plane, while x is the coordinate in the scattering plane.

$$p(X) = \frac{e^{j\frac{2\pi}{\lambda Z}X_m^2}}{Z} FT[pb(x)]\left(\frac{X}{\lambda Z}\right)$$

Eq.4. 2

where Z is the depth of the scattering plane. Often the complex exponential term is removed by aligning the signals in receive, but this is not the case in this work.

The spatial correlation R_P of the received pressure field between 2 array elements m and n is then

$$R_P(X_m, X_n) = < p(X_m)\overline{p(X_n)} >$$
$$= < \frac{e^{j\frac{2\pi}{\lambda Z}X_m^2}}{Z}\int p_i(x)r(x)e^{\frac{j2\pi X_{mi}x}{\lambda Z}}dx \cdot \frac{e^{-j\frac{2\pi}{\lambda Z}X_n^2}}{Z}\int \overline{p_i(x)r(x)}e^{-\frac{j2\pi X_{nj}x}{\lambda Z}}dx >$$
$$= \frac{e^{j\frac{2\pi}{\lambda Z}\left(X_m^2 - X_n^2\right)}}{Z^2}\int p_i(x_1)\overline{p_i(x_2)} < r(x_1)\overline{r(x_2)} > e^{\frac{j2\pi X_{mi}x_1}{\lambda Z}}e^{-\frac{j2\pi X_n x_2}{\lambda Z}}dx_1 dx_2$$

Eq.4. 3

where the bracket symbols < > stand for the expected value, which would be obtained by averaging on an infinite number of realizations of the random variable.

We used the development of a product of two integrals

$$\int f(x)dx \cdot \int g(x)dx = \int f(x_1)g(x_2)dx_1 dx_2$$

Eq.4. 4

and the fact that only r(x) is a random variable and depend on the realizations.

Using the fully developed speckle model (4.II.A.2) stating that there is no correlation between neighbor scatterers, we can write

$$< r(x_1)\overline{r(x_2)} > = {r_0}^2 \delta(x_1 - x_2)$$

Eq.4. 5

where $\delta(x)$ is the Dirac function, and r_0 is a function of frequency. The scattering coefficient r(x) has then the same statistics as a white noise. Using Eq.4. 5 in Eq.4. 3 yield

$$R_P(X_m, X_n) = \frac{e^{j\frac{2\pi}{\lambda Z}\left(X_m^2 - X_n^2\right)}}{Z^2} \int p_i(x_1)\overline{p_i(x_1)} \cdot {r_0}^2 e^{\frac{j2\pi X_{mi} x_1}{\lambda Z}} e^{-\frac{j2\pi X_n x_1}{\lambda Z}} dx_1$$
$$= \left(\frac{r_0}{Z}\right)^2 e^{j\frac{2\pi}{\lambda Z}\left(X_m^2 - X_n^2\right)} \int \left|p_i(x_1)\right|^2 e^{\frac{j2\pi(X_m - X_n)x_1}{\lambda Z}} dx_1$$
$$= \left(\frac{r_0}{Z}\right)^2 e^{j\frac{2\pi}{\lambda Z}\left(X_m^2 - X_n^2\right)} FT[\left|p_i(x)\right|^2]\left(\frac{X_m - X_n}{\lambda Z}\right)$$

Eq.4. 6

where the notation FT[f(x)](X) is the Fourier Transform of f(x) evaluated at abscissa X Eq.4. 6 shows that the spatial correlation function of the field backscattered by speckle is given by the Fourier transform of the intensity distribution of the incident pressure field. This formula is known as the Van Cittert Zernike theorem. It has been demonstrated here in the case of the Fraunhoffer approximation for simplicity, but still holds under the more general Fresnel approximation (Mallart and Fink 1994).

An important result is that the spatial correlation function depends only on the distance X_i-X_j between the 2 elements. We can then write

$$R_p(X_m, X_n) = R_p(X_m - X_n)$$

Eq.4. 7

This is no longer exactly true when one account for the directivity of the transducers, or the attenuation.

In practice, the measured signal is not the pressure p, but the output of each transducer. Let $S_j(\omega)$ be the signal measured on element m. The signal is proportional to

the element width and to the acousto-electric response. Both will be regrouped in the factor $A_{el}(\omega)$, which yields

$$S_j = A_{el} P(X_j)$$

Eq.4. 8

for the output of the j^{th} element.

Eq.4. 6 and Eq.4. 8 lead to the expression of the spatial cross-correlation $R_S(m,n)$ between the signals S_m and S_n, received by transducers m and n.

$$\begin{aligned} R_S(m,n) &= < S_m S_n^{*} > \\ &= |A_{el}|^2 < p(X_m)\overline{p(X_n)} > \\ &= |A_{el}|^2 \, R_p(X_m - X_n) \\ &= \left(\frac{r_0 \,|\, A_{el} \,|}{Z}\right)^2 e^{j\frac{2\pi}{\lambda Z}\left(X_m^2 - X_n^2\right)} FT[\,|p_i(x)|^2\,]\left(\frac{X_m - X_n}{\lambda Z}\right) \\ &= \beta \cdot e^{j\frac{2\pi}{\lambda Z}\left(X_m^2 - X_n^2\right)} \cdot P\left(\frac{X_m - X_n}{\lambda Z}\right) \end{aligned}$$

Eq.4. 9

where $P(X) = FT[\,|p_i(x)|^2\,]$ and $\beta = \left(\frac{r_0 \,|\, A_{el} \,|}{Z}\right)^2$.

The derivations have been performed for a signal at one temporal frequency, which is the type of signal we are using in the FDORT formalism. The result can also be expressed in the time domain (Walker and Trahey 1997) and (Silverstein 2001).The term cross-spectrum is sometimes used (Waag and Astheimer 2005; Waag and Astheimer 2006) instead of cross-correlation, to highlight the fact that it is built in the temporal frequency domain. Rigorously, it is a cross-spectrum regarding to the temporal domain,

but a cross-correlation regarding to the spatial domain. Therefore, the term spatial cross-correlation will be used in this document.

The spatial correlation matrix

In this work, the spatial correlation matrix is an important tool. It is noted R_{SS} to make the difference with the spatial correlation function. It is the matrix whose coefficients are the cross-correlation between the signals received by pairs of transducers. Thus

$$\left(R_{SS}\right)_{m,n} = R_S(m,n) =< S_m S_n^{*} >$$

The Van Cittert Zernike Theorem in presence of an aberrator

In presence of an aberration, the theorem is slightly modified. In the frequency domain, the aberrator is represented by the complex function Ab(X,ω). Neglecting the variation of the amplitude

$$Ab(X) = e^{j\phi^{Ab}(X)}$$

In presence of aberration, using eq. Eq.4. 2 and Eq.4. 8, the signal on the mth element becomes

$$S_j = e^{j\left(\phi^{Ab}(X)+\frac{2\pi}{\lambda Z}X_m^2\right)}\frac{A_{el}}{Z}FT[p_b^{Ab}(x)]\left(\frac{X_j}{\lambda Z}\right)$$

where the index Ab in p_b^{Ab} highlight the fact that the phase aberration is affecting the transmit. Then the spatial correlation becomes

$$\left\langle S_m S_n^{*}\right\rangle = \exp j\left((\phi^{Ab}(X_m)-\phi^{Ab}(X_n)+\frac{2\pi}{\lambda Z}\left(X_m^2 - X_n^2\right)\right)\cdot\beta\cdot P^{Ab}\left(\frac{X_m - X_n}{\lambda Z}\right)$$

Eq.4. 10

The main difference with the homogeneous case is that the differential phase aberration appears in the phase term. This is the base of phase aberration estimation algorithm, as will be later. Moreover, the aberration modifies the distribution of the transmit intensity, and therefore the shape of the amplitude of the spatial correlation. The correlation function is no longer a triangle. Usually, in presence of aberration, the intensity distribution is broader as the focus is not as good, and then the spatial correlation function is narrower, as shown in Figure 77.

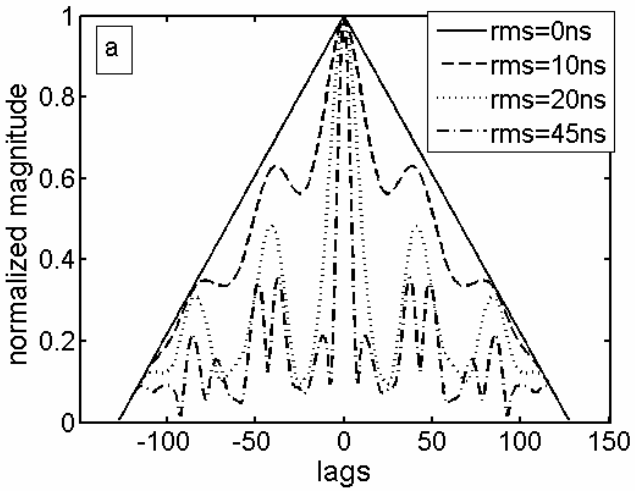

Figure 77 Amplitude of the spatial correlation in an homogeneous medium (straight line), and in the presence of phase aberration of different strength. The spatial correlation is a triangle in an homogeneous medium and become narrower as the aberration strength increases. The width of the main lobe is the coherence length of the signal.

The Van Cittert Zernike theorem in function of the aperture auto-correlation

Another form of the theorem can be expressed in function of the transmit aperture. This form will be especially helpful for aberration correction, as it will be possible to express the spatial correlation function in function of the aberrator.

In the Fresnel approximation, the pressure distribution $p_i(x)$ in the focal plane is related to the signal in the transmit aperture, $A_{Tx}(X)$, by a Fourier Transform. Therefore, from the property of the Fourier transform, $FT(f(x) \otimes \overline{g(-x)}) = FT[f](X) \times \overline{FT[g](X)}$, the intensity distribution $\left|P_i(x)\right|^2$ in the focal plane is related to the Fourier transform of the auto-convolution of the aperture function, $A_{Tx}(X) \otimes \overline{A_{Tx}(-X)}$, that we note simply $R_{ATx}(X)$. Injecting this in the Van Cittert Zernike theorem, Eq.4. 10, yields

$$\left\langle S_m S_n^* \right\rangle = \exp j\left((\phi^{Ab}(X_m) - \phi^{Ab}(X_n) + \frac{2\pi}{\lambda Z}\left(X_m^2 - X_n^2\right)\right) \cdot \beta \cdot R_{ATx}(X)$$

Eq.4. 11

The amplitude of the spatial correlation is given by the autocorrelation of the aperture function. In a homogeneous medium, the aperture function is a gate that has the dimension of the transmit aperture, and the auto-correlation gives a triangle. However, in presence of aberration, the transmit aperture has to be multiplied by the aberration term $Ab(X) = e^{j\phi^{Ab}(X)}$. Therefore, the amplitude of the spatial correlation function is given by the autocorrelation of the aberration. The spatial correlation can then be linked to the auto-correlation of the aberrator. In general, if an aberrator has a phase that varies fast and with large amplitude, and leads to a narrower correlation function than an aberrator that varies slowly with low amplitude. Closed relationships between the aberrator profile and the spatial correlation function are derived in (Mallart and Fink 1994)

2. The focusing criterion, C

The focusing criterion C has been introduced by (Mallart and Fink 1994).The focusing criterion is an objective measure of the quality of focusing. It is a number that can vary from 0 to 1, the upper bound being reached only for signal from point scatterers. In speckle, its value depends on how well the received signals are correlated, which in turns, from the VanCittert Zernike theorem, depends on the quality of focusing. The criterion is defined as a ratio of the coherent intensity and the incoherent intensity. Let us then define these quantities first.

The coherent intensity

Let $S(\omega)$ contain the Ne signals $S_i(\omega)$ received by each of the Ne array elements. $S(\omega)$ is then a Ne*1 vectors

$$S(\omega) = \begin{pmatrix} S_1(\omega) \\ \vdots \\ S_i(\omega) \\ \vdots \\ S_{Ne}(\omega) \end{pmatrix}$$

Let V(ω) be the Ne*1 complex vector used to beamform the received signal. It can be seen as a filter applied on the receive signal, and can be used for aberration correction. The amplitude of V(ω) is the apodisation and the phase is related to the time delay law applied on each element. *V* is usually the Green function of the desired focal point. The beamformed amplitude is then

$$A = \sum_{n=1}^{Ne} S_n V_n^{\ *} = V^H S$$

Eq.4. 12

Now, the coherent intensity is

$$I_C = AA^* = V^H S\left(V^H S\right)^H = V^H S S^H V$$

Eq.4. 13

where SS^H forms a matrix whose element (*m*,*n*) is $S_m S_n^*$. The expected coherent intensity, or average speckle brightness, is

$$\left\langle I_c \right\rangle = V^H \left\langle SS^H \right\rangle V \ .$$

We used the fact that V is independent of the realizations. $\left\langle SS^H \right\rangle$ is a matrix whose element (*m*,*n*) is $\left\langle S_m S_n^* \right\rangle$, and therefore it is the spatial correlation matrix R_{SS}. Finally

$$< I_C >= V^H \mathbf{R}_{\mathbf{SS}} V$$

The coherent intensity, or speckle brightness, increases as the signals get more coherent and add constructively. It is then a good relative criterion to asset the strength of the aberration.

An explicit expression of the coherent intensity in function of the spatial correlation function can be derived (in Appendix 4.A).

$$\langle I_C \rangle = \beta \int R_{ATx}(X) R_{ARx}(X) dX$$

Eq.4. 14

where $R_{ATx}(X)$ is the autocorrelation of the transmit aperture or the Fourier transform of the transmit intensity distribution in the focal plane, and $R_{ARx}(X)$ is the same for the receive aperture. In general, if the same aperture is used in transmit and receive, the functions are the same. Eq.4. 14 relates the coherent intensity to the area under the spatial correlation function. Indeed the integral of a function can be interpreted as the area under the function plot. As shown in Figure 77, the spatial correlation gets narrower when the aberration is stronger and therefore the area under the plot decreases.

However it is not an absolute criterion as it does not depend only on the quality of the focusing, but also on other parameters like the speckle echogeneicity or the array parameters. Looking at one value of the coherent intensity does not allow us to conclude on the quality of focusing without knowing what the maximum value is. Hence the idea to normalize the intensity to get an absolute criterion.

The incoherent intensity

Using the Schwartz inequality, $0 \le \left| \sum_i a_i b_i \right|^2 \le \sum_i a_i^2 \sum_i b_i^2$, with $a_i=V_i$ and $b_i=S_i$,

we find

$$0 \le < I_C > \le < \sum_i^{Ne} |V_i|^2 \sum_i^{Ne} |S_i|^2 >$$

Choosing V such as it is a unit vector (its l^2-norm $\sqrt{\sum_i^{Ne} |V_i|^2}$ is equal to 1), which will be the case in the following as we will be considering eigenvectors of the correlation matrix (a correlation matrix has the hermitian symmetry and therefore has orthonormal eigenvectors), the inequality becomes

$$0 \le < I_C > \le \sum_i^{Ne} < |S_i|^2 >$$

where $\langle I_{inc} \rangle = \sum_i^{Ne} < |S_i|^2 >$ can be interpreted as the expected total incoherent intensity, which is the sum of the intensity received by each element. This differs from the coherent intensity where the signals are summed on an amplitude basis and can therefore interfere – constructively or destructively. Our definition of incoherent intensity differs from (Mallart and Fink 1994) by a factor N that comes from the fact that we are using a normalized vector V. The incoherent intensity can also be expressed in function of the spatial correlation matrix

$$\langle I_{Inc} \rangle = \sum_{i=1}^{Ne} \left\langle |S_i|^2 \right\rangle = \sum_{i=1}^{Ne} R_{SS}(i,i) = Tr(R_{SS})$$

Eq.4. 15

where *Tr* is the trace of a matrix.

Focusing criterion

When normalizing the expression of the coherent intensity in function of the spatial correlations functions given in Eq.4. 14, a similar formula is obtained for the focusing criterion (in Appendix 4.A)

$$C = \int \rho_{ATx}(l_{array} \cdot X)\rho_{ARx}(l_{array} \cdot X)dX$$

Eq.4. 16

Where $\rho_{ATx}(X) = \frac{R_{ATx}(X)}{R_{ATx}(0)}$ is the normalized auto-correlation function of the aperture, also known as coherence function. Unlike the coherent intensity in Eq.4. 14 the expression for *C* does not depend on any numerical factor, and the correlation functions are fully normalized so that they no longer depends on any array parameters, as shown in Figure 78

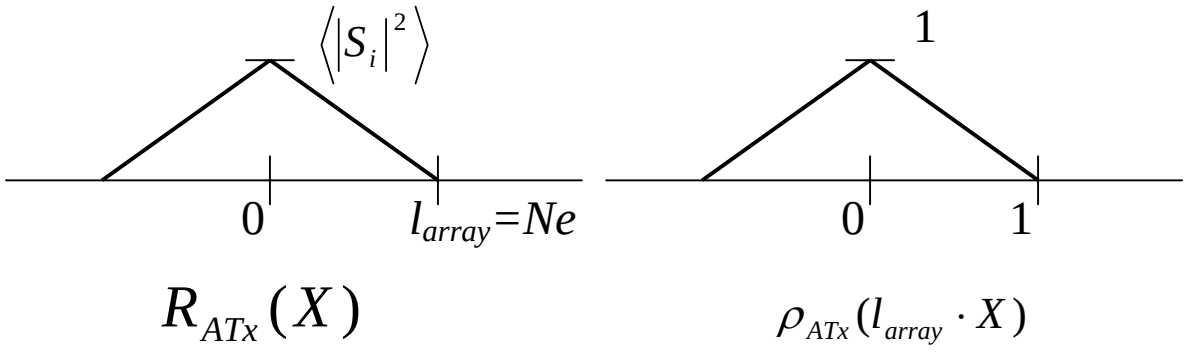

Figure 78 The spatial correlation function (left) depends on many parameters of the array. After normalization by the total incoherent intensity, it becomes independent of the parameters.

In a homogeneous medium (perfect focusing), the normalized spatial correlation function $\rho_{ATx}(l_{array} \cdot X)$ is a triangle whose base is equal to the 2, and C was shown in[8] to be equal to 2/3 in this case (C is the area of the triangle to the square). However this is not exactly the maximum value that C can reach in speckle, as it is for a square apodization. With other apodizations higher value of C can be reached, and value close to 0.75 have been observed during simulations. Other parameters like the transducers directivity can influence C. C drops quickly when the focusing degrades, and a good rules of thumb seems to consider that the focusing is decent if C is above 0.5.

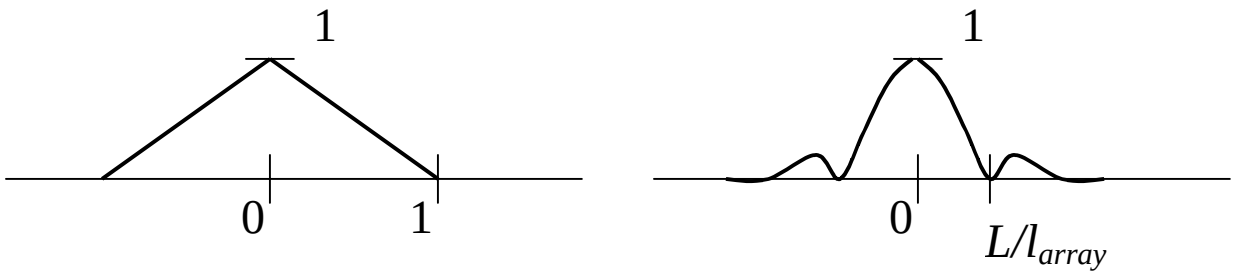

Figure 79 $\rho_{ATx}(l_{array} \cdot X)$ in an homogeneous medium and in presence of the aberration. The area under the plot to the square, that gives the focusing criterion, decreases in the last cases, and is proportional to the ratio between the coherence length and the array.

An explicit relationship between C and the coherence length of the signal can be derived. The spatial correlation function for a backscattered signal of coherence length L can be roughly approximated by a triangle of base $2*L/l_{array}$. It results that C would be $2/3\frac{L}{l_{array}}$ in this case, where *D* is the full array width. Indeed when the base of the triangle was equal to $2.l_{array}$, C was 2/3. The coefficient 2/3 in this case is not really

important as it depends on the shape of the correlation function (2/3 is for a triangle), but the main result is the proportionality between C and $\frac{L}{l_{array}}$. The focusing criterion is basically inversely proportional to the number of coherent cells in the array.

3. Correlation between signals originating from different speckle region

Another 2nd order statistics result will be very helpful for the following. It concerns the correlation between signals arriving from neighbor region of speckle. Indeed, to reduce the variance of the estimates with speckle, it is interesting to average the results on different region of speckle. In order to have a good averaging, one wants to add uncorrelated signals. It is then helpful to know how fast the echos decorrelate from one region to another. The signals are not completely correlated because they originate from different scattering volume, that have different random scattering distribution. Intuitively, the correlation between the signals is proportional to the overlap between their scattering volumes. This is rigorously derived in the following.

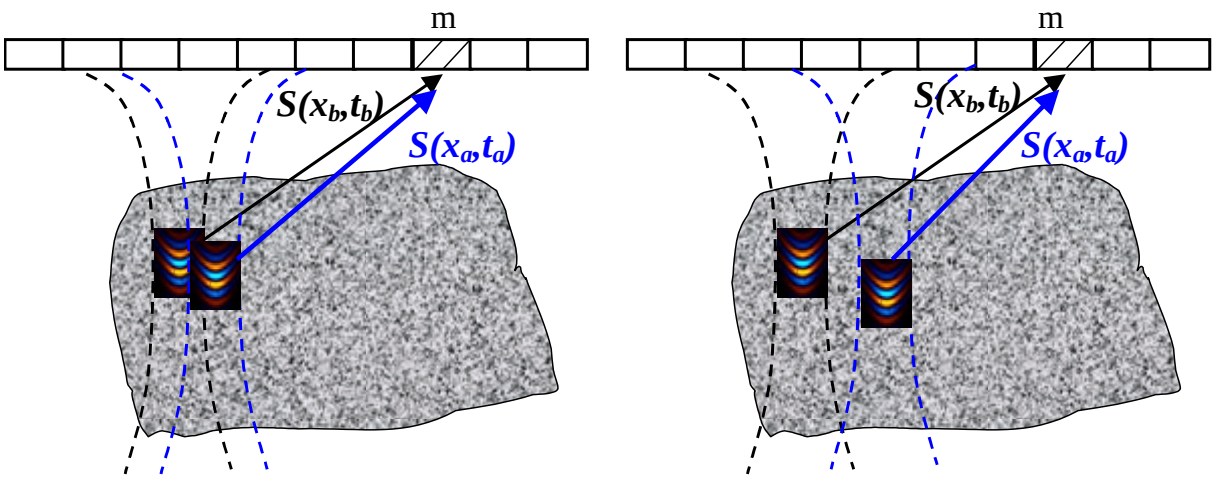

Figure 80 The correlation between signals generated by different scattering volumes (different transmit or arrival time) is proportional to the overlap between the scattering volumes. Left: the two scattering volume overlap, so the resulting signals $S(x_b,t_b)$ and $S(x_a,t_a)$ are correlated. Right: the two scattering volumes do not overlap, so the resulting signals $S(x_b,t_b)$ and $S(x_a,t_a)$ are uncorrelated. They give independent realizations of the signal.

We consider here the correlation of two regions displaced in azimuth or in depth. We consider first the correlation between 2 time samples of signal. For simplicity, the signals are received by the same transducer so that the only cause of the decorrelation is the fact that the signals originates from different region. If different transducers as used in receive, an additional decorrelation due to the Van Cittert Zernike theorem is introduced.

Let $S(x_a,t_a)$ be the signal received at time t_a, when the transmits is focused at the lateral position (azimuth) x_a. $S(x_a,t_a)$ is the sum of the contribution of all scatterers located in the scattering volume at time t_a. As explained in 4.II.A, the volume is delimited by the wave-front at frozen time t_a for a transmit at x_a.

Rigorously, the wave-front should be noted $w(x,z,x_a,t_a)$ because the wave-front varies in two dimensions (x and z) and because it depends on the transmit azimuth (x_a)

and on the time considered (the wave-front propagates with time) However, it can be considered that the wave-front for a transmit can be deduced from the wave-front for another transmit by a translation, which is a good approximation. This is called shift-invariance in azimuth. As only signals from around the focal depth are considered in this work, we can also consider that the wave-front is shift-invariant with depth. These approximations allow to write $w(x- x_a,z-z_a)$ with $z_a=1/2ct_a$ which simplifies the derivation.

The signal received at time t is then expressed as

$$S(x,t) = \iint w(x - x_a, z - z_a) r(x,z) dx dz$$

where $r(x,z)$ is the random scattering distribution, and can be seen as a higher-order equivalent of the random mirror introduced in the previous section.

The assumption that the speckle is full developed translate here in

$$< r(x_1,z_1) r(x_2,z_2)^* >= {r_0}^2 \delta(x_1 - x_2, z_1 - z_2)$$

The correlation between $S(x_a,t_a)$ the signal sample received at time t_a for a transmit focusing at azimuth x_a and $S(x_b,t_b)$ the signal sample received at time t_b for a transmit focusing at azimuth x_b is thus

$$\begin{aligned}
\left\langle S(x_a,t_a) S(x_b,t_b)^* \right\rangle &= \left\langle \iint w(x_1 - x_a, z_2 - z_a) r(x_1,z_1) dx_1 dz_1 \iint w(x_2 - x_b, z_2 - z_b)^* r(x_2,z_2)^* dx_2 dz_2 \right\rangle \\
&= \iint\iint\iint w(x_1 - x_a, z_2 - z_a) w(x_2 - x_b, z_2 - z_b)^* \left\langle r(x_1,z_1) r(x_2,z_2)^* \right\rangle dx_1 dz_1 dx_2 dz_2 \\
&= {r_0}^2 \iint w(x_1 - x_a, z_2 - z_a) w(x_1 - x_b, z_1 - z_b)^* dx_1 dz_1 \\
&= {r_0}^2 \iint w(x', z') w(x' - (x_b - x_a), z' - (z_b - z_a))^* dx' dz'
\end{aligned}$$

In the last step, $x'=x_1-x_a$ was used. The last integral express the auto-correlation of the wave-front, at lag $(x_b - x_a)$ and $(z_b - z_a)$. Thus

$$\left\langle S(x_a,t_a)S(x_b,t_b)^* \right\rangle = r_0{}^2 R_w(x_b - x_a, z_b - z_a)$$

This equation states that the correlation between two samples of received signals is proportional to the overlap between the corresponding round-trip wave-fronts.

A normalized version can be derived, noting that $\left\langle S(x_a,t_a)S(x_a,t_a)^* \right\rangle$ is the incoherent intensity I_{Inc}, and defining the normalized correlation function, also called coherence function

$$\sigma_w(x_b - x_a, z_b - t_a) = \frac{R_w(x_b - x_a, z_b - z_a)}{R_w(0,0)}$$

The normalized equation is then

$$\left\langle S(x_a,t_a)S(x_b,t_b)^* \right\rangle = I_{Inc}\sigma_w(x_b - x_a, z_b - z_a)$$

Eq.4. 17

In this work, temporal frequency domain signals are considered. In order to compute the Fourier Transform of the signals, one time sample is not enough. A sequence of several time sample is needed. To perform FDORT in speckle, the signals are gated in time. The size of the gate is typically one pulse length. Doing this is equivalent to convolve the receive signal *S(x,t)* by a gate that has a linear phase corresponding to the desired frequency. Convolving by such a function does modify the round-trip wave-front. An accurate derivation should take this into account. However, as long as the size of the gate is of the order of the pulse-length, the modification is negligible, and the formula for time sample will be used.

Consequently, Eq.4. 17 can be used to compute the correlation for the coefficients of the FDORT matrix. It gives the condition for two signals to be independent. The coherence area has the size of the resolution cell (or point spread function). In azimuth, two transmits separated by the beam-width, $\frac{\lambda z}{D}$, where *D* is the size of the aperture are uncorrelated. In depth, two signals are uncorrelated if they are separated by the round-trip pulse-length.

D. Basics of estimation theory

We will be introducing estimate of the correlation function in section III. We present quickly the basics about estimation theory.

The i^{th} realization of the signal received by element *m* is S_m^i. In practice we do not have access directly to the expected cross-correlation between two signals received by elements *m* and *n*, $< S_m \cdot S_n^* >$. We have access to a mere estimate of the cross-correlation, which is an average of *I* realizations of the cross-correlation. The estimate, $\tilde{R}_{mn}$ is defined as

$$\tilde{R}_{mn} = \frac{1}{I}\sum_{m=1}^{M} S_m^i S_n^i *$$

The following results are valid for the estimate of any quantities, not only the cross-correlation. The expected value of the estimate is equal to the expected cross-correlation (the estimate is said non-biased)

$$\left\langle \tilde{R}_{mn} \right\rangle = < S_m \cdot S_n^* >$$

The variance of the estimate is defined as

$$\left\langle \left(\tilde{R}_{mn} - < \tilde{R}_{mn} > \right)^2 \right\rangle = \left\langle \tilde{R}_{mn}{}^2 \right\rangle - < \tilde{R}_{mn} >^2$$

and the standard deviation is the square root of the variance. The standard deviation can be interpreted as the average error made on the estimate. If the *I* realizations are independent, the standard deviation of the estimate is proportional to $1/\sqrt{I}$, which means that the error decreases when the number of independent realization increases.

For a complex signal, like $\tilde{R}_{mn}$, an exact expression of the variance is not simple. It depends both on the number of realizations and on the coherence between the signals (the coherence, $\mu(m,n)$, is the normalized cross-correlation. It is equal to 1 for perfectly coherent signals). Probability clouds are shown in Figure 105. For a large number of realizations, and a decent coherence, the following formula can be given (see (Priestley 1988) p.703, and the appendix B of this chapter for a derivation of the results for continuous fields)

$$\mathrm{var}\left[\left|\left(\tilde{R}_{mn}\right)\right|\right] \approx \frac{< \tilde{R}_{mn} >^2}{I} \frac{1 + \left|\mu(m,n)\right|^2}{\left|\mu(m,n)\right|^2}$$

$$\mathrm{var}\left[angle\left(\tilde{R}_{mn}\right)\right] \approx \frac{1}{I} \frac{1 - \left|\mu(m,n)\right|^2}{\left|\mu(m,n)\right|^2}$$

In the following, we will be estimating Green's function. The standard deviation of the phase of the Green's function is particularly important, as the quality of focusing depends mainly on the phase. The standard deviation of the phase of the Green's function is also proportional to $1/\sqrt{I}$.

III. INTERPRETATIONS OF KK^H

In the previous chapters, it has been shown that, in the case of deterministic, well-resolved scatterers, KK^H could be interpreted as a time reversal operator for a virtual array. The Time Reversal Operator interpretation of KK^H is fundamental, as it yields physical meaning to the eigenvectors and eigenvalues using a thought experiment of Time reversal iteration. . Indeed, the Green's functions of well resolved scatterers are invariants of the Time reversal process. When one transmit a Green's function, only the corresponding scatterer is insonified, and the received echo is the time reversed version of the transmit Green's function. One can time reverse the signal and iterate the process, and still get the same signal.

Speckle is formed from a very large number of sub-resolved scatterers. In this case a thought experiment of iterative Time Reversal no longer helps predicting the behavior of the eigenvector, nor their focusing properties, , as many scatterers are insonified at the same time. Therefore, a new interpretation has to be proposed.

A. Spatial correlation matrix, or Van Cittert Zernike matrix

1. Link between KK^H and the spatial correlation matrix

In the FDORT method, the volume of scatterers insonified by each transmit can be limited in depth (from $z-\Delta z$ to $z+\Delta z$) by the time gating, as seen in Figure 81, before taking the Fourier transform. In speckle, we select scattering volumes around the focal depth. Therefore, we are exactly in the conditions of the Van Cittert Zernike theorem, illustrated in Figure 73 and Figure 74, and the coefficient $K_{im}(\omega)$ of K is the same as $S_m(x_i,\omega)$ used in Section.4.II. In the following, $S_m(x_i,\omega)$ will be noted simply S_m^i.

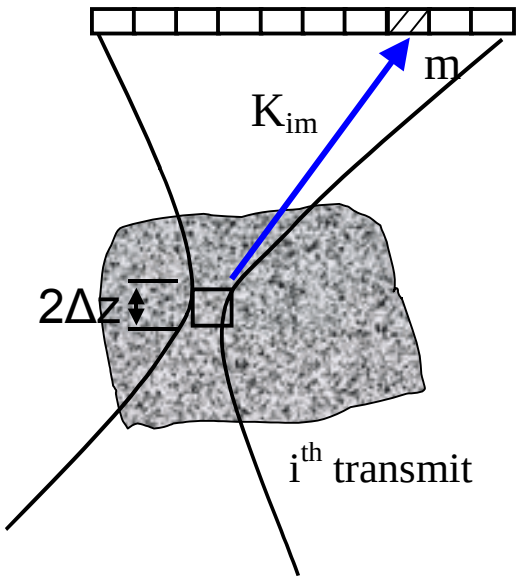

Figure 81 Acquisition of the transfer matrix in the FDORT method. The focused transmit i insonify the medium. The signal received by array element j is time gated to select the signal from depth $z-\Delta z$ to $z+\Delta z$, and its Fourier coefficient at frequence ω gives the matrix coefficient K_{im}. In speckle Δz is taken to be about the pulse-length.

Thus the beam pattern at the focal depth is now noted $p(x)$. For a homogeneous medium, $p(x)$ is a sinc function. Each of the N transmits insonify a similar scattering

volume, as the transmits are translated version of each other, but with a different set of scatterers and therefore gives a different realization of the random backscattered signal. This is equivalent to the problem where we fire *N* times the same transmit (instead of using *N* consecutive transmit) but with a different random medium each time. In our case however, the insonified volumes for each transmits are in slightly different locations. Better results are obtained if this is taken into account by a modification of the FDORT algorithm. Indeed, the echoes resulting from a focal spot at depth Z and azimuth x=0, have typically a wavefront curvature proportional to

$$\frac{2\pi}{\lambda}\sqrt{Z^2+X^2} \propto \left(Z+\frac{X^2}{2Z}\right)\frac{2\pi}{\lambda}$$

Eq.4. 18

where X is the coordinate in the array plane, and using the Fresnel aproximation. For another transmit whose focal spot is at abscissa x_i, we have

$$\frac{2\pi}{\lambda}\sqrt{Z^2+(X+x_i)^2} \propto \left(Z+\frac{1}{2Z}(X^2+x_i^2+2X\cdot x_i)\right)\frac{2\pi}{\lambda}$$

Eq.4. 19

In order to have signals that really look like two realizations of the same signals, it is necessary to remove the part depending on x_i in the wavefront curvature. This is done by time delaying the echo for the ith transmit by

$$\left(1/2x_i^2+X\cdot x_i\right)\frac{\pi}{\lambda Z}$$

Eq.4. 20

This is described in **Figure 82**. As a result, it looks like the two realizations come from the same location, but that it is the medium that has moved between the two insonifications. Alternatively, the signal can be completely aligned. In this case, the complete curvature is removed using a time-delay given by Eq.4. 19. This is interesting in the case where there is no interest in the whole Green function, and only the perturbation due to heterogeneities is of interest, like in phase aberration correction.

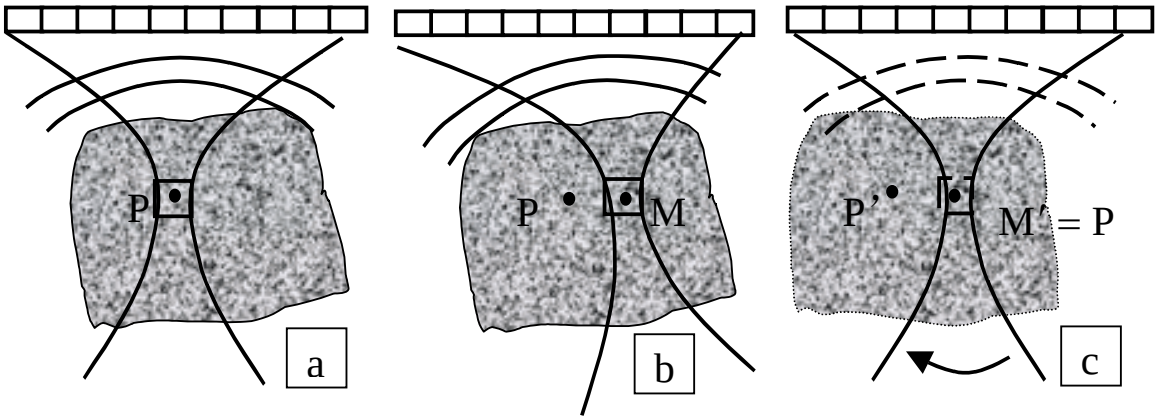

Figure 82 a) A transmit focusing at a point P and the corresponding received wave front. In speckle, ideally, to estimate the Green function at point P, we would like to fire several times the same transmit focusing at P, but with a different speckle distribution each time, to provide a good averaging of the randomness. b) Instead, we use a neighbor beam focusing at M close to P (the distance between M and P is exaggerated here). c) By properly shifting the wave front of the received signal, it looks like the whole medium is virtually translated and M', the new position of M, corresponds to P. Thus a new realization of the signal coming from P is obtained, with a different scatterer distribution. By virtually translating the phantom by different amounts, several realizations are obtained.

Now, K_{im} or $S_m{}^i$ is the i^{th} realization of the backscattered signal received by the m^{th} array element. Developing the product KK^{H} yields for the coefficient (m,n) of KK^{H}:

$$\left(KK^{H}\right)_{m,n} = \sum_{i=1}^{I} S_m^i S_n^{i^*} = I\left(\frac{1}{I}\sum_{m=1}^{M} S_m^i S_n^{i^*}\right)$$

Eq.4. 21

This is I times the average, over the I realizations of the speckle (in this case I is the number of transmits), of the product of the signals received by element m and by element n. This is, at frequency ω, an estimate of $\left\langle S_m S_n^* \right\rangle$, the cross-correlation of the signals received on elements m and n (see SectionII.D). Thus KK^H can be interpreted as an estimate of the spatial correlation matrix $R_{SS.}$

There is a difference between R_{SS} and KK^H, which is only an estimate of R_{SS} from a limited number of realizations (the transmits). In particular, the estimate KK^H has a variance which depends on the number of transmits. It is only one possible estimate of $R_{SS,}$ and most of the results derived here would apply to other estimates of R_{SS}.

2. Link to the Van Cittert Zernike theorem

In speckle, the FDORT matrix is then an estimate of the spatial correlation matrix, which contains the spatial cross-correlation for every pair of array elements. Following the Van Cittert Zernike theorem derived in Section 4.II.C.1, the spatial cross-correlation for a pair of elements (m,n) only depends on the distance between the elements, $X_m - X_n$, and is proportional to the Fourier Transform of the square of $p(x)$:

$$\left\langle S_m S_n^* \right\rangle = \exp j\left((\phi^{Ab}(X_m) - \phi^{Ab}(X_n) + \frac{2\pi}{\lambda Z}\left(X_m^2 - X_n^2\right)\right) \cdot \beta \cdot P\left(\frac{X_m - X_n}{\lambda Z}\right)$$

Eq.4. 22

where $P(X) = FT[|p(x)|^2]$

Eq.4. 23

β is a real constant, $\frac{2\pi}{\lambda Z}\left(X_m^2 - X_n^2\right)$ is the difference of geometric curvature between the 2 elements, that is the difference of propagation path in an homogeneous medium, and $\phi^{Ab}(X_m) - \phi^{Ab}(X_n)$ is the differential aberration phase between elements *m* and *n*, that is due to the presence of an inhomogeneity in the medium. In the usual near-field screen approximation, where the aberration introduces a mere time delay τ_i on the element *i* , $\phi^{Ab}(X_i) = \omega\tau_i$.

The amplitude of the spatial correlation is particularly interesting. In a homogeneous medium, *p(x)* is the sinc function, and therefore its Fourier transform is the triangle function. The amplitude of the cross-correlation for a pair of element decreases as a triangle function when the distance between elements increases. This is the pattern one can observe when the amplitude of the KK^H matrix is plot (Figure 83).

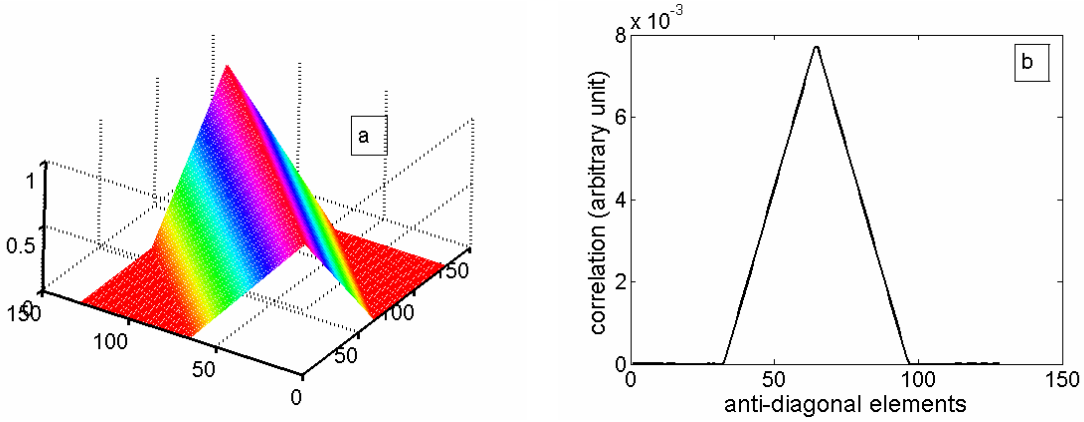

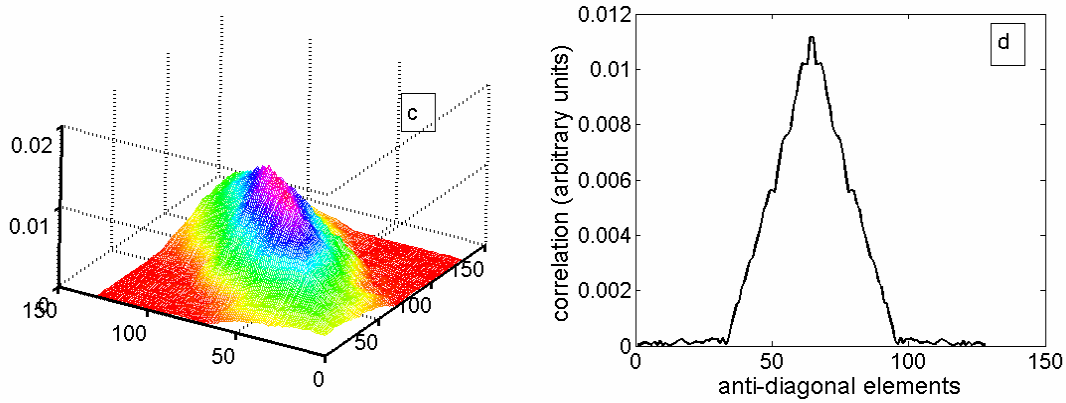

Figure 83 a,b)Theoretical amplitude of the spatial correlation matrix (a) and projection on the anti-diagonal (b) in homogeneous media as predicted by the VanCittert Zernike theorem. The triangular shape that arises from the Fourier Transform of sinc^2 is easily identifiable. 64 of the 128 elements were used in transmission, which is why the triangle base is 64 elements wide. c, d) Experimental amplitude of the FDORT matrix , for a 60 mm focus. The differences observed for the edge elements are mainly due to the transducers directivity, which was not taken into account in the VanCittert Zernike prediction.

In inhomogeneous medium, the focus is broader, and therefore the spatial correlation function decreases faster. This is also observed for the amplitude of the matrix, as seen in Figure 84.

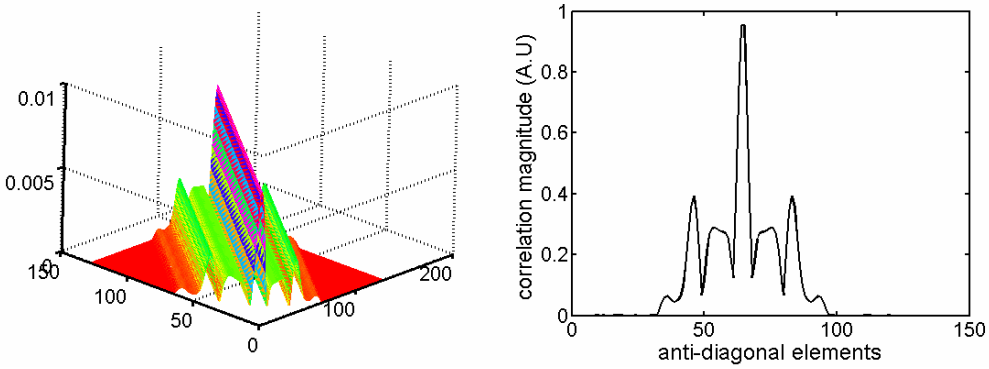

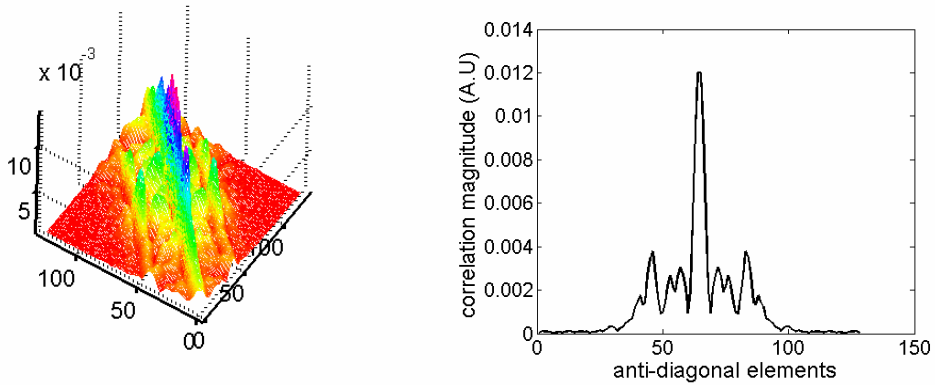

Figure 84 Same as Figure 83 for the aberrated case. The amplitude of the spatial correlation matrix is now given by the autocorrelation of the aberrated aperture.

In conclusion, in speckle, KK^H is an estimate of the spatial correlation matrix – or Van Cittert Zernike matrix- that is fully described by the Van Cittert Zernike theorem. This interpretation of the matrix will be helpful to interpret the eigenvalues. It is also interesting because correlation matrices are a very important tool in random signal processing, and is the base of numerous algorithm (Trees 2002).

This interpretation of the FDORT matrix as a correlation matrix is not surprising. For deterministic scatterers, it has already been shown (Prada and Thomas 2003; Gruber, Marengo et al. 2004) that the Time Reversal Operator can be interpreted as a correlation matrix of the received signal.

B. Time Reversal Operator for an equivalent virtual object

As said in the previous Section, in speckle, it does not make sense, *a priori*, to interpret directly KK^H as a Time Reversal Operator. However, we can play a trick and interpret it as the Time Reversal operator for an equivalent deterministic object. Everything happens as if we were performing a Time Reversal experiments on an object

whose reflectivity is proportional to $p(x)^2$, the beam intensity. Indeed, it is shown in the following, that for such an experiment, and under Fraunhoffer approximation, the transfer matrix, that we can call K_{eq} has the same coefficient as the spatial correlation matrix described in Sec. III.A. Intuitively, it is easy to see where this virtual object comes from. In fact, the speckle can be considered as a random mirror (Mallart and Fink 1994), that *reflects* an image of the transmit beam *p(x)*. If only one transmit, or realization, is available, this image is very blurred. However, by averaging on several realizations, the random mirror is smoothed, and the object is revealed.

More rigorously, one can compare the equation expressing the coefficients of the spatial correlation matrix (Eq.4. 22), to the equation expressing the coefficient of the transfer matrix *K* for an extended object in Chapter 3 (Eq.3. 5). They are both identical, if we choose the object scattering distribution to be equal to $p(x)^2$. (There is a difference in the arguments; in one case it is $X_m + X_n$, and in the other case $X_m - X_n$. Consequently one of the matrices is deduced from the other by a column flip, but this kind of symmetry does not affect the singular vectors)

Thus from a mathematical standpoint, everything happens as if the focused transmit was creating a virtual scatterer at the focal spot and we were doing DORT on it. The first eigenvector is then the Green function of the focal spot. As the focal spot is not a perfect point, but has a finite size given by the resolution of the array, there is not a single eigenvector, but several one, as observed with extended object (Chapter 3). If the focal spot is sufficiently small, the 1st eigenvector can still be considered to be the Green's function of the focal point. It is therefore important to use the whole aperture in transmit to keep the focal spot as small as possible.

To illustrate this point, we show in Figure 85, the eigenvalues distribution and the amplitude of the 2 first eigenvectors, when the full transmit is used. In Figure 86, we show the same thing for a narrow transmit aperture, and therefore a larger beam pattern.

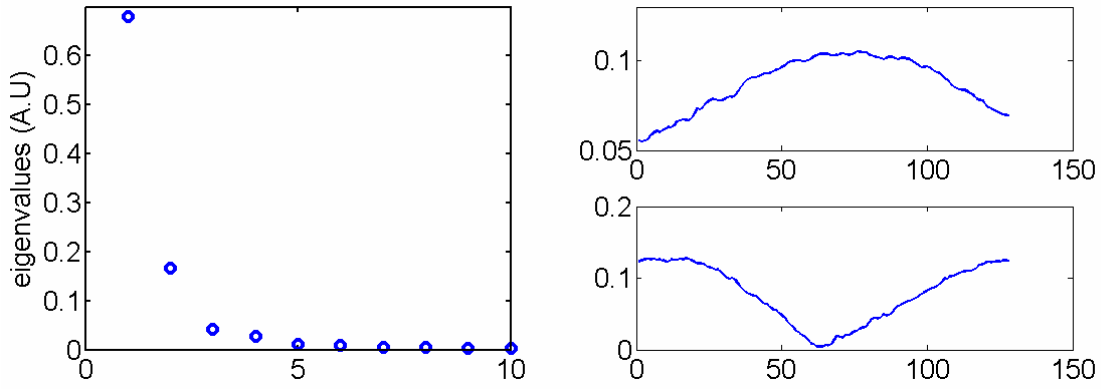

Figure 85 Normalized eigenvalue distribution, and amplitude of the 2 first eigenvectors when the full transmit aperture is used (optimal setting for FDORT in speckle). It is very similar to what was obtain for a small object about the size of the resolution cell in chapter 3 (here the object is the beam pattern to the square) It will be shown in III.D that the 1st eigenvalue is about 2/3.

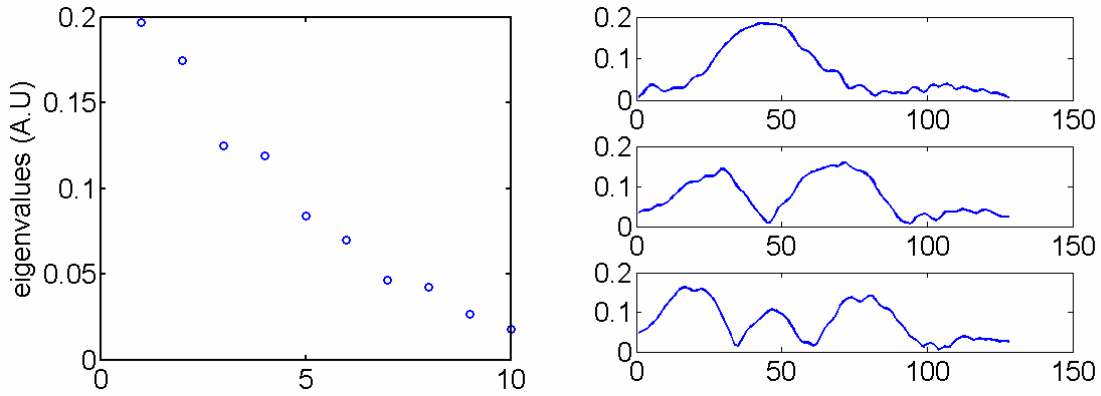

Figure 86 Same for a narrow transmit aperture (20 elements out of 128) In this case the virtual object is larger, and there are more non-zero eigenvalues (the variation of the eigenvalues is different than in Chapter 3 because the object is not a rectangle but a sinc to the square) The amplitude of the eigenvectors look similar to the case of an object larger than the resolution cell in Chapter 3. The

width of the 1st eigenvector' s amplitude is narrow. Therefore is not good for focusing (low resolution)

C. Variance and standard deviation of the estimation

We have determined asymptotic expressions and properties for the FDORT matrix in speckle. However, in a random media like speckle, one can only talk in statistical terms. The asymptotic properties have to be considered as mean values, obtained only if one could average on an infinite number of realizations of the signal. The estimated coefficients of the matrix, and therefore the eigenvectors, will in practice fluctuate from this mean value. The random fluctuation is characterized by a standard deviation (see Section II.D). The variance (square of the standard deviation) is usually used in the literature (Astheimer, Pilkington et al. 2006; Msoy, Angelsen et al. 2007).The standard deviation seems to have more physical meaning though, as the quality of focusing depends on the standard deviation of the phase of the Green's function, rather than its variance. The results given here apply to the standard deviation of most estimated quantities in this paper (amplitude and phase of the estimated Green's functions, coefficients of KK^H)

Expressions of the standard deviation are given in Section. II.D and the main result is that the standard deviation is proportional to the square root of the number of independent realizations. In our case, the different realizations are given by the different transmits. It has been shown in Section.II.C that two transmits yield independent (or non-correlated) realizations if they are separated by a distance equal to the width of the transmit resolution cell $\frac{\lambda Z}{D}$. Therefore the number of realizations that one can extract

from a part of medium of width L is $\frac{LD}{\lambda Z}$. L is usually limited because we assume (Section. III.A) that the curvature of the wave-fronts coming from all the locations that we use differs only by a linear term that we remove before averaging. It makes sense that if we want to estimate the Green's function at a specific location, only the region of medium with the same Green's function can be used. Removing the linear term enables to use the region where the Fresnel approximation holds. However, in most cases, we are interested by estimating the Green's function in inhomogeneous medium. In this case, the Green's function can vary quickly from one location to another. The region where we can still make the assumption that the Green's function differs only by a linear term is called the isoplanatic patch. In medical ultrasound, a typical isoplanatic patch in the breast is 1 mm laterally and 2 mm axially (Dahl, Soo et al. 2005). Therefore, the number of independent realizations that one can take laterally is given by the lateral size of the isoplanatic patch divided by $\frac{\lambda Z}{D}$, which is typically 0.4 mm. Consequently, only 3 or 4 independent realizations can be taken laterally.

As a limited number of realizations can be taken laterally, the variance can be further reduced by taking realizations from different depth. As shown in Figure 87, signals from a few depths surrounding the focal depths can be selected by time gating. Two different windows in depth yield independent realization if they are separated by the pulse-length, which, depending on the frequency of the probe typically varies from 0.2 to 0.5 mm.

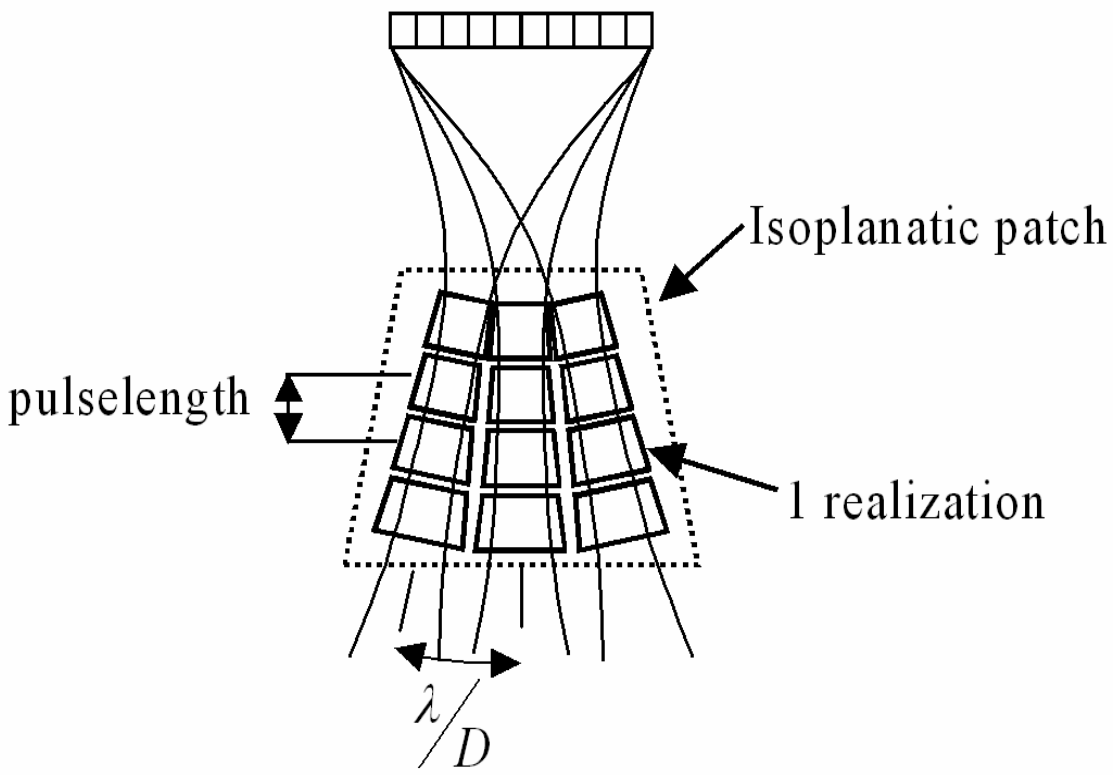

Figure 87 Independent realizations in the isoplanatic patch. The number of independent realizations is equal to the number of resolution cells.

In our simulations, 4 realizations were selected laterally, and 6 axially which yield 24 realizations, and the standard deviation is reduced by a factor 5. With a 2D array (Waag and Astheimer 2005; Waag and Astheimer 2006) and 3D imaging, the number of realizations can be increased by taking additional realizations in the elevation dimension (the 3rd dimension). In (Waag and Astheimer 2005; Waag and Astheimer 2006) 70 realizations are typically taken in a 3D volume.

To summarize, in speckle, the variance of the estimate decreases with the number of realizations, and the number of realizations is given by the area of the isoplanatic patch divided by the area of the resolution cell $\frac{\lambda Z}{D} \cdot pulselength$. In 3D, the number of

realizations would be given by the volume of the isoplanatic patch divided by the volume of the resolution cell.

One could be tempted to increase the transmit density (by reducing the distance between consecutive transmits) in order to have more realizations and decrease the variance further. However, the additional realizations would not be independent from the initial realizations. Therefore, they do not bring additional information. They bring only redundancy. Doing this would slow the acquisition process, as more transmit are required, but would not reduce further the variance. In fact, it is proved rigorously in Appendix B, that even if one take an infinity of continuous realizations in a given volume (by varying continuously the position (x,t)), the maximum variance reduction is given by the number of realization cells in the volume. This derivation is, to our knowledge, new in acoustics, but is placed in Appendix in reason of its technical difficulty.

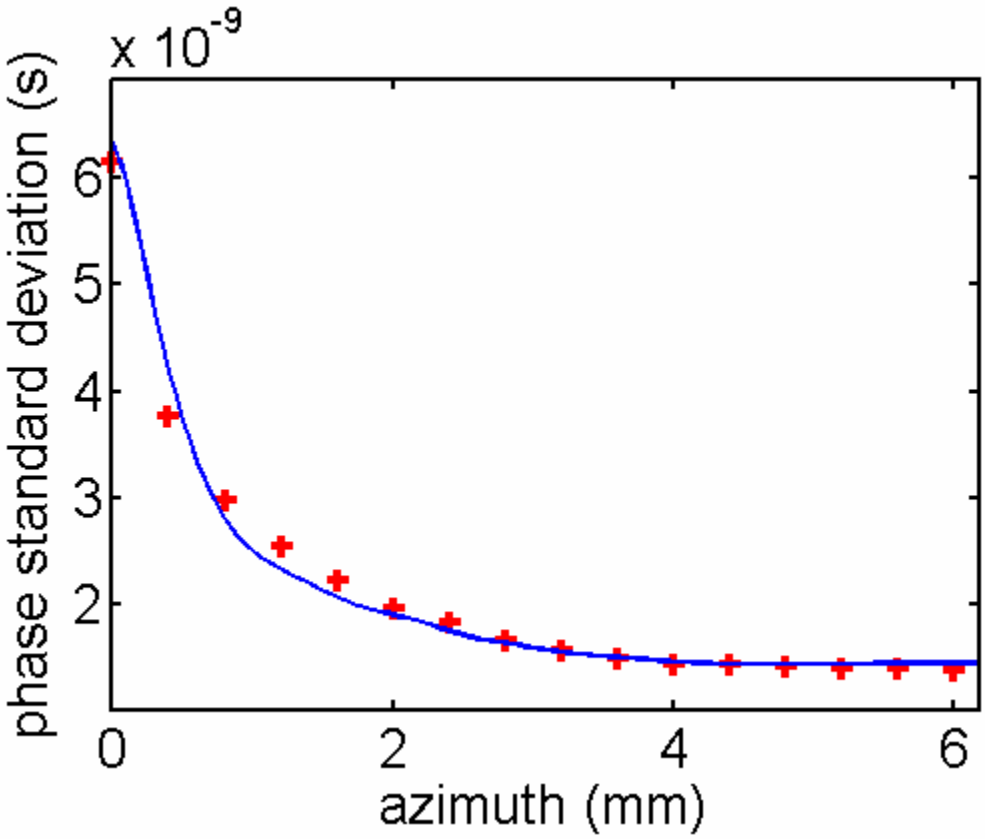

Figure 88 Standard deviation of the phase in function of the lateral size of the speckle region. In blue, the transmits are very close from each other (0.01 mm) while in red, the transmits used in the estimation were separated by the beam width (0.4 mm). It is clear that taking more transmits than required by the condition to have independent realizations does not improve the estimation.

The number of resolution cell in a volume is a good measure of the quantity of information (number of degree of freedom) one can extract from the volume. This is also equivalent to the *space-bandwidth* product, a well-known measure of information quantity in engineering, which is equal to the area interrogated times the area of the spectrum (k-space) of the system. The area in k-space can be approximated by the product of the temporal bandwidth B/c, and the spatial bandwidth $D/\lambda F$. Therefore, the space-bandwidth product is $Area_{Isoplanatic\_patch} \cdot B/c \cdot D/\lambda F$.

It is shown in Appendix, that in a 1st approximation, this result is still valid in presence of a near-field phase screen aberration.

D. Interpretation of the first eigenvalue in speckle

1. Interest of the focusing criterion

We use here the statistical interpretation developed in Sec.III.A. to show that the first eigenvalue in speckle has an important interpretation: if it is properly normalized, it is the focusing criterion C introduced in Section II.C.2.

The focusing criterion is equal to the ratio of the coherent intensity and incoherent intensity. Now, we need to express this quantity in term of the spatial correlation matrix.

2. Link between first eigenvalue and coherent intensity

(Varslot, Krogstadt et al. 2004). demonstrated that the first eigenvector of the spatial correlation matrix (or FDORT matrix) gives the receive focal law and apodization that maximizes the speckle brightness and can therefore be used to correct an aberration. Indeed, let V be the $N_{el} \times 1$ complex vector used to beamform the signal in receive. The phase term of V is a focal law, and the amplitude term is an apodization law. V is usually the Green function of the desired focal point.

An expression of the expected coherent intensity in function of the spatial correlation matrix and of the vector V used to beamform the signal has been derived in Section II.C.2

$$\left\langle I_c \right\rangle = V^H R_{SS} V$$

An estimate of the coherent intensity averaged on the few transmits used in FDORT is therefore $V^H K K^H V$.

It is well known (Donnell 1982; Nock, Trahey et al. 1989) that the coherent intensity, or speckle brightness increases with the quality of focusing. Therefore the best focusing is obtained by maximizing the coherent intensity. Now, let us show that the normalized vector V that maximizes the coherent intensity is the 1st eigenvector of the spatial correlation matrix.

Indeed let $\mathbf{e_i}$ be the ith eigenvector. The eigenvectors form an orthonormal basis, then one can decompose $\mathbf{V}$ in that basis $\mathbf{V} = \sum < \mathbf{V} \mid \mathbf{e_i} > \mathbf{e_i}$ and therefore

$$\mathbf{V}^H R_{SS} \mathbf{V} = \sum < \mathbf{V} \mid \mathbf{e_i} >^2 \lambda_i$$
$$\leq \sum < \mathbf{V} \mid \mathbf{e_i} >^2 \lambda_1 = \lambda_1$$

where λ_i is the ith eigenvalue. We used the fact that the norm of $\boldsymbol{V}$ is 1. The inequality is reached when $\boldsymbol{V = e_1}$.

Consequently, the 1st eigenvector of the spatial correlation matrix maximizes the coherent intensity, and hence the focusing (this confirms the result we derived using Time Reversal on the equivalent object in Sec.III.B) and the 1st eigenvalue is the corresponding coherent intensity. In practice, estimates of these parameters are given by the 1st eigenvector and eigenvalue of KK^H.

The coherent intensity is proportional to the focusing quality, however, it is only a relative criterion. Looking at the 1st eigenvalue by itself does not allow to conclude on the quality, as it depends on many parameters like the transmitted power, the scatterer reflectivity. This is where the criterion C is interesting, because it is an absolute criterion.

3. Link between the incoherent intensity and the sum of the eigenvalues

The expected incoherent intensity is the sum of the intensity received by each elements

$$\left\langle I_{Inc} \right\rangle = \sum_{i=1}^{Ne} \left\langle \left| S_i \right|^2 \right\rangle = \sum_{i=1}^{Ne} R_{SS}(i,i) = Tr(R_{SS})$$

where *Tr* is the trace of a matrix, that is, the sum of its diagonal elements. The *Trace* is conserved when the matrix is expressed in another basis. In the eigenvectors basis, the matrix is diagonal, and the diagonal elements are the eigenvalues. Thus the incoherent intensity is also equal to the sum of all eigenvalues.

$$\left\langle I_{Inc} \right\rangle = \sum_{i=1}^{Ne} \lambda_i$$

The incoherent intensity can be estimated by the sum of the eigenvalues of KK^H.

4. Link between C and the normalized 1st eigenvalue

The focusing criterion C is the ratio of the coherent intensity over the incoherent intensity. Thus, an estimate of C is given by

$$C_1 = \frac{\lambda_1}{Tr(KK^H)} = \frac{\lambda_1}{\sum_{n=1}^{Nel} \lambda_i}$$

The notation C_1 is used to highlight the fact that it is the focusing criterion obtained when the first eigenvector $\mathbf{e_1}$ is used to beamform the received signal.

Alternatively, a normalized version of the spatial correlation matrix can be built

$$\overline{\overline{KK^H}} = \frac{KK^H}{Tr(KK^H)}$$

This matrix has the same eigenvector as $\mathbf{KK^H}$ as it just differs by a scaling factor, but its first eigenvalue is directly C_1.

Thus, the decomposition of the FDORT matrix not only provides an estimate of the Green's function, $\mathbf{e_1}$, but also provides a direct measure of how well the aberration is corrected, or in other words, a measure of the quality of the image. For example, a 1st normalized eigenvalue above 0.5 means that the estimate of the Green's function is good. A poor value of the 1st normalized eigenvalue means that an iteration is needed (this will be elaborated in Sec.IV). With other aberration correction methods, such a criterion has to be computed separately(Lacefield and Waag 2002).

IV. APPLICATION TO FOCUSING IN HETEROGENEOUS MEDIUM

A. Equivalent virtual object and iteration of the method

It has been shown that performing FDORT in speckle was equivalent to performing DORT on an equivalent virtual object which has the shape of the transmit. In homogeneous media, a virtual scatterer is created at the focal spot, and the 1st eigenvector is the Green's function of the focal spot.

However, in presence of phase aberration, the transmit is no longer well focused and the virtual object is more complex In order to illustrate the effects of phase aberration, an FDORT experiment in speckle has been simulated using Field II (J.A.Jensen 1996). A 1-D linear array of 128 elements at 7.3 MHz central frequency is simulated. It focuses at 60 mm depth through a near-field phase screen. All the elements are used in transmit in order to get the best possible estimation of the phase screen, as has been explained in Section II.C. The statistics of the phase screen are 45ns average delay

variation, 4 mm spatial correlation length of the variation. The delay profile is shown in Fig.8, along with its estimate after 1 and 5 iterations of the FDORT method. The speckle phantom is generated with 15 scatterers per-resolution cell. 24 realizations are used (4 realizations laterally and 6 axially) for the measurement of the transfer matrix.

In Figure 89.*a*.we see that the beampattern through the aberrator appears as a collection of points that are not well resolved. In the case of such an object, the 1st eigenvector is mainly the Green's function of the brightest spot but as it is not well separated from the other points, it is perturbated by the signal from the other points[5]. As a result, the focusing obtained by backpropagation of the 1st eigenvector is not very good (Figure 89.*b*), but it is better than the original transmit. The process can therefore be iterated: the transmits are partially corrected using the 1st estimate of the Green's function and a new KK^H matrix is built. The virtual object correspond now to Figure 89.*b*. One point is now clearly brighter than the other and the new 1st eigenvector will be mainly the Green's function from this point, with less interferences from the other points than during the 1st iteration. As seen in Figure 89.*c* the focusing properties improved. By iterating the process a few times, the interferences decreases to zero and the 1st eigenvector converges to the Green's function of the brightest spot of the initial virtual object. This yields a very good focusing through the inhomogeneous media (Figure 89.*d*).

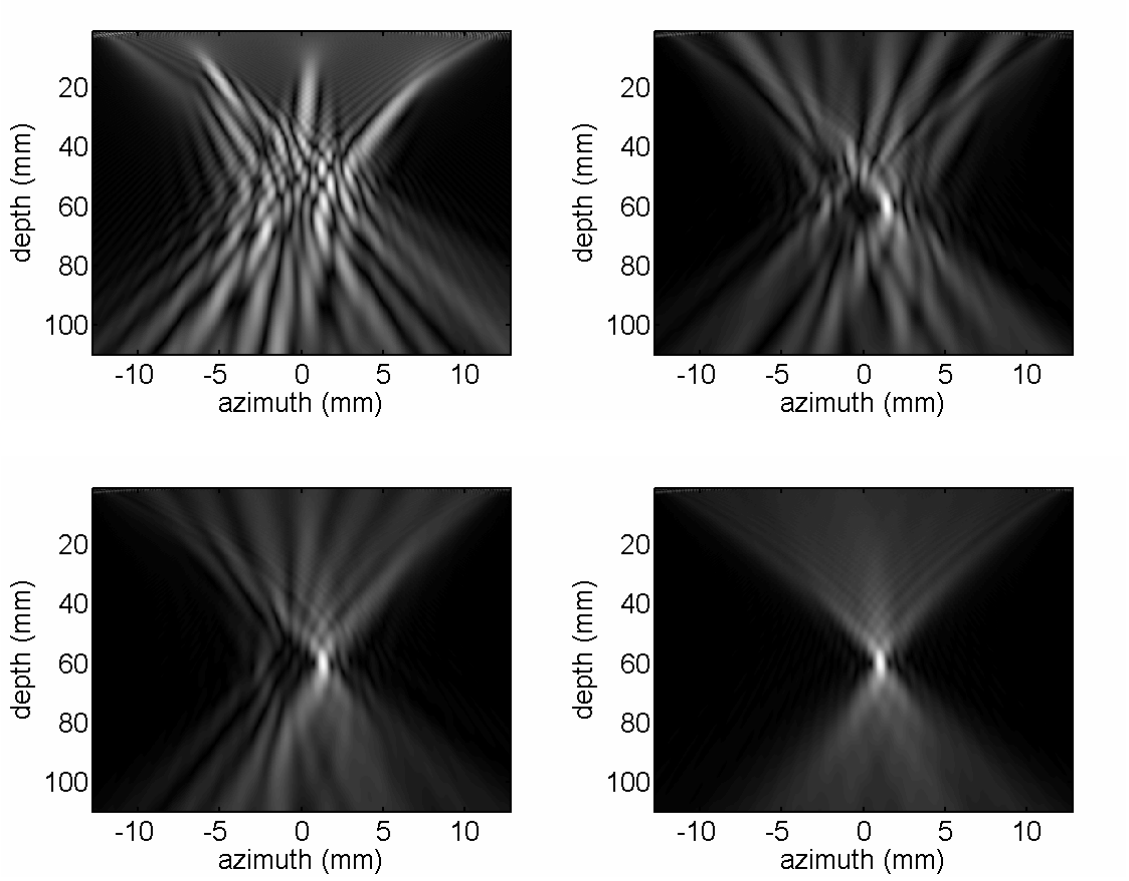

Figure 89 Simulated transmit fields at 7.3 Mhz in presence of the near field phase aberrator for different number of iteration of the algorithm a) Initial transmit: it is based on the Green function in homogeneous medium, and therefore the focusing is very poor. It is the equivalent virtual object for the 1st FDORT iteration b) The 1st eigenvector obtained in the 1st iteration is back-propagated. It focuses mainly on the brightest spot of the 1st transmit, but with significant interferences. The focusing criterion C is only 0.3. It is used to correct the transmit for the 2nd iteration of FDORT c) First eigenvector from the 2nd iteration. The focusing has improved. It is used to correct the transmit for the 3rd iteration. d) Fifth iteration: the 1st eigenvector yield now a very good focusing. It is an accurate estimate of the Green function in presence of the phase aberrator. C is now equal to 0.7.

Our interpretation of the 1st eigenvalue as the focusing criterion C is very helpful here. Indeed, it is an objective assessment of the quality of focusing. It indicates when the

iteration should be stopped. Indeed, as soon as C reaches a certain threshold, we know that we have a good focusing, and a good estimate of the Green's function. The evolution of C in function of the number of iteration is shown in Figure 90.

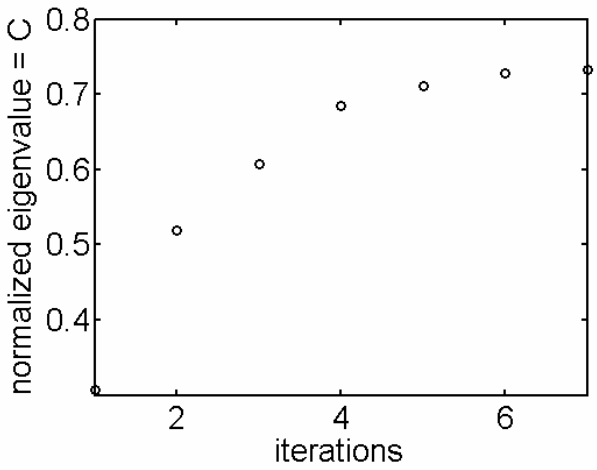

Figure 90 Evolution of the normalized 1st eigenvalue in speckle with a simulated near-field phase screen. The normalized 1st eigenvalue is equal to the focusing factor C. At the 1st iteration, C is about 0.3, which is the sign of a bad focusing related to the phase screen. After a few iterations, the algorithm converges and C passes 0.7, which means that the focusing is excellent. The corresponding transmit fields are displayed in Figure 89.

The phase profile of the near-field phase screen can be estimated from the Green's function phase, by removing the geometrical phase law corresponding to propagation in the homogeneous media. The estimated profiles at the center frequency are displayed in Figure 91. The phase has been converted in time by dividing by ω. As expected, the estimation is not good at the 1st iteration, but converges toward the true applied profile after a few iterations.

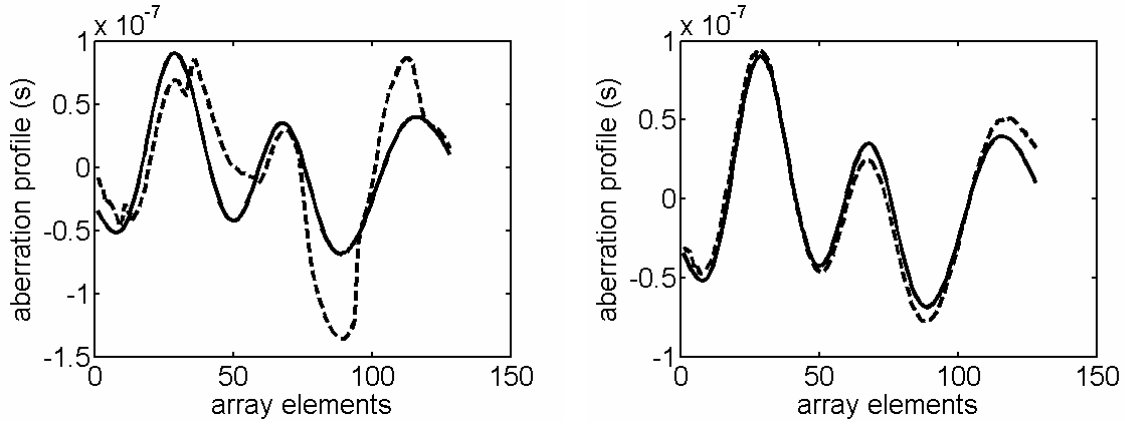

Figure 91 The phase of the estimated Green functions is unwrapped and the geometrical curvature removed to show an estimate of the aberrator delay profile. The estimate (dash line) is compared with the true profile (solid line), after the 1st iteration (a) and after 5 iterations (b). The estimate is not very good at the first iteration but converges after a few iterations.

We have learnt to auto-focus in a speckle medium using iteration of the FDORT method. This can be applied to imaging through heterogeneous medium. A phantom of pure speckle containing cyst has been simulated. The absence of bright scatterers ensures that only speckle signal is used to auto-focus. The 45ns, 4 mm FWHM near-field phase screen used in the previous example is applied and result in a severe distortion of the image. The estimate of the Green's function after 5 iterations is used to correct the image and restore a good focusing. Practically, the aberrator delay profile is estimated as described above (Figure 91) and is used to correct the beamforming process. Results before and after correction are shown in Figure 92.

The image quality improvement can be quantified by the cyst contrast. It is defined by

$$Cyst\_contrast = 20 \cdot \log\left(\frac{backgroundlevel}{lesionlevel}\right)$$

where lesionlevel is the average level in the lesion, and backgroundlevel the average level in a region having the same shape located in the speckle, close to the lesion. The cyst contrast before correction is found to be 4 dB. After correction, the contrast is 22 dB, which is close from the 23 dB obtained in a reference unaberrated medium.

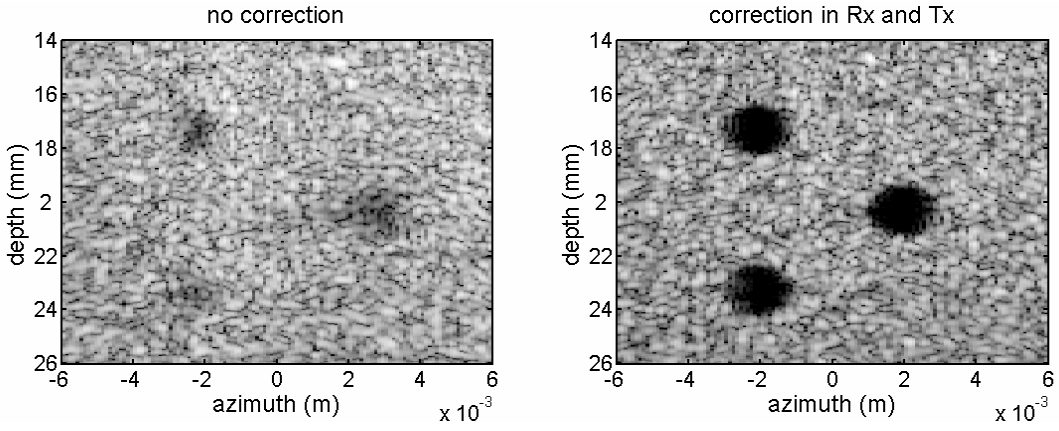

Figure 92 Image of a simulated speckle phantom containing, in presence of a near fild phase screen, before and after correction.

B. Focusing through a far-field phase screen

In the previous example (Figure 89 and Figure 90), the heterogeneity was modeled by a *near-field phase screen*. This is a good model if the heterogeneity is localized in a thin slice close to the transducer. This model is also the easiest to correct, as it can be corrected by simple time-delays. In the frequency domain, that we consider here, it translates by a phase correction $\phi_i = \omega\tau_i$. Another advantage of the *near-field phase screen*, is that the isoplanatic patch discussed in Sec.III.C. is large, like in the homogeneous case. Thus, more realizations can be taken.

A more difficult case is obtained if the phase screen is no longer close to the array, but deeper in the medium (far-field phase screen, see Chapter1.I.B.4). In this case, the effect in the array plane can no longer be modeled by simple time-delays, but by phase and amplitude (because of the interferences) variations at each frequency. The phase is a-priori no longer linear in function of the frequency. An additional difficulty results in the limited size of the isoplanatic patch in this case.

The same phase-screen as in Sec.IV.A. is simulated, but it is now located at a depth of 20 mm. The focal depth was chosen to be 80 mm. Results are shown in Figure 93. Again, the 1st eigenvector lock on the brightest point of the initial transmit field (equivalent object) and the focusing is improved after a few iterations.

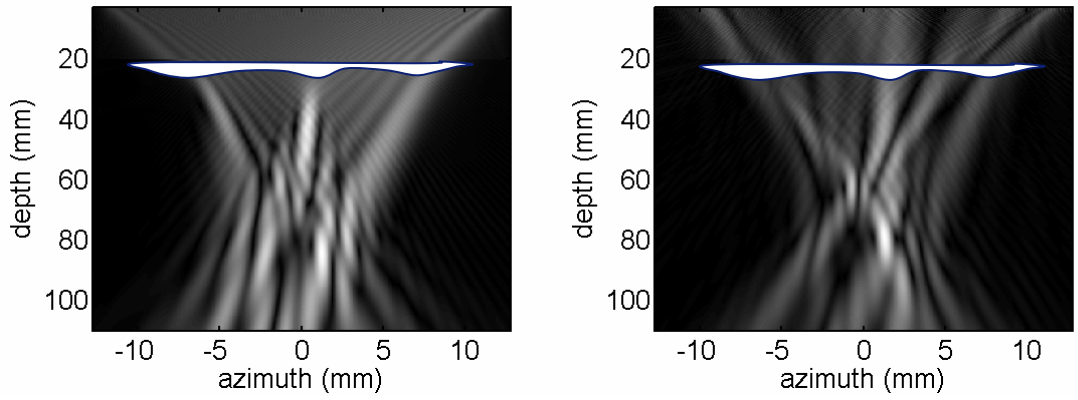

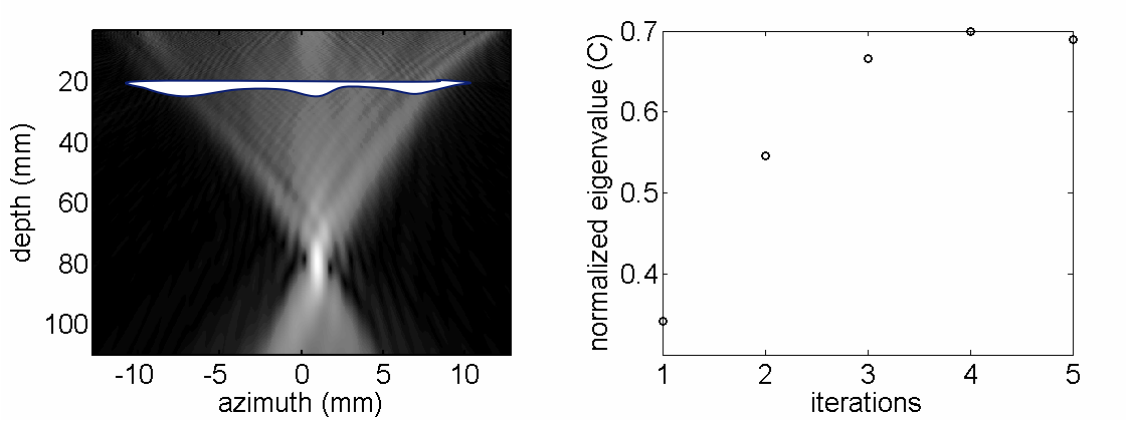

Figure 93 Simulated transmit fields at 7.3 Mhz in presence of the far field phase aberrator (drawn on each transmit in white) located at depth 20 mm, for different number of iteration of the algorithm a) Initial transmit: it is based on the Green function in homogeneous medium, and therefore the focusing is very poor. It is the equivalent virtual object for the 1st FDORT iteration b) Field obtained after back-propagation of the 1st eigenvector obtained in the 1st iteration. It focuses mainly on the brightest spot of the 1st transmit, but with interferences. C is 0.35 c) 1st eigenvector after the 4th iteration. C is 0.7 d) Evolution of the normalized eigenvalue, or C factor. Even if the screen is not close to the array, the convergence is reached quickly.

As in the case of the near-field phase screen, the convergence of the iteration is reached after a few iterations, with a focusing criterion close to 0.7. Now, the 1st eigenvector has an amplitude variation, as expected with the screen in the far-field. Backpropagation of the eigenvector (amplitude plus phase) yields a good focusing (Figure 93.*c*).

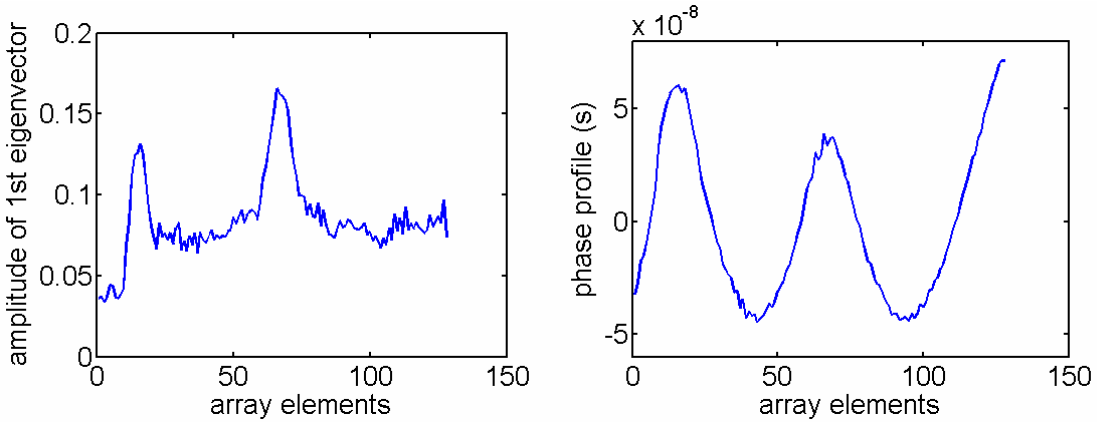

Figure 94 Amplitude and delay profile for the 1st eigenvector at the center frequency. As the phase screen is at 20 mm from the array, interferences occur and lead to amplitude variations. The FDORT method gives both the amplitude variation and the phase variation.

To summarize, FDORT has the ability to estimate accurate Green's functions in speckle in the more general model of a far-field phase screen.

C. Medical phantom results

Medical phantom data were obtained using a phased array at 2.7 MHz, and the Philips HDI-5000 scanner.

In a real experimental setup, two main things are differing from the simulations. First, the nature of the signal is different. In simulation, a perfect fully-developed was simulated, and no noise or bright scatterers (that can act as off-axis interference) were present. Second, a real aberrator will probably differ from the simple model used. In order to separate the influence of these two factors, two sets of experiments have been performed.

Experimental data and simulated aberrator

In the first experiment, the goal was to check that the method was working with real signals. Thus an experimental data set from an unaberrated phantom was used, and the data was artificially aberrated in the computer by delaying the signals. Therefore, the nature of the aberration is the same as in the simulation. The aberrated phantom is shown in Figure 96. The region of speckle used for FDORT was 2mm wide and 2 mm deep, and was located in the center right part of the phantom. About 25 realizations were selected in the region. The statistic of the phase screen was 45ns, 4 mm FWHM.

Discussion: The evolution of the 1st eigenvalue is shown in Figure 95. The maximum is reached after 3 iterations, and the focusing criterion is close to 0.6. The value is lower than in simulation, which is due to the transducers directivity and to the noise. However, 0.6 is already an excellent value. The images before correction, and corrected using the aberrator estimation after the 1st and 3rd estimations are shown in Figure 96 to Figure 98. An amplitude and delay correction was used. After the 3rd iteration, a very good focusing is achieved and it yield a good image quality.

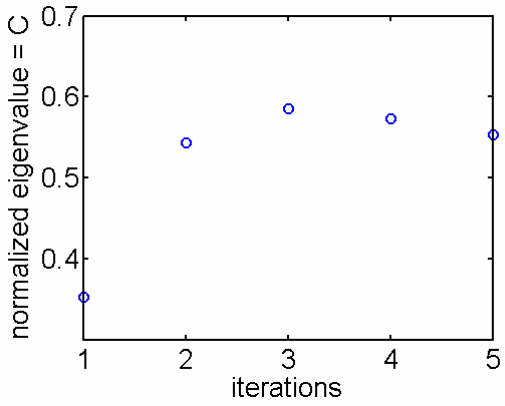

Figure 95 Evolution of the 1st eigenvalue after a few iterations.

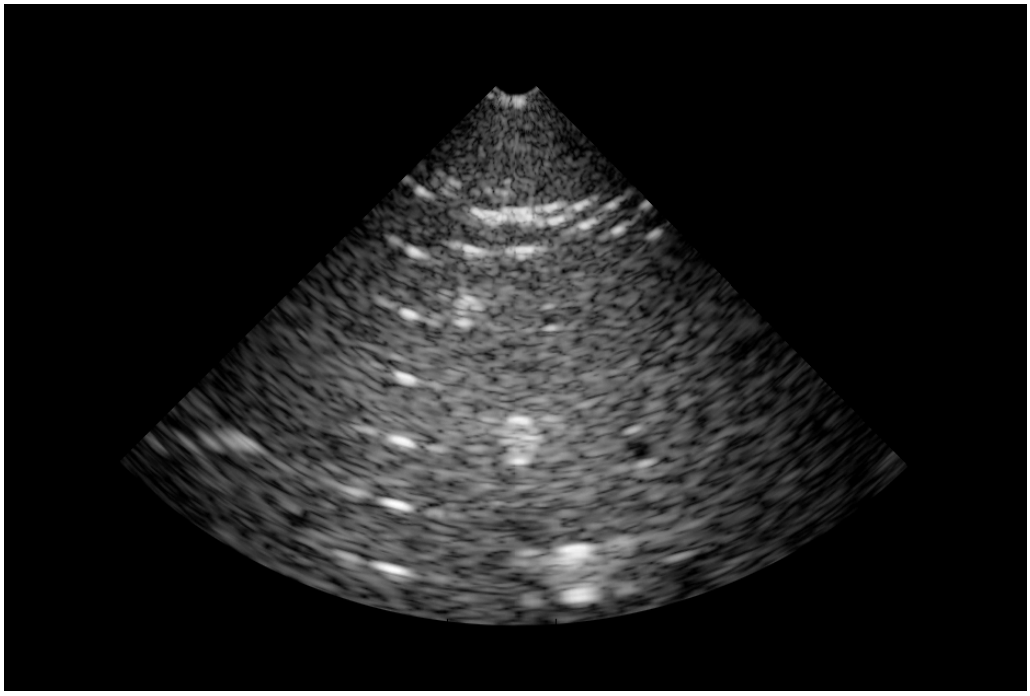

Figure 96 Image of the artificially aberrated phantom without correction.

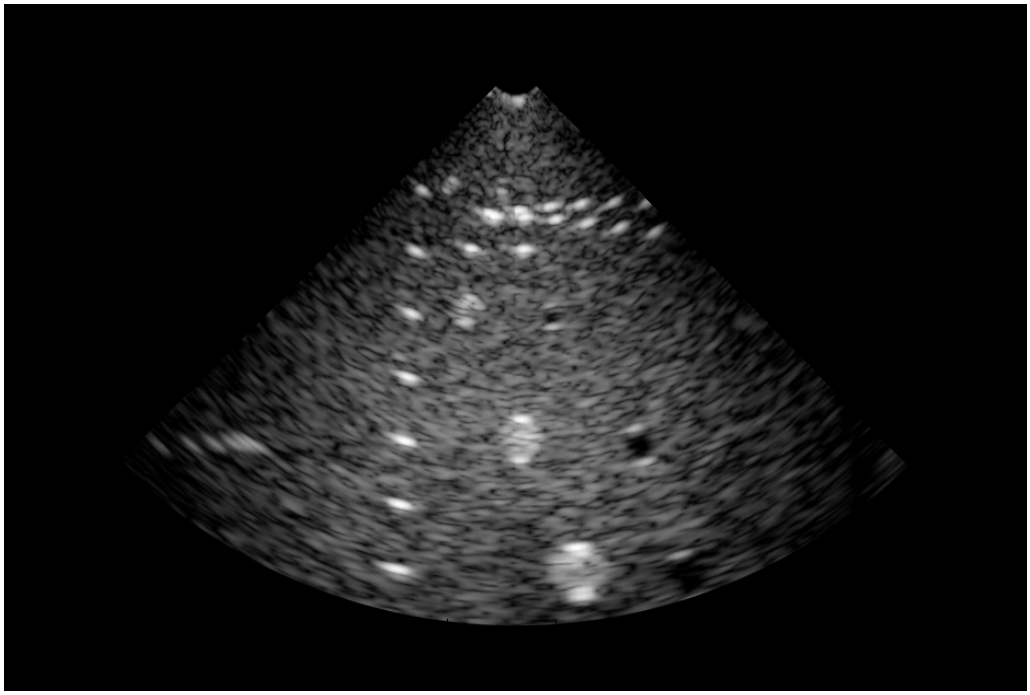

Figure 97 Image of the artificially aberrated phantom corrected after the 1st iteration of FDORT.

The points in the near field are not very well resolved yet.

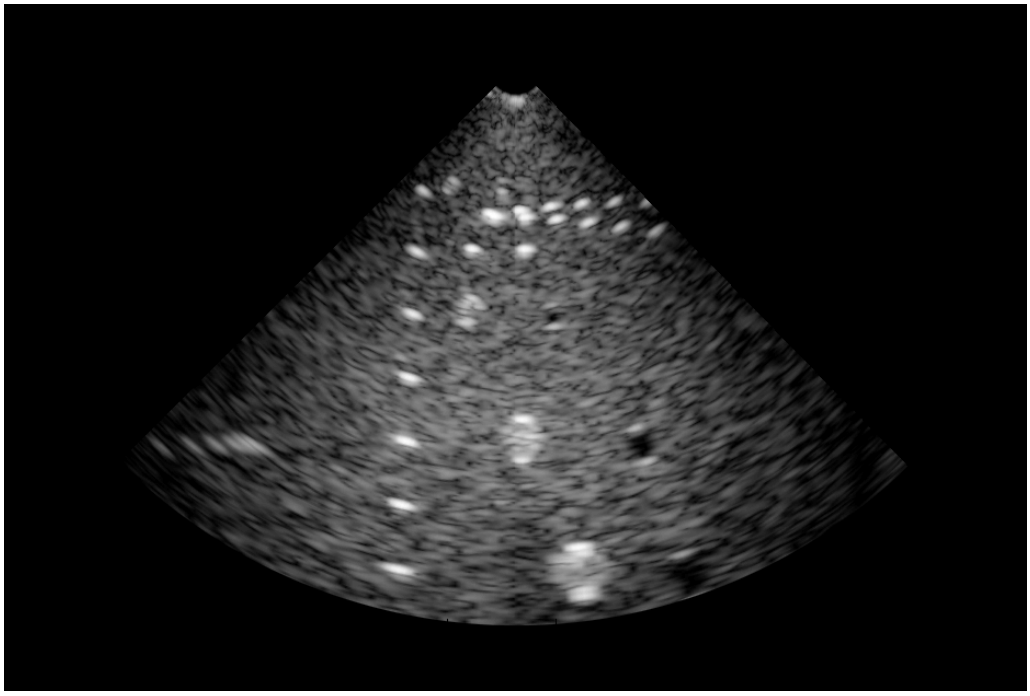

Figure 98 Image of the artificially aberrated phantom corrected after the 3rd iteration of FDORT. The focusing is excellent.

Experimental data with rubber aberrator

Now, experimental data of a phantom with a rubber aberrator is used. The rubber aberrator is characterized by a 75 ns rms delay and a 3 mm FWHM. It is then stronger than the simulated one. The aberrator was positioned between the phantom and the array. The aberrated image can be seen in Figure 99. The speckle area used for the estimation was the same as in the previous case. The corrected image after 5 iterations of FDORT is shown in Figure 100.

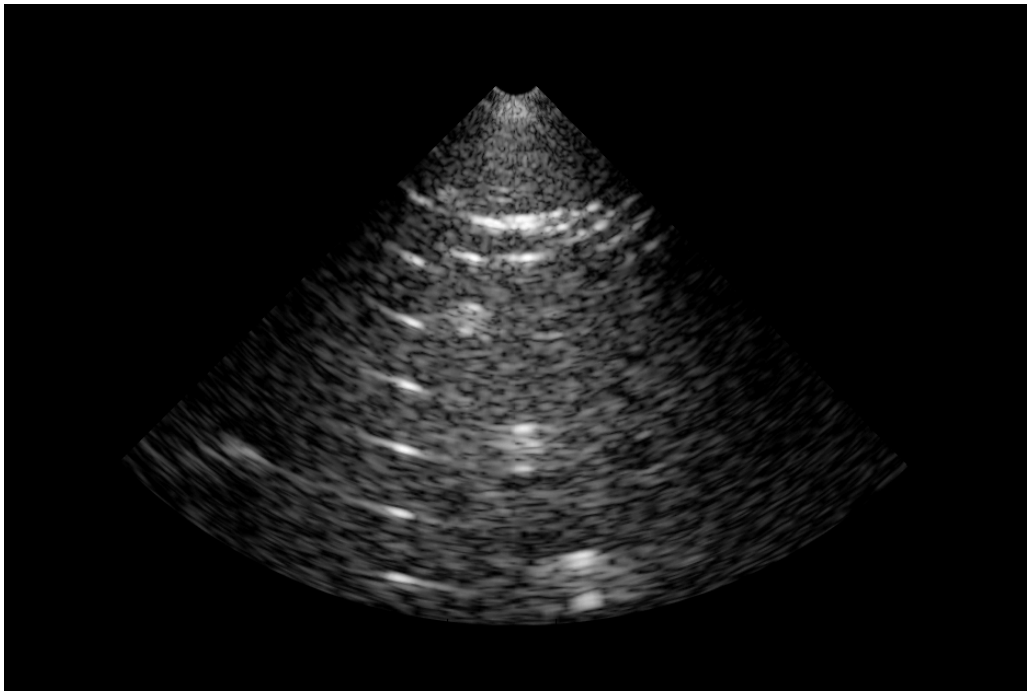

Figure 99 Image of the phantom with rubber aberrator without correction.

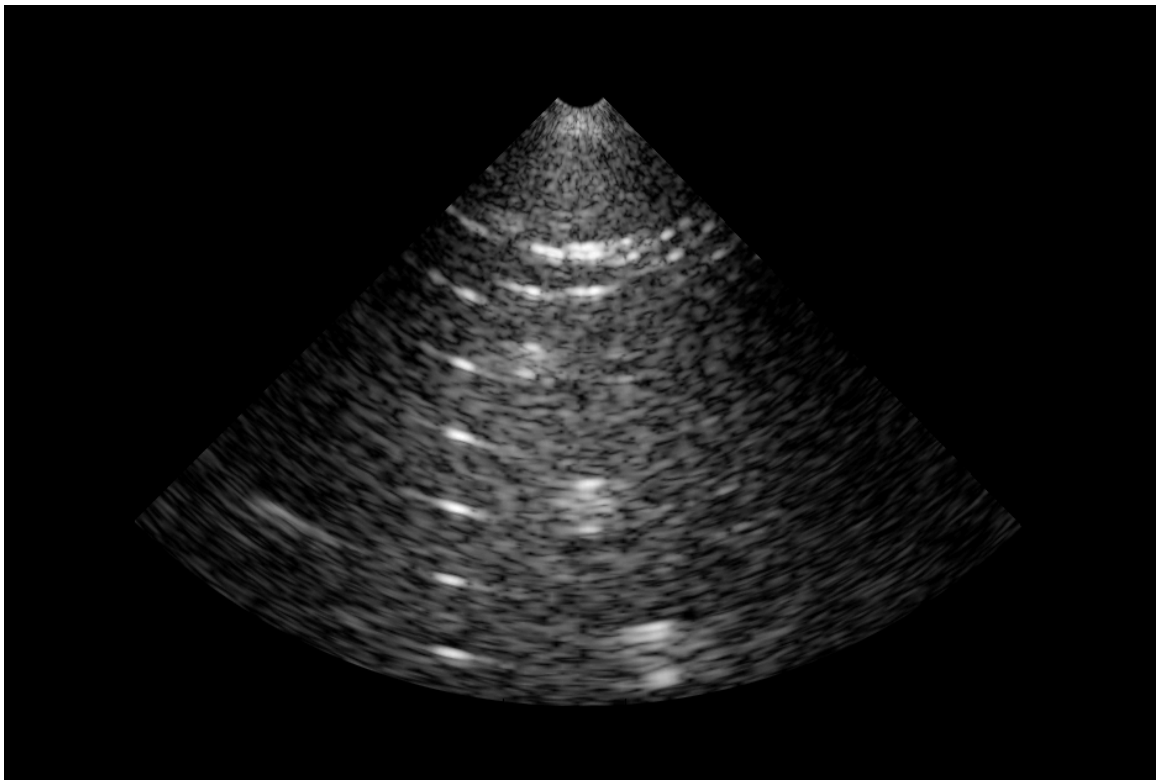

Figure 100 Image of the phantom with rubber aberrator corrected after the 5^{th} iteration of FDORT.

Discussion: Some improvement is seen in the resolution of the points scatterers on the left side near the speckle region, but the image still looks globally distorted. The focusing criterion stayed under 0.4 even after 10 iterations. As a comparison, FDORT has also been performed on one of the point scatterer, and the Green's function of the point scatterer used to correct the image. The result was similar to Figure 100. Other aberration correction methods gave similar results.

There are two main possible explanations for the difficulty to correct the image:

- Isoplanatic patch: as discussed in Section II.B., once the Green's function of a point has been estimated, the Green's function of the neighbor points can be deduced by the addition of a steering term. This works as long as the points are in a region surrounding the 1st point. This region is the isoplanatic patch. Despite the rubber aberrator is located in the near field, and thus should a large isoplanatic patch was expected, the results seems to show this is not the case. Indeed, the focusing seems to be good close to the region that has been used for the estimation, but it degrades rapidly away from this region.
- Two dimensional nature of the aberrator: the rubber aberrator varies in both azimuthal and elevational dimension, but as a 1D array is used, only the azimuthal dimension is corrected. This is the reason why most aberration correction schemes uses 2D array (Lacefield and Waag 2002; Fernandez, Gammelmark et al. 2003; Fernandez and Trahey 2003; Waag and Astheimer 2005; Waag and Astheimer 2006)

V. LINK WITH OTHER ABERRATION CORRECTION METHOD IN SPECKLE

A few aberration correction methods have been presented in Chapter1. The aim of this section is to interpret several of these methods with the spatial correlation matrix formalism and show that they are more similar than they appear.

A. 1-lag cross-correlation (O'Donnell)

This method has first been proposed in the time-domain by (Flax and O'Donnell 1988; O'Donnell and Flax 1988). It consists in computing the cross-correlation between the signals in pairs of adjacent elements. In the time domain, the maximum of the cross-correlation indicates the average difference of arrival time between the 2 elements and provide thus an estimate of the delay due to the aberrator. The method can also be implemented in the temporal frequency domain. This can be understood easily using our formalism. Indeed, an estimate of the cross-correlation between adjacent elements *m* and *m+1* is given by the coefficients $\left\langle S_m S_{m+1}^* \right\rangle = \left(R_{SS}\right)_{m,m+1}$ on the 1st extra-diagonal of the spatial correlation matrix.

Such a coefficient can be expressed, following Eq.4. 10, as

$$\left\langle S_m S_{m+1}^* \right\rangle = \exp j\left(\left(\phi^{Ab}(X_m) - \phi^{Ab}(X_{m+1})\right)\cdot \beta \cdot P\left(\frac{X_m - X_{m+1}}{\lambda Z}\right)\right.$$

Eq.4. 24

The phase term corresponding to the geometrical curvature of the wave-front has been removed, as the wave-fronts are usually aligned in aberration estimation method.

Taking the phase (noted $\angle$) of both side of the expression yield

$$\angle(\langle S_m S_{m+1}^* \rangle) = \phi^{Ab}(X_{i+1}) - \phi^{Ab}(X_i) + \angle\left(P\left(\frac{X_m - X_{m+1}}{\lambda Z}\right)\right)$$

Eq.4. 25

The phase of the coefficient (*m,m+1*) of the spatial correlation matrix is proportional to the phase difference between the 2 neighbor elements plus another term, which is the phase of the Fourier transform of the intensity distribution in the focal plane. In general, the Fourier transform of a function is complex, and the phase is non-zero. However, the term depends only on the separation between elements and thus is identical for all couple of neighbor elements. The last term of Eq.4. 25 is then the same constant for all elements on the 1st extra-diagonal of the matrix. Let A be this constant. Eq.4. 25 becomes

$$\angle(\langle S_m S_{m+1}^* \rangle) = \phi^{Ab}(X_{m+1}) - \phi^{Ab}(X_m) + A$$

and the phase estimate is obtained by integrating

$$\langle \tilde{\phi}^{Ab}(X_n) \rangle = \sum_{m=1}^{n-1} \angle(\langle S_m S_{m+1}^* \rangle)$$
$$= \phi^{Ab}(X_n) - \phi^{Ab}(X_1) + (n-1) \times A$$
$$= \phi^{Ab}(X_n) - \phi^{Ab}(X_1) + \left(\frac{X_n - X_1}{pitch}\right) \times A$$

In this case the bias is then reduced to a mere linear phase shift $\left(\frac{X_i - X_1}{pitch}\right) \times A$. In this technique, like in most aberration estimation technique, the estimated profile is detrended (suppression of linear phase shift). A linear bias will therefore not have any influence on the estimated profile. Thus, this method is said to be unbiased.

In practice, the estimate $\tilde{\phi}^{Ab}(X_n)$ can be obtained by integration of the phase of the elements $\left(KK^H\right)_{m,m+1}$ of the 1st extra-diagonal of the FDORT matrix.

This technique is very simple to implement, as no SVD is required, and only the terms on the 1st extra-diagonal have to be computed. Moreover, it does not, *a priori* requires any iteration, unlike FDORT. In practice, though, iterations may be required. Indeed the variance of the estimate depends on the spatial correlation that is low at the 1st iteration, as the transmit is not well focused. To obtain an estimate with an acceptable variance, at least one iteration is usually required.

The main drawback of this method compared to FDORT is in the presence of multiple signals, like off-axis scatterers. This problem is the object of the Section.4.V. Another drawback of the method can be noticed when one or several elements have a low signal. As the method relies only on correlation between neighbor elements, a discontinuity in the estimated aberrator profile can be observed at the location of the low signal elements.

B. Maximum Speckle Brightness

The speckle brightness increases with the quality of focusing. This is back-up by the expression of the speckle brightness in function of the spatial correlation in Section.II.B. Therefore, an aberration correction method consists in maximizing the brightness in a region of interest, corresponding usually to the isoplanatic patch, by adjusting the delays on the array elements. The brightness is maximized when the delay corrects the aberration.

As seen in Section.4.III.E., the 1st eigenvector of FDORT maximizes the speckle brightness. Thus, the maximum speckle brightness algorithm is very close to the FDORT method. The main difference, is that, in the speckle brightness algorithm, only the 1st eigenvector is obtained, which is a limitation in the case of multiple signals discussed in Section.4.V. Also, FDORT provides directly an objective criterion, C. The speckle brightness is only a relative criterion and is not as useful.

C. Eigenfunction analysis of backscattering signal

This method has been proposed by (Varslot, Krogstadt et al. 2004) and involves the decomposition of the spatial correlation matrix. It is then similar to our method. However, in (Varslot, Krogstadt et al. 2004) no practical way to build an estimate of the matrix is proposed. We propose to use the FDORT matrix as such an estimate. Moreover, our interpretation of the 1st eigenvalue enables to make the iteration process automatic as it provides a criterion for the convergence.

D. Multi-lag cross-correlation (LMS algorithm)

The multi-lag cross correlation technique is similar to the 1-lag cross-correlation technique, except that the cross-correlation is not only performed between adjacent elements, but also between pair of neighboring elements (up to a few elements apart). The differential delays are deduced from the correlation function maximums. Finally, the aberrator profile that fit the best the differential delays for all the pair of elements is found using a Least Mean Square (LMS) fitting that minimizes the least mean square error between the aberrator estimate and the differential delays (Fernandez, Gammelmark et al. 2003) and (Gauss, Trahey et al. 2001)The fact that not only delays between adjacent

elements but also delays between other pair of elements are used improves the robustness of the estimation, as more information is available. However, as the distance between elements in a pair increases, the Van Cittert Zernike theorem predicts a decrease in the correlation between the signals. When the correlation becomes too low, the differential delay estimate for the pair of element is very noisy and the benefits of using more pair of elements is overcame by the low quality of the additional delay estimate.(Fernandez, Gammelmark et al. 2003) and (Gauss, Trahey et al. 2001) are therefore using only near-neighbor pair of elements, up to 3 elements apart.

Another solution would be to use all pair of elements, but to weight the differential delay estimate given by each pair by the spatial correlation coefficients. Thus, pairs of elements that have a good correlation and thus provide a robust estimate have a large weight, while pairs of elements with a low correlation and therefore a large error in the estimate have a small weight. A variant of such a method is proposed by (Msoy, Angelsen et al.), in the temporal frequency domain.

We are now showing that it is also exactly what FDORT is doing. This is not surprising because Eq.4. 24 shows that the spatial correlation matrix, or FDORT matrix, contains the differential phase term for every pair of elements.

Indeed, rewriting Eq.4. 16 with discrete formalism yield

$$C = \frac{1}{Ne} \sum_{i=-Ne}^{Ne} \rho_{ATx}(i) \rho_{ARx}(i)$$

Eq.4. 26

$\rho_{ATx}(i)$ is the coherence of the signals for a pair of elements separated by i elements (lag i). It depends on the aberration in transmits. It is the triangle function if the transmit is not

aberrated. Let assume it is still a real positive function in presence of an aberrator. $\rho_{ARx}(i)$ is the autocorrelation of the receive aperture. The receive aperture phase comprises 2 terms: the receive aberration, $\phi^{Ab}(i)$ and a correction applied during the beamforming process, $\tilde{\phi}(i)$. It is then possible to write the receive aperture as

$$A_{Rx}(i) = \exp(j(\phi^{Ab}(i) - \tilde{\phi}(i)))$$

At lag 1 for example, the autocorrelation $\rho_{ARx}(i=1)$ is

$$\rho_{ARx}(1) = \sum_{i=1}^{Ne-1} \exp(j(\phi^{Ab}(i+1) - \phi^{Ab}(i)) - (\tilde{\phi}(i+1) - \tilde{\phi}(i)))$$

Eq.4. 27

This expression is a sum of exponential whose arguments are the differences between the true differential phase and the estimated differential phase. Similar expressions are obtained for other lags.

The 1st eigenvector of FDORT try to maximize the value of *C* by adjusting $\tilde{\phi}(i)$, the estimated phase term. *C* is maximized if each of the $\rho_{ARx}(i)$ is maximized. At lag 1, (Eq.4. 27), it is obtained if all the exponential of the sum have the same phase, so that the sum is constructive (the sum can be seen geometrically as a sum of vectors of length 1, the resulting vector is the longest if all the vectors are aligned) thus, for every i

$$\tilde{\phi}(i+1) - \tilde{\phi}(i) = \phi^{Ab}(i+1) - \phi^{Ab}(i) + A$$

Eq.4. 28

where *A* is a constant At lag 2, maximization of $\rho_{ARx}(i=2)$ is equivalent to

$$\tilde{\phi}(i+2)-\tilde{\phi}(i)=\phi^{Ab}(i+2)-\phi^{Ab}(i)+A'$$

Eq.4. 29

C is maximized only if *A=A'*, so that the term at lags 1 and 2 have the same phase and add constructively in Eq.(16). This is possible only if *A=0.* Indeed

$$\begin{aligned}\tilde{\phi}(i+2)-\tilde{\phi}(i) &= \tilde{\phi}(i+2)-\tilde{\phi}(i+1)+\tilde{\phi}(i+1)-\tilde{\phi}(i)\\ &= \phi^{Ab}(i+2)-\phi^{Ab}(i)+2A\end{aligned}$$

Eq.4. 30

using Eq.4. 28 twice. Eq.4. 29 and Eq.4. 30 are compatible with *A=A'* only if *A=A'=0.* Eq.4. 28 with *A=0* means that the difference between the true and estimated differential phase is minimized. Eq.4. 29 states the minimization of the difference between true and estimated 2-lag differential phase. Thus the phase of the 1st eigenvector is the estimation that fit the best the differential phase for all lags.

According to Eq.4. 26, the contribution of each lag in *C* is weighted by $\rho_{ATx}(i)$, which is the coherence of the received signals for this lag. Therefore, the lags for which the signals are the most coherent have large weights, while signals that are very weakly correlated (and therefore result in a high variance in the estimation) have small weights and have a low contribution to the estimate.

While the LMS algorithm minimizes the the least mean square error between the aberrator estimate and the differential delays, FDORT minimizes the error function $1-C$.

VI. GREEN FUNCTION ESTIMATION AND FOCUSING IN PRESENCE OF STRONG INTERFERING SIGNALS

The FDORT method is quite complex to implement as it involves singular value decomposition of the spatial correlation matrix. As seen in the previous section, methods involving a simple summation of the coefficients in the 1st extra-diagonal only yield an estimate of the phase of the Green's function as accurate as FDORT. A question one may ask is then what is then the advantage of the FDORT method? A first advantage has already been discussed before: unlike the other methods, FDORT provides both the phase and the amplitude of the Green's function. In addition, it provides a measure of the focusing quality through the 1st eigenvalue. However, all this quantities could also be estimated independently.

There is another important advantage of using FDORT, which is similar to the advantage of using the DORT (or FDORT) method with point scatterers. The fundamental advantage of the DORT method is that it is able to separate the wave-fronts form different scatterers. Each eigenvector correspond to a different scatterer. It is then able to separate the signal of the target of interest from other signals (other scatterers, interferences..) This property is fundamentally linked to the interpretation as a covariance matrix (Gruber, Marengo et al.) and principal component analysis (Rao 1964) (Cooley and Lohnes 1971)

In the same fashion, the fact that the FDORT method in speckle involves the decomposition of the spatial correlation matrix enables it to separate signals. Let us consider a simple example where one try to estimate a Green's function from speckle signal in presence of a strong interference. In our case, the interference is a signal coming

from “infinite”. In practice, the interference can be due to an active source (a boat in underwater acoustic for example). In medical ultrasound, the interference could be a bright off-axis scatterer. A simple aberration method does not separate the signals, so the estimated phase will be an average of the interference Green’s function and of the Green’s function that one wants to estimate (Dahl and Trahey 2003). If the interference is much stronger than the speckle signal, then the estimate gives the phase of the interference and it is impossible to know the desired Green’s function. However FDORT has the ability to separate the 2 signals as long as they are orthogonal (resolved). The 1st eigenvector will typically be the interference Green’s function, while the 2nd eigenvector will be the desired speckle Green’s function. It does not matter how much stronger is the interference signal.

Simulation

The setup is illustrated in Figure 101. The speckle is placed behind a phase screen. This setup has been simulated with an interference signal 1000 times stronger (60 dB) than the speckle signal of interest. The magnitude of the interference is exaggerated to demonstrate the efficiency of the FDORT algorithm.

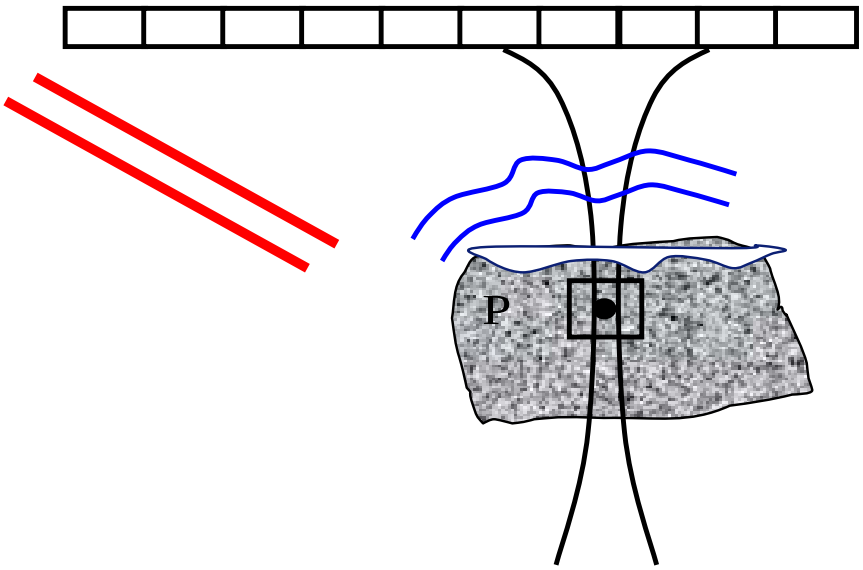

Figure 101 Setup for the simulation: the goal is to estimate the Green's function of point P in speckle (blue wave-front) using focused transmit, in presence of a strong interferer signal (red wave-front). The signal from point P travels through an heterogeneity, but the interferer does not. In order to estimate the parameters of the heterogeneity it is necessary to isolate the wave-front of P from the interferers. In the simulation, the interferer is 1000 times stronger than the signal.

The phases for the 1st and 2nd eigenvector of FDORT are displayed in Figure 102. The geometrical delay law has been subtracted from the 2nd eigenvector for clarity. It is clear that the 1st eigenvector corresponds to the interference and the 2nd eigenvector to the speckle target. The distortion due to the heterogeneity is seen in the phase of the speckle Green's function, and not in the phase of the interference as the interference signal did not go through the heterogeneity.

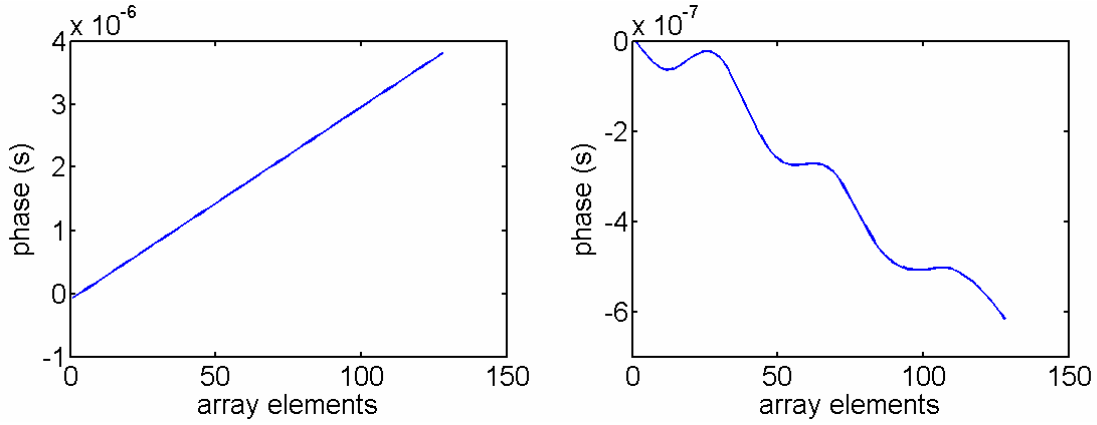

Figure 102 Phase for the 1st and 2nd eigenvector of FDORT, corresponding to the setup of Figure 101. The 1st eigenvector corresponds clearly to the interference, while the 2nd corresponds to the speckle, and carries information on the heterogeneity.

Backpropagation of the eigenvectors, shown in Figure 103 confirms that the 2 signals are very well separated. In addition, it shows that the estimate of the speckle Green'function is excellent as one is able to achieve very good focusing through the heterogeneity. The eigenvectors shown here were obtained after 4 iterations, where the 2nd eigenvector was used to correct the transmit.

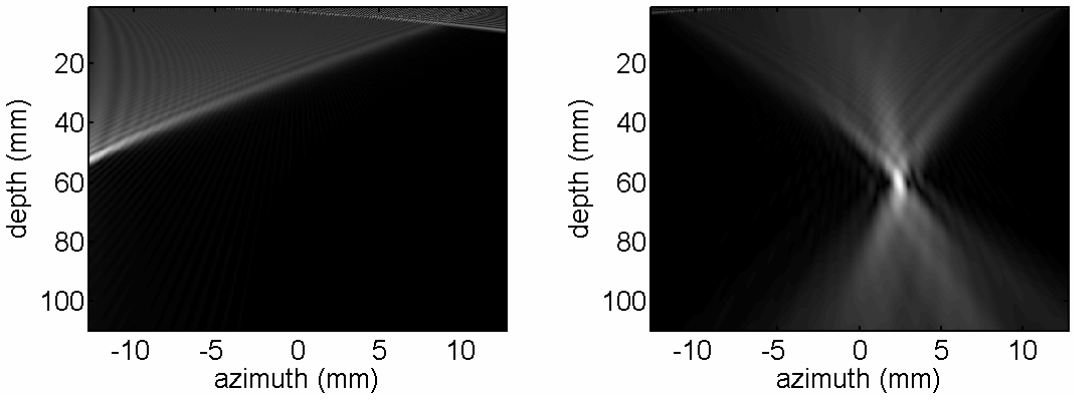

Figure 103Fields after numerical backpropagation of the 1st (left) and 2nd eigenvectors. This confirms that the 1st eigenvector corresponds to the interference, while the 2nd eigenvector corresponds to the desired speckle signal. The eigenvector corresponding to the speckle is a very good estimate of the

Green’s function and leads to a good focusing through the heterogeneity despite the presence of the strong interfering signal.

It is remarkable that such an accurate estimate of the speckle Green’s function is possible in presence of an interfering signal 1000 times stronger. This is an important property of FDORT.

With another estimation method, like the 1 lag cross correlation method, this is not possible. The phase profile estimated with the 1-lag method is shown in Figure 104. It is completely dominated by the strong interference. It is difficult to extract any information about the heterogeneity from this curve, and the focusing in speckle cannot be achieved using this method.

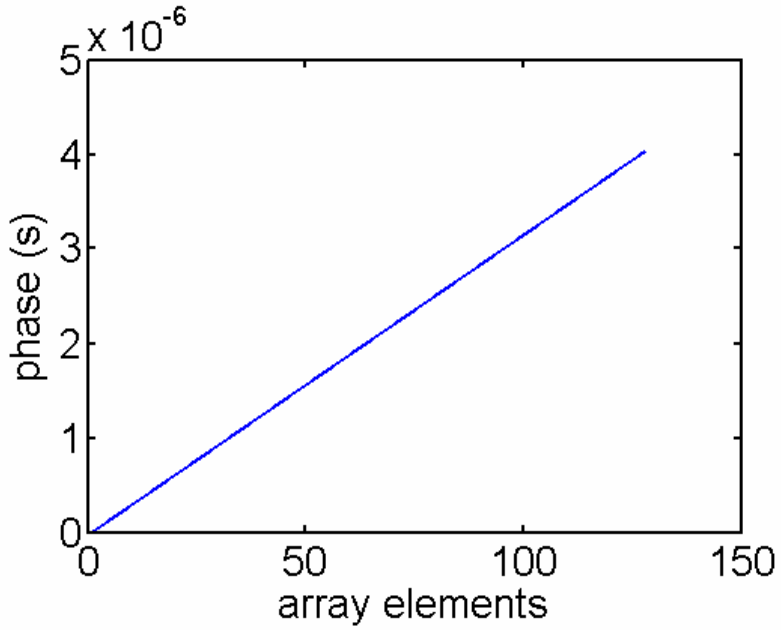

Figure 104 Phase estimate obtained with the 1-lag cross-correlation method. The estimate is completely dominated by the interference, and it is not possible to extract any information about the heterogeneity.

Some application of this signal separation property also arises when there are a few bright scatterers in a speckle medium. If one try to estimate the Green's function in a region of pure speckle, there are chances that one receives not only echoes from the speckle region, which is the region insonified by the transmits, but also from bright scatterers outside of the region. This happens even though one focus in transmit far from the bright scatterers because there is some energy in the side lobes of the transmit. In this case we talk about off-axis scatterers. This can be an important problem in aberration correction if the off-axis scatterer is not in the isoplanatic patch of the speckle. In this case the wave-fronts of the speckle and of the off-axis scaterrers are distorted by different aberrations, and a classic estimation method will yield an average of the two aberrations, which will not lead to a very good focusing on the speckle region, nor on the off-axis scatterer. FDORT can separate the aberration profiles.

One can note that even though FDORT can separate the Green's function of two scatterers, the order of the Green's function can change when the method is iterated. For example, in an experiment, FDORT was used to estimate the Green's function in a speckle region in the phantom of Figure 96, close from a bright scatterers. For the 10 first iterations, the 1st eigenvector was corresponding to the speckle, and the scatterer's eigenvector was 2nd. However, after 10 iterations, the bright scatterer's eigenvector took the first position.

VII. CONCLUSION

It has been shown that FDORT could be used to extract Green's functions from speckle signal as well as from resolved scatterers. With resolved scatterers, the operator KK^H, built with the FDORT method, is connected to Time Reversal. In speckle, it has

been shown that KK^H was connected to another fundamental theorem of acoustics, the Van Cittert Zernike theorem. This yields an interpretation of the 1st eigenvalue of the FDORT matrix as the focusing criterion C, which is a measure of the quality of the focusing, and has been used in number of publications. In speckle KK^H can alternatively be interpreted as a canonical Time Reversal Operator for an equivalent virtual object that has the shape of the transmit. This leads to an intuitive understanding of the eigenvectors. Thus, the first eigenvector focuses on and is the Green function of the brightest point of the transmit beam pattern, which, in homogeneous medium is the focal spot of the transmit. In heterogeneous medium, a few iterations of the method are often needed to converge on the Green's function of a point. The interpretation of the 1st eigenvalue of KK^H is of particular interest, as it indicates objectively when the focusing is good enough and the iteration can be stopped. The focusing properties of the 1st eigenvector of KK^H have been demonstrated for different model of heterogeneities. Finally, a main feature of the FDORT method is its ability to separate wave-fronts. In particular, it is able to separate the signal of interest from interferences and off-axis scatterers.

APPENDIX A COHERENT INTENSITY AND FOCUSING CRITERION IN FUNCTION OF THE SPATIAL CORRELATION FUNCTION

From Eq.4. 12 and Eq.4. 13, the coherent intensity is

$$I = < \sum_{i=1}^{Ne} S_i V_i^* \left(\sum_{i=1}^{Ne} S_i V_i^* \right)^* >$$
$$= < \sum_{i=1}^{Ne} \sum_{j=1}^{Ne} S_i S_j^* V_i^* V_j >$$
$$= \sum_{i=1}^{Ne} \sum_{j=1}^{Ne} < S_i S_j^* > V_i^* V_j$$

Using Eq.4. 10 yields

$$I = \beta \sum_{i=1}^{Ne} \sum_{j=1}^{Ne} e^{j\phi^{Ab}(X_i)} V_i e^{-j\phi^{Ab}(X_j)} V_j R_{ATx}(X_i - X_j)$$

We introduced earlier a transmit aperture function. Similarly, the receive aperture function in presence of the aberrator is

$$A_{Rx}(X) = e^{j\phi^{Ab}(X_i)} V(X)^*$$

Eq.4. 31

V(X) is an apodization function, that can also be complex to allow for aberration correction. Using the continuous formalism

$$I = \gamma \iint A_{Rx}(X_i) A_{Rx}(X_j)^* R_{ATx}(X_i - X_j) dX_i dX_j$$

Letting ΔX be X_i-X_j leads to

$$I = \gamma \iint A_{Rx}(\Delta X + X_j) A_{Rx}(X_j) R_{ATx}(\Delta X) d\Delta X dX_j$$
$$= \gamma \int \left[\int A_{Rx}(\Delta X + X_j) A_{Rx}(X_j)^* dXj \right] R_{ATx}(\Delta X) d\Delta X$$

we recognize in the first integral $\int A_{Rx}(\Delta X + X_j)\overline{A_{Rx}(X_j)}dXj$ the autocorrelation function of the equivalent receive aperture denoted $R_{ARx}(X)$. Now

$$I = \gamma \int R_{ATx}(\Delta X) R_{ARx}(\Delta X) d\Delta X$$

Eq.4. 32

We also need to express the incoherent intensity. Eq.4. 15 yield $I_{Inc}=Ne.R_S(i,i)$

From Eq.4. 11, $R_{SS}(i,i) = \beta R_{ATx}(0)$

And in the continuous formalism, we can write $Ne=l_{array}$, the array length. Finally,

$$\langle I_{Inc} \rangle = \beta R_{ATx}(0) \cdot l_{array}$$

Eq.4. 33

Now, we can derive an expression of the coherence factor by taking the ratio of equation Eq.4. 32 and Eq.4. 33. Let us first introduce a normalized version of the aperture autocorrelation function, known as the coherence function

$$\rho_{ATx}(X) = \frac{R_{ATx}(X)}{R_{ATx}(0)}$$

The maximum of the coherence function, reached for X=0, is 1, for any aperture used.

For the receive aperture, Eq.4. 31 yields $R_{ARx}(0) = \int_{ARx} |v(X)|^2 \, dX = 1$ since v(X) has a unit norm. Then $\rho_{ARx}^{Eq}(X) = R_{ARx}^{Eq}(X)$. Thus,

$$C = \frac{\int \rho_{ATx}(X)\rho_{ARx}(X)dX}{l_{array}} = \int \rho_{ATx}(l_{array}.X)\rho_{ARx}(l_{array}.X)dX$$

the last step was obtained using a change of variable.

Appendix B**. VARIANCE OF THE ESTIMATION**

It was mentioned in Section III.C. that the maximum variance reduction that one can achieve in a given volume of speckle is equal to the number of resolution cells in the volume. We provide here a more rigorous derivation of this.

For simplicity, we start deriving the result for the amplitude of the coefficients of the spatial correlation matrix (or FDORT matrix). The case of the phase will then be dealt with.

A. Variance of the amplitude of the spatial correlation coefficients

The estimate of the spatial correlation between the signals received by element i and element j is given by

$$\left(KK^{H}\right)_{m,n} = \sum_{i=1}^{I} S_m^i S_n^{i*} = I\left(\frac{1}{I}\sum_{m=1}^{M} S_m^i S_n^{i*}\right)$$

Eq.4. 34

This is the average value on I realizations of the product of the signals received by the transducers. As explained in III.C, the realizations can be taken by transmitting at different azimuths *x*, and by selecting signals from different depths (different arrival time *t*). To highlight this, let us note one realization of the signal received by element m $S_m(x,t)$. Let us now imagine that we average on every realizations from a given volume of speckle (here, as we are considering a 2D geometry, it is more rigorously an area of speckle). The dimension of the volume is *X* in azimuth, and *T* in arrival time (depth). The estimate of the spatial correlation coefficient can thus be rewritten, using continuous notations instead of discrete ones

$$\left(KK^{H}\right)_{m,n} = \frac{1}{XT}\iint_{area} S_m(x,t)\cdot S_n(x,t)^{*}\,dxdt$$

The integral on the area of speckle is the continuous equivalent of the sum in Eq.4. 34. Each position *(x,t)* defines here a realization, that was indexed by i in the discrete formulation.

Let us first check that the expected value of the estimation is the spatial correlation between the signals. The expected value is

$$<\left(KK^{H}\right)_{m,n}>=\frac{1}{XT}\iint_{area}<S_m(x,t)\cdot S_n(x,t)^{*}>\,dxdt$$

By definition,

$$<S_m(x,t)\cdot S_n(x,t)^{*}>=<S_m\cdot S_n^{*}>$$

Eq.4. 35

is the spatial correlation. It is independent of the index *(x,t).* Of course, this rely on the position *(x,t)* being in the isoplanatic patch, close to the focal depth, and on the wave-fronts being properly shifted as explained in **Figure 82**, so that the $S_m(x,t)$ can be considered as different realizations of the same signal. Then

$$< \left(KK^H\right)_{m,n} >= \frac{1}{XT} \iint_{area} < S_m \cdot S_n^{\ *} > dxdt$$
$$= \frac{< S_m \cdot S_n^{\ *} >}{XT} \iint_{area} dxdt$$
$$= \frac{< S_m \cdot S_n^{\ *} >}{XT} XT$$
$$=< S_m \cdot S_n^{\ *} >$$

Indeed, $\iint_{area} dxdt$ is the total area and is thus equal to XT. We have shown that in average, the coefficients of the FDORT matrix, $\left(KK^H\right)_{m,n}$, are equal to the spatial correlation coefficients. This seems obvious as $\left(KK^H\right)_{m,n}$ is an estimate of the spatial correlation coefficients, but it is not the case for all estimators in statistics. $\left(KK^H\right)_{m,n}$ is said to be a non-biased estimation of the spatial correlation coefficient.

More interesting is the variance of the estimation. The variance is defined by

$$\left\langle \left(\left(KK^H\right)_{m,n} - < \left(KK^H\right)_{m,n} > \right)^2 \right\rangle = \left\langle \left(KK^H\right)_{m,n}^{\ 2} \right\rangle - < \left(KK^H\right)_{m,n} >^2$$

Eq.4. 36

The second term is the square of the expected value derived before.

$$< \left(KK^H\right)_{m,n} >^2 =< S_m \cdot S_n^{\ *} >^2$$

Let us focus on the 1st term.

$$\left(KK^{H}\right)_{m,n}{}^{2} = \frac{1}{XT}\iint\limits_{area} S_m(x1,t1)\cdot S_n(x1,t1)^{*}\,dx1dt1\cdot\left(\frac{1}{XT}\iint\limits_{area} S_m(x2,t2)\cdot S_n(x2,t2)^{*}\,dx2dt\right)^{*}$$
$$= \frac{1}{(XT)^2}\iiint\iint S_m(x1,t1)\cdot S_n(x1,t1)^{*} S_m(x2,t2)^{*}\cdot S_n(x2,t2)dx1dt1dx2dt2$$

and thus

$$\left\langle\left(KK^{H}\right)_{m,n}{}^{2}\right\rangle = \frac{1}{(XT)^2}\iiint\iint\left\langle S_m(x1,t1)\cdot S_n(x1,t1)^{*} S_n(x2,t2)\cdot S_m(x2,t2)^{*}\right\rangle dx1dt1dx2dt2$$

Eq.4. 37

The derivation of the variance involves a product of 4 terms, and is therefore 4th order statistics. 4th order moments are usually very difficult to compute. However, in the case of jointly Gaussian variable, as it is the case with speckle signal, the 4th order moment can be expressed as a sum of 2nd order moments. This is the known as the Gaussian moment theorem (also known as Wick theorem) (Goodman 1985). Let u_1, u_2, u_3, and u_4 be 4 jointly Gaussian random variables. The Wick formula says [eq.(2.8.-22) in (Goodman 1985)]

$$\left\langle u_1 u_2{}^{*} u_3 u_4{}^{*}\right\rangle = \left\langle u_1 u_2{}^{*}\right\rangle\left\langle u_3 u_4{}^{*}\right\rangle + \left\langle u_1 u_4{}^{*}\right\rangle\left\langle u_3 u_2{}^{*}\right\rangle$$

In our case, this yield

$$\left\langle S_m(x1,t1)\cdot S_n(x1,t1)^{*} S_n(x2,t2)\cdot S_m(x2,t2)^{*}\right\rangle$$
$$= \left\langle S_m(x1,t1)\cdot S_n(x1,t1)^{*}\right\rangle\left\langle S_n(x2,t2)\cdot S_m(x2,t2)^{*}\right\rangle + \left\langle S_m(x1,t1)\cdot S_m(x2,t2)^{*}\right\rangle\left\langle S_n(x2,t2)\cdot S_n(x1,t1)^{*}\right\rangle$$

Eq.4. 38

The 1st term simplifies using Eq.4. 35. to yield

$$\left\langle S_m(x1,t1)\cdot S_n(x1,t1)^{*}\right\rangle\left\langle S_m(x2,t2)\cdot S_n(x2,t2)^{*}\right\rangle = < S_m\cdot S_n{}^{*} >^2$$

This term will cancel out with the 2nd term of Eq.4. 36 as will be shown later. For now let us focus on the 2nd term of Eq.4. 38, which is responsible for the variance. $\left\langle S_m(x1,t1)\cdot S_m(x2,t2)^*\right\rangle$ represents the correlation between the signal from a window located at position *(x1,t1)* and the signal from a window located at position *(x2,t2)*. This has been derived in Section II.C.2.. It is independent on the receiver *m* and leads to

$$\left\langle S(x_1,t_1)S(x_2,t_2)^*\right\rangle = I_{Inc}\,\sigma_w(x_2-x_1,z_2-z_1)$$

Injecting this in Eq.4. 38 yield

$$\left\langle S_m(x1,t1)\cdot S_n(x1,t1)^* S_m(x2,t2)\cdot S_n(x2,t2)^*\right\rangle = < S_m\cdot S_n^* >^2 + I_{Inc}{}^2\sigma_w(x_2-x_1,t_2-t_1)^2$$

Equation Eq.4. 37 becomes

$$\left\langle \left(KK^H\right)_{m,n}{}^2\right\rangle = \frac{< S_m\cdot S_n^* >^2}{(XT)^2}(XT)^2 + \frac{I_{Inc}{}^2}{(XT)^2}\iiint \sigma_w(x_2-x_1,z_2-z_1)^2\,dx1dt1dx2dt2$$

Finally, the variance expressed in Eq.Eq.4. 36 becomes

$$\left\langle \left(KK^H\right)_{m,n}{}^2\right\rangle - <\left(KK^H\right)_{m,n}>^2 = < S_m\cdot S_n^* >^2 + \frac{I_{Inc}{}^2}{(XT)^2}\iiint \sigma_w(x_2-x_1,z_2-z_1)^2\,dx1dt1dx2dt2 - < S_m\cdot S_n^* >^2$$

$$= \frac{I_{Inc}{}^2}{(XT)^2}\iiint \sigma_w(x_2-x_1,z_2-z_1)^2\,dx1dt1dx2dt2$$

Changing the variable to $x_1=x+x_2$ and $t_1=t+t_2$ yields

$$\left\langle \left(KK^H\right)_{m,n}{}^2\right\rangle - <\left(KK^H\right)_{m,n}>^2 = \frac{I_{Inc}{}^2}{(XT)^2}\iint dx2dt2\iint \sigma_w(x,z)^2\,dxdz$$

and finally noticing that $\iint dx2dt2 = XT$ leads to the expression of the variance

$$\left\langle \left(KK^H\right)_{m,n}{}^2\right\rangle - <\left(KK^H\right)_{m,n}>^2 = \frac{I_{Inc}{}^2}{XT}\iint \sigma_w(x,z)^2\,dxdz$$

Now *XT* is the area of speckle interrogated, and the integral term also has the dimension of an area. $\sigma_w(x,z)$ is a function which is basically non-zero only on a zone that has the size of the resolution cell, and whose maximum value is 1. If the area of integration is larger than the resolution cell, then $\iint \sigma_w(x,z)^2\,dxdz$ is about the area of the resolution cell (modulo a numerical factor that depends on the bandwidth and apodization). Therefore, the variance is proportional to the number of resolution cell in the total area. In general, with a 2D array, the reduction in variance of the estimate is proportional to the number of resolution cell in the volume of speckle used for the estimate.

$$\left\langle \left(KK^H\right)_{m,n}{}^2 \right\rangle - < \left(KK^H\right)_{m,n} >^2 \propto I_{Inc}{}^2 \frac{A_{resolution\_cell}}{A_{total}} \propto \frac{I_{Inc}{}^2}{N_{resolution\_cell}}$$

A very important conclusion, is that even if a continuum of realizations (each realization corresponding to a pair *(x,t)*) is used, the variance is reduced only by a finite amount. In other words, there are only a finite number of realizations in the speckle volume, which is the number of resolution cells, $N_{resolution\_cell}$. There is then no use to use more than $N_{resolution\_cell}$ realizations if they are well chosen so that they are independent.

Another interesting parameter is the *space-bandwidth* product. It is easily shown that $\iint \sigma_w(x,z)^2\,dxdz$ is roughly equal to the inverse of the area of the spectrum $A_{k-space}$ of the wave-front. The spatial frequency domain is also known as k-space. The variance is inversely proportional to the product of the area of speckle by the area of the spectrum of the system. Then another expression of the variance is

$$\left\langle \left(KK^H\right)_{m,n}{}^2 \right\rangle - < \left(KK^H\right)_{m,n} >^2 \propto \frac{I_{Inc}{}^2}{XT \cdot A_{k-space}} \propto \frac{I_{Inc}{}^2}{X \cdot T \cdot B \cdot D/\lambda F}$$

We used the fact that the area in k-space could be approximated by the product of the temporal bandwidth B and the spatial bandwidth $D/\lambda F$.

The expression in function of the area of the spectrum is particularly important. Indeed, the amplitude of the spectrum, and then its area, is independent of the depth (Zemp and Insana 2004).In particular it is the same at the focal depth and at other depth. Only the phase of the spectrum is changing, which does not affect the area. Also in a good approximation, the amplitude of the spectrum is not affected by a near field phase aberration. This means, that, counter intuitively, the quantity of information is the same out of the focus, or in presence of a phase aberration.

B. Variance of the phase

Computing the variance of the phase is more technical. Such a derivation is done in chapter 6.2 of (Goodman 1985), for a one-dimensional (time) signal. This can be easily generalized to our 2-dimensional model (azimuth-time) using the derivation in Section 4.VI.A. Only the main results are given here.

The 1st step is to compute the variance for the real part and the imaginary part of the spatial correlation coefficients. This is very similar to the derivation of the previous section (4.VI.A.) The only difference is that it involves computing correlation like $\left\langle S_m(x1,t1)\cdot S_n(x2,t2)^* \right\rangle$ where both the speckle region and the receive element are different. This is half way between the Van Cittert Zernike theorem and the result of II.C.2. A rough approximation made by Goodman is

$$\left\langle S_m(x1,t1)\cdot S_n(x2,t2)^* \right\rangle = I_{Inc}\sigma_w(x_2-x_1,z_2-z_1)\mu(m,n)$$

This allows to compute easily the mean value and variances

$$\left\langle \mathrm{Re}\left(\left(KK^H\right)_{m,n}\right)\right\rangle = I_{Inc}\left|\mu(m,n)\right|$$

$$\mathrm{var}\left[\mathrm{Re}\left(\left(KK^{H}\right)_{m,n}\right)\right] = \frac{{I_{Inc}}^{2}}{N_{resolution\_cell}} \frac{1+\left|\mu(m,n)\right|^{2}}{2}$$

$$\left\langle \mathrm{Im}\left(\left(KK^{H}\right)_{m,n}\right)\right\rangle = 0$$

$$\mathrm{var}\left[\mathrm{Im}\left(\left(KK^{H}\right)_{m,n}\right)\right] = \frac{{I_{Inc}}^{2}}{N_{resolution\_cell}} \frac{1-\left|\mu(m,n)\right|^{2}}{2}$$

The variance of the phase can then be represented graphically by representing a *cloud* of probability for the complex coefficient $\left(KK^{H}\right)_{m,n}$ as shown in Figure 105. The variance does not depend only on the number of resolution cell, but also on the coherence of the signals received by a pair of element. According to the Van Cittert Zernike theorem, neighbor coefficients have a high coherence, and $\left|\mu(m,n)\right|$ is close to 1. In this case the variance of the phase is small. This makes sense, as when the signals are perfectly coherent, their phase difference is constant. For elements further apart, especially in a heterogeneous medium where the coherence length is decreased, $\left|\mu(m,n)\right|$ can be close to zero, and the variance of the phase is important. In all cases, it decreases inversely proportionally to the number of resolution cells.

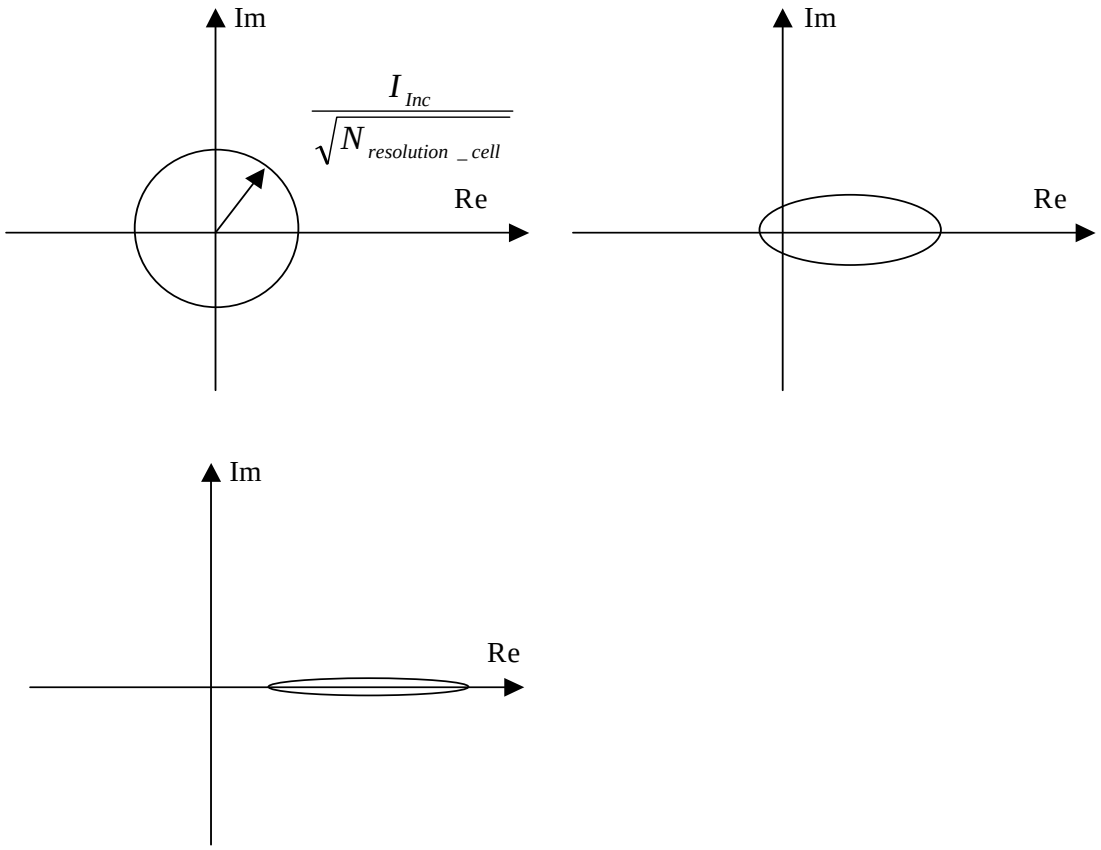

Figure 105 Probability clouds for the spatial correlation, for 3 values of the coherence. From top left to bottom: $|\mu(m,n)|$ =0, $|\mu(m,n)|$ =0.5, $|\mu(m,n)|$ =0.98. As the coherence increases, the phase variance decreases.

In the limit where the number of realizations is important and $|\mu(m,n)|$ is not to small, a closed formula can be derived for the variance of the phase (6.2.-3 in (Goodman 1975))

$$\mathrm{var}\left[angle\left(\left(KK^{H}\right)_{m,n}\right)\right]=\frac{1-|\mu(m,n)|^{2}}{N_{resolution\_cell}\cdot|\mu(m,n)|^{2}}$$

This formula is a general version of the one derived by (Walker and Trahey 1995).In our case, the realizations are taken from a volume, (or area) of speckle. In his case, the only averaging was in time.

Dorme, C. and M. A. Fink (1996). "Ultrasonic beam steering through inhomogeneous layers with a time reversal mirror." Ultrasonics, Ferroelectrics and Frequency Control, IEEE Transactions on **43**(1): 167-175.

Fink, M., J.-F. Cardoso, et al. (1984). "Analyse des effets de la diffraction en echographie medicale " Acta Electronica **26**(1-2): 59-80.

Goodman, J. W. Statistical Optics, Wiley Classics Library.

Raoul, M. and F. Mathias (1994). "Adaptive focusing in scattering media through sound-speed inhomogeneities: The van Cittert Zernike approach and focusing criterion." The Journal of the Acoustical Society of America **96**(6): 3721-3732.

Roger, Z. and F. I. Michael (2007). "Imaging with unfocused regions of focused ultrasound beams." The Journal of the Acoustical Society of America **121**(3): 1491-1498.

Walker, W. F. and G. E. Trahey (1995). "A fundamental limit on delay estimation using partially correlated speckle signals." Ultrasonics, Ferroelectrics and Frequency Control, IEEE Transactions on **42**(2): 301-308.

Astheimer, J. P., W. C. Pilkington, et al. (2006). "Reduction of variance in spectral estimates for correction of ultrasonic aberration." Ultrasonics, Ferroelectrics and Frequency Control, IEEE Transactions on **53**(1): 79-89.

Cooley, W. W. and P. R. Lohnes (1971). Multivariate Data Analysis, John Wiley & Sons.

Dahl, J. J., M. S. Soo, et al. (2005). "Spatial and temporal aberrator stability for real-time adaptive imaging." Ultrasonics, Ferroelectrics and Frequency Control, IEEE Transactions on **52**(9): 1504-1517.

Dahl, J. J. and G. E. Trahey (2003). Off-axis scatterer filters for improved aberration measurements.

Donnell, M. O. (1982). "Quantitative ultrasonic backscatter measurements in the presence of phase distortion." The Journal of the Acoustical Society of America **72**(6): 1719-1725.

Fernandez, A. T., K. L. Gammelmark, et al. (2003). "Synthetic elevation beamforming and image acquisition capabilities using an 8 /spl times/ 128 1.75D array." Ultrasonics, Ferroelectrics and Frequency Control, IEEE Transactions on **50**(1): 40-57.

Fernandez, A. T. and G. E. Trahey (2003). Two-dimensional phase aberration correction using an ultrasonic 1.75D array: case study on breast microcalcifications.

Fink, M., J.-F. Cardoso, et al. (1984). "Analyse des effets de la diffraction en echographie medicale " Acta Electronica **26**(1-2): 59-80.

Flax, S. W. and M. O'Donnell (1988). "Phase-aberration correction using signals from point reflectors and diffuse scatterers: basic principles." Ultrasonics, Ferroelectrics and Frequency Control, IEEE Transactions on **35**(6): 758-767.

Gauss, R. C., G. Trahey, et al. (2001). "Wavefront estimation in the human breast." Proc. SPIE **4325**: 172-181.

Goodman, J. W. (1975). Statistical Properties of Speckle Pattern. Laser Speckle and Related Phenomena. J. C. Dainty. Berlin, Springer-verlag**:** 9-75.

Goodman, J. W. (1985). Statistical Optics, Wiley Classics Library.

Gruber, F. K., E. A. Marengo, et al. (2004). "Time-reversal imaging with multiple signal classification considering multiple scattering between the targets." The Journal of the Acoustical Society of America **115**(6): 3042-3047.

J.A.Jensen (1996). "Field: A program for simulating ultrasound systems." Med. Biol. Eng. Comp., col. 10th Nordic-Baltic Conference on Biomedical Imaging **4**(1): 351-353.

Lacefield, J. C. and R. C. Waag (2002). "Spatial coherence analysis applied to aberration correction using a two-dimensional array system." The Journal of the Acoustical Society of America **112**(6): 2558-2566.

Mallart, R. and M. Fink (1994). "Adaptive focusing in scattering media through sound-speed inhomogeneities: The van Cittert Zernike approach and focusing criterion." The Journal of the Acoustical Society of America **96**(6): 3721-3732.

Msoy, S.-E., B. Angelsen, et al. (2004). "Estimation of ultrasound wave aberration with signals from random scatterers." The Journal of the Acoustical Society of America **115**(6): 2998-3009.

Msoy, S.-E., B. Angelsen, et al. (2007). "Variance analysis of arrival time and amplitude estimates from random speckle signal." The Journal of the Acoustical Society of America **121**(1): 286-297.

Msoy, S.-E., T. Varslot, et al. (2005). "Iteration of transmit-beam aberration correction in medical ultrasound imaging." The Journal of the Acoustical Society of America **117**(1): 450-461.

Nock, L., G. Trahey, et al. (1989). "Phase aberration correction in medical ultrasound using speckle brightness as a quality factor." The Journal of the Acoustical Society of America **85**(5): 1819-1833.

O'Donnell, M. and S. W. Flax (1988). "Phase-aberration correction using signals from point reflectors and diffuse scatterers: measurements." Ultrasonics, Ferroelectrics and Frequency Control, IEEE Transactions on **35**(6): 768-774.

Prada, C. and J. L. Thomas (2003). "Experimental subwavelength localization of scatterers by decomposition of the time reversal operator interpreted as a covariance matrix." The Journal of the Acoustical Society of America **114**(1): 235-243.

Priestley, M. B. (1988). Spectral analysis and time series Academic Press.

Rao, C. R. (1964). "The Use and Interpretation of Principal Component Analysis in Applied Research." Sankhya **A 26**: 329 -358.

Silverstein, S. D. (2001). "Ultrasound scattering model: 2-D cross-correlation and focusing criteria-theory, simulations, and experiments." Ultrasonics, Ferroelectrics and Frequency Control, IEEE Transactions on **48**(4): 1023-1030.

Trees, H. V. (2002). Optimum Array Processing - Detection, Estimation, and Modulation Theory, Wiley-Interscience.

Varslot, T., H. Krogstadt, et al. (2004). "Eigenfunction analysis of stochastic backscatter for characterization of acoustic aberration in medical ultrasound imaging." The Journal of the Acoustical Society of America **115**(6): 3068-3076.

Waag, R. C. and J. P. Astheimer (2005). "Statistical estimation of ultrasonic propagation path parameters for aberration correction." Ultrasonics, Ferroelectrics and Frequency Control, IEEE Transactions on **52**(5): 851-869.

Waag, R. C. and J. P. Astheimer (2006). "Statistical estimation of ultrasonic propagation path parameters for aberration correction." The Journal of the Acoustical Society of America **119**(5): 3376.

Walker, W. F. and G. Trahey (1997). "Speckle coherence and implications for adaptive imaging." The Journal of the Acoustical Society of America **101**(4): 1847-1858.
Walker, W. F. and G. E. Trahey (1995). "A fundamental limit on delay estimation using partially correlated speckle signals." Ultrasonics, Ferroelectrics and Frequency Control, IEEE Transactions on **42**(2): 301-308.
Zemp, R. and M. F. Insana (2004). Spatial coding with curved wavefronts.

Chapter 5. Spatio-temporal invariants of The Time Reversal Operator

I. INTRODUCTION

The DORT (and FDORT) method is a powerful technique to extract monochromatic Green's function from a medium. However, in medical ultrasound, like in several other modalities, broadband signals are used. The broadband nature of the signal offers one great advantage, which is the axial (in depth) resolution of the scatterers in an image. With one frequency, or narrow-band signals, the scatterers are badly resolved in depth. A shadow can also be observed. With the broad-band signals used in medical ultrasound (the bandwidth is usually about 60% of the central frequency and even more with the new generation of transducers) an axial resolution of the order of the wave-length is achieved.

Sometimes, enough information can be extracted from the Green's function at the central frequency. For example, in the near-field phase screen model, the aberration is modeled as a delay, and therefore the knowledge of the phase at one frequency is enough. However, most of the time, it is essential to have broad-band (or temporal) Green's function. For example, to focus on a scatterer by time reversal, one needs the temporal Green's function. In wave-guides (Folegot, Prada et al. 2003; Prada, Rosny et al. 2006) or in any case of multiple reflections (multiple reflections are observed in medical imaging) temporal Green's function are also required to see the multiple arrivals. Finally, in a general model of aberration, where the aberration phase depends on the frequency, it is necessary to know the Green's function for every frequency sample of the bandwidth.

One solution is to compute the invariants of theTime Reversal Operator at every frequency sample, and then to do a Fourier Transform to obtain the invariant in the time

domain. This is what we have done in the previous chapters when we have been showing temporal Green's function. This approach works well when only one scatterer, or a few scatterers with different reflectivities are present. However, if there are a few scatterers with similar reflectivity (and therefore similar singular values), or if their reflectivities vary differently in function of the frequency, we usually observe a permutation problem. In other words, the order of the singular vectors changes with the frequency. For example, one scatterer might be the brightest, at low frequencies, and therefore it will correspond to the first singular vector (the one with the higher singular value), and another scatterer might be brighter at higher frequencies. This problem is illustrated in

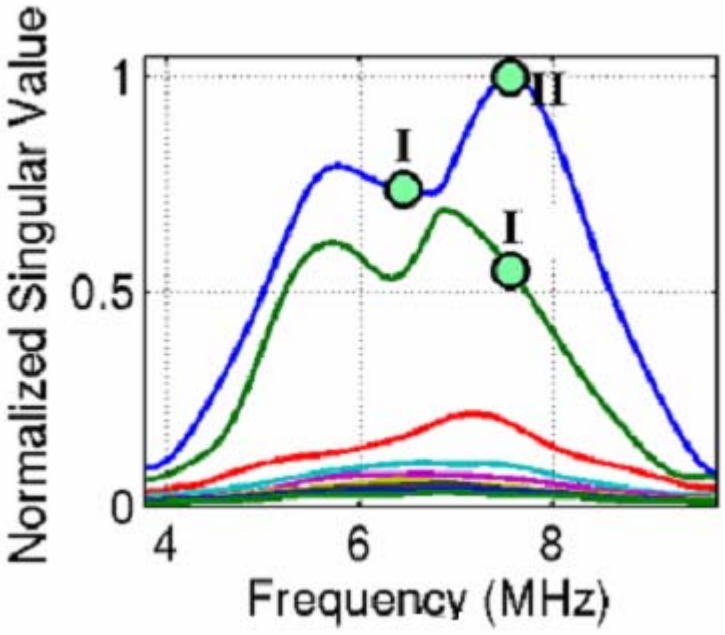

Figure 106 Permutation problem for two scatterers (in-vivo microcalcifications). The 1st singular vector of DORT (blue) corresponds to the scatterer I at low frequency, and to the scatterer II at high frequency, because the reflectivity functions of the scatterers cross each other.

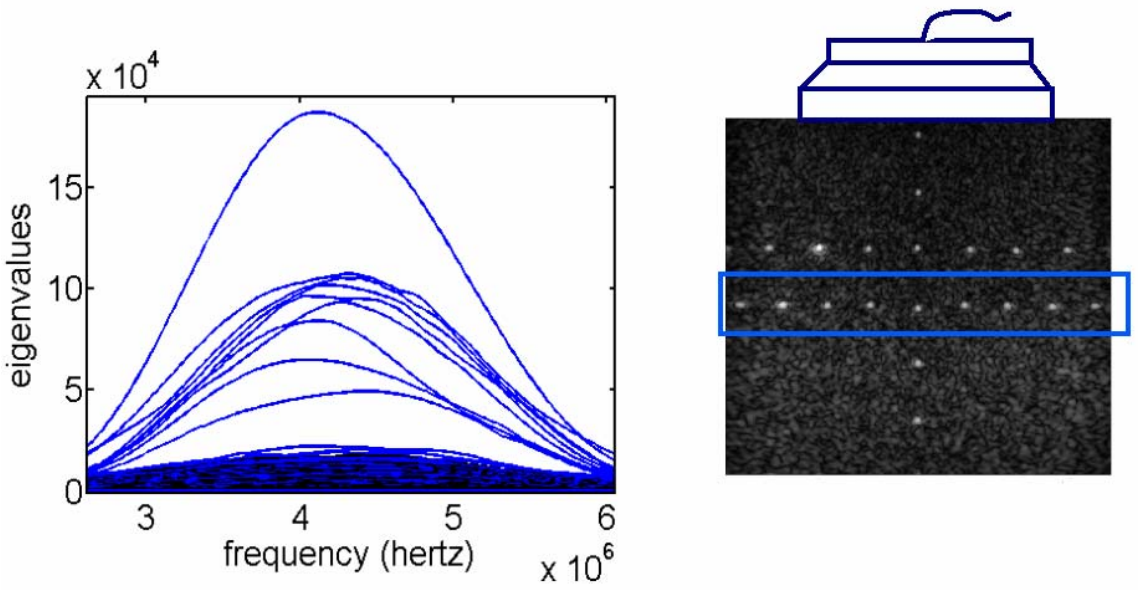

Figure 107 Permutation problem in the case of 9 wires in a medical phantom (depitcted on the right in the blue box) One wire is significantly brighter than the other, but the other wires have similar level of reflectivity, therefore the singular values cross eact others.

In this case, taking the Fourier Transform of the 1st singular vector will give a mixture of several Green's functions.

The main objective of this Chapter is to derive methods to solve this problem, and obtain proper time-domain Green's function. Other less important limitation of the monochromatic approach will be addressed:

- One of them has been solved partially in Chapter 2.V.: while the DORT method yield a good lateral separation of the scatterers, the axial separation is very weak (two scatterers with same azimuth but different depths are likely to be coupled: the two singular vectors will be a combination of the scatterers' Green functions) The DORT method does not take advantage of the temporal resolution offered by broadband signals. Fourier transforming the frequency domain singular vectors does not help.

- Moreover, the temporal signals obtained by Fourier transforming the monochromatic singular vectors are not really invariants of the time reversal process. They are invariant spatially, but not temporally. The transfer function of the transducers, foe example, spread the signal at each time reversal process.

Since it is difficult to reconstruct the time-domain Green's function from the frequency domain ones, the best solution seems to compute directly the invariants of the Time Reversal in the time domain. This is the object of the Section II. We will show how to build this operator that takes the form of a tensor, and how to decompose it. However, we will see that the solutions do not fulfill all our wishes and we will explain why physically.

A method based on the decomposition of a Focused tensor, that mixes the tensor approach with the focused beams, is then proposed. This method is a good solution for our problem. However, we will see that it requires *a-priori* information on the medium.

II. SPATIO-TEMPORAL INVARIANTS OF THE TIME REVERSAL

II.A Heuristics

In order to compute the invariants to the Time Reversal in the time domain, we need to build the Time Reversal Operator in the time domain. In the frequency domain, the Time Reversal Operator was represented by a matrix. In the time domain, things become more complicated mathematically, and we need to introduce higher order tensor. In Section II.B, a rigorous mathematic formalism is introduced. But we first want to justify intuitively the need for the tensor representation.

II.A.1 Reminder: frequency domain formalism

In the frequency domain (Prada and Fink 1994; Prada, Manneville et al. 1996), the received signal vector $R(\omega)$ is linked to the transmitted (emitted) signal vector $E(\omega)$ by the transfer matrix $K(\omega)$

$$R(\omega) = K(\omega)E(\omega)$$

Eq.5. 1

In order to show explicitly the dimensions of the quantity considered, we introduce Einstein's notations. The indexes are explicitly shown, and the summation is done on the repeated index (m in Eq.5. 2). Eq.5. 1 is rewritten

$$R_i(\omega) = K_{i,m}(\omega)E_m(\omega)$$

Eq.5. 2

In Eq.5. 2, the index k refers to an array element in receive (spatial sample in receive) and the index j to an array element in transmit. The Time Reversal Operator is KK^H. Usually, the singular value decomposition of K is used to compute the invariants of the time Reversal Operator.

II.A.2 Time Domain Formalism

In the frequency domain, the signals were represented by vectors. Each element corresponded to a spatial sample. In the time domain, we need two dimensions to describe the signals: the spatial dimension (array elements) and the time dimension. Therefore, a signal is represented by a matrix. A typical time domain emitted signal is represented in Figure 108. This signal is represented by the matrix $E_{m,n}$. The index n refers to a time sample in the observation window.

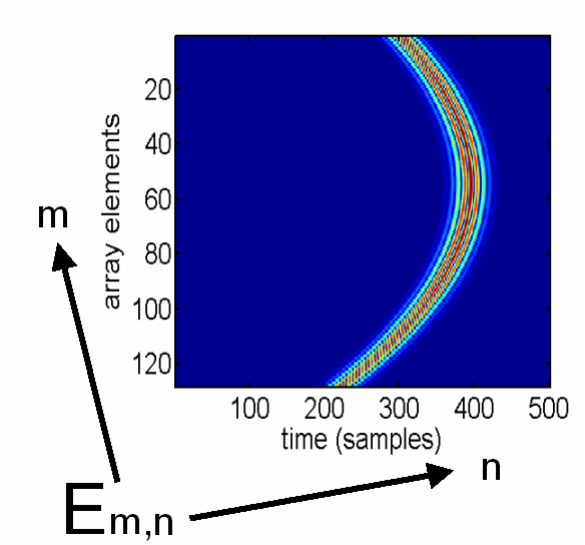

Figure 108 A time domain transmitted signal. Two indexes are required to describe the signal. *m* refers to the spatial dimension, and *n* referes to the time dimension

Similarly, the received signal is represented by the matrix $R_{i,j}$. Now, the received signal can be linked to the transmitted signal by a transfer tensor (a tensor is the generalization of a vector or matrix to any dimension) As we need two indexes to describe the transmit signal, and two other to describe the receive signal, the transfer tensor has 4 indexes: *i,j,m,n*. It is a 4th order tensor. Eq.5. 2 becomes

$$R_{i,j} = K_{i,j,m,n} E_{m,n}$$

Eq.5. 3

$K_{i,j,m,n}$ represents the signal received on element *i*, at time sample *j* when a pulse is transmitted by element *m* at time sample *n*. (In practice, it is not required to transmit a pulse at each time sample to acquire the tensor. Indeed, the process is time shift invariant, therefore the received signal when a pulse is transmitted at time sample *n+1* can be deduced from the received signal when a pulse is transmitted at time sample *n* by a shift in time)

In practice, we are not using the transfer tensor, but the Time Reversal Operator described in the next section. Indeed, the observation window in receive is too large with the transfer tensor: the echo coming from scatterers at very different depths will arrive with a large delay between them. Decomposing such large tensor is computationally prohibitive. However, when the echos are time reversed and retransmitted, the echos from all scatterers (after 1 time reversal cycle) will arrive simultaneously, which reduces greatly the size of the observation window.

II.B The Time Reversal Operator in the Time Domain

II.B.1 Expression of the Time Reversal process in the time domain

We are now using continuous notation for the time dimension, and discrete notation for the spatial dimension (array element). This gives more physical meaning to the derivations. The signal received by element *i* is now $R_i(t)$. Einstein convention is still used for the discrete dimension (implicit summation on the repeated index) Eq.5. 3 becomes

$$R_i^0(t) = \int_0^T K_{i,m}(t-\tau) E_m^0(\tau) d\tau$$

Eq.5. 4

where T is the length of the transmitted pulse, $E^0_m(t)$. We can write $K_m(t-\tau)$ instead of $K_{i,m}(t,\tau)$ because of the time shift invariance. The upper index 0 is used to differentiate the signals at the different iterations of the time reversal.

The signal is time-reversed ($E^1_i(t) = R^0_i(-t)$) and transmitted back to the medium. A new echo, $R^1_k(t)$ is received

$$
\begin{aligned}
R_k^1(t) &= \int_{-\infty}^{\infty} K_{k,i}(t-\tau_1) E_i^1(\tau_1) d\tau_1 \\
&= \int_{-\infty}^{\infty} K_{k,i}(t-\tau_1) R_i^0(-\tau_1) d\tau_1 \\
&= \int_{-\infty}^{\infty} K_{k,i}(t-\tau_1) \int_0^T K_{i,m}(-\tau_1-\tau_2) E_m^0(\tau_2) d\tau_2 d\tau_1 \\
&= \int_0^T E_m^0(\tau_2) \left[\int_{-\infty}^{\infty} K_{k,i}(t-\tau_1) K_{i,m}(-\tau_1-\tau_2) d\tau_1 \right] d\tau_2
\end{aligned}
$$

Eq.5. 5

The second time integral is *infinite* as the received signal $R^0_i(-t)$ can be very long, as explained at the end of Section.II.A.2. (Extending the integration to negative times has no consequence as the signals are equal to zero for negative times) Let $\tau' = -\tau_1 - \tau_2$; the quantity inside the brackets becomes

$$
\int_{-\infty}^{\infty} K_{k,i}(t-\tau_1) K_{i,m}(-\tau_1-\tau_2) d\tau_1 = \int_{-\infty}^{\infty} K_{i,m}(\tau') K_{k,i}(\tau'+(\tau_2+t)) d\tau'
$$

Eq.5. 6

Invoking the spatial reciprocity principle yield $K_{k,i}(t) = K_{i,k}(t)$. In Eq.5. 6, the summation on the repeated index *i* was implicit. Writing it explicitly yield

$$
\int_{-\infty}^{\infty} K_{k,i}(t-\tau_1) K_{i,m}(-\tau_1-\tau_2) d\tau_1 = \sum_{i=0}^{N} \int_{-\infty}^{\infty} K_{i,m}(\tau') K_{k,i}(\tau'+(\tau_2+t)) d\tau'
$$

Eq.5. 7

where *N* is the number of array elements.

$\int_{-\infty}^{\infty} K_{i,m}(\tau') K_{k,i}(\tau'+(\tau_2+t)) d\tau'$ is the cross-correlation between the impulse responses received by element *k* and element *m*, when a pulse is transmitted by element *i*, evaluated at lag $\tau_2 + t$. In the left side of Eq.5. 7, we recognized this cross-correlation function, averaged on all transmits *i*. The realizations of this correlation function are then taken both in time and in space. Let $C_{k,m}(\tau_2 + t)$ be this correlation function

$$C_{k,m}(t) = \sum_{i=0}^{N} \int_{-\infty}^{\infty} K_{i,m}(\tau') K_{k,i}(\tau'+t) d\tau'$$

Eq.5. 8

Using Eq.5. 8 in Eq.5. 5, the receive signal after the Time Reversal process becomes

$$R_k^1(t) = \int_0^T C_{k,m}(\tau_2 + t) E_m^0(\tau_2) d\tau_2$$

Eq.5. 9

Finally, the input for the next iteration is the time reversed version of $R_k^1(t)$.

$$E_k^2(t) = R_k^1(-t) = \int_0^T C_{k,m}(\tau_2 - t) E_m^0(\tau_2) d\tau_2$$

Eq.5. 10

with, still, implicit summation on the repeated index *m*. Eq.5. 10 defines the time domain Time Reversal Operator.

II.B.2 Time Domain Invariants of the Time Reversal Operator

The invariants are given by $E^2(t) = \mu E^0(t)$. As $E^0(t)$ is of finite length *T*, then $E^2(t)$ must also be of finite length *T*. We are then only interested by Eq.5. 10 for $0 < t < T$. This yield

$$\mu E_k^0(t) = \int_0^T C_{k,m}(\tau_2 - t) E_m^0(\tau_2) d\tau_2 \qquad 0 < t < T \qquad 1 < k < N$$

Eq.5. 11

II.B.3 Discrete formulation: the Time Reversal Tensor

We are now discretizing the time. $E_k^0(t)$ becomes $E_{k,l}^0$, and $E_m^0(\tau_2)$ becomes $E_{m,n}^0$. The integral (continuous summation) is replaced by the discrete (implicit) summation on the index *n*. Eq.5. 11 becomes

$$\mu E^0_{k,l} = C_{k,l,m,n} E^0_{m,n}$$

Eq.5. 12

with $$C_{k,l,m,n} = C_{k,m}(t_n - t_l) = C_{k,m}(\frac{n-l}{f_s}) = C_{k,m}[n-l]$$

Eq.5. 13

where f_s is the temporal sampling frequency, and using signal processing notation in the last equality.

The tensor $C_{k,l,m,n}$ is the time domain Time Reversal Operator. The link between Time Reversal Operator and correlation (covariance) matrices has already been pointed out in the monochromatic case(Prada and Thomas 2003; Gruber, Marengo et al. 2004) It is very clear in the time domain: the coefficients of the Time reversal Operator are given by the cross-correlation of the signals received by two elements, averaged on all the transmits.

To summarize, the coefficient $C_{k,l,m,n}$ is obtained by the following processing:

- A pulse is transmitted with the 1st element; and the signal is received by elements *k* and *m*. The cross-correlation function of the two signals is computed.
- The process is repeated for each transmit elements. The cross-correlation functions obtained for all transmits are averaged to form $C_{k,m}(t)$
- The coefficient $C_{k,l,m,n}$ is the [n-l] time sample of $C_{k,m}(t)$

The time domain invariants of the Time Reversal Operator are found by decomposing the tensor $C_{k,l,m,n}$. The method for the decomposition is given in Section II.C.

II.C. Decomposition of the Tensor

II.C.1 Existence of the decomposition

Using the spatial reciprocity principle, and a shift in time in Eq.5. 8, we find

$$C_{k,l,m,n} = C_{k,m}(t_n - t_l) = C_{m,k}(-(t_n - t_l)) = C_{m,n,k,l}$$

Eq.5. 14

which ensures the existence of a eigen-decomposition of the tensor (Cardoso 1991).

II.C.2 Maping of the tensor to a matrix

The decomposition of high-order tensor is not unique, unlike the 2D (matrix) case. There exists several generalization of the SVD, depending on the properties one is looking for. The decomposition that we propose here is the one that leads to the spatio-temporal invariants of the operator, which is *a priori* what we are looking for.

The 4th order problem may be transformed in a matrix eigen-problem that can be numerically solved. Each pair (*k,l*) may be indexed by a number α, $1 \le \alpha \le K \cdot L$, where *K* and *L* are the number of samples in space and time (*K=N*, the number of elements and $L = T \cdot f_s$ where *T* is the length of the observation window (in s), *fs* is the sampling frequency and therefore $T \cdot f_s$ is the number of time samples). In general, we can choose, $\alpha = (l-1) \cdot K + k$. This is equivalent to *unwrap* the tensor and matrices, and is shown in Figure 109. Each pair (*m,n*) may also be indexed by β, $1 \le \beta \le N \cdot T \cdot f_s$., and finally Eq.5. 12 becomes

$$\mu E^0_\alpha = C_{\alpha,\beta} E^0_\beta$$

and the decomposition of $C_{\alpha,\beta}$ is computed using a conventional matrix decomposition. The singular (or eigen) vectors obtained have to be remapped into singular matrices. For example, the SVD of $C_{\alpha,\beta}$ yield $C_{\alpha,\beta} = U_\alpha S V_\beta$, and U_α is remapped into $U_{k,l}$.

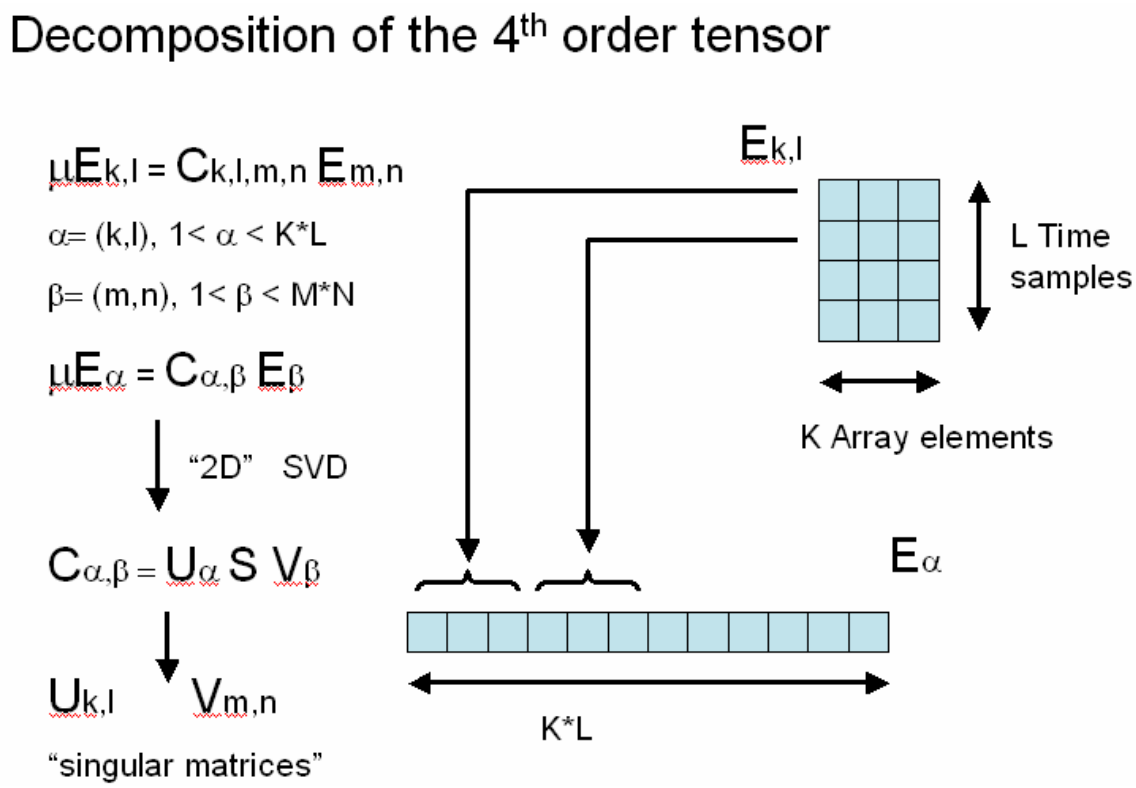

Figure 109 Unwrapping a matrix into a tensor. By remapping the indexes, the four dimensionnal problem is transformed into an easily solvable 2D problem.

II.D. Practical implementation and results

II.D.1. Practical implementation

The matrix $C_{\alpha,\beta}$ can become very large ($1 \le \alpha, \beta \le N \cdot T \cdot f_s$). To be able to perform its decomposition using software like Matlab, it is necessary to limit its size. The number of spatial samples is the number of array elements and cannot easily be reduced. However, the number of times samples can be kept low by selecting a small observation window, and using the minimum sampling frequency (given by the Nyquist limit). In our

implementations, we had 60 samples in time and a 64 elements array. The pitch was 0.4 mm, and the center frequency 7 MHz.

We used Field II for the simulations, and Matlab for the signal processing. Only the first few singular vectors are computed.

II.D.2 Results with two well-resolved scatterers

Two resolved point-scatterers are simulated at a depth of 50 mm. They were separated by 5 mm. We are expecting to obtain the Time domain Green's functions of the scatterers. The results are shown in Figure 110.

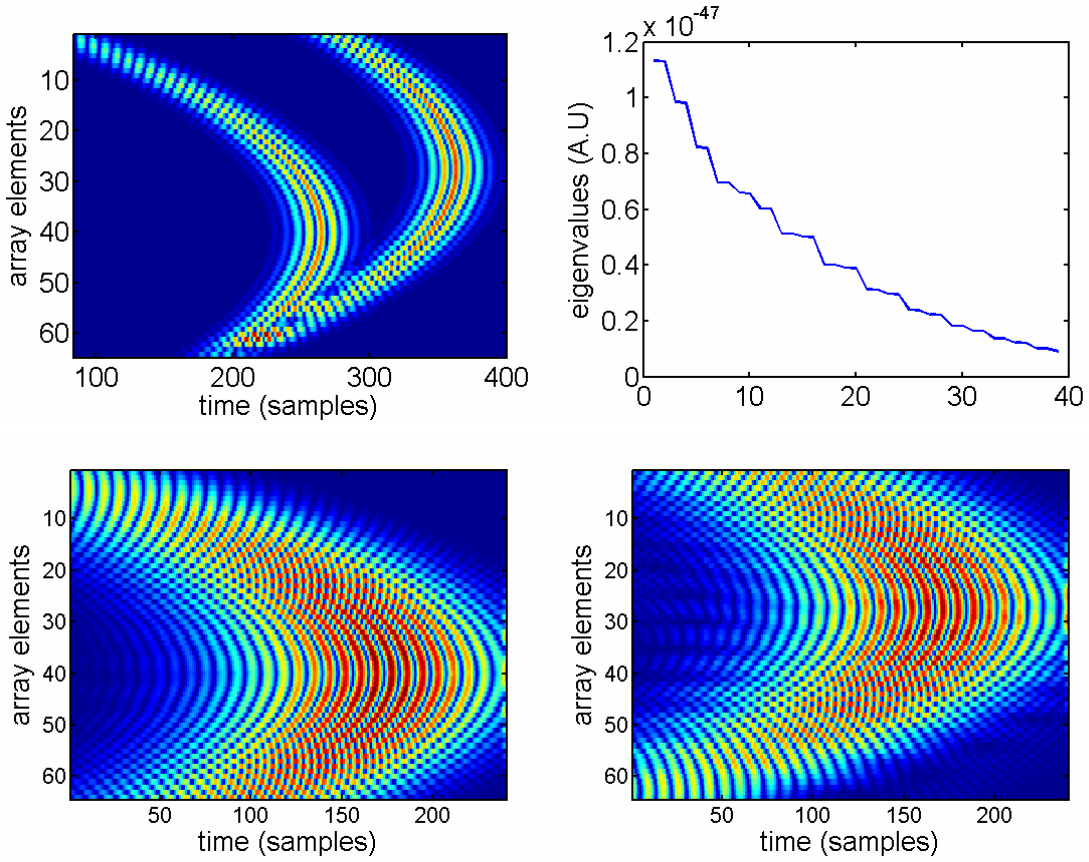

Figure 110 Top left: signal received for one transmit showing the two scatterer's echos. Top right: singular values of the time domain Time Reversal Operator. Bottom: first invariants for each of the scatterer.

As expected, we obtains two singular matrices that looks like the scatterers Green's function. However, the wave-fronts are larger in time than the original wave-fronts. Moreover, there is not only two non-zero singular values, as we could have expected by generalizing the monochromatic results, but nearly 20. These results are analyzed in the following Section, and it will be shown that they are coherent with the Time Reversal Invariance.

II.D.3 Interpretation

To understand the results, a single scatterer has been simulated. The results are shown in Figure 111 to Figure 113.

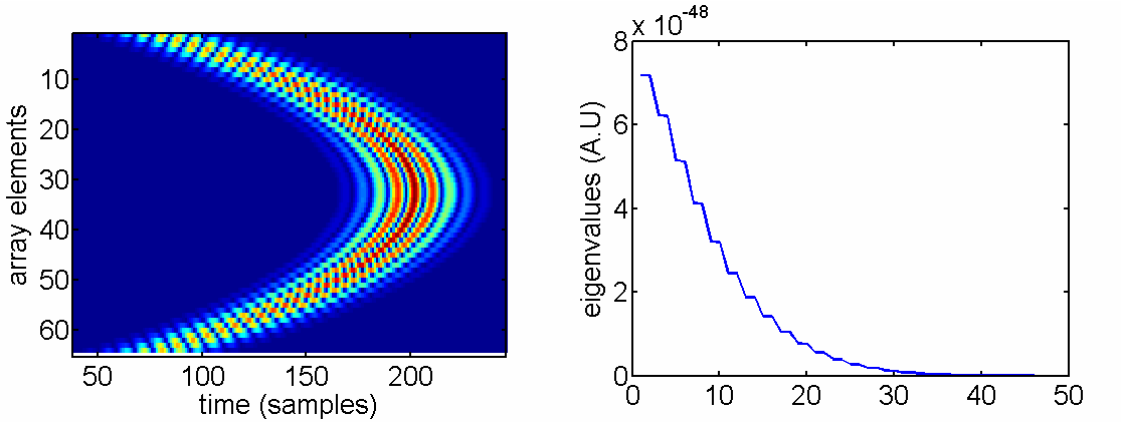

Figure 111 Left: Echo from one transmit ; Right singular value decomposition for a single scatterers. Multiple non-zero singular values are presents.

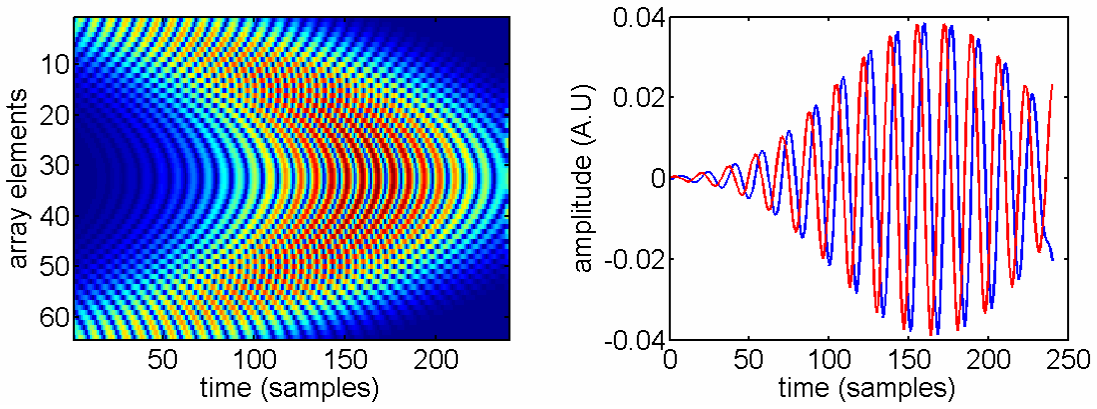

Figure 112 Left: First temporal invariant. The 2nd invariant has a very similar shape. Right: the signal on one element for the two first invariants are compared. They correspond to a sine and cosine modulation, and have the same eigenvalue.

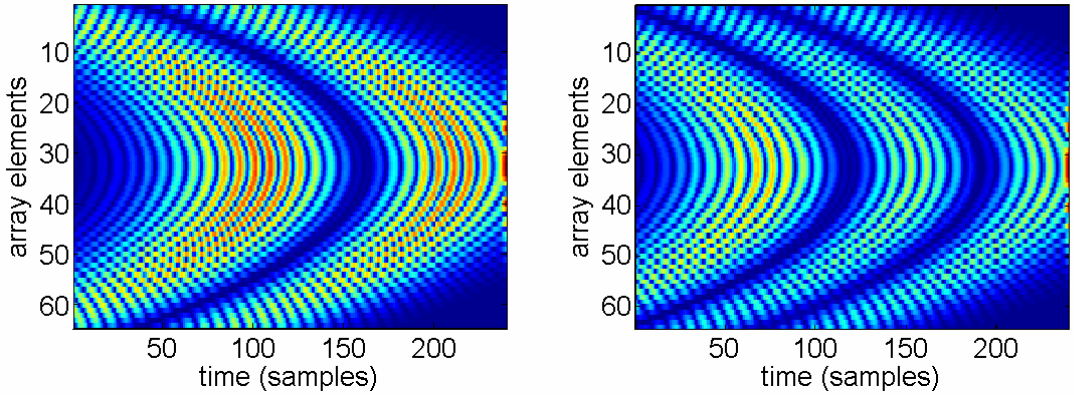

Figure 113 Third and fifth invariants. The 4th, resp. 6th, invariant has the same envelope as the 3rd,resp. 5th invariant but a sine modulation.

Even for a single scatterer, several non-zero singular values are observed. This is at first surprising, but is finally coherent with what we are looking for: the Invariants of the Time Reversal Operator. Indeed, if one wave-front is invariant of the Time Reversal, the same wave-front shifted in time will also be an invariant (Figure 114). The singular matrices are combinations of the different shifted versions of the scatterer Green's function, which is why they appear so large. Physically, there is then no reason to have only one spatio-temporal invariant for each scatterer.

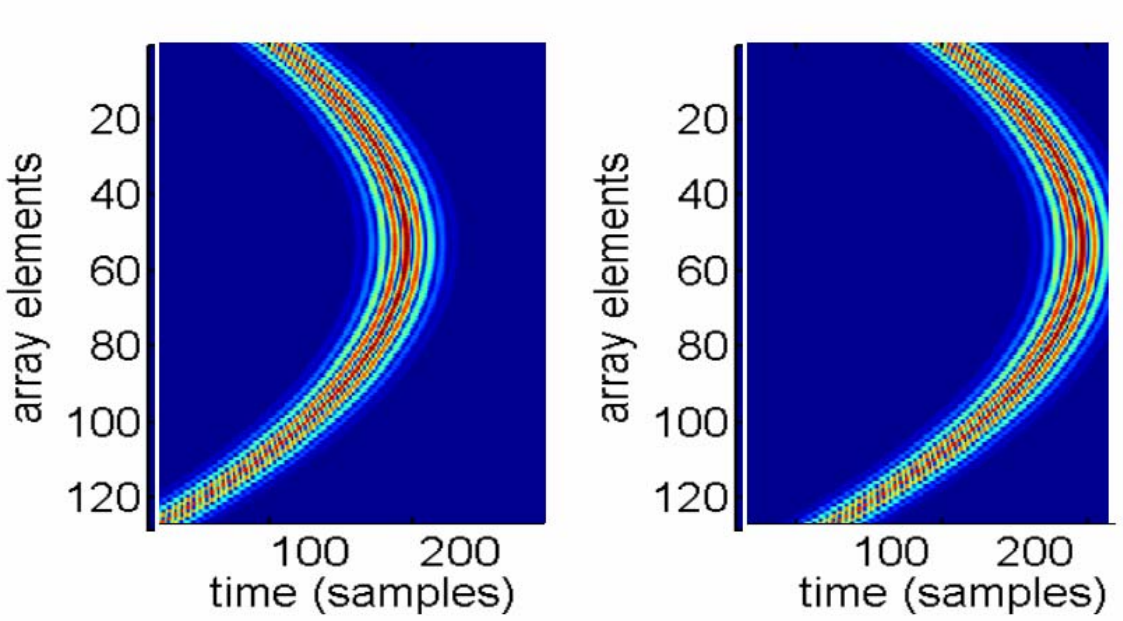

Figure 114 Left: a scatterer Green's function. Right: the same Green's function shifted in time. If the first one is an invariant of the Timr Reversal Operator, then the second is also an invariant. The singular matrices (Figure 112 and Figure 113) are combination of these shifted signals.

For each singular value, we observe two singular matrices that have identical singular values. They correspond to the same wave-front, but shifted by a quarter of a wave-length. They correspond to sine and cosine modulation of the signal (Figure 112)

Physically, there could be an infinite number of invariants for each scatterer (obtained by shifting a 1st invariant in time by different amount) In practice, the number of invariant is limited by the size of the observation window. The number of non-zero singular values is related to the number of wave-fronts that can fit in the Observation Window. This is given by the time-bandwidth product WT (W is the bandwidth and T is the observation window). In fact, the problem is very similar to the extended object problem presented in Chapter 3. For an extended object (at a given frequency), the number of invariants is given by the number of resolution cell that fit in the object, or the product of the object length D by the spatial bandwidth $L/\lambda Z$ (the size of the array is L). If

the bandwidth of the transducer was square, instead of typically Gaussian, the different time-domain invariants would be given by the Prolate functions. The cosine and sine modulation arises from the fact that the bandwidth has both positive (centered around +7Mhz) and negative frequencies (-7MHz).

The problem may actually be considered as a 2D problem (2D array, 2D objects) The 2nd array dimension being the time-window, and the 2nd object dimension being the temporal frequencies. The equivalent object is plotted in Figure 115.

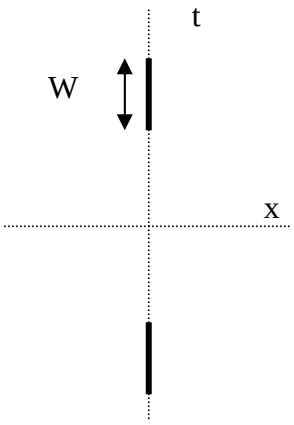

Figure 115 Equivalent 2D objects for the spatio-temporal problem, for a point scatterer. The temporal dimension appears has an extended object in both case, the size of the object been given by the bandwidth W. There is one object in the positive frequencies and another in the negative frequencies, which double the number of invariants.

Note: The singular matrices of the time domain Time Reversal Operator are invariants in space and time of the time reversal, and thus they keep the same shape after several iterations, which is not the case for wave front reconstructed from the monochromatic singular vectors of the DORT method.

To summarize, the decomposition of the time domain Time Reversal Operator does not yield one unique invariant for each scatterer, but several ones. The invariants are

the combination of different time-shifted versions of the Green's function. The 1st invariant can be seen as a large, narrower bandwidth version of the desired Green's function.

The nice properties of the monochromatic invariant of the Time Reversal Operator (the number of non-zero singular values is equal to the number of scatterers, and the singular vectors are the Green's function) are not conserved in the Time Domain.

In fact the monochromatic properties are linked to the Covariance matrix interpretation and the Principal Component analysis (Rao 1964). In 2D (matrices) there is a unique singular value decomposition, and the singular vectors enjoy many properties. At higher dimensions, there is several generalization of the SVD, but none of them offers all the benefits of the 2D SVD. Principal Component Analysis generalization to higher order is an active topic. Several algorithms have been proposed. Most of them need a priori information about the problem and are very specific to a given problem.

II.D.4 Improvement

It is possible to improve the method to have less invariants for each scatterer, and have invariants less spread in time.

One solution to reduce the observation window length T (the number of invariant being related to the number of wave-fronts that can fit in the window). However the wave front is partially cut, as seen in Figure 116.

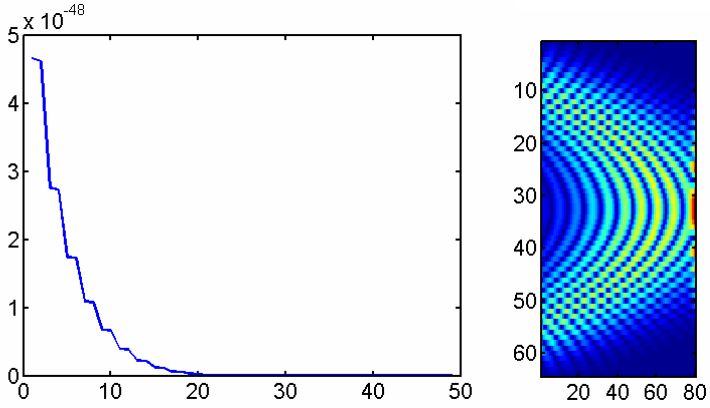

Figure 116 Singular values and 1st singular matrices for the same scatterer as in Figure 111, but using a smaller observation window. The number of singular values decreases, but the wave-front is partially cut.

A better solution is to use an asymmetrical tensor $C_{k,l,m,n}$. We can reduce the observation window corresponding to the index *n*, while keeping a large window for the index *l*. The number of invariants is considerably reduced, as seen in Figure 117, but the wave-front is still observe entirely, because we plot the singular matrice $U_{k,l}$, corresponding to the full time window. Good results were obtained, especially when *n* is reduced to only one sample. However, this method is not as good to separate nearby scatterers. Indeed, the Green's function of the scatterers will be separated by the SVD if both the singular matrices $U_{k,l}$ and $V_{m,n}$ are orthogonal. When *n* is reduced to 1 sample, $V_{m,n}$ correspond to a single line of the wave-front Figure 118. Typically, only the low frequency component of the wave-front is encoded on this line, and the resolution is not as good. Therefore, the separation of 2 Green's function for nearby scatterer may not be complete (Figure 119)

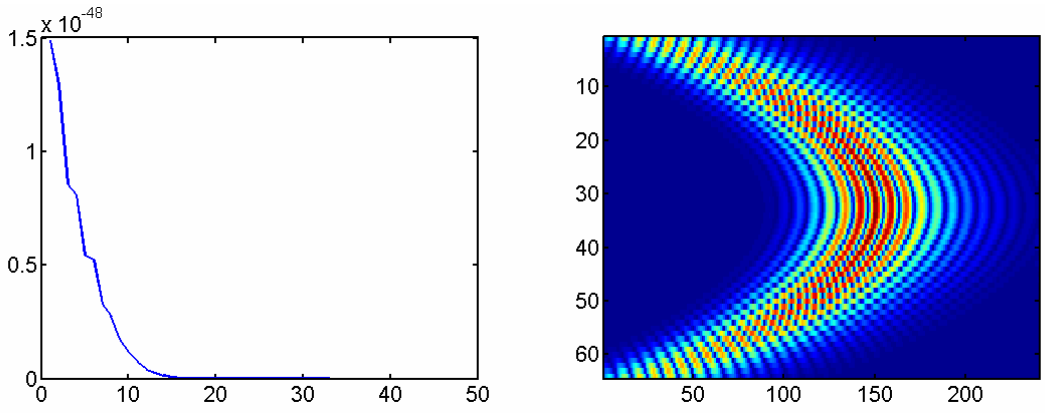

Figure 117 Singular values and 1st singular matrice ($U_{k,l}$) obtained with a full time-window in transmit on the left side of the tensor (index *l*), but a time window reduced to 1 sample on the right side (index *n)*. The number of invariants is reduced and the invariant is more concentrated in time. Moreover, the method has a low processing cost.

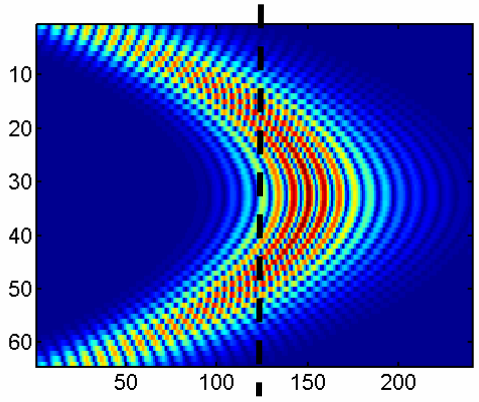

Figure 118 $V_{m,n}$ is reduced to only one line when the observation window is reduced to one sample in the dimension *n*. Two Green's function are then less likely to be orthogonal and separated by the SVD, because all spatial frequencies are not encoded in this line (the low frequencies are typically at the front of the wave-front, while the high frequencies are in the *tails*) Therefore the separation of Green's function is less good

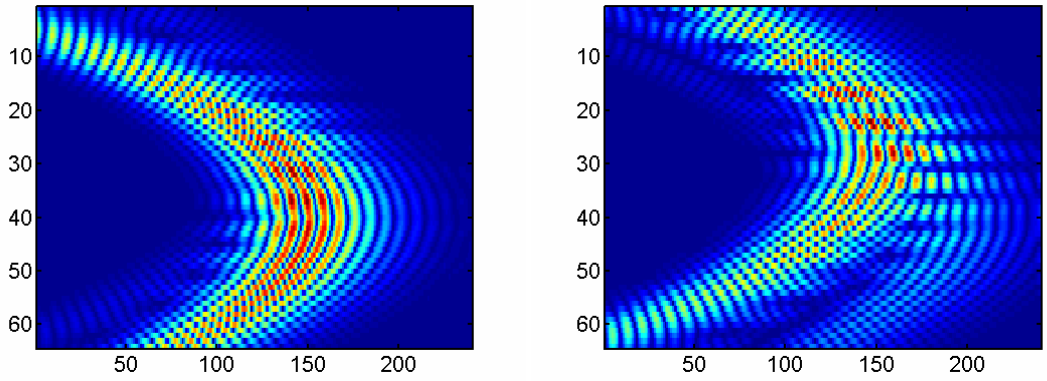

Figure 119 Separation of 2 scatterers responses when *n* is reduced to one sample. The Green's function are not as well resolved as with the full method Figure 110.

II.D.5 Invariants for an extended objects

The temporal invariants for an extended objects are very difficult to reconstruct from the monochromatic invariants, because the singular values are very similar and therefore the order of singular vector changes easily in function of the frequency. Time domain invariants are easily found by decomposition of the Time Reversal Tensor. The spatial variation is typical from the Prolate functions (Chapter 3).

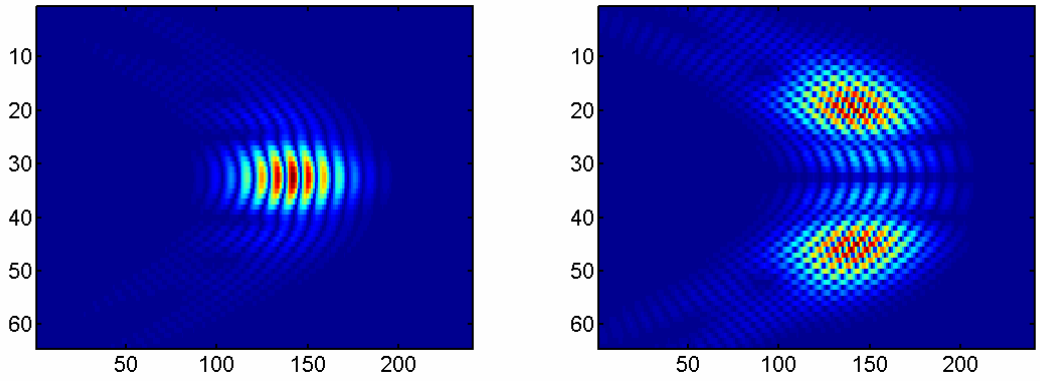

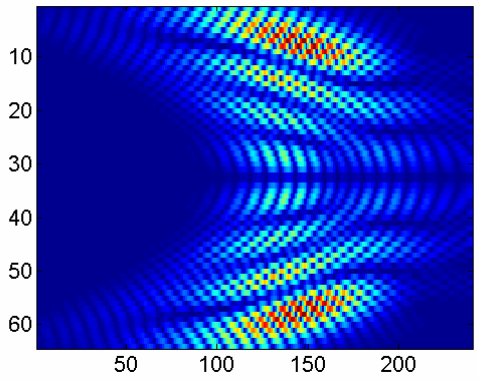

Figure 120 A few invariants for an extended objects.

III. DECOMPOSITION OF THE FOCUSED TENSOR

The decomposition of the time domain Time Reversal Operator provides the spatio-invariants of the Time Reversal, but do not offer a generalization of the properties of the monochromatic invariants. There is not a unique non-zero singular values for each point-scatterers, the first singular matrices is a narrower-band version of the desired Green's function. Moreover, the method does not offer the additional property that one can expect from a time domain method: the separation of scatterers at the same azimuth but different depth, reminded in Introduction.

We propose here a method to achieve these objectives when some *a-priori* information is known about the medium. More precisely, the method requires to be able to achieve a good focusing in the medium. This means that it will work well in homogeneous medium or slightly heterogeneous medium. The performance will be degraded for strongly heterogeneous medium. This is a drawback compared to the monochromatic DORT method, that performs equally well in any heterogeneous medium, as long as the attenuation is negligible.

III.A The Focused Tensor

The focused tensor can be seen as a generalization of the method FDORT with time gating exposed in Chapter 2.V. This is not a surprise as the method was designed to separate the Green's function from scatterers at different depth. The method was a mix of impulsive and monochromatic approaches. The impulsive approach was used to separate the signal in depth, and the monochromatic approach was used to separate the signals laterally by the mean of the SVD. We now have the tools to perform the SVD directly in the time domain by doing a tensor decomposition. Therefore we can implement the method entirely in the time domain.

The Focused tensor, $F_{k,l,m,n}$ is built by using the following process:

- The k^{th} focused beam is transmitted.
- The echo is recorded by every element. The signal is gated in time to select the echos originating from a particular depth. The position of the time gate is refered by the index *l*.
- The selected signal is placed in a matrix full of zero. The spatial dimension of this matrix corresponds to the index *m* while the time dimension is the index *n*. This matrix is a slice of the tensor $F_{k,l,m,n.}$ This is shown in Figure 121. The length of the gate is the pulse-length.
- Another gate is selected, leading to a new slice of the tensor (index *l+1)* (Figure 122). The spacing between two consecutive gates center is the pulse-length.
- When all the gates have been selected, the process is repeated for the next focused transmit (index *k+1)*

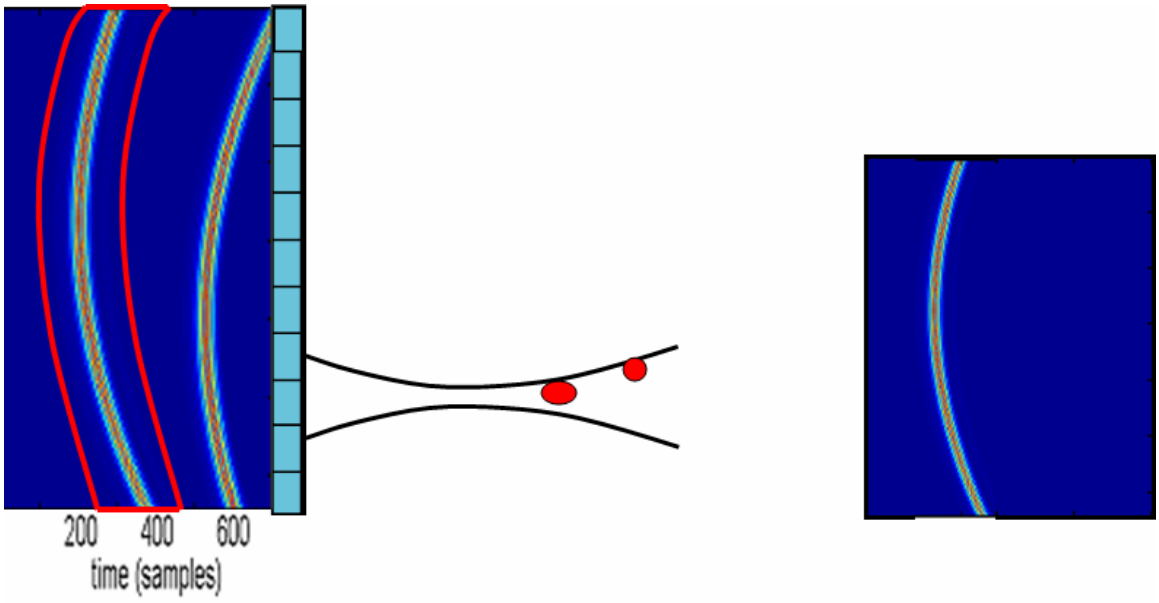

Figure 121 The echo originating from a particular depth is selected using a time gate. This gives a slice of the tensor.

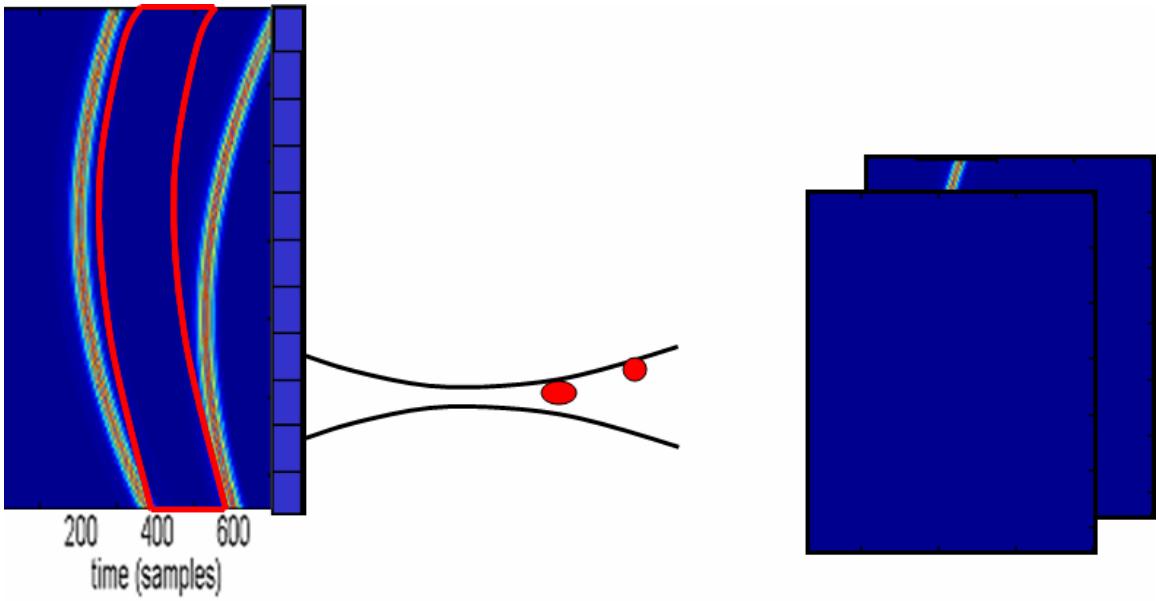

Figure 122 The gate is displaced to select the signal from the next depth. This gives another slice of the tensor.

The Focused tensor is not exactly the Time Reversal Operator in the focused basis. Else the decomposition would provide the same results as in section II.

III.B Decomposition of the Focused Tensor

The focused tensor is decomposed by mapping into a matrix, as explained in Section.II.C. Two Green's function will be separated if both the singular matrices $U_{k,l}$ and $V_{m,n}$ are orthogonal. $V_{m,n}$ provides the signal in the canonical basis, in function of the time. This is similar to what was obtained in Section.II.

However, $U_{k,l}$ provides a different information. k is the transmit number, or n other word the lateral position of the transmit resolution cell. l refers to position of the time gate, or in other words to the axial position (depth) of the resolution cell. Consequently, $U_{k,l}$ gives the signal in a "resolution cell basis" or in a "image pixel basis". This will become clear after a few examples.

Two Green's function will be separated if the matrices $V_{m,n}$ are orthogonal, which is the usual Green's function orthogonality condition, but also if their representations in the image basis, $U_{k,l,}$ are orthogonal. In practice, that means that the two scatterers are in different resolution cells, which is why the scatterers separation depends on the quality of focusing.

III.C. Results

III.C.1 Two well-resolved scatterers

The Focused tensor has been built with the 2 scatterers simulation described in II.D.2. The transmits were focused at the scatterers depth. The results are shown in Figure 123. There are two dominant singular values corresponding to the two scatterers, and the singular matrices $V_{m,n}$ correspond to the scatterer Green's functions. The two wave-fronts are perfectly separated, and they are not spread in time.

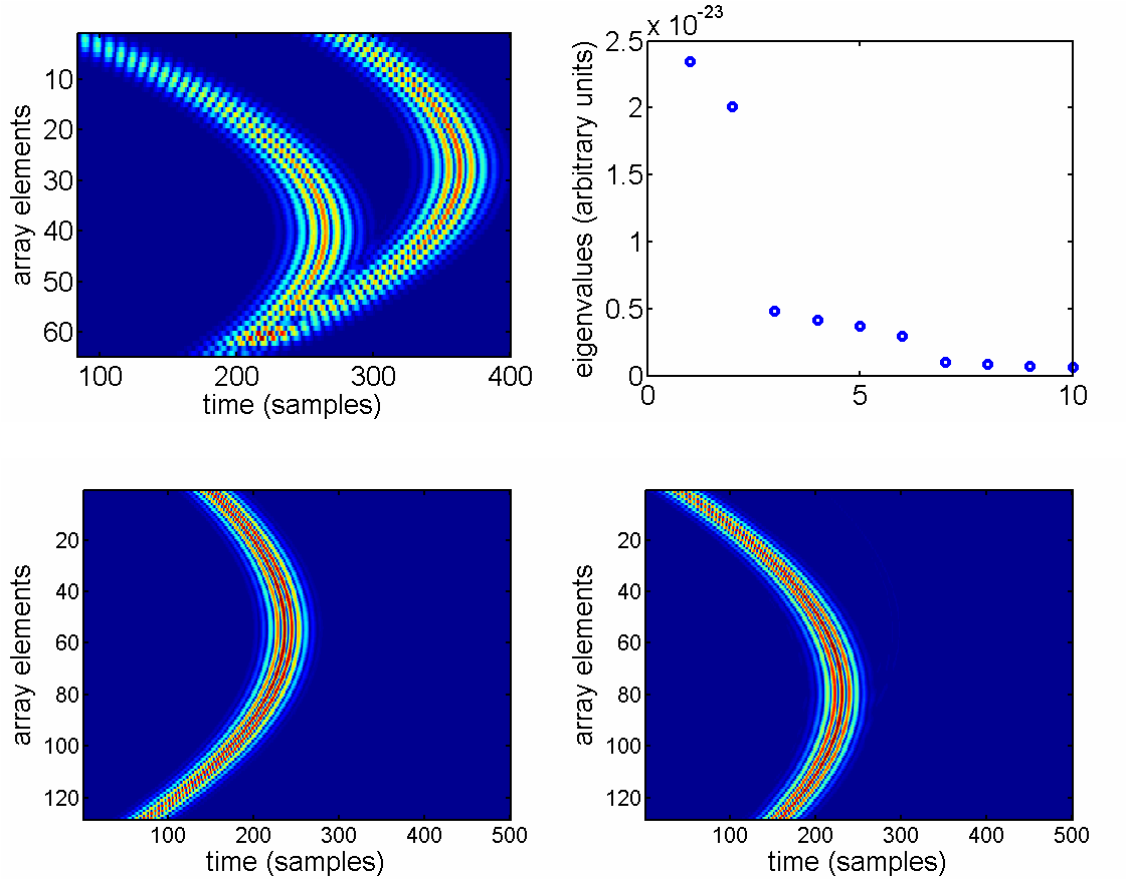

Figure 123 Simulation of two scatterers in a homogeneous medium. Top left: typical received signal, showing the echo of the 2 scatterers. Top right: singular values distribution for the Focused tensor; two dominant singular values are observed, they correspond to each scatterer. Bottom: singular matrices $V_{m,n}$. They give the scatterers Green's function.

III.C.2 Two point scatterers in inhomogeneous medium

The focused tensor method works ideally in a homogeneous medium. We are now showing that it can still be used in slightly inhomogeneous medium. The same two point-scatterers are simulated with a near-field phase screen (30ns average delay variation and 4.5 mm spatial correlation). The results are shown in Figure 124.

The Green's functions are slightly less well separated, but the result is satisfactory. When the strength of the aberration increases, the separation degrades. Indeed, as said in III.B, the quality of the separation depends on the quality of focusing. For stronger aberration, it is possible to use an iterative method: the first estimate of the

aberration is found and used to correct the transmit focusing for the 2nd iteration (similarly to the speckle algorithm, described in Chapter 4.IV)

In the case of wave-guides, the method can still be used to obtain Green's function. However, it will not take advantage of the super-resolution of the wave guide (because the transmit focusing assumes an homogeneous medium) and very close scatterers may not be separated.

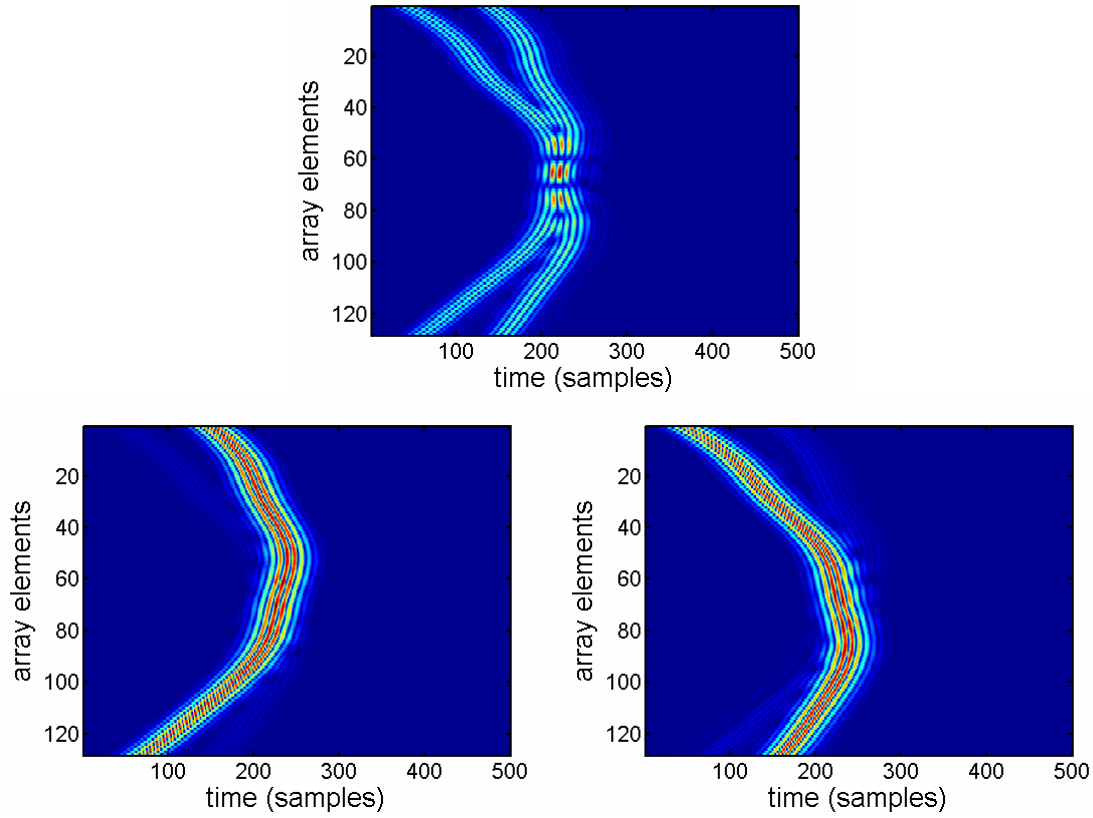

Figure 124 Simulation of two scatterers (5mm apart) in an inhomogeneous medium, modeled by a near-field phase screen, with 30ns average delay variation and 4.5 mm spatial correlation. Top left: typical echo showing the two wave-fronts. Bottom: singular matrices $V_{m,n}$. They correspond to the time domain Green's function of the scatterers. The separation is not as good as in the homogeneous medium, but still decent.

III.C.3 Separation of scatterers from different depths

The phantom data set introduced in Chapter.2.V is now used. We want to demonstrate that the decomposition of the Focused tensor also leads to a separation of scatterers at different depth, which is expected from a time domain method (the axial resolution is linked to the pulse width)

It is best to focus the transmit beams at any depth (to optimize the scatterers separation) If the region of interest is shallow, focusing at the center is usually enough. The dynamic focusing in transmit can be achieved by acquiring a full data set (single elements transmit) first, and adding the different transmits with the relevant delays to achieve the focusing.

The phantom used for the experiment is showed in Figure 125. The region of interest is shown in blue. Using the monochromatic method (DORT) was shown to lead to coupling between the scatterers at different depth and speckle. The results of the decomposition of the Focused Tensor are shown in Figure 126.

The Green's function of the scatterers are given by the singular matrices $V_{m,n}$. They are well separated, there is no coupling with wires or speckle from other depths. We are also showing the singular matrices $U_{k,l}$ for the same scatterers. As mentioned in Section III.B, they correspond to the projection of the Green's functions on the resolution cells, or image pixels. Therefore, they give an image of the scatterer in the region of interest. They enable to locate the scatterer, without the need for a back-propagation.

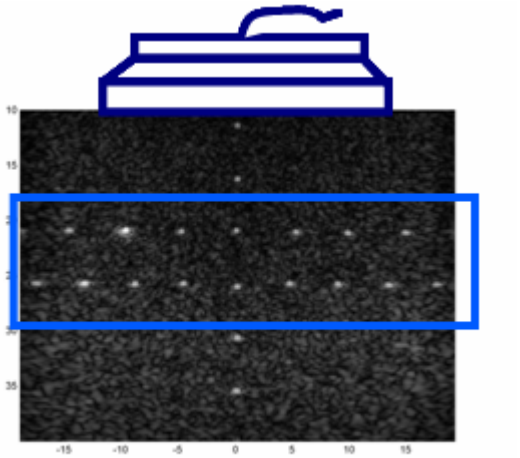

Figure 125 Phantom used for the experiment with the region of interest in blue

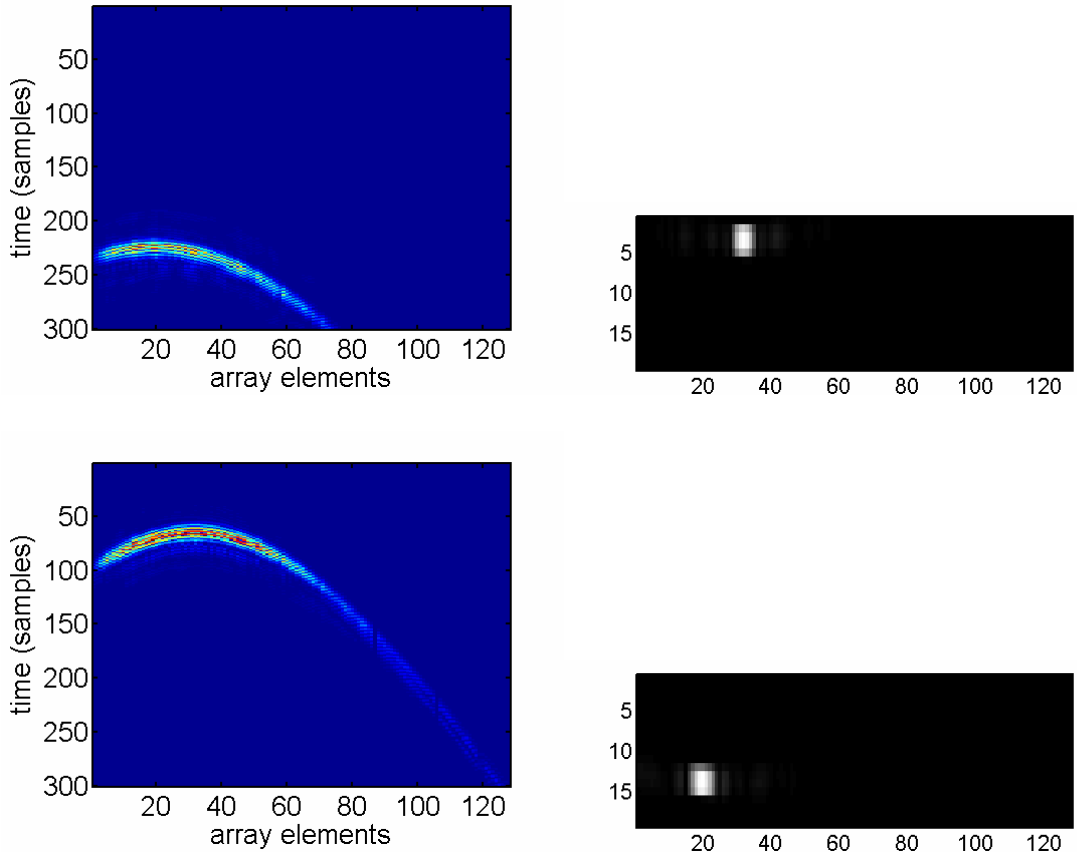

Figure 126 Two first singular matrices of the Focused Tensor. We show both the $V_{m,n}$ that corresponds to the Green' s functions (wave-fronts), and the $U_{k,l}$ that corresponds to the projection on the image pixels and therefore provides an image of the scatterers.

With the monochromatic methods (DORT), the number of scatterers that can be detected in theory is limited by the number of array elements (number of degrees of freedom, or dimension of the space) Now the broad-band nature of the method brings extra degrees of freedom. The number of scatterers that can be theoretically detected is now basically equal to the number of resolution cells in the region of interest. Axially, the size of the resolution cell is of the order of the wave-length. Laterally, it is $\lambda z / D$ for a linear array (D is the aperture size and z is the depth) or λ / D for a phased array (see Chapter 2).

IV. RECONSTRUCTION OF THE TEMPORAL GREEN'S FUNCTION BY CORRELATION OF MONOCHROMATIC GREEN'S FUNCTIONS

IV.1 Theory

We propose here an alternative method to obtain the temporal Green's function. The problem when one tries to reconstruct the time-domain Green's function from the frequency-domain ones is that the order of the singular vectors changes with the frequency. Therefore we need a method that enables us to link a singular vector at one frequency with the singular vector corresponding to the same scatterer at another frequency.

A solution to this problem is to compute the cross-correlation (in fact scalar product) between a singular vector at a certain frequency, and all the singular vectors at another frequency. The idea is that the singular vector corresponding to the same scatterer will be more similar, and therefore it will have a better correlation.

However, things are not as simple. The phase of the Green's function for a given scatterer changes with the frequency. Indeed, it is proportional to $\omega t_i(P)$, where $t_i(P)$ is the propagation time between a transducer and a scatterer as given by Eq.1.1. Thus, the correlation between two singular vectors corresponding to the same scatterer is close to one if the frequencies are close, but decreases when the frequency lag increases. The correlation is then given by $\int e^{j\frac{\Delta\omega}{c}\sqrt{z^2+(x-X)^2}} \Big/ \sqrt{z^2+(x-X)^2}\, dX$, where $\Delta\omega$ is the frequency difference, (x,z) are the coordinates of the scatterer, and X is the coordinate of the transducers. The function is plot in Figure 127. The position of the 1st minimum is given by The function decreases faster when the resolution increases.

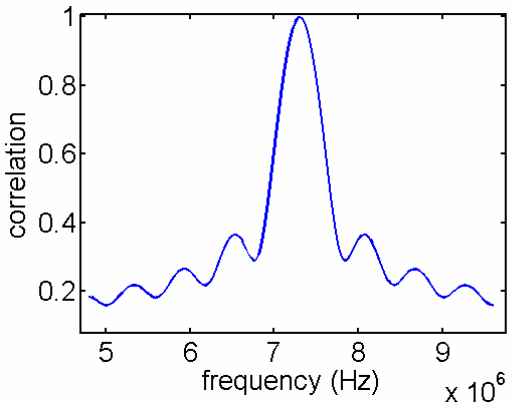

Figure 127 Correlation (scalar product) between the singular vector corresponding to a scatterer for *f=7.3* Mhz, and the singular vectors for the same scatterers at other frequencies. The singular vectors are normalized, so the peak is equal to 1.

In Figure 128, the correlation between the Green's function of a point *P* at the central frequency and the Green's function of every point at the same depth as *P* and for every frequency of the bandwidth is shown. For frequencies close to the central frequency, only the Green's function located in the same resolution cell as *P* have a

strong correlation. When the frequency lag increases, more and more points have a similar correlation. It becomes increasingly difficult to link the singular vectors.

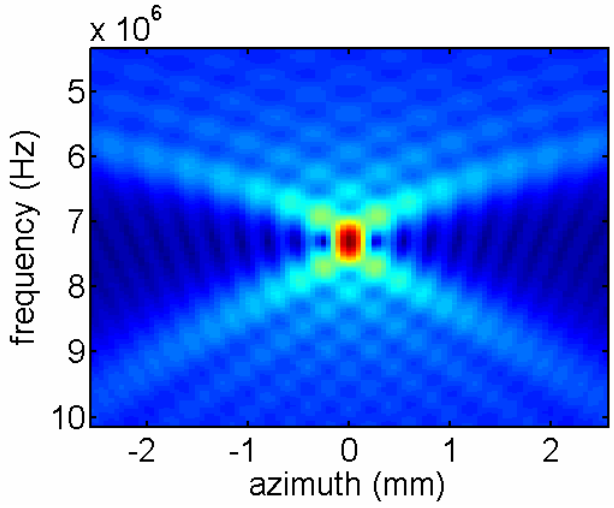

Figure 128 Correlation (scalar product) between the singular vector at 7.3 MHz for a scatterer located at 0 mm, and the singular vectors for other scatterers and other frequencies.

Therefore it is preferable to use a short frequency lag $\Delta\omega$, in the high-correlation area. By correlation the Green's function separated by a frequency lag, say ω and $\omega+\Delta\omega$, we can link the singular vectors. Then we can do the same between $\omega+\Delta\omega$ and $\omega+2\Delta\omega$, $\omega+2\Delta\omega$ and $\omega+3\Delta\omega$ and so forth. Finally, we can link all the singular vectors in the bandwidth.

However, we have to take another effect into account. At the points where the singular values cross each other, there is usually a coupling between the singular vectors that have similar singular values. The singular vectors around these points are a mixed of Green's function corresponding to both scatterers. Thus, if $\Delta\omega$ is smaller than the frequency interval where the coupling occur, we will lose the tracking of the singular vectors. Therefore, it is important not to choose $\Delta\omega$ to small. $\Delta\omega=$ VALUE is appropriate.

It actually correspond to the Nyquist number that correspond to an observation window (the window where the temporal functions are shown) of about the size of the wave-front.

IV.2 Experiments

Two scatterers with different frequency response are simulated, using Field II (J.A.Jensen). The singular values and reconstructed first temporal invariants using the classical DORT method is shown in Figure 129. The order of the singular vectors changes at about 6 MHz. Therefore, the first time-domain invariant is a mix of both scatterers.

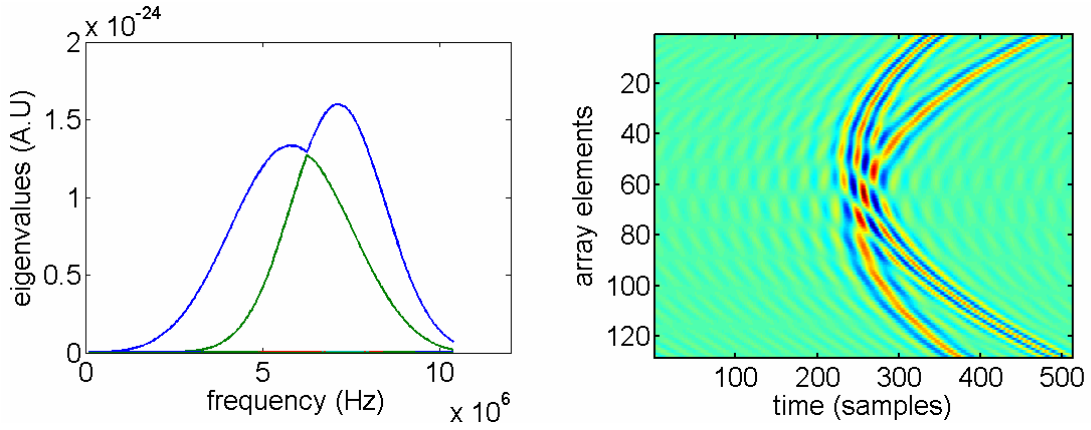

Figure 129 Singular values (left) and first temporal invariant (reconstructed by Fourier Transform of the frequency domain invariants) with the classical DORT method.

The scalar product between singular vectors at consecutive frequencies has been computed, and used to match each singular vector with the corresponding one at a different frequency. We used here a lag = DGYFD for the sampling in frequency domain.

For example, we compute the scalar product between the 1st singular vector at a given frequency and the 1st and 2nd singular vector at the following frequency. The maximum correlation indicates if the singular vectors have been switching order. This is shown in Figure 130. In this case the shift takes place at 6 MHz. This is used to find the

position of a given singular vector, as seen in Figure 130 (right). Once the position of the singular vectors has been identified, it is possible to take the Fourier Transform and to obtain the time domain Green's function.

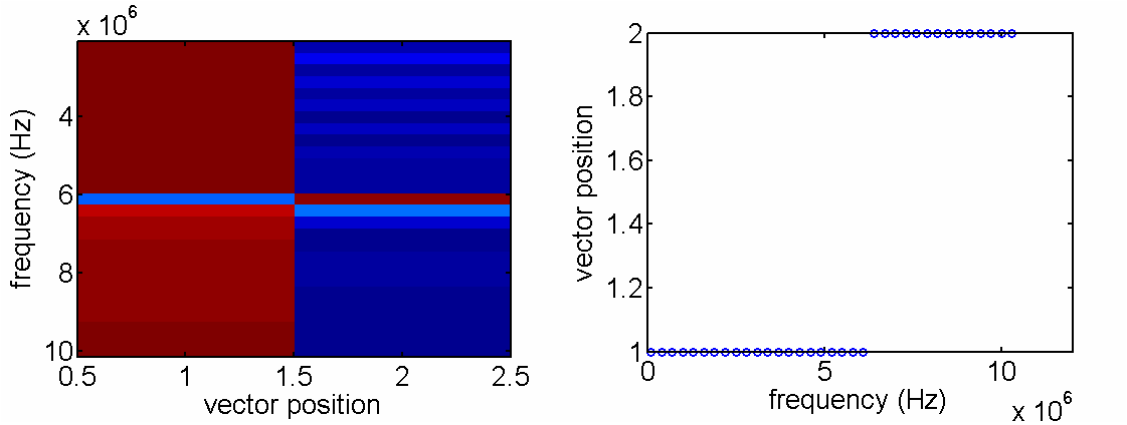

Figure 130 Left: Correlation coeficient between the 1st singular vector at each frequency and the 1st and 2nd singular vector at the next frequency. Red indicates a high correlation, while blue is a low correlation. At 6 Mhz, the 2nd singular vector has the highest correlation, which indicates that the order has switched. The correlations are used to find the position of the singular vector corresponding to a given scatterer (right)

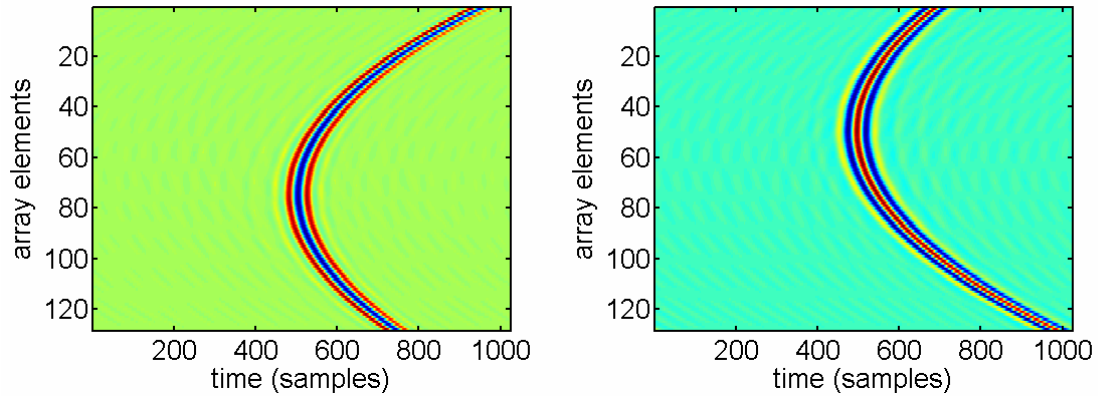

Figure 131 Temporal invariants reconstructed by Fourier Transform of the frequency domain singular vectors, after their position has been adjusted.

This method yield good results, and does not require any a priori knowledge of the medium. However, the method may failed when the area where the singular vectors are coupled is too large, especially in the case where the resolution is high. Indeed, in this case the coherence length of the singular vectors at different frequencies decreases. The

singular vectors needs to be well separated in the frequency domain. Thus, this method does not resolve scatterers from different depth.

V.CONCLUSION

We have shown how to build the Time Reversal Operator in the time domain. It takes the form of a fourth order tensor. A method to decompose the tensor and find the spatio-temporal invariants of the Time Reversal has been proposed. However, the spatio-temporal invariants no longer have the properties of the monochromatic invariants given by the DORT method. There is several spatio-temporal invariants for each scatterer, and the 1st invariant is a combination of several time-shifted version of the Green's function, and appear as a spread in time (narrower band) version of the Green's function. The decomposition of the time domain Time Reversal Operator is then not a good solution to the problem of extracting Green's functions.

We have proposed to use a Focused tensor instead. The Focused tensor offers a perfect solution to the problem in a homogeneous, or slightly heterogeneous, medium. It also has the property to separate the Green's functions of scatterers at the same azimuth, but different depth (axial resolution) which is not the case of a monochromatic method. With the DORT method (monochromatic), the maximum number of scatterers that can be detected is limited by the number of array element. Thanks to the resolution in time, the number of scatterers that one can detect with the focused tensor is in theory equal to the number of resolution cells in the region of interest. Another interest of the Focused tensor is that it provides at the same time the Green's functions in the right side singular matrix and an image in the left-side singular matrix. However, the Focused Tensor method

requires *a priori* information about the medium. Its performance is dependent on the quality of focusing. For very inhomogeneous medium, an iterative method might be a solution.

Finally, we proposed a method to match the monochromatic singular vectors obtained at different frequencies with the classical DORT method. This is based on the strong correlation between two singular vectors corresponding to the same scatterers but having slightly different frequencies. The method has been demonstrated on a simple case.

REFERENCES

Cardoso, J. F. (1991). "Super-symmetric decomposition of the fourth order cumulant tensor. Blind identification of more sources than sensors." Proceedings ICASSP: 3109-3112.

Folegot, T., C. Prada, et al. (2003). "Resolution enhancement and separation of reverberation from target echo with the time reversal operator decomposition." The Journal of the Acoustical Society of America **113**(6): 3155-3160.

Gruber, F. K., E. A. Marengo, et al. (2004). "Time-reversal imaging with multiple signal classification considering multiple scattering between the targets." The Journal of the Acoustical Society of America **115**(6): 3042-3047.

J.A.Jensen (1996). "Field: A program for simulating ultrasound systems." Med. Biol. Eng. Comp., col. 10th Nordic-Baltic Conference on Biomedical Imaging **4**(1): 351-353.

Prada, C. and M. Fink (1994). "Eigenmodes of the time reversal operator: a solution to selective focusing in multiple-target media." Wave motion **20**: 151-163.

Prada, C., S. Manneville, et al. (1996). "Decomposition of the time reversal operator: Detection and selective focusing on two scatterers." The Journal of the Acoustical Society of America **99**(4): 2067-2076.

Prada, C., J. d. Rosny, et al. (2006). "Decompostion of the time reversal operator applied to detection and focusing in a 12-m-deep channel in Brest Bay." The Journal of the Acoustical Society of America **119**(5): 3428-3429.

Prada, C. and J. L. Thomas (2003). "Experimental subwavelength localization of scatterers by decomposition of the time reversal operator interpreted as a covariance matrix." The Journal of the Acoustical Society of America **114**(1): 235-243.

Rao, C. R. (1964). "The Use and Interpretation of Principal Component Analysis in Applied Research." Sankhya **A 26**: 329 -358.

Conclusion

Au cours de cette these, une serie de résultats permettant l'application de methodes basees sur le Retournement Temporel en imagerie medicale ont ete etablis.

Dans le chapitre 2, nous avons vu adapte la methode de decomposition de l'operateur retournement temporel a partir de transmission focalisees, comme c'est le cas en echographie. Nous avons vu que le probleme pouvait etre vu comme un probleme de retournement temporel classique entre deux barettes : la barette physique d'une part, et une barette virtuelle, dont les transducteurs correspondent aux foci des transmissions. La methode focalisee permet de gagner en rapport signal sur bruit par rapport a la methode classique, et elle est plus robuste lorsque le milieu est en mouvement (typique pour le corps humain) De plus elle permet une implementation plus rapide lorsque l'on ne s'interesse qu'a une region reduite de l'espace. En effet, un nombre limite de rayon insonifie une region donnee de l'espace. Une application prometteuse est le probleme de l'ecran de phase en champs lointain (Chapitre I.B.4). En choisissant convenablement la position des foci, on peut transformer le probleme de l'ecran en champ lointain en un probleme d'ecran en champ proche, beaucoup plus simple a corriger. En effet, cela revient a generer une barette virtuelle, situe immediatement derriere l'ecran de phase. Du point de vue de cette barette virtuelle, l'ecran est en champ proche. Enfin, nous avons presente un algorithme base sur les transmissions focalisees qui permet de resoudre les diffuseurs en profondeur, en utilisant certains avantages de la nature large bande des signaux. Cela permet entre autre une nette amelioration de la detection de diffuseurs ponctuels entoures de speckle.

Au cours du chapitre 3, nous nous sommes interesses au probleme des diffuseurs etendus. C'est par exemple le cas d'un vaisseaux ou d'une microcalcification en imagerie medicale. Nous avons montre que dans le cas ou la taille du diffuseur est suffisament petite devant la longueur d'onde et la profondeur, les solutions sont une famille de fonctions connues appellees Spheroidal Prolate Wave-functions. Le nombre de valeur propre de l'operateur Retournement temporel differente de zero dans ce cas est proportionel a la taille de l'objet, exprimee en nombre de cellule de resolution. Si l'objet est suffisamment petit, le premier vecteur propre de l'operateur retournement temporel peut etre considere comme une fonction de Green d'un point de l'objet. L'une des applications les plus prometteuses est la caractérisation de petits objets, dont la taille est de l'ordre de la cellule de resolution. Ces objets, qui ont un role crucial dans la detection de cancer du sein par exemple, sont mal caractérisé par un mode d'imagerie classique, Les vecteurs propres de l'operateur retournement temporel sont la base naturelle d'algorithme d'inversion, qui permettent d'obtenir une image a tres haute resolution des objets.

Dans le chapitre 4, nous avons montre que la methode FDORT permettait d'extraire des fonctions de Green a partir du speckle, sans avoir besoin de la presence d'un diffuseur ponctuel brillant. C'est un aspect particulierement important pour l'imagerie medicale et la correction d'aberration. Le rayon transmis cree en quelque sorte un objet virtuel dans le speckle. Le premier vecteur propre est en general la fonction de Green du point focal du rayon. Nous avons etabli un formalisme statistique de la methode pour les mileux aleatoire, et fait le lien avec un theoreme important, le theoreme de Van Cittert Zernike. En particulier, cela permet d'interpreter la premiere valeur propre

normailsee en tant que critere de focalisation. Lorsque la premiere valeur propre est proche de 2/3, cela signifie que la focalisation est bonne. En milieu heterogene, la methode doit etre iterer quelques fois avant de converger vers la fonction de Green. Nous avons montre que la methode permettait d'estimer des fonctions de Green et de focaliser a la fois dans les modeles de l'ecran de phase en champ proche et en champ lointain. Un avantage de la methode FDORT par rapport a d'autres algorithmes de correction d 'aberration et sa capacite a separer le signal d'interet des interferences, meme si celles-ci sont plus intenses.

Enfin dans le Chapitre 5, nous avons essaye d'exploiter les proprietes larges bandes du signal echographique en developpant des methodes pour obtenir les fonctions de Green directement dans le domaine temporel. En effet, la reconstruction des fonctions de Green temporelle a partir des fonctions de Green monochromatique est rendu difficile par un probleme de permutation des vecteurs propres. Nous avons tout d'abord montre comment construire l'operateur retournement temporel dans le domaine temporel. Il prend la forme d'un tenseur du 4eme ordre. Nous avons explique comment decomposer ce tenseur pour obtenir les invariants spatio-temporel du retournement temporel. Malheureusement, ces invariants ne generalisent pas les proprietes interessantes des invariants monochromatique, ce qui est explique en terme physique. Nous avons ensuite propose d'utiliser le Tenseur Focalise. Cette methode offre une bonne solution pour les milieux homogenes ou legerement heterogenes. Elle permet en outre de separer les diffuseurs a differente profondeurs, et le nombre maximum de diffuseurs que l'on peut detecter est egale au nombre de cellules de resolution dans le milieu. La matrice singuliere droite du Tenseur focalise est la fonction de Green temporelle du diffuseur,

tandis que la matrice singuliere gauche offre directement une image permettant de localiser le diffuseur dans le milieu. Cependant, cette methode necessite de l'information a priori sur le milieu, et depend de la qualite de la focalisation. Finalement nous avons presente une methode permettent de relier les invariants monochromatiques de la methode DORT classique, correspondant au meme diffuseurs mais a frequence differente. Cela permet, au moins dans le cadre d'exemple simple, de resoudre le probleme de permutation.